A Study on Moisture-dependent Viscoelasticity of Bio-based Composites

by

Yu Chen

A thesis submitted in partial fulfillment of the requirements for the degree of

Doctor of Philosophy

Department of Mechanical Engineering
University of Alberta

Abstract

Bio-based composites made from bio-renewable and biodegradable constituents have been proposed as alternatives to petroleum-based composites for a variety of applications. However, studies have shown that in many cases, these bio-based composites are hydrophilic, and their viscoelasticity can be affected by moisture absorbed from humid ambient environment. Thus, to address this problem, this thesis focuses on the understanding and describing the moisture-dependent viscoelasticity of these bio-based composites using analytical and experimental tools.

The mechanical properties of composites are closely related to the constituents' assembly structure and their mechanical properties. Therefore, to model the moisture-dependent viscoelasticity of the bio-based composites, the moisture-dependent viscoelasticity of the constituents needs to be modeled first. Based on existing studies, the diffused water molecules within those hydrophilic polymers can cause both plasticization and anti-plasticization effect. However, the existing well recognized Reimschuessel model only considers the plasticization effect, leading to an underestimation of the material's stiffness at intermediate moisture level. Therefore, a simple yet important modification was introduced to the Reimschuessel model which considered the anti-plasticization effect. Together with Burgers model as the constitutive relation, the proposed model was validated with the experimental results in the literature with reasonably good accuracy.

With the proposed modified Burgers-Reimschuessel model, an experimental methodology that can comprehensively evaluate the moisture-dependent viscoelasticity of hydrophilic polymers was proposed. The proposed methodology was used to evaluate

the moisture-dependent viscoelasticity of polylactic acid (PLA), a commonly used bio-based thermoplastic polymer, and a significant anti-plasticization effect was discovered from the experimental results. The modified Burgers-Reimschuessel model was found to be able to predict the effect of moisture on the viscoelasticity of PLA and the results highlighted the importance of considering the moisture's anti-plasticization effect.

A model was developed to predict the moisture-dependent viscoelasticity of homogeneously distributed and randomly oriented short fiber reinforced bio-based composites based on micromechanical framework. The development is divided into two steps. In the first step, a micromechanical model was developed by extending Halpin-Tsai-Pagano model to linear viscoelastic regime according to correspondence principle. The model was validated against the experimental results of regenerated cellulose fibers (RCF) reinforced PLA bio-based composites with different RCF concentrations. Good agreement was found, and it provides a solid foundation to the next step. In the second step, a two-layer model with two empirical parameters were introduced to describe the moisture distribution, fiber-matrix swelling mismatch and fiber/matrix interface debonding during the moisture diffusion process. In order to validate the model, sheet samples of 5.6 wt% RCF reinforced PLA bio-based composites were produced. The samples were conditioned under 98% RH to acquire equilibrium moisture content and tested under 24% RH. Results indicate that the developed model is able to describe the effect of non-equilibrium moisture diffusion on the creep compliance of this bio-based composites.

The model developed in this thesis can be used to predict the performance of products made by these bio-based composites. It can also provide guidance to the design and optimization of the products made by theses bio-based composites.

Preface

This thesis is based on a collection of published, submitted or soon to be submitted journal articles, which were completed in collaboration with my supervisors.

Chapter 1 provides an introduction of the thesis including motivation, background, and objectives of the thesis.

A version of Chapter 2 of this thesis has been published in the *Journal of Polymer Science* as ***Y. Chen, C. Ayranci, T. Tang, "Modified Burgers-Reimschuessel model for moisture-sensitive polymers", vol. 60, no. 9, pp. 1539-1549, 2022.*** I contributed to the modeling conceptualization and development, code writing in MATLAB, model validation and the preparation of the original draft of the manuscript. Drs. Tang and Ayranci contributed to modeling conceptualization, funding acquisition, supervision, as well as reviewing and editing the manuscript.

A version of Chapter 3 of this thesis has been published in the *Journal of Applied Polymer Science* as ***Y. Chen, T. Tang, C. Ayranci, "Moisture-induced Anti-plasticization of Polylactic Acid: Experiments and Modeling", vol. 139, no. 24, pp. 52369, 2022.*** I contributed to experimental methodology conceptualization, code writing in MATLAB, sample production and testing, data analysis and the preparation of the original draft of the manuscript. Drs. Tang and Ayranci contributed to experimental methodology conceptualization, funding acquisition, supervision, as well as reviewing and editing the manuscript.

A version of Chapter 4 of this thesis is in the process of being submitted as ***Y. Chen, T. Tang, C. Ayranci, "Linear viscoelasticity of bio-based composites of polylactic acid and regenerated cellulose fibers: modeling and***

experimental validation". The author contributed to modeling conceptualization and development, experimental methodology conceptualization, code writing in MATLAB, sample production and testing, data analysis and the preparation of the original draft of the manuscript. Drs. Tang and Ayranci contributed to modeling conceptualization, experimental methodology conceptualization, funding acquisition, supervision, as well as reviewing and editing the manuscript.

A version of Chapter 5 will be submitted to a peer-review journal for publication. I contributed to modeling conceptualization and development, experimental methodology conceptualization, code writing in MATLAB, sample production and testing, data analysis and the preparation of the original draft of the manuscript. Drs. Tang and Ayranci contributed to modeling conceptualization, experimental methodology conceptualization, funding acquisition, supervision, as well as reviewing and editing the manuscript.

Chapter 6 provides a conclusion of the thesis and recommendations to the future works.

Acknowledgements

First and foremost, I would like to express my sincere gratitude to my supervisors Dr. Cagri Ayranci and Dr. Tian Tang for their continuous support in every aspect during my PhD program. Their motivation, enthusiasm, and immense knowledge helped me grow from a student interested in research into a researcher I am today. I truly enjoy the weekly meeting with them and their suggestions would always inspire me, help me to solve the problems encountered during this project. I know PhD is always not an easy journey, but they made my journey enjoyable. They are not only my supervisors, but also my friends and my mentors. I always feel comfortable chatting and consulting with them on any topics other than research such as career path, teaching, camping, etc.

I would like extend my thanks to Dr. David Nobes for being a member of my supervisory committee and provide me with valuable suggestions and insights during our committee meetings, as well as the candidacy exam. I would like to thank Dr. Chong-Qing Ru and Dr. Anastasia Elias to be my examiners for my candidacy exam and provided inspiring questions during the exam.

I gratefully acknowledge the support from the Natural Sciences and Engineering Research Council of Canada (NSERC), Alberta Innovates, Alberta Graduate Excellence Scholarship, Alberta Innovates Graduate Student Scholarship, Westmoreland Coal Company Graduate Scholarship in Environmental Engineering and University of Alberta Doctoral Recruitment Scholarship.

I also want to say thanks to my friends and lab mates Dr. Irina Garces, Dr. Eyup Can Demir, and Miss Jiawei Chen. Thanks for all the trainings, helps, and I enjoy

working with you all for every projects and management of this lab. I would also like to thank other lab mates during this journey for creating this friendly and interesting working environment, they are Samir, Abiy, Xiaoang, Panxi, Devin, Abdelhaq, Alan, and Zongyu.

I am especially grateful to my wife, Xinyuan He, for encouraging me to realize my dream and for your accompany during my PhD study. I cannot overcome all the hardships and difficulties without your constant love and support. Thank you so much! A special thank to my kitty Mahjong who came to our home right at the time when this thesis was proposed. He is a stress reliever and is growing up with this thesis.

Last but not the least, I would like express my thanks to my parents Yu-Fang Xia and Dong-Dong Chen, for their encouragement and financial support during my study. Thank you for giving birth to me at the first place, providing me with good education and supporting me spiritually throughout my life.

Table of Contents

List of Tables

List of Figures

List of Symbols

Constants

ΔH_{mf}	Heat of fusion of fully crystallized PLA	$93.1\, J/g$

Latin

a_C	Moisture shifting factor	
B_1	The first empirical parameter of WLF function	
B_2	The second empirical parameter of WLF function	$wt\%$
C	Moisture content	$wt\%$
C_0	Reference moisture content	$wt\%$
C_c	Moisture content of the composites	$wt\%$
C_e	Equilibrium moisture content	$wt\%$
C_{C-a}	Actual equilibrium moisture content of the composites	$wt\%$
C_{C-p}	Predicted equilibrium moisture content of the composites	$wt\%$
C_{da}	Effective fiber damage coefficient due to interface debonding and hygroscopic mismatch of fiber and matrix	
C_{fe}	Equilibrium moisture content of fiber	$wt\%$
C_{me}	Equilibrium moisture content of matrix	$wt\%$
D	Diffusivity	m^2/s
d	Diameter	mm
d_f	Fiber diameter	μm
D_q	Intermediate parameters of closed form solution of Halpin-Tsai-Pagano model in Laplace transformed domain	
E	Young's modulus	GPa
E_0	Initial level of Young's modulus in Reimschuessel model	GPa

E_c	Young's modulus of composites	GPa
E_f	Young's modulus of the fibers	GPa
E_s	Saturation level of Young's modulus in Reimschuessel model	GPa
E_{10}	Initial level of the first elastic parameter in Modified Burgers-Reimschuessel model	GPa
E_{1s}	Saturation level of the first elastic parameter in Modified Burgers-Reimschuessel model	GPa
E_1	The first elastic parameter in Burgers model	GPa
E_{20}	Initial level of the second elastic parameter in Modified Burgers-Reimschuessel model	GPa
E_{2s}	Saturation level of the second elastic parameter in Modified Burgers-Reimschuessel model	GPa
E_2	The second elastic parameter in Burgers model	GPa
E_{c1}	Young's modulus of aligned short fiber composites in longitudinal direction	GPa
E_{c2}	Young's modulus of aligned short fiber composites in transverse direction	GPa
E_{f-eff}	Effective fiber Young's modulus after moisture damage	GPa
E_{i-WBAP}	Term to describe WBAP effect on elastic parameters in modified Burgers-Reimschuessel model	GPa
E_{m1}	The first elastic parameter in Burgers model for matrix	GPa
E_{m2}	The second elastic parameter in Burgers model for matrix	GPa
E_m	Young's modulus of the matrix	GPa
$f(t)$	Areal fraction of the inner layer for the two-layer model	
F_p	Intermediate parameters of closed form solution of Halpin-Tsai-Pagano model in Laplace transformed domain	
$\hat{G}_c$	Laplace transformed Stress relaxation modulus of the randomly oriented short fiber reinforced composites	
$\hat{G}_{c1}$	Laplace transformed stress relaxation modulus of the aligned short fiber reinforced composites in longitudinal direction	
$\hat{G}_{c2}$	Laplace transformed stress relaxation modulus of the aligned short fiber reinforced composites in transverse direction	

$\hat{G}_{f-eff}$	Laplace transformed effective stress relaxation modulus of fibers	
$\hat{G}_m$	Laplace transformed stress relaxation modulus of matrix	
G	Stress relaxation modulus	GPa
G_I	Inner layer stress relaxation modulus	GPa
G_s	Surface layer stress relaxation modulus	GPa
ΔH_c	Heat of crystallization	J/g
ΔH_m	Heat of fusion	J/g
$\hat{J_{c1}}$	Laplace transformed creep compliance of aligned short fiber composites in longitudinal direction	
$\hat{J_{c2}}$	Laplace transformed creep compliance of aligned short fiber composites in transverse direction	
$\hat{J}_c$	Laplace transformed creep compliance of composites	
$\hat{J}_f$	Laplace transformed creep compliance of fiber	
$\hat{J_m}$	Laplace transformed creep compliance of matrix	
J	Creep compliance	$1/GPa$
J_c	Creep compliance of the composites	$1/GPa$
J_m	Creep compliance of matrix	$1/GPa$
K	A representation of a general viscoelastic property	
k	Slope of the initial linear portion of moisture absorption curve	$wt\%/s^{0.5}$
k_A	Anti-plasticization constant in modified Reimschuessel model	
k_D	Anti-plasticization decay constant in modified Reimschuessel model	
k_E	Plasticization decay constant for Young's modulus in Reimschuessel model	$1/wt\%$
k_p	Plasticization decay constant in modified Reimschuessel model	
k_w	Inner layer thickness variation constant	$1/s$
$k_{\mu i}$	Plasticization decay constant for viscous parameters in modified Burgers-Reimschuessel model	$1/wt\%$
$k_{A\mu i}$	Anti-plasticization constant in modified Reimschuessel model for viscous parameters of Burgers model	$GPa \cdot s/wt\%$
k_{AEi}	Anti-plasticization constant in modified Reimschuessel model for elastic parameters of Burgers model	$GPa/wt\%$

$k_{D\mu i}$	Anti-plasticization decay constant in modified Reimschuessel model for viscous parameters of Burgers model	$GPa \cdot s/wt\%$
k_{da}	Constant to describe the effective fiber damage	$1/\%$
k_{DEi}	Anti-plasticization decay constant in modified Reimschuessel model for elastic parameters of Burgers model	$GPa \cdot s/wt\%$
k_{Ei}	Plasticization decay constant for elastic parameters in modified Burgers-Reimschuessel model	$1/wt\%$
L_f	Fiber length	mm
m	mass	kg
P	Material parameters in modified Reimschuessel model	
P_0	Initial level of parameter in modified Reimschuessel model	
p_1	Intermediate parameter in stress relaxation modulus solution	
p_2	Intermediate parameter in stress relaxation modulus solution	
P_s	Saturation level of parameter in modified Reimschuessel model	
q_1	Intermediate parameter in stress relaxation modulus solution	
q_2	Intermediate parameter in stress relaxation modulus solution	
r_1	Intermediate parameter in stress relaxation modulus solution	
r_2	Intermediate parameter in stress relaxation modulus solution	
s	Independent variable in Laplace transformed domain	
S_a	Proportional constant in Shen-Springer model	
S_b	Exponential constant in Shen-Springer model	
S_c	Elastic compliance of the composites	$1/GPa$
S_f	Fiber elastic compliance	$1/GPa$
S_m	Elastic compliance of the matrix	$1/GPa$
S_{c1}	Elastic compliance of aligned short fiber composites in longitudinal direction	$1/GPa$
S_{c2}	Elastic compliance of aligned short fiber composites in transverse direction	$1/GPa$
T	Temperature	$^\circ C$
t	Time	s

V_f	Fiber volume fraction	%
V_m	Matrix volume fraction	%
W_f	Weight fraction of the fiber	%
W_m	Weight fraction of the matrix	%
X_c	Crystallinity	%

Greek

η	Halpin-Tsai modulus ratio parameter	
η_θ	Empirical parameter for fiber orientation effect	
η_i	Halpin-Tsai intermediate parameter	
η_l	Empirical parameter for fiber length effect	
μ_{10}	Initial level of the first viscous parameter in Modified Burgers-Reimschuessel model	$GPa \cdot s$
μ_{1s}	Saturation level of the first viscous parameter in Modified Burgers-Reimschuessel model	$GPa \cdot s$
μ_1	The first viscous parameter in Burgers model	$GPa \cdot s$
μ_{20}	Initial level of the second viscous parameter in Modified Burgers-Reimschuessel model	$GPa \cdot s$
μ_{2s}	Saturation level of the second viscous parameter in Modified Burgers-Reimschuessel model	$GPa \cdot s$
μ_2	The second viscous parameter in Burgers model	$GPa \cdot s$
μ_{i-WBAP}	Term to describe WBAP effect on viscous parameters in modified Burgers-Reimschuessel model	$GPa \cdot s$
μ_{m1}	The first viscous parameter in Burgers model for matrix	$GPa \cdot s$
μ_{m2}	The second viscous parameter in Burgers model for matrix	$GPa \cdot s$
ϕ	Relative humidity	%
σ	Stress	GPa
σ_0	Creep stress	GPa
σ_c	Composites stress	GPa
σ_f	Fiber stress	GPa
σ_I	Inner layer stress	GPa

σ_m	Matrix stress	Gpa
σ_S	Surface layer stress	GPa
τ	Integration variable	s
ε	Strain	
ε_0	Constant strain in stress relaxation test	
ε_c	Composites strain	
ε_f	Fiber strain	
ε_I	Inner layer strain	
ε_m	Matrix strain	
ε_S	Surface layer strain	
ξ_i	Halpin-Tsai empirical parameter	

Abbreviations

DP degree of polymerization.

DSC differential scanning calorimetry.

MEMS micro-electromechanical systems.

Micro-CT microcomputed tomography.

NMMO N-Methyl morpholine N-oxide.

PA polyamide.

PBS poly(butylene succinate).

PEG polyethylene glycol.

PET polyethylene terephthalate.

PEVA poly(ethylene-vinyl acetate).

PGA polyglycolic acid.

PHA polyhydroxyalkanoates.

PHBV poly(3-hydroxybutyrate-co-3-hydroxyvalerate).

PLA polylactic acid.

PS polystyrene.

PVA polyvinyl alcohol.

PVAc polyvinyl acetate.

PVC polyvinyl chloride.

RCF regenerated cellulose fibers.

RH relative humidity.

TMS time-moisture superposition.

TTS time-temperature superposition.

WBAP water bridge anti-plasticization.

WLF Williams-Landel-Ferry.

Chapter 1

Introduction

1.1 Background and Research Motivation

Starting from mid-20th century, the applications of fiber reinforced polymer composites materials have increased significantly [1]. These materials are conventionally composed of petroleum-based matrices and reinforcements as constituents. In recent years however, the elevated environmental concerns lead to critical discussions on the use of these traditional composite materials [2–4] due to their production and recycling at the end of their life cycles.

Bio-based composites have been proposed and became promising alternatives to the currently utilized petroleum-based composites in order to address the aforementioned shortcomings [2, 5]. Bio-based composites are defined as composites consist of constituents that are sourced using bio-renewable resources and that are often biodegradable [4]. Some examples of bio-based matrix phase are thermoplastic starch, polylactic acid (PLA), polyhydroxyalkanoates (PHA), polyhydroxybutyrate-co-valerate (PHB), etc. [2, 5] They possess similar mechanical properties and share similar processing techniques with those petroleum-based polymers such as polystyrene (PS) and polyethylene terephthalate (PET). Some examples of bio-based reinforcement phases include hemp, kenaf, sisal, ramie, and regenerated cellulose fibers (RCF) [2, 4–6]. Although these fibers offer slightly lower stiffnesses, they are still promising alternatives to those fibers such as Kevlar and glass fibers used in traditional petroleum-based

composites [6]. In fact, these bio-based composites are used in automotive and construction applications [4]. Due to the promising future of bio-based composites, the number of publications related to bio-based composites has increased drastically since the beginning of 21th century, as shown in Figure 1.1.

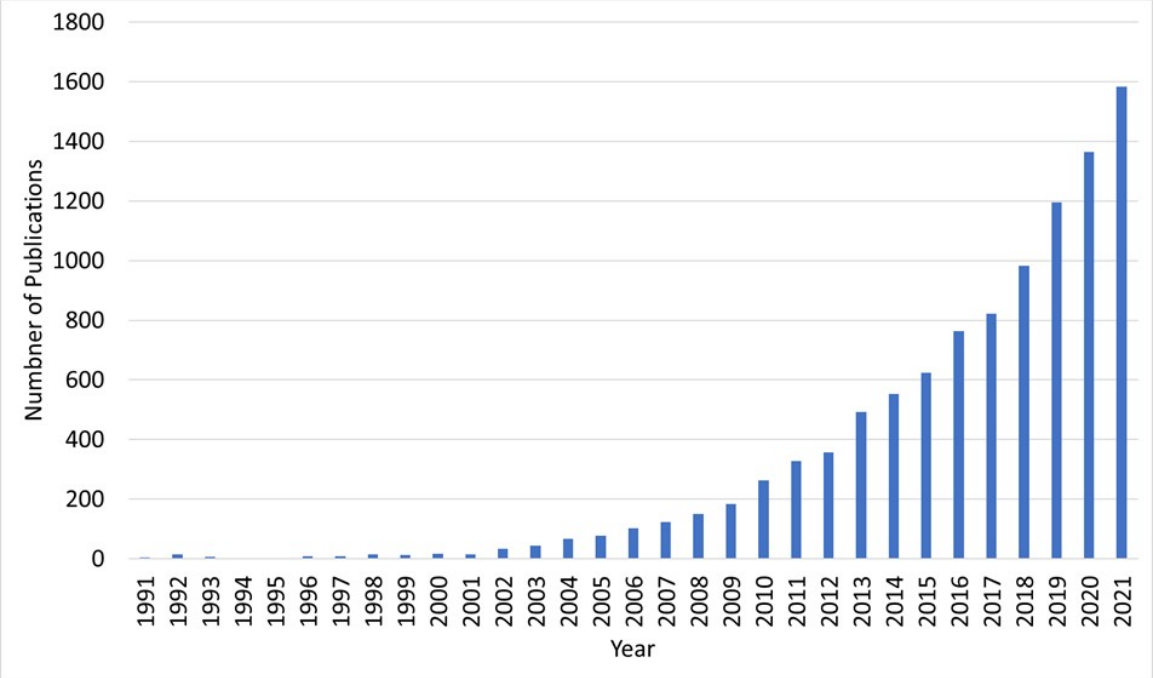

Figure 1.1: Number of publications with keyword "bio-based composites" or "bio-composites" in Web of Science database, retrieved on Oct 6, 2022.

In the development and application of bio-based composites, characterizing and modeling the mechanical properties is one of the most crucial aspects [1]. Bio-based composites are made from biopolymers, which mostly belong to viscoelastic materials [7]. Thus, for this type of material to be used as structural components under long-term loadings, its time-dependent viscoelastic behavior needs to be characterized, modeled, and accounted for in the designs [7–9]. In many cases, both matrix and reinforcement phases of bio-based composites are hydrophilic biopolymers that can absorb moisture under humid environments [10–17]. Also, it has been discovered that the viscoelasticity of hydrophilic polymers can be significantly changed by moisture absorption since the water molecules will cause both plasticization and anti-

plasticization effect [18–27]. Existing models only considers the effect of plasticization [22, 26–28] while the lack of consideration on anti-plasticization effect caused deviations between model prediction and the experimental results at intermediate moisture levels [22, 26]. Furthermore, studies have discovered that, other than plasticization and anti-plasticization effect on the constituents, the diffused moisture may cause complex phenomena such as fiber/matrix swelling mismatch and interface debonding, which both could weaken the mechanical properties of the bio-based composites [29–31]. An analytical model that comprehensively considers the effect of these phenomena on the viscoelasticity of bio-based composites was not discovered among the existing studies. These challenges have motivated the current study. The goal of this thesis is to contribute to the fundamental understanding and modeling of moisture-dependent viscoelasticity of bio-based composites and to promote their real-life applications.

1.2 Thesis Objectives

The mechanical properties of composites are closely related to the constituents' assembly structure and their mechanical properties [1]. To characterize and model the moisture-dependent viscoelasticity of bio-based composites, the moisture-dependent viscoelasticity of its constituents needs to be characterized and modeled first. Next, a micromechanical model that can predict the viscoelasticity of bio-based composites based on constituents' viscoelastic constitutive relation and assembly structure of them needs to be established as a framework. Finally, based on the framework of this micromechanical model, a model to describe the moisture-dependent viscoelasticity of bio-based composites can be developed. Therefore, the objectives of this thesis are shown below:

1. To develop a model that can predict the moisture-dependent viscoelasticity of hydrophilic polymers.

2. To develop an experimental methodology that can characterize the moisture-dependent viscoelasticity of hydrophilic polymers and bio-based composites.

3. To develop a model that can describe the viscoelasticity of bio-based composites with given constituents' mechanical properties.

4. To develop a model that can describe the moisture-dependent viscoelasticity of bio-based composites under moisture diffusion.

1.3 Literature review and overview of the thesis

Over the last sixty years, researchers have undertaken various investigations to study the effect of moisture on the viscoelasticity of hydrophilic polymers. When water molecules enter the hydrophilic polymers, it can cause plasticization effect by forming water clusters and anti-plasticization effect by forming water bridges [32–34]. The plasticization effect would soften the polymers since the water clusters may increase the inter-molecular distance and release some topological entanglements between the molecular chains [27, 35, 36]. Some water molecules can form hydrogen bonds and establish bridge-like links between the polymer chains [35–37]. These bond water could stiffen the polymers by restricting the mobility of the polymer chains (a.k.a anti-plasticization effect) [20]. Both effects have been observed directly or indirectly in the literature [20, 22, 35, 37–39]. Thus, it is important to predict the moisture-dependent viscoelasticity of these polymer by considering both plasticization and anti-plasticization effects.

Among the existing studies, time-moisture superposition principle (TMS) analogous to time-temperature superposition (TTS) principle, has been proposed and applied to describe the effect of moisture on viscoelasticity of hydrophilic polymers [26, 27]. However, due to the lack of consideration on anti-plasticization effect, this model has been discovered to apply only to cases in which the plasticization effect is more significant and anti-plasticization effect is negligible [23, 26, 28, 40, 41]. In

addition, Reimschuessel [22] proposed a relation to describe the effect of moisture on the Young's modulus of hydrophilic polymers and the model has been applied to the experimental results of Nylon 6 [38] and polyurethane-based shape memory polymers [42]. However, it was found that at intermediate level of moisture content (below 2 wt%), the model underestimated the experimental values [22, 42], indicating the lack of consideration on anti-plasticization effect of this model. To address this shortcoming, an essential modification has been introduced to the Reimschuessel's model (in Chapter 2) that considers anti-plasticization effect. The proposed model is also validated against the experimental results in the literature.

The proposed model has many parameters, which can only be fitted with experimental results. Thus, a systematic experimental approach is needed to extract the model parameters for a specific hydrophilic polymer. In addition, the proposed model predicts a stiffening effect at low moisture content, which was only indirectly observed by Schmid et al. [20] on SU-8, a hydrophilic polymer for micro-resonator fabrication. For this purpose, a polymer with weak hydrophilicity would be the best candidate to observe the anti-plasticization effect since, under the same condition, this polymer will absorb a minor amount of moisture and show a more significant anti-plasticization effect. Therefore, in Chapter 3 of this thesis, an experimental methodology has been developed and PLA, which has a contact angle of around 75° [43–46], was characterized using the developed methodology. Anti-plasticization effect has been observed when PLA absorbs less than 1 wt% of moisture.

The existing studies that focus on prediction of mechanical properties of bio-based polymer composites are limited only to the linear elastic regime. Pan and Zhong [47–51] formulated a Helmholtz free energy of the composite system and the moisture diffusion was considered as a thermodynamically irreversible process. The model can be generally applied to various bio-based composites including unidirectional long fiber reinforced bio-based composites [48], bidirectional long fiber reinforced bio-based composites [52], evenly distributed and randomly oriented short fiber reinforced bio-

based composites [53], wood cell wall [49], and hybrid bio-based composites [54]. Despite that, the limitation of this model is that it was only demonstrated to predict the elastic properties, such as Young's modulus of the composites, while these bio-based composites have been presented with viscoelasticity [12]. The second category that provided by the same research group [29, 50] is to introduce modifications to existing micromechanical models to account for the moisture effect. The fiber/matrix swelling mismatch was considered by modifying the fiber stiffness tensor based on fiber swelling strain. Kamau et al. [55] further extended this model to account for the fiber-matrix interface debonding. Similar to the previous model, no work has been found that can predict the viscoelasticity during moisture diffusion. Consequently, in this thesis, a model has been developed to describe the viscoelasticity of homogeneously distributed, randomly oriented short fiber reinforced bio-based composites during moisture diffusion, which is currently missing in the literature. The development has been divided into two steps. In the first step, Chapter 4, a micromechanical model that combines Halpin-Tsai model [56] and Tsai-Pagano model [57] is developed. The model is extended from linear elastic regime to linear viscoelastic regime based on correspondence principle to describe the viscoelasticity of homogeneously distributed, randomly oriented short fiber reinforced bio-based composites with no moisture content. In the second step, Chapter 5, two modifications are introduced to account for the moisture effect. One of them is to describe the moisture diffusion while the other one is to consider the weakening caused by fiber-matrix swelling mismatch and fiber-matrix interface debonding.

To validate the model, a type of bio-based composite that has hydrophilic matrix and reinforcement was produced. One of the most widely used biopolymers, PLA, is chosen for the matrix of bio-based composites [58]. PLA's mechanical properties, bio-renewability, biodegradability and processability lead to its wide-spread application in the manufacturing of bio-based composites [59–64]. In terms of reinforcement phase, regenerated cellulose fibers (RCF), is chosen. RCF has proven advantages

over those cellulosic natural fibers since RCF have fewer surface impurities and their properties do not vary with the production batches [15, 65–67]. Because of these reasons, RCF/PLA composites has been widely used and studied [12, 61, 65–71]. In this thesis, sheet samples of RCF/PLA bio-based composites have been manufactured using a two-step extrusion method. In Chapter 4, produced dry sheet samples were tested to validate the developed micromechanical model. In Chapter 5, the produced samples were conditioned under 98% RH to acquire equilibrium moisture content. Then, tensile creep tests were conducted under 24% RH. The effect of moisture diffusion was shown on the experimental results and the model was validated against the results.

1.4 Structure of the thesis

The structure of the thesis is shown in the flowchart in Figure 1.2. The thesis is written in journal paper format. As such, some versions of the main chapters of the thesis are published, or submitted/will be submitted to be published, in peer-reviewed journals.

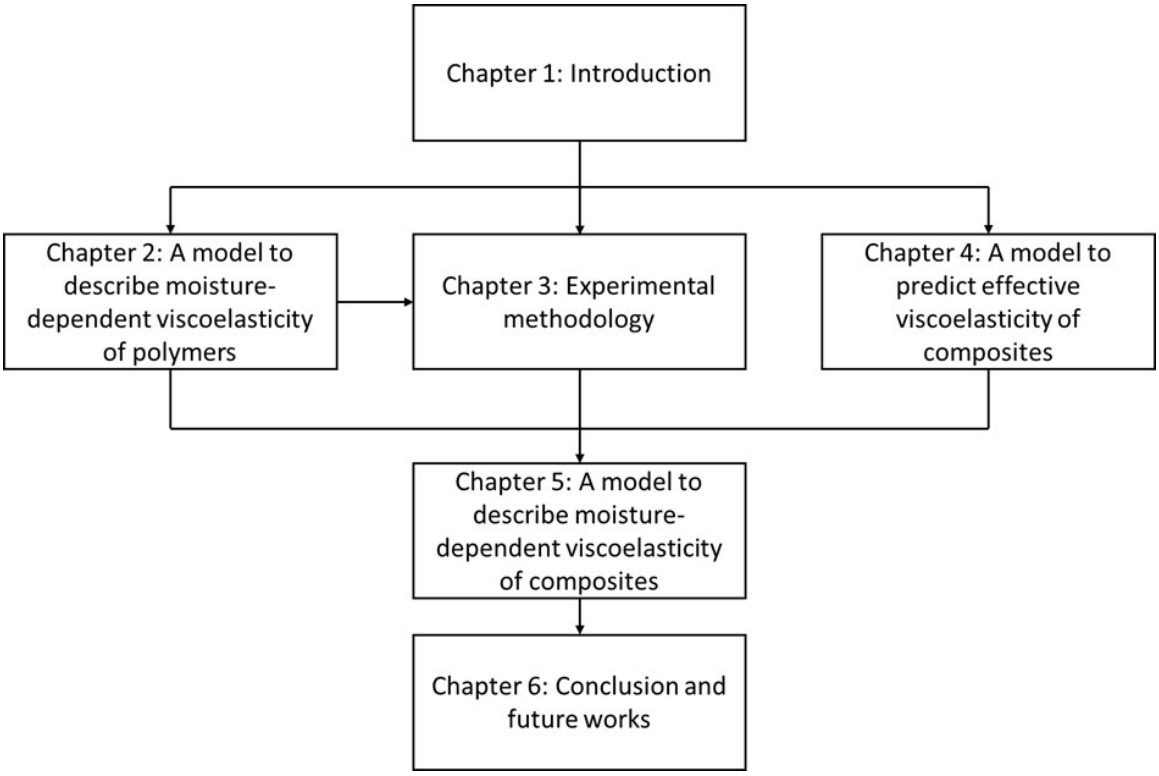

Figure 1.2: Structure of the thesis.

The effect of moisture on the viscoelasticity of hydrophilic polymers is studied in Chapter 2. Findings outline that the moisture can cause both plasticization and anti-plasticization. A modification is introduced to Reimschuessel's model [22] to consider both effects and the model is validated with experimental results obtained by Onogi et al. [26] A version of this chapter has been published in *Journal of Polymer Science* [72].

In Chapter 3, based on the developed model, an experimental methodology to comprehensively characterize the viscoelasticity of hydrophilic polymers has been proposed. The developed methodology is applied to characterize the moisture-dependent viscoelasticity of PLA. The anti-plasticization effect proposed by the model developed in Chapter 2 was also observed in the experimental results in this chapter. A version of this chapter has been published in *Journal of Applied Polymer Science* [73].

In Chapter 4, a model that combines Halpin-Tsai model and Tsai-Pagano model

is developed and extended into linear viscoelastic regime to predict the creep behavior of homogeneously distributed and randomly oriented short fiber reinforced bio-based composites. RCF/PLA sheet samples with different RCF concentration were produced using a two-step extrusion method and creep tests were conducted on the samples. Good agreement is observed between the prediction and experimental results, indicating this micromechanical model can be used as a solid framework for the modeling of the moisture effect. A version of this chapter is in the process of being submitted.

Chapter 5 introduces two additional parameters to describe the moisture diffusion and the weakening effect caused by fiber/matrix swelling mismatch and fiber/matrix interface debonding. Sheet samples of 5.6 wt% RCF reinforced PLA bio-based composites has been produced and conditioned to obtain equilibrium moisture content under 98% RH while creep tests were conducted under 24% RH. It has been discovered that the developed model can describe the creep behavior of this composites under moisture desorption. A version of this chapter is prepared to be submitted to a peer-reviewed journal.

Chapter 6 draws a conclusion to the entire thesis and provides some future recommendations.

References

[1] A. K. Kaw, *Mechanics of Composite Materials*, 2nd ed. CRC Press, 2006, p. 491.

[2] A. K. Mohanty, M Misra, and G Hinrichsen, "Biofibres, biodegradable polymers and biocomposites: An overview," *Macromolecular Materials and Engineering*, vol. 277, pp. 1–24, 2000.

[3] D. Bondeson and K. Oksman, "Dispersion and characteristics of surfactant modified cellulose whiskers nanocomposites," *Composite Interfaces*, vol. 14, pp. 617–630, 7-9 Sep. 2007, ISSN: 09276440. DOI: 10.1163/156855407782106519.

[4] A. K. Mohanty, M. Misra, and L. T. Drzal, *Natural fibers, biopolymers, and biocomposites*. Taylor and Francis, 2005.

[5] T. Gurunathan, S. Mohanty, and S. K. Nayak, "A review of the recent developments in biocomposites based on natural fibres and their application perspectives," *Composites Part A: Applied Science and Manufacturing*, vol. 77, pp. 1–25, Jun. 2015, ISSN: 1359835X. DOI: 10.1016/j.compositesa.2015.06.007.

[6] J. K. Pandey, S. H. Ahn, C. S. Lee, A. K. Mohanty, and M. Misra, "Recent advances in the application of natural fiber based composites," *Macromolecular Materials and Engineering*, vol. 295, pp. 975–989, 11 Nov. 2010, ISSN: 14387492. DOI: 10.1002/mame.201000095.

[7] M. T. Shaw and W. J. MacKnight, *Introduction to Polymer Viscoelasticity*, 3rd ed. John Wiley and Sons, Inc., 2005, p. 327.

[8] D. Gutierrez-Lemini, *Engineering Viscoelasticity*. Springer, 2014, p. 353.

[9] R. A. Schapery, *Viscoelastic Behavior and Analysis of Composite Materials*, 1st ed., G. P. Sendeckyj, Ed. Academic Press, 1974, pp. 85–168.

[10] A. Atmakuri, A. Palevicius, M. Siddabathula, A. Vilkauskas, and G. Janusas, "Analysis of mechanical and wettability properties of natural fiber-reinforced epoxy hybrid composites," *Polymers*, vol. 12, pp. 1–15, 12 Dec. 2020, ISSN: 20734360. DOI: 10.3390/polym12122827.

[11] K. E. Mazur *et al.*, "Analysis of the effect of photo and hydrodegradation on the surface morphology and mechanical properties of composites based on pla and phi modified with natural particles," *Materials*, vol. 15, 3 Feb. 2022, ISSN: 19961944. DOI: 10.3390/ma15030878.

[12] L. Rozite, J. Varna, R. Joffe, and A. Pupurs, "Nonlinear behavior of pla and lignin-based flax composites subjected to tensile loading," *Journal of Thermoplastic Composite Materials*, vol. 26, pp. 476–496, 4 May 2013, ISSN: 08927057. DOI: 10.1177/0892705711425846.

[13] B. Baghaei and M. Skrifvars, "Characterisation of polylactic acid biocomposites made from prepregs composed of woven polylactic acid/hemp-lyocell hybrid yarn fabrics," *Composites Part A: Applied Science and Manufacturing*, vol. 81, pp. 139–144, Feb. 2016, ISSN: 1359835X. DOI: 10.1016/j.compositesa.2015.10.042.

[14] C. A. Murphy and M. N. Collins, "Microcrystalline cellulose reinforced polylactic acid biocomposite filaments for 3d printing," *Polymer Composites*, vol. 39, pp. 1311–1320, 4 Apr. 2018, ISSN: 15480569. DOI: 10.1002/pc.24069.

[15] J. W. Park, T. H. Lee, J. H. Back, S. W. Jang, H. J. Kim, and M. Skrifvars, "Phenyl silane treatment and carding process to improve the mechanical, thermal, and water-absorption properties of regenerated cellulose lyocell/polylactic acid bio-composites," *Composites Part B: Engineering*, vol. 167, pp. 387–395, Jun. 2019, ISSN: 13598368. DOI: 10.1016/j.compositesb.2019.02.064.

[16] A. Smoca, "Water absorption properties of hemp fibres reinforced pla biocomposites," *Engineering for Rural Development*, vol. 18, pp. 1079–1083, 2019, ISSN: 16915976. DOI: 10.22616/ERDev2019.18.N522.

[17] M. A. Sawpan, M. R. Islam, M. D. H. Beg, and K. Pickering, "Effect of accelerated weathering on physico-mechanical properties of polylactide biocomposites," *Journal of Polymers and the Environment*, vol. 27, pp. 942–955, 5 2019, ISSN: 15662543. DOI: 10.1007/s10924-019-01405-2. [Online]. Available: http://dx.doi.org/10.1007/s10924-019-01405-2.

[18] R. A. Jurf and J. R. Vinson, "Effect of moisture on the static and viscoelastic shear properties of epoxy adhesives," *Journal of Materials Science*, vol. 20, pp. 2979–2989, 8 1985, ISSN: 00222461. DOI: 10.1007/BF00553063.

[19] F. Huber, H. Etschmaier, H. Walter, G. Urstöger, and P. Hadley, "A time temperature moisture concentration superposition principle that describes the relaxation behavior of epoxide molding compounds for microelectronics packaging," *International Journal of Polymer Analysis and Characterization*, vol. 25, pp. 467–478, 6 2020, ISSN: 15635341. [Online]. Available: https://doi.org/10.1080/1023666X.2020.1807680.

[20] S. Schmid, S. Kühne, and C. Hierold, "Influence of air humidity on polymeric microresonators," *Journal of Micromechanics and Microengineering*, vol. 19, 6 2009.

[21] M. B. Satterfiield and J. B. Benziger, "Viscoelastic properties of nafion at elevated temperature and humidity," *Journal of Polymer Science Part B: Polymer Physics*, vol. 47, pp. 11–24, 2009. [Online]. Available: http://arxiv.org/abs/cond-mat/0406218%0Ahttp://dx.doi.org/10.1002/polb.

[22] H. K. Reimschuessel, "Relationships on the effect of water on glass transition temperature and young's modulus of nylon 6," *Journal of Polymer Science Part A: Polymer Chemistry*, vol. 16, pp. 1229–1236, 6 1978.

[23] I. Widiastuti, I. Sbarski, and S. H. Masood, "Mechanical behavior of a fluid-sensitive material during liquid diffusion," *Mechanics of Time-Dependent Materials*, vol. 18, pp. 387–406, 2 2014, ISSN: 13852000. DOI: 10.1007/s11043-014-9233-9.

[24] I. Widiastuti, I. Sbarski, and S. H. Masood, "Mechanical response of poly(lactic acid)-based packaging under liquid exposure," *Journal of Applied Polymer Science*, vol. 131, pp. 1–10, 16 2014.

[25] I. Widiastuti, I. Sbarski, and S. H. Masood, "Creep behavior of pla-based biodegradable plastic exposed to a hydrocarbon liquid," *Journal of Applied Polymer Science*, vol. 127, pp. 2654–2660, 4 2013, ISSN: 00218995. DOI: 10.1002/app.37575.

[26] S. Onogi, K. Sasaguri, T. Adachi, and S. Ogihara, "Time–humidity superposition in some crystalline polymers," *Journal of Polymer Science*, vol. 58, pp. 1–17, 166 1962.

[27] H. Fujita and A. Kishimoto, "Diffusion-controlled stress relaxation in polymers. iii. stress relaxation in a swelling polymer," *Journal of Polymer Science*, vol. 28, pp. 569–585, 118 1958.

[28] I. Emri and V. Pavsek, "On the influence of moisture on the mechanical properties of polymers," *Materials Forum*, vol. 16, pp. 123–131, 2 1992.

[29] Y. Pan and Z. Zhong, "A micromechanical model for the mechanical degradation of natural fiber reinforced composites induced by moisture absorption," *Mechanics of Materials*, vol. 85, pp. 7–15, Aug. 2015, ISSN: 01676636. DOI: 10.1016/j.mechmat.2015.02.001.

[30] Z. Huo, "Modeling and evaluation of moisture diffusion in polymer composite materials," Missouri University of Science and Technology, 2016.

[31] D. Roy, *Biocomposites for high-performance applications: current barriers and future needs towards industrial development*. Woodhead Publishing, 2017.

[32] S. Koltzenburg, M. Maskos, and O. Nuyken, *Polymer chemistry*. Springer, 2017.

[33] P. Gilormini and J. Verdu, "On the role of hydrogen bonding on water absorption in polymers," *Polymer*, vol. 142, pp. 164–169, 2018. DOI: 10.1016/j.polymer.2018.03.033. [Online]. Available: https://hal.archives-ouvertes.fr/hal-01743020.

[34] U. W. Gedde, *Polymer Physics*. Springer, 1999, p. 301.

[35] R. M. Hodge, T. J. Bastow, G. H. Edward, G. P. Simon, and A. J. Hill, "Free volume and the mechanism of plasticization in water-swollen poly(vinyl alcohol)," *Macromolecules*, vol. 29, pp. 8137–8143, 25 1996, ISSN: 00249297. DOI: 10.1021/ma951073j.

[36] X. Fan, "Mechanics of moisture for polymers: Fundamental concepts and model study," 2008.

[37] R. M. Hodge, G. H. Edward, and G. P. Simon, "Water absorption and states of water in semicrystalline poly(vinyl alcohol) films," *Polymer*, vol. 37, pp. 1371–1376, 8 1996, ISSN: 00323861. DOI: 10.1016/0032-3861(96)81134-7.

[38] K. Inoue and S. Hoshino, "Swelling of nylon 6 film due to water sorption.," *Journal of Polymer Science Part B: Polymer Physics*, vol. 14, pp. 1513–1526, 8 1976, ISSN: 00981273. DOI: 10.1002/pol.1976.180140812.

[39] K. M. Zakir, A. J. Parsons, C. D. Rudd, I. Ahmed, and W. Thielemans, "Mechanical , crystallisation and moisture absorption properties of melt drawn polylactic acid fibres," *European Polymer Journal*, vol. 53, pp. 270–281, 2014, ISSN: 0014-3057. DOI: 10.1016/j.eurpolymj.2014.02.001. [Online]. Available: http://dx.doi.org/10.1016/j.eurpolymj.2014.02.001.

[40] A. Ishisaka and M. Kawagoe, "Examination of the time-water content superposition on the dynamic viscoelasticity of moistened polyamide 6 and epoxy," *Journal of Applied Polymer Science*, vol. 93, pp. 560–567, 2 2004.

[41] R. D. Maksimov, E. A. Sokolov, and V. P. Mochalov, "Effect of temperature and moisture on the creep of polymeric materials 1. one-dimensional extension under stationary temperature-moisture conditions," *Mechanics of Composite Materials*, vol. 11, pp. 334–339, 3 1975.

[42] I. T. Garces, S. Aslanzadeh, Y. Boluk, and C. Ayranci, "Effect of moisture on shape memory polyurethane polymers for extrusion-based additive manufacturing," *Materials*, vol. 12, 2 2019, ISSN: 19961944.

[43] S. M. Bhasney, R. Patwa, A. Kumar, and V. Katiyar, "Plasticizing effect of coconut oil on morphological, mechanical, thermal, rheological, barrier, and optical properties of poly(lactic acid): A promising candidate for food packaging," *Journal of Applied Polymer Science*, vol. 134, p. 45 390, 41 Nov. 2017.

[44] V. Marturano *et al.*, "Light-responsive nanocapsule-coated polymer films for antimicrobial active packaging," *Polymers*, vol. 11, p. 68, 1 Jan. 2019.

[45] A. Orue, A. Eceiza, C. Peña-Rodriguez, and A. Arbelaiz, "Water uptake behavior and young modulus prediction of composites based on treated sisal fibers and poly(lactic acid)," *Materials*, vol. 9, p. 400, 5 2016.

[46] M. Esmaeili, G. Pircheraghi, R. Bagheri, and V. Altstädt, "Poly(lactic acid)/coplasticized thermoplastic starch blend: Effect of plasticizer migration on rheological and mechanical properties," *Polymers for Advanced Technologies*, vol. 30, pp. 839–851, 4 Apr. 2019.

[47] Y. Pan and Z. Zhong, "Modeling of the mechanical degradation induced by moisture absorption in short natural fiber reinforced composites," *Composites Science and Technology*, vol. 103, pp. 22–27, Oct. 2014, ISSN: 02663538. DOI: 10.1016/j.compscitech.2014.08.010.

[48] Y. Pan and Z. Zhong, "A nonlinear constitutive model of unidirectional natural fiber reinforced composites considering moisture absorption," *Journal of the Mechanics and Physics of Solids*, vol. 69, pp. 132–142, 1 2014, ISSN: 00225096. DOI: 10.1016/j.jmps.2014.04.007.

[49] Y. Pan and Z. Zhong, "Analysis of creep and modulus loss of the wood cell wall," *Acta Mechanica*, vol. 227, pp. 3191–3203, 11 Nov. 2016, ISSN: 00015970. DOI: 10.1007/s00707-015-1532-y.

[50] Y. Pan and Z. Zhong, "Micromechanical modeling of the wood cell wall considering moisture absorption," *Composites Part B: Engineering*, vol. 91, pp. 27–35, Apr. 2016, ISSN: 13598368. DOI: 10.1016/j.compositesb.2015.12.038.

[51] Z. Zhong and F. Tian, "Modeling of mechanical behaviors for natural fiber reinforced composites under hygrothermal ageing," *Science China: Physics, Mechanics and Astronomy*, vol. 60, 12 Dec. 2017, ISSN: 18691927. DOI: 10.1007/s11433-017-9103-3.

[52] K. F. Wang and B. L. Wang, "A mechanical degradation model for bidirectional natural fiber reinforced composites under hydrothermal ageing and applying in buckling and vibration analysis," *Composite Structures*, vol. 206, pp. 594–600, Dec. 2018, ISSN: 02638223. DOI: 10.1016/j.compstruct.2018.08.063.

[53] Y. H. Pan and Z. Zhong, "Relative humidity and temperature dependence of mechanical degradation of natural fiber composites," *Science China: Physics, Mechanics and Astronomy*, vol. 59, 6 Jun. 2016, ISSN: 16747348. DOI: 10.1007/s11433-015-0520-0.

[54] Y. Pan and Z. Zhong, "The effect of hybridization on moisture absorption and mechanical degradation of natural fiber composites: An analytical approach," *Composites Science and Technology*, vol. 110, pp. 132–137, Apr. 2015, ISSN: 02663538. DOI: 10.1016/j.compscitech.2015.02.005.

[55] K. Kamau-Devers and S. A. Miller, "Using a micromechanical viscoelastic creep model to capture multi-phase deterioration in bio-based wood polymer composites exposed to moisture," *Construction and Building Materials*, vol. 314, Jan. 2022, ISSN: 09500618. DOI: 10.1016/j.conbuildmat.2021.125252.

[56] J. C. Halpin and J. L. Kardos, "The halpin-tsai equations: A review," *Polymer Engineering and Science*, vol. 16, pp. 345–352, 5 1976.

[57] S. W. Tsai and N. J. Pagano, "Invarient properties of composite materials," Air Force Materials Laboratory, May 1968.

[58] R. A. Ilyas *et al.*, "Polylactic acid (pla) biocomposite: Processing, additive manufacturing and advanced applications," *Polymers*, vol. 13, 8 Apr. 2021, ISSN: 20734360. DOI: 10.3390/polym13081326.

[59] E Castro-aguirre, F Iñiguez-franco, H Samsudin, X Fang, and R Auras, "Poly (lactic acid) — mass production , processing , industrial applications , and end of life," *Advanced Drug Delivery Reviews*, vol. 107, pp. 333–366, 2016, ISSN: 0169-409X. DOI: 10.1016/j.addr.2016.03.010. [Online]. Available: http://dx.doi.org/10.1016/j.addr.2016.03.010.

[60] D. Tzetzis, K. Tsongas, and G. Mansour, "Determination of the mechanical properties of epoxy silica nanocomposites through fea-supported evaluation of ball indentation test results," *Journal of Materials Research*, vol. 20, pp. 1571–1578, 6 Nov. 2017, ISSN: 15161439. DOI: 10.1590/1980-5373-MR-2017-0454.

[61] N. Kurokawa and A. Hotta, "Regenerated cellulose nanofibers fabricated through electrospinning and saponification of cellulose acetate as reinforcement of polylactide composites," *Cellulose*, vol. 26, pp. 7797–7808, 13-14 Sep. 2019, ISSN: 1572882X. DOI: 10.1007/s10570-019-02623-6.

[62] R. Auras, L. Lim, S. M. Selke, and H. Tsuji, *Polylactic Acid, Synthesis, Structures, Properties, Processing, and Applications*. John Wiley and Sons, 2010.

[63] N. F. Zaaba and M. Jaafar, "A review on degradation mechanisms of polylactic acid: Hydrolytic, photodegradative, microbial, and enzymatic degradation," *Polymer Engineering and Science*, vol. 60, pp. 2061–2075, 9 2020, ISSN: 15482634. DOI: 10.1002/pen.25511.

[64] M. Funabashi, F. Ninomiya, and M. Kunioka, "Biodegradability evaluation of polymers by iso 14855-2," *International Journal of Molecular Sciences*, vol. 10, pp. 3635–3654, 8 Aug. 2009, ISSN: 14220067. DOI: 10.3390/ijms10083635.

[65] M. Shibata, S. Oyamada, S.-I. Kobayashi, and D. Yaginuma, "Mechanical properties and biodegradability of green composites based on biodegradable polyesters and lyocell fabric," *Journal of Applied Polymer Science*, vol. 92, pp. 3857–3863, 2004.

[66] M. S. Huda, A. K. Mohanty, L. T. Drzal, E Schut, and M Misra, "Green composites from recycled cellulose and poly(lactic acid): Physico-mechanical and morphological properties evaluation," *Journal of Materials Science*, vol. 40, pp. 4221–4229, 2005.

[67] A. K. Bledzki, A. Jaszkiewicz, and D. Scherzer, "Mechanical properties of pla composites with man-made cellulose and abaca fibres," *Composites Part A: Applied Science and Manufacturing*, vol. 40, pp. 404–412, 4 Apr. 2009, ISSN: 1359835X. DOI: 10.1016/j.compositesa.2009.01.002.

[68] B. Bax and J. Müssig, "Impact and tensile properties of pla/cordenka and pla/flax composites," *Composites Science and Technology*, vol. 68, pp. 1601–1607, 7-8 Jun. 2008, ISSN: 02663538. DOI: 10.1016/j.compscitech.2008.01.004.

[69] M. S. Huda, L. T. Drzal, A. K. Mohanty, and M. Misra, "Chopped glass and recycled newspaper as reinforcement fibers in injection molded poly(lactic acid) (pla) composites: A comparative study," *Composites Science and Technology*, vol. 66, pp. 1813–1824, 11-12 Sep. 2006, ISSN: 02663538. DOI: 10.1016/j.compscitech.2005.10.015.

[70] B. Geissler, M. Feuchter, S. Laske, M. Fasching, C. Holzer, and G. R. Langecker, "Strategies to improve the mechanical properties of high-density polylactic acid foams," *Journal of Cellular Plastics*, vol. 52, pp. 15–35, 1 Jan. 2016, ISSN: 15307999. DOI: 10.1177/0021955X14538274.

[71] B. Baghaei, M. Skrifvars, M. Rissanen, and S. K. Ramamoorthy, "Mechanical and thermal characterization of compression moulded polylactic acid natural fiber composites reinforced with hemp and lyocell fibers," *Journal of Applied Polymer Science*, vol. 131, 15 Aug. 2014, ISSN: 10974628. DOI: 10.1002/app.40534.

[72] Y. Chen, C. Ayranci, and T. Tang, "Modified burgers-reimschuessel model for moisture-sensitive polymers," *Journal of Polymer Science*, vol. 60, pp. 1539–1549, 9 Oct. 2021.

[73] Y. Chen, T. Tang, and C. Ayranci, "Moisture-induced anti-plasticization of polylactic acid: Experiments and modeling," *Journal of Applied Polymer Science*, vol. 139, 24 Jun. 2022, ISSN: 10974628. DOI: 10.1002/app.52369.

Chapter 2

Modified Burgers-Reimschuessel Model for Moisture-sensitive Polymers

2.1 Introduction

Polymers are one of the most common engineering materials used in our daily lives [74]. Mechanical properties of polymers are crucial in their applications. Almost all polymers exhibit viscoelasticity, and their time-dependent properties must be considered when used as a structural component under long-term loading [7]. This becomes more critical for hydrophilic polymers, whose viscoelastic properties are typically sensitive to moisture. A number of studies have reported that, viscoelastic properties of hydrophilic polymers can be significantly affected by moisture, resulting in drastic changes in the deformation as moisture content increases [18, 19, 21, 22, 24, 26–28, 40, 41, 75–82]. However, to the best of our knowledge, modeling the moisture effect on viscoelastic properties has been limited, which calls for further investigations [19, 22, 24, 28, 41].

At molecular level, the effect of moisture is originated by the interaction between the molecular chains and the water molecules [22]. When small molecules, like water, penetrate the hydrophilic polymer's molecular structure, they can increase the inter-chain distance and break the physical bonds between the chains. As a result,

the polymers are softened [83]. These small molecules are commonly referred to as plasticizers and the softening phenomenon is referred to as plasticization. The plasticization phenomenon induced by water has been widely observed in a variety of polymers such as polyamide 6 (Nylon 6) [22], polyvinyl alcohol (PVA) [35] and polylactic acid (PLA) [39]. On the other hand, water molecules can also form hydrogen bonds with the polar groups on the polymer chains [33]. These water molecules become immobilized between the polymer chains and restrict the chain-mobility. The reduced molecular mobility can cause stiffening of the polymers, known as the anti-plasticization effect [34], which has been indirectly observed in the literature. For example, Schmid et al.[20] reported that, in low RH (3-10%) environment, there was an increase in the resonance frequency of SU-8, a hydrophilic polymer commonly used in the fabrication of micro-resonators. This increase in the resonance frequency at low moisture content was attributed to the increased stiffness of SU-8 due to water's anti-plasticization effect while the decrease of the resonance frequency at high moisture content was caused by the plasticization effect.

It is important to understand and be able to predict the effect of both plasticization and anti-plasticization on moisture-sensitive polymers prior to any design and structural applications. In the literature, attempts have been made to model the effect of moisture on the mechanical behaviors of polymers, among which the time-moisture superposition (TMS) principle is the most widely used. TMS states that for a time-dependent property such as creep compliance or stress relaxation modulus, the effect of increasing moisture content is equivalent to that of extending the time scale [26, 27]. Mathematically, the principle can be represented by

$$K(t, C_0) = K(\frac{t}{a_C}, C_e) \tag{2.1}$$

where $K(t, C_0)$ is the property at a reference moisture content C_0, $K(t, C_e)$ is the property at equilibrium moisture content C_e, and $a_C(C_e)$ is the moisture shifting factor which is a function of C_e. C_e is usually defined as the ratio between the weight

of the absorbed moisture and the original weight of the dry polymer. In practice, when plotting the time-dependent property with respect to time in logarithmic scale, the curves corresponding to different C_e values can be collapsed into a single master curve by a horizontal shift [28]. Therefore, knowing a_C and the curve under C_0, the time-dependent property under other moisture contents can be predicted. Fujita et al. [27] reported that, for a linear amorphous polymer above its second-order transition temperature, material softening with increased moisture content was solely due to plasticization whereas the anti-plasticization effect was negligible at high temperature. As a result, the TMS principle held. Onogi et al. [26] attempted to apply the TMS principle to PVA and Nylon 6 at room temperature (20-25°C). The TMS principle was found to work well for the stress relaxation modulus of Nylon 6 while it failed to provide a good fit for PVA at very low moisture content. It is highly possible that the poor agreement was due to the omission of anti-plasticization effect which could be significant for PVA at room temperature. Later, Emri et al. [28] proposed that, to adopt the TMS principle in real applications, the shift factor a_C may follow the Williams-Landel-Ferry (WLF) function [84]:

$$\ln a_C = \frac{-B_1(C_e - C_0)}{B_2 + C_e - C_0} \tag{2.2}$$

where B_1 and B_2 are empirical parameters to be determined by fitting experimental data. Emri et al. [28] successfully applied the WLF function to fit the shear creep compliances measured for cylindrical specimens of polyvinyl acetate (PVAc) containing different moisture contents. Ishisaka et al. [40] also attempted to use the WLF function on the storage modulus of Nylon 6 and epoxy. Although the shift factor in the form of Equation 2.2 worked for Nylon 6, it did not hold for epoxy. A possible explanation could be that the covalent bonds between the epoxy chains restricted the molecular mobility. Consequently, water molecules cannot significantly increase the inter-molecular distance and plasticize the material. The authors also discovered that the glass transition temperature was not significantly lowered even after the moisture

absorption, suggesting that the plasticization effect is rather limited [40]. This study agreed with the findings by Onogi et al. [26] where the TMS principle was only applicable to Nylon 6. Under the framework of TMS, Maksimov et al. [41] proposed a second order polynomial for the relation between $\ln a_c$ and C_e. This relation was successfully applied to predict the creep compliance of polyester, although to the best of our knowledge it has not been used for any other polymers due to the lack of physical interpretation. Widiastuti et al. [23] used Burgers model to describe the viscoelasticity of a PLA-based polymer while considering moisture-dependent parameters. The WLF function was used to predict the retardation time while other parameters were assumed to be polynomials of moisture content C_e. At the highest C_e (6 wt%), more than 25% of discrepancy was observed for the creep compliance between the model prediction and experimental results [23].

Reimschuessel [22] proposed a model for the change of Young's modulus E with respect to moisture, based on the tensile test results of Inoue and Hoshino [38]. One underlying assumption was that the sample was fully saturated and the moisture was uniformly distributed during the tests. This was a reasonable assumption given that the time scale of the tensile tests (around 30 s) was two orders of magnitude smaller than that of moisture diffusion (around 8000 s) [38]. Experimentally for Nylon 6, E was found to decay faster at low moisture content and slower at high moisture content, eventually approaching a limiting value. Based on those observations, Reimschuessel proposed the relation in Equation 2.3 to describe the change of E with respect to C_e:

$$E(C_e) = E_s + (E_0 - E_s)\exp(-k_E C_e) \tag{2.3}$$

where k_E is a positive constant, E_0 is the Young's modulus of dry Nylon 6 and E_s is the limiting (saturation) value for large C_e. This relation was explained by water plasticization causing the breakage of secondary bonds between the polymer chains and the increase of inter-molecular distance [22]. Garces et al. [42] successfully applied this model to predict the Young's modulus of one type of polyurethane-based

shape memory polymer. However, in Reimeschuessel's work, it was found that the agreement between model and experiments was poor at intermediate moisture levels [22]. In particular, the experimental value of E was approximately 19% higher than the prediction at C = 2 wt% [22]. This suggests the overestimation of the plasticization effect, or the lack of consideration on anti-plasticization, by the Reimschuessel model.

In this chapter, we introduce a simple, yet important, modification to the Reimschuessel's model, by considering both plasticization and anti-plasticization induced by water molecules. Isothermal condition is assumed, to avoid the coupled effect of temperature and moisture. The model is validated by the experimental stress relaxation data presented by Onogi et al. for four different types of polymers, namely PVA with degree of polymerization (the number of monomer units in the polymer, DP) 600, PVA with DP 2060, original Nylon 6, and heat-treated Nylon 6 [26]. The proposed modified Reimschuessel model predictions compare well with the aforementioned experimental data for the stress relaxation moduli of the materials for a range of moisture content (0 to 16 wt%). The proposed model can provide valuable information for critical uses of other types of moisture-sensitive polymers when their performance and service life under ambient conditions need to be predicted prior to design.

2.2 Model

A great amount of work has been done to model the viscoelasticity of polymers and the majority of them were based on phenomenological mechanical analogs consisting of elastic and viscous elements [34, 85].The present work adopts the Burgers model since it is one of the simplest models that capture the essential features of polymer viscoelasticity [86]. The behaviors of the elastic and viscous elements are considered to change with moisture. The change is mathematically described by considering plasticization and anti-plasticization caused by two different forms of water that exists

in moisture-sensitive polymers: free water and bound water [36, 87–90].

2.2.1 Burgers Model

The Burgers model is schematically shown in Figure 2.1 and quantitatively described by Equation 2.4, where $\varepsilon(t)$ and $\sigma(t)$ are strain and stress, respectively [91]. Although generally considered as a phenomenological model, the parameters (E_1, E_2, μ_1 and μ_2) in the Burgers model, to some degree, capture the molecular responses of the polymers [7]. The elastic parameters E_1 and E_2 represent the ability of the polymer chains to recover from a deformation [7]. They are affected by the fraction of closely compacted crystalline region (crystallinity) and the number of topological entanglements between the polymer chain coils within the amorphous regions [34, 83, 86]. The viscous parameters μ_1 and μ_2 represent the resistance caused by the non-covalent bonds between the polymer chains when they slide past one another under the external load [83]. The free volume within the polymers and the number of the inter-chain non-covalent bonds affects these viscous parameters [7, 83].

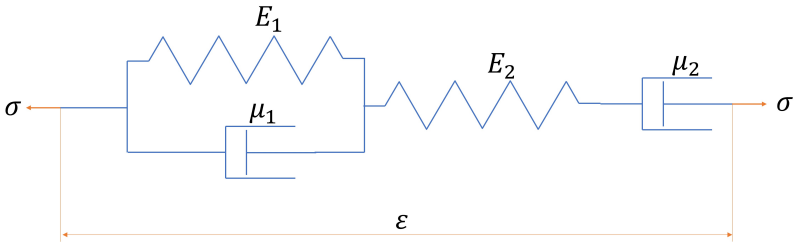

Figure 2.1: Schematic representation of Burgers model

$$\frac{\mu_1\mu_2}{E_1}\frac{d^2\varepsilon}{dt^2} + \mu_2\frac{d\varepsilon}{dt} = \frac{\mu_1\mu_2}{E_1E_2}\frac{d^2\sigma}{dt^2} + \left(\frac{\mu_1}{E_1} + \frac{\mu_2}{E_1} + \frac{\mu_2}{E_2}\right)\frac{d\sigma}{dt} + \sigma \tag{2.4}$$

2.2.2 Plasticization caused by free water

Water molecules has little effect on the crystalline regions due to their closely compacted nature [22]. Under constant temperature, when water molecules enter the amorphous regions, it can exist in two forms, free and bound as shown in Figure 2.2a

and 2.2b, respectively [36, 37, 92]. Free water corresponds to molecules that do not have significant interaction with the polymer chains and therefore are free to move within the network. They usually form clusters as illustrated by the blue filled circles in Figure 2.2a, and can increase the inter-molecular distance, leading to increased free volume [35, 36, 89]. As a result, the polymer is softened by the enhanced molecular mobility [27].

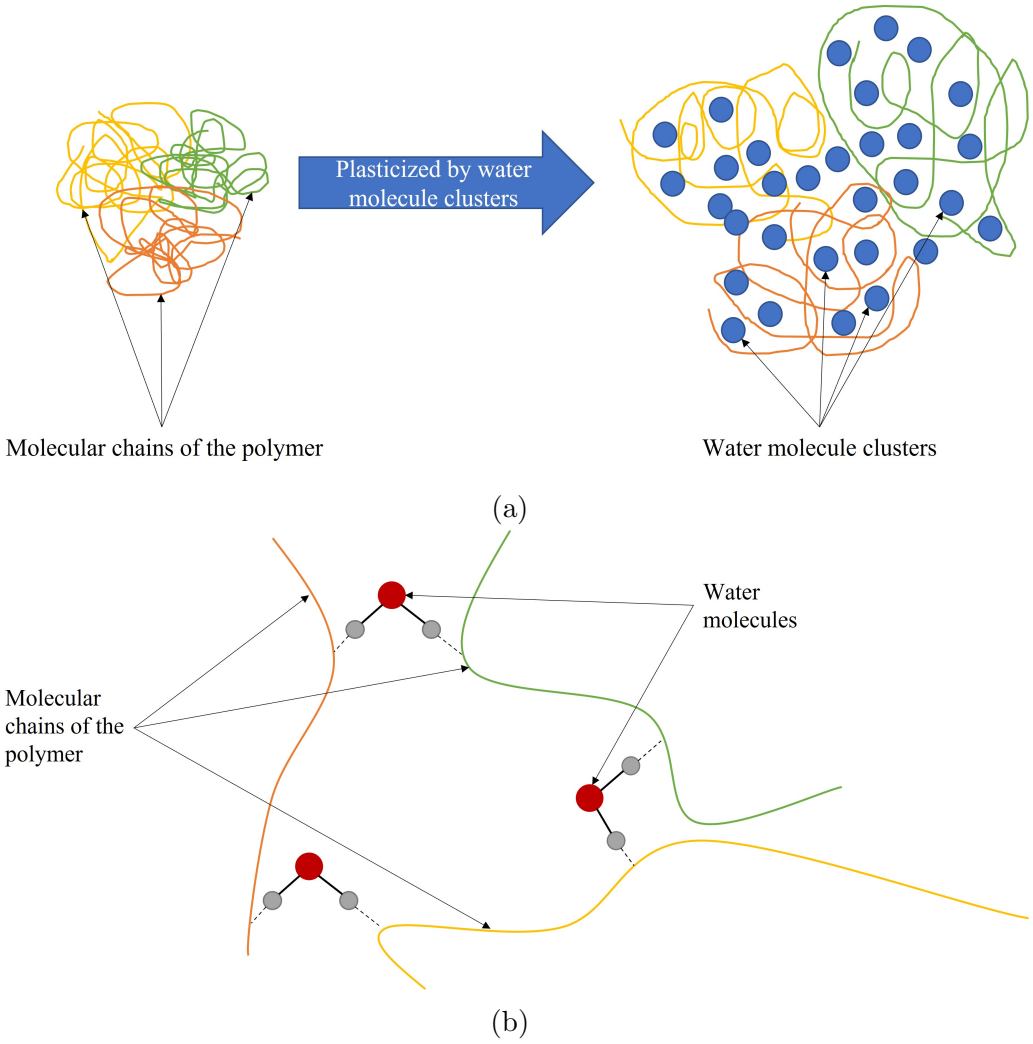

Figure 2.2: Schematic representation of (a) free water clusters and (b) bridging water molecules within the polymer network [22, 92, 93]

The effect of free water on the Burgers model parameters are qualitatively illustrated by the red curve in Figure 2.3. E_1 and E_2 mainly represent the enthalpic

elasticity of the crystalline region and the entropic elasticity of the amorphous region, which are affected by the crystallinity and topological entanglements within the polymer. Water molecules that diffuse into the polymer network can increase the free volume and release some of the topological entanglements, causing the elastic moduli to decrease. However, E_1 and E_2 may not decrease to zero even if there is a significant amount of absorbed moisture. This is because of the finite number of topological entanglements that can be released, the existence of entropic elasticity of the polymer coils, the little impact free water has on the closely compacted crystalline regions, and the residual non-covalent interactions between the polymer chains such as van der Waals force and water bridges (to be discussed in section 2.2.3). Therefore, as in the Reimschuessel model [22], Equation 2.5 is proposed to describe the change of elastic parameters with respect to moisture content C_e, under the effect of plasticization:

$$\frac{dE_i}{dC_e} = -k_{Ei}\left(E_i(C_e) - E_{is}\right) \tag{2.5}$$

where $i = 1, 2;$, k_{Ei} are positive constants; and E_{is} are the limiting values for large C_e. The initial condition, corresponding to the dry polymer, is given by Equation 2.6

$$E_i(C_e = 0) = E_{i0} \tag{2.6}$$

which renders the following solution to Equation 2.5:

$$E_i(C_e) = E_{is} + (E_{i0} - E_{is})\exp(-k_{Ei}C_e) \tag{2.7}$$

The viscous parameters μ_1 and μ_2 are affected by free water in a similar way, where the increased inter-molecular distance reduces the probability of forming non-covalent bonds between chains. As a result, μ_1 and μ_2 are expected to decrease with moisture content and approach their respective limiting values at large C_e. Therefore, as proposed by Reimschuessel [22], μ_1 and μ_2 change with C_e in the following form

$$\mu_i(C_e) = \mu_{is} + (\mu_{i0} - \mu_{is})\exp(-k_{\mu i}C_e) \tag{2.8}$$

where $i = 1, 2$; $k_{\mu i}$ are positive constants; μ_{is} are the limiting values at large C_e; and μ_{i0} are the viscous parameters of the dry polymer.

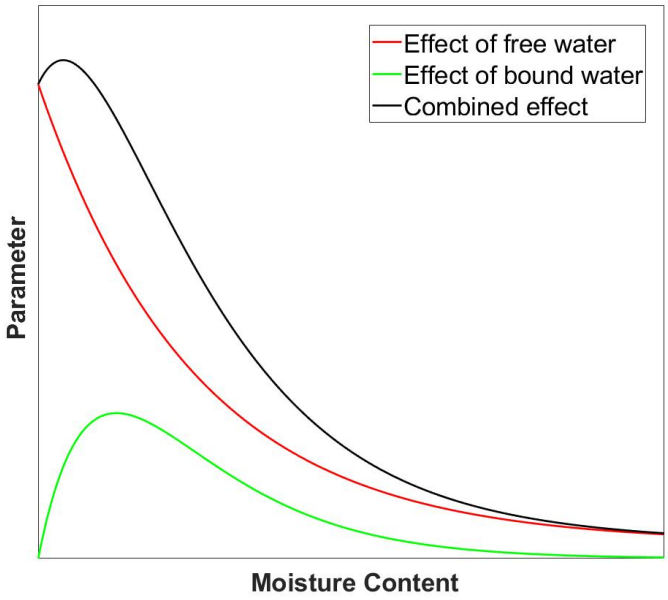

Figure 2.3: Illustration of the effects of free and bridging water on the Burgers model parameters (E_1, E_2, μ_1, μ_2)

2.2.3 Anti-plasticization caused by bridging water

Some of the water molecules that diffuse into the polymer network do not form clusters with other water molecules. Instead, they become immobilized due to their interactions with the polymer chains [35–37], and hence are referred to as bound water [36]. For example, the hydrogen and oxygen atoms on a water molecule can form hydrogen bonds with polar groups on the polymer chains [40, 92, 93]. Through the hydrogen bonds, water molecules can establish bridge-like links between the polymer chains shown in Figure 2.2b and restrain these chains' relative motions. This phenomenon, referred to as the water-bridge-anti-plasticization (WBAP) effect, has been found in microcrystalline cellulose by Hancock et al. [94], as well as in Nylon 6 by Inoue and Hoshino [38]. In both works it was reported that the decreasing rate of Young's modulus with respect to C is smaller at low C_e.

The WBAP effect caused by water bridges shown in Figure 2.2b slows down the plasticization caused by water clusters shown in Figure 2.2a and provides a stiffening mechanism. To capture this effect, we propose to add a single term to the Reimschuessel model given by Equations 2.7 and 2.8. At low C_e, the bridges formed by bridging water molecules in Figure 2.2b act as weak cross-links between polymer chains and occupy some of the free volume. As a result, the chain mobility is restrained, and the Burgers model parameters are expected to increase with C_e. Higuchi and Iijima [90] discovered that when the amount of water that diffuses into the polymer network is small, the majority of the water molecules are bridging water and forming bridges between the polymer chains. Consequently, the number of water bridges and hence the term describing the WBAP effect are approximated to be linear in C_e for small C_e. As C_e increases, the probability of forming water clusters becomes larger, which increases the inter-chain distance and can break the existing water bridges, weakening the anti-plasticization [95]. Therefore, the stiffening mechanism will eventually decrease, reaching a constant value at high moisture content. The effect of bridging water can be qualitatively illustrated by the green curve in Figure 2.3. Based on these physical considerations, the WBAP effect is captured by introducing a term, varying non-monotonically with C_e, to each elastic (E_i) and viscous (μ_i) parameter:

$$\begin{aligned} E_{i-WBAP} &= (k_{AEi}C_e)\exp(k_{DEi}C_e) \\ \mu_{i-WBAP} &= (k_{A\mu i}C_e)\exp(k_{D\mu i}C_e) \end{aligned} \tag{2.9}$$

In Equation 2.9 k_{AEi} and $k_{A\mu i}$ are coefficients that describe the approximately linear relation at small C_e, whereas k_{DEi} and $k_{D\mu i}$ describe the exponential decay that occurs at larger C_e. All these parameters are positive constants for a given material under isothermal condition. Equation 2.9 predicts, for each parameter, an increasing branch at low C_e, a skewed peak at intermediate C_e, and a decreasing branch at large C_e. It is recognized that the term associated with the WBAP effect does not necessarily decay to zero at high C_e. However, any residual contribution from the WBAP effect can be captured by the limiting values, E_{is} and μ_{is} in Equations 2.7 and 2.8, when the

plasticization and WBAP effects are combined. Therefore, to minimize the number of parameters in the model, no additional constants are introduced in Equation 2.9. Performing Taylor series expansion on Equation 2.9, near $C_e = 0$, Equation 2.9 is reduced to $E_{i-WBAP} = k_{AEi}C + O(C^2)$ and $\mu_{i-WBAP} = k_{A\mu i}C + O(C^2)$, which captures the anticipated linear variation of the moduli with respect to C_e at small C_e. At large C_e, Equation 2.9 is dominated by the exponential decay, representing the diminishing of anti-plasticization as water bridges break. The exponential decay is a characteristic of first-order kinetics, used in many empirical models such as the original Reimschuessel model. Compared with the polynomial form suggested by Maksimov et al. [41] and Widiastuti et al. [23], Equation 2.9 proposed here is simple (containing only a single term instead of a series), has stronger physical interpretations (linear increase for small C_e and exponential decay for large C_e), and can be readily integrated into the existing Reimschuessel model which possesses terms in similar forms.

2.2.4 Modified Burgers-Reimschuessel model

Combining the formulations in sections 2.2.2 and 2.2.3, the change of any of the model parameters P (E_1, E_2, μ_1 or μ_2) with respect to moisture content under isothermal condition can be described by the modified Burgers-Reimschuessel model below:

$$P(C_e) = P_s + (P_0 - P_s)\exp(-k_pC_e) + (k_AC_e)\exp(-k_DC_e) \tag{2.10}$$

where $P(C_e)$ is the value of the parameter as a function of C_e; P_0 corresponds to the dry polymer; P_s is the limiting value at large C_e; k_p is a positive constant that describes the exponential decay due to plasticization; and k_A and k_D are positive constants that describes the WBAP effect. The overall trend of $P(C)$ is illustrated by the black curve in Figure 2.3.

With Equation 2.10 and the constitutive relation given in Equation 2.4, the viscoelastic behavior of the polymer under different loading and moisture conditions

can be predicted. Two quantities of general interest are the creep compliance $J(t)$ and the stress relaxation modulus $G(t)$, which can be respectively extracted from creep and stress relaxation tests. Similar to the original Reimschuessel model used for the Young's modulus extracted from tensile tests, it is assumed that the creep and relaxation tests were either much faster than moisture diffusion or performed under well controlled humidity condition. As such, the moisture can be considered uniformly distributed within the sample during the tests, and spatial variations of the creep compliance or stress relaxation modulus are neglected. In a creep test, an instantaneous stress σ_0 is applied at $t = 0$ and the strain ε is measured with respect to time. The creep compliance is given by $J(t) = \varepsilon(t)/\sigma_0$, and for the Burgers model it is given by Equation 2.11 [91].

$$J(t) = \frac{t}{\mu_2} + \frac{1}{E_2} + \frac{1}{E_1}\left[1 - \exp\left(-\frac{E_1}{\mu_1}t\right)\right], \qquad t \geq 0 \tag{2.11}$$

In a stress relaxation test, an instantaneous strain ε_0 is applied at $t = 0$ and the stress σ is measured with respect to time. The stress relaxation modulus is given by $G(t) = \sigma(t)/\varepsilon_0$, which for the Burgers model is given by Equation 2.12 [91].

$$G(t) = \frac{1}{\sqrt{p_1^2 - 4p_2}}[(q_1 - q_2 r_1)\exp(-r_1 t) - (q_1 - q_2 r_2)\exp(-r_2 t)], \qquad t \geq 0 \tag{2.12}$$

where

$$\begin{aligned} p_1 &= \frac{\mu_1}{E_1} + \frac{\mu_2}{E_1} + \frac{\mu_2}{E_2} \\ p_2 &= \frac{\mu_1 \mu_2}{E_1 E_2} \\ q_1 &= \mu_2 \\ q_2 &= \frac{\mu_1 \mu_2}{E_1} \\ r_1 &= \frac{p_1 - \sqrt{p_1^2 - 4p_2}}{2p_2} \\ r_2 &= \frac{p_1 + \sqrt{p_1^2 - 4p_2}}{2p_2} \end{aligned} \tag{2.13}$$

2.3 Validation and Discussion

The above modified Burgers-Reimschuessel model is validated against the data obtained by Onogi et al. [26] In their work, four different types of materials were used, namely PVA with DP 600, PVA with DP 2060, original Nylon 6 and heat-treated Nylon 6. PVA films were fabricated by solvent casting and Nylon 6 films were fabricated by inflation method. Some of the Nylon 6 samples were heat-treated for 8 min under 150-155 °C, leading to increased crystallinity and slightly decreased molecular weight. All samples were conditioned under constant temperature (20 °C for PVA with DP 600; 25 °C for PVA with DP 2060, original Nylon 6 and heat-treated Nylon 6) in chambers with different relative humidity until an equilibrium moisture content was reached. The conditioning chambers were produced by using various saturated salt solutions in a vessel at the bottom of the chambers. To maintain the moisture content during stress relaxation tests, a glass cell with saturated salt solutions were used on a table model of Instron Tensile Tester. The stress relaxation test was conducted on each sample in the same chamber where it was conditioned, so that the moisture content in the sample stayed uniform and at the equilibrium level during the test. Stress relaxation modulus as a function of time was plotted with respect to time for different moisture content.

Since the constitutive relations for the tested polymers were not provided in Onogi et al. [26], the stress relaxation modulus was fitted using Equation 2.12 to extract the elastic (E_1 and E_2) and viscous (μ_1 and μ_2) parameters under different C_e. Then Equation 2.10 was used to extract P_0, P_s, k_p, k_A and k_D in the modified Burgers-Reimschuessel model. Table 2.1 lists the values of these parameters and the adjusted R^2 for the fittings. All the adjusted R^2 values are greater than 0.98, suggesting the good quality of the fit. P_0 for the dry polymers are of similar magnitude to what was reported for PVA [96] and Nylon 6 [97], confirming that the results were physically reasonable. As expected, the limiting values P_s for all polymers are either

0 or significantly lower than the corresponding P_0 values, indicating the dominance of the plasticization effect at large C_e. The magnitude of coefficients k_A emphasize the significance of the anti-plasticization effect at small C_e. As an example, the fitting of E_2 using both Reimschuessel model and the modified Reimschuessel model proposed in this work is shown in Figure 2.4 for heat-treated Nylon 6 and PVA with DP 2060. Consistent with what was reported, the original Reimschuessel model underestimated the values at lower C_e, which was corrected by the modified Reimschuessel model.

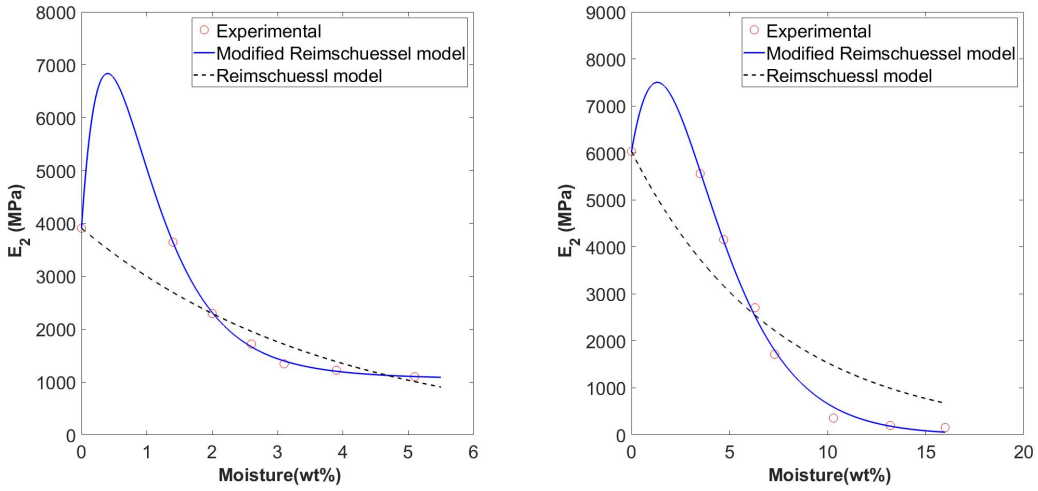

(a) (b)

Figure 2.4: Comparison between Reimschuessel's model in [22] and the modified Reimschuessel model proposed in this work for (a) E_2 of heat-treated Nylon 6, (b) E_2 of PVA with DP 2060.

Table 2.1: Fitted modified Reimschuessel model parameters for Onogi et al.[26]'s data and quality of fitting

	P_0 (unit)	P_s (unit)	k_p (1/wt%)	k_A (unit/wt%)	k_D (1/wt%)	Adjusted R^2
PVA with DP 600						
E_1 (MPa)	20637	422.3	0.7191	37720	0.7177	0.98949
E_2 (MPa)	5590	61.48	0.9989	10100	0.4987	
μ_1 ($\times 10^6$ MPa·s)	1.819	0	0.97920	8.981	0.9880	
μ_2 ($\times 10^6$ MPa·s)	127.6	2.857	0.8134	497.1	0.9519	
PVA with DP 2060						
E_1 (MPa)	25679	414.5	7.076	367300	1.087	0.99737
E_2 (MPa)	6030	0	1.001	8462	0.4848	
μ_1 ($\times 10^6$ MPa·s)	4.018	0	0.9663	17.92	0.9901	
μ_2 ($\times 10^6$ MPa·s)	225.4	1.456	0.6437	1453	1.059	
Original Nylon 6						
E_1 (MPa)	47311	0	1.797	3665	0.1821	0.99234
E_2 (MPa)	4233	617.5	0.3613	1029	15.76	
μ_1 ($\times 10^6$ MPa·s)	5.466	0.2258	2.504	0.09683	21.26	
μ_2 ($\times 10^6$ MPa·s)	310.3	0	9.961	44.42	0.2412	
Heat-treated Nylon 6						
E_1 (MPa)	153890	5792	4.063	7501000	4.578	0.99225
E_2 (MPa)	3910	1055	0.8116	21110	2.052	
μ_1 ($\times 10^6$ MPa·s)	107.25	0	2.227	0.06016	0	
μ_2 ($\times 10^6$ MPa·s)	514.05	0	1.042	29.59	0.1902	

Parameters in Table 2.1 were used to generate the time-dependent stress relaxation modulus predicted by the modified Burgers-Reimschuessel model. Figure 2.5 shows the comparisons between the model and experimental results. Unlike the TMS principle adopted by Onogi et al. [26], which failed to predict the behavior of PVA at low moisture content, all the model predictions in Figure 2.5 are accurate which demon-

strates the capability of the model to capture the change of viscoelastic properties with moisture content. The only exception is heat-treated Nylon 6 under 2.0 wt% moisture, for which a discrepancy of 17% was observed between the model prediction and experimental results. However, this discrepancy is still smaller than the model proposed by Widiastuti et al., which is more than 25% [23]. The discrepancy found in this particular case (heat-treated Nylon 6 containing 2.0 wt% moisture) arises from the relatively poor fitting of μ_2 (Figure 2.6). Since this deviation was not observed in other types of polymers, there is a high probability that the deviation is caused by the heat treatment. According to Onogi et al., the heat treatment of Nylon 6 films was conducted at 150-155°C for 8 min [26]. The treatment might have induced imperfect crystallites [98, 99], which could have allowed water molecules to penetrate into them and affect the viscoelasticity of the material in a different way. In addition, the cooling process after the heat treatment was not reported in Onogi et al. [26] which, if not well controlled, could have induced residual stresses in the samples. The diffusion of water molecules might release the residual stress and change the conformation of the polymer chains. These potential factors are not considered in the modified Burgers-Reimschuessel model.

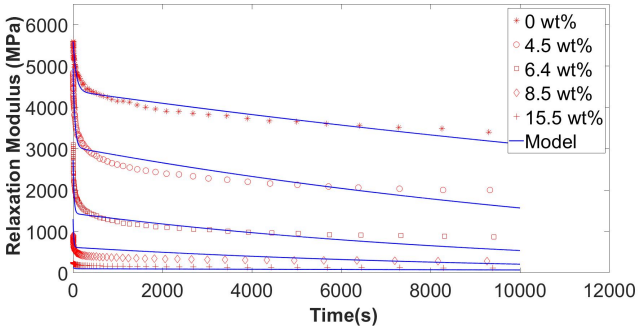

(a)

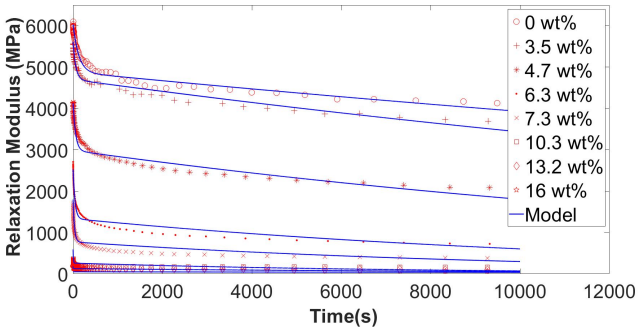

(b)

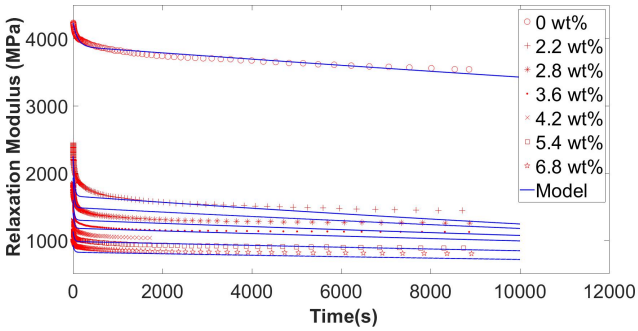

(c)

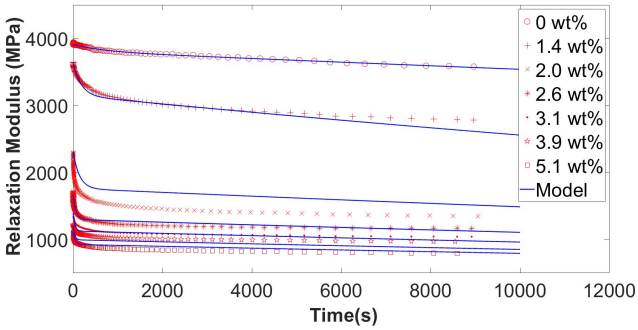

(d)

Figure 2.5: Stress relaxation modulus with different moisture content for (a) PVA with DP 600, (b) PVA with DP 2060, (c) Original Nylon 6, (d) Heat-treated Nylon 6. Red symbols represent experimental data from Onogi et al. [26] and blue solid curves are predictions using the proposed modified Burgers-Reimschuessel model.

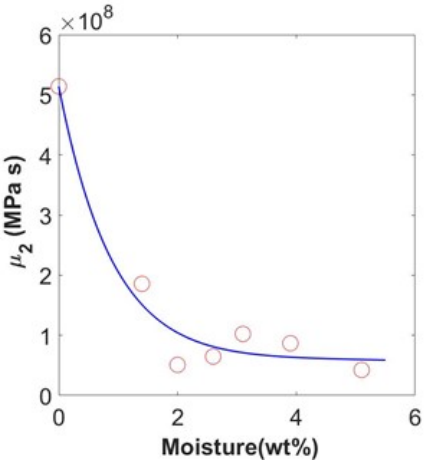

Figure 2.6: Change of μ_2 with respect to moisture for heat-treated Nylon 6. Red circles represent values obtained from fitting the Burgers model to stress relaxation data, and blue solid curve is prediction using the proposed modified Burgers-Reimschuessel model.

Compared with other models reviewed in the Introduction, the greatest advantage of the modified Burgers-Reimschuessel model is its simplicity. The WBAP effect is included by a simple modification as given in Equation 2.9, and all the Burgers model parameters have the same form as shown in Equation 2.10. Wide applicability of this model presents another advantage. In contrast to the TMS principle coupled with the WLF function, whose success has been limited to few polymers such as Nylon 6, the current model can be applied to a variety of hydrophilic polymers.

Hydrophilic polymers have been widely used in a broad range of engineering applications that may be subject to humid or aqueous environment. For example, PVA is a hydrophilic polymer that has a well-documented history to be used as load-bearing components in tissue engineering scaffolds [100], surgical thread [101], and vascular stents [102]. PVA have been reported to show deteriorations in mechanical properties as moisture content increases, which could affect the performance of these products [26, 40]. With the modified Burgers-Reimschuessel model, the performance and service life for these polymer products under given working condition can be estimated. Since the model establishes a relation between the moisture content and the viscoelas-

tic parameters, if the moisture content of a polymer product can be determined as a function of time, the material parameters can be predicted after exposure to the ambient environment for a period of time. Taking the data of PVA with DP 600 as an example, Figure 2.7 shows the prediction of the Burgers model parameters normalized by the respective values of the dry counterpart. The intersects between the blue curves and the black horizontal lines correspond to moisture content at which the Burgers model parameters reduce to 20% of their original values. If 80% of reduction is a critical level at which the polymer product can no longer support its designed load, then one can conclude that the service life of this PVA product is at the time when the moisture content of the product reaches around 5 wt%, which can be estimated from the rate of diffusion of water in PVA.

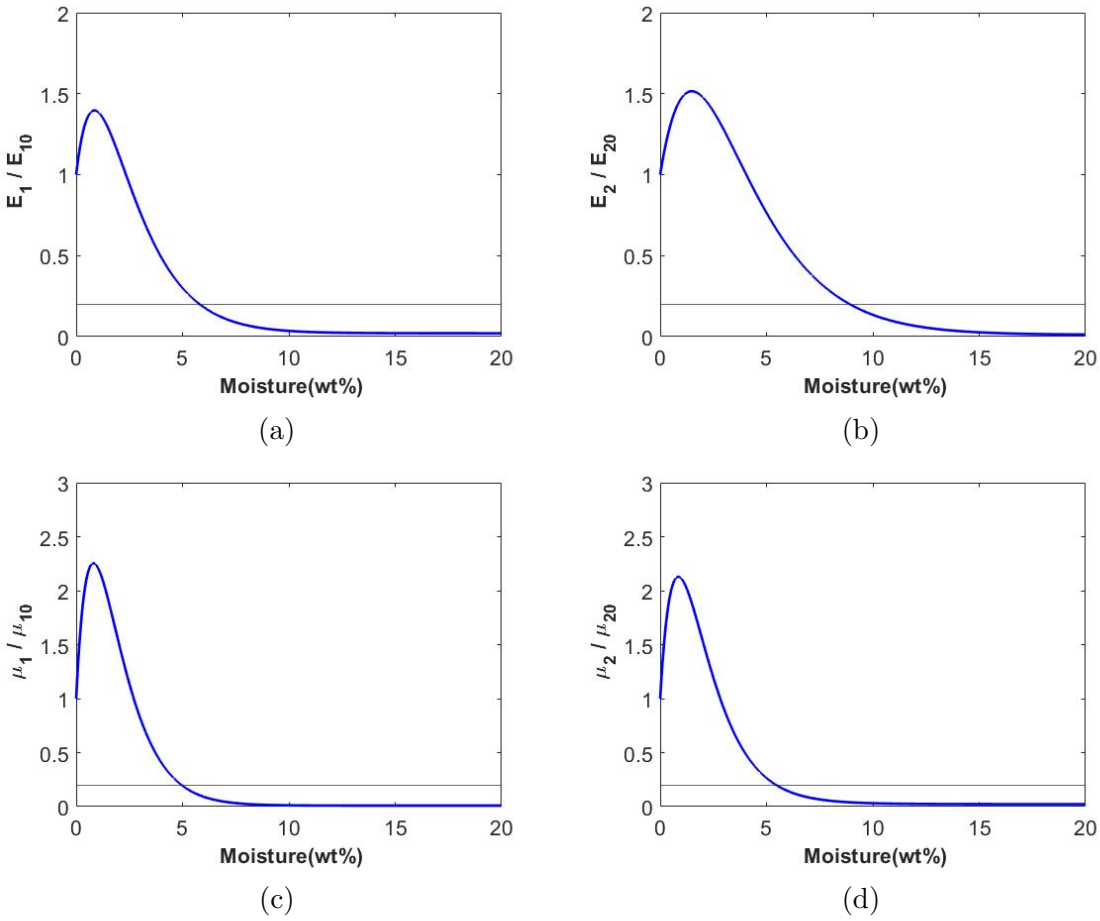

Figure 2.7: Prediction of the Burgers model parameters of PVA with DP 600, normalized by the respective values of the dry PVA (a) E_1/E_{10}, (b) E_2/E_{20}, (c) μ_1/μ_{10}, (d)μ_2/μ_{20}

This study may also provide guidance on how to manufacture polymer products to reduce the effect of moisture. The most apparent approach is to increase the limiting values P_s, which can be achieved by creating more entanglements between the polymer chains during synthesis and manufacturing, by increasing the crystallinity of the material with added nucleating agents, by properly selecting the processing parameters, or by using manufacturing techniques such as injection molding instead of extrusion so that the polymer chains are in a more compacted structure. Compacting the polymer network has another advantage, namely it increases the anti-plasticization effect. More closely compacted polymer chains have their polar groups located closer to each

other. Thus, it is potentially easier for water molecules to find anchor points to form bridges. The probability that water molecules gather together to form clusters and cause plasticization is also decreased.

In industry, mechanical properties of some intrinsically brittle materials such as polyvinyl chloride (PVC) and PLA are tailored by adding compatible plasticizers, which reduce the hardness and stiffness of the polymers by increasing the intermolecular distance and decreasing the amount of secondary bonds such as hydrogen bonds and van der Waals forces [83, 103, 104]. Li et al. [103] discovered that less than 10 wt% of polyethylene glycol (PEG) with molecular weight of 400 g/mol could significantly reduce the stiffness of PLA. On the other hand, Gedde [34] pointed out the presence of anti-plasticization effect for a variety of polymers and plasticizers which was caused by interaction between the low molecular weight plasticizers and the polymer chains. A similarity can be recognized between the role of these small plasticizers and that of moisture. Therefore, the model proposed here may be able to describe the effect of plasticizers, with the moisture content C_e replaced by the weight percentage of the plasticizers.

It is worth pointing out a few limitations of this model and future perspectives. First, the model is based on the isothermal assumption, and validated against experiments performed under a constant temperature. The effect of temperature on the constitutive relation of the polymers is not included. In practical applications, especially in outdoor environments, both temperature (T) and C_e can influence the viscoelastic properties of polymers and their effects are often coupled. Huber et al. [19] pointed out that the increase of T could increase the vibration of water molecules, which might further increase the free volume within the polymer network and lead to increased plasticization. Baschek et al. [105] reported that at T below 0°C, water within the polymer network could provide a reinforcing effect since the free water was frozen. Future work can be done to describe the coupled effect of T and C_e, by introducing T-dependent parameters $k_p(T)$, $k_A(T)$, etc., and/or adding terms as

functions of both T and C_e to Equation 2.10.

The model presented here is empirical in nature, i.e., it is developed based on phenomenological description of the influence from free and bridging water. Macroscopically, the model captures the anticipated behaviors at small and large moisture contents and supports indirect experimental evidence for anti-plasticization. However, there are microscopic phenomena which are not considered by the model, for example, the release of residual stress during moisture diffusion, or the penetration of water molecules into imperfect crystallites. Future work can be done to study the effects of these microscopic phenomena and provide modifications to the model. The empirical nature of the model also implies that values of the parameters in Equation 2.10 need to be acquired by fitting experimental data. Efforts can be devoted to study the correlation between these parameters and the intrinsic and extrinsic properties of polymers such as the molecular weight, free volume, and density of polar functional groups on the polymer chains. Such correlation can benefit the design and synthesis of the polymers to achieve desired performance.

Finally, this work revealed the possibility that a small amount of moisture may be able to stiffen the material. Both shown in Figure 2.7 and Figure 2.4, when the moisture content is less than 1 wt%, all four Burgers model parameters are larger compared with the dry material. Theoretically, this stiffening effect is possible due to the more likelihood of water molecules to form bridges rather than clusters when their concentration is low. While the lack of data in the low moisture regime (Figure 2.4 and Figure 2.5) in Onogi et al. [26] does not provide direct evidence, future testing in this regime may generate insights into this potential transient stiffening.

2.4 Conclusion

A modified Burgers-Reimschuessel model was proposed to describe the viscoelasticity of moisture-sensitive polymers. Plasticization caused by free water and anti-plasticization induced by bridging water were both considered. The proposed model

was validated against the data from Onogi et al. [26] for four different polymers, which demonstrated good accuracy. Due to the anti-plasticization effect, properties of moisture-sensitive polymers may be tailored by a small amount of moisture, or equivalently, a small amount of low molecular weight plasticizers. The model can be used to evaluate the performance and estimate the service life of products made from moisture-sensitive polymers. It can also be used to assist in the design and manufacturing of these polymers.

References

[7] M. T. Shaw and W. J. MacKnight, *Introduction to Polymer Viscoelasticity*, 3rd ed. John Wiley and Sons, Inc., 2005, p. 327.

[18] R. A. Jurf and J. R. Vinson, "Effect of moisture on the static and viscoelastic shear properties of epoxy adhesives," *Journal of Materials Science*, vol. 20, pp. 2979–2989, 8 1985, ISSN: 00222461. DOI: 10.1007/BF00553063.

[19] F. Huber, H. Etschmaier, H. Walter, G. Urstöger, and P. Hadley, "A time temperature moisture concentration superposition principle that describes the relaxation behavior of epoxide molding compounds for microelectronics packaging," *International Journal of Polymer Analysis and Characterization*, vol. 25, pp. 467–478, 6 2020, ISSN: 15635341. [Online]. Available: https://doi.org/10.1080/1023666X.2020.1807680.

[20] S. Schmid, S. Kühne, and C. Hierold, "Influence of air humidity on polymeric microresonators," *Journal of Micromechanics and Microengineering*, vol. 19, 6 2009.

[21] M. B. Satterfiield and J. B. Benziger, "Viscoelastic properties of nafion at elevated temperature and humidity," *Journal of Polymer Science Part B: Polymer Physics*, vol. 47, pp. 11–24, 2009. [Online]. Available: http://arxiv.org/abs/cond-mat/0406218%0Ahttp://dx.doi.org/10.1002/polb.

[22] H. K. Reimschuessel, "Relationships on the effect of water on glass transition temperature and young's modulus of nylon 6," *Journal of Polymer Science Part A: Polymer Chemistry*, vol. 16, pp. 1229–1236, 6 1978.

[23] I. Widiastuti, I. Sbarski, and S. H. Masood, "Mechanical behavior of a fluid-sensitive material during liquid diffusion," *Mechanics of Time-Dependent Materials*, vol. 18, pp. 387–406, 2 2014, ISSN: 13852000. DOI: 10.1007/s11043-014-9233-9.

[24] I. Widiastuti, I. Sbarski, and S. H. Masood, "Mechanical response of poly(lactic acid)-based packaging under liquid exposure," *Journal of Applied Polymer Science*, vol. 131, pp. 1–10, 16 2014.

[26] S. Onogi, K. Sasaguri, T. Adachi, and S. Ogihara, "Time–humidity superposition in some crystalline polymers," *Journal of Polymer Science*, vol. 58, pp. 1–17, 166 1962.

[27] H. Fujita and A. Kishimoto, "Diffusion-controlled stress relaxation in polymers. iii. stress relaxation in a swelling polymer," *Journal of Polymer Science*, vol. 28, pp. 569–585, 118 1958.

[28] I. Emri and V. Pavsek, "On the influence of moisture on the mechanical properties of polymers," *Materials Forum*, vol. 16, pp. 123–131, 2 1992.

[33] P. Gilormini and J. Verdu, "On the role of hydrogen bonding on water absorption in polymers," *Polymer*, vol. 142, pp. 164–169, 2018. DOI: 10.1016/j.polymer.2018.03.033. [Online]. Available: https://hal.archives-ouvertes.fr/hal-01743020.

[34] U. W. Gedde, *Polymer Physics*. Springer, 1999, p. 301.

[35] R. M. Hodge, T. J. Bastow, G. H. Edward, G. P. Simon, and A. J. Hill, "Free volume and the mechanism of plasticization in water-swollen poly(vinyl alcohol)," *Macromolecules*, vol. 29, pp. 8137–8143, 25 1996, ISSN: 00249297. DOI: 10.1021/ma951073j.

[36] X. Fan, "Mechanics of moisture for polymers: Fundamental concepts and model study," 2008.

[37] R. M. Hodge, G. H. Edward, and G. P. Simon, "Water absorption and states of water in semicrystalline poly(vinyl alcohol) films," *Polymer*, vol. 37, pp. 1371–1376, 8 1996, ISSN: 00323861. DOI: 10.1016/0032-3861(96)81134-7.

[38] K. Inoue and S. Hoshino, "Swelling of nylon 6 film due to water sorption.," *Journal of Polymer Science Part B: Polymer Physics*, vol. 14, pp. 1513–1526, 8 1976, ISSN: 00981273. DOI: 10.1002/pol.1976.180140812.

[39] K. M. Zakir, A. J. Parsons, C. D. Rudd, I. Ahmed, and W. Thielemans, "Mechanical , crystallisation and moisture absorption properties of melt drawn polylactic acid fibres," *European Polymer Journal*, vol. 53, pp. 270–281, 2014, ISSN: 0014-3057. DOI: 10.1016/j.eurpolymj.2014.02.001. [Online]. Available: http://dx.doi.org/10.1016/j.eurpolymj.2014.02.001.

[40] A. Ishisaka and M. Kawagoe, "Examination of the time-water content superposition on the dynamic viscoelasticity of moistened polyamide 6 and epoxy," *Journal of Applied Polymer Science*, vol. 93, pp. 560–567, 2 2004.

[41] R. D. Maksimov, E. A. Sokolov, and V. P. Mochalov, "Effect of temperature and moisture on the creep of polymeric materials 1. one-dimensional extension under stationary temperature-moisture conditions," *Mechanics of Composite Materials*, vol. 11, pp. 334–339, 3 1975.

[42] I. T. Garces, S. Aslanzadeh, Y. Boluk, and C. Ayranci, "Effect of moisture on shape memory polyurethane polymers for extrusion-based additive manufacturing," *Materials*, vol. 12, 2 2019, ISSN: 19961944.

[74] C. Hall, *Polymer Materials, An Introduction for Technologists and Scientists*, 1st ed. The MacMillan Press Ltd., 1981, p. 208.

[75] S. M. Zhou and K. Tashiro, "Confirmation of universality of time-humidity superposition principle for various water-absorbable polymers through dynamic viscoelastic measurements under controlled conditions of relative humidity and temperature," *Journal of Polymer Science Part B: Polymer Physics*, vol. 39, pp. 1638–1650, 14 2001.

[76] P. Myllytie, L. Salmén, E. Haimi, and J. Laine, "Viscoelasticity and water plasticization of polymer-cellulose composite films and paper sheets," *Cellulose*, vol. 17, pp. 375–385, 2 2010, ISSN: 09690239. DOI: 10.1007/s10570-009-9376-z.

[77] O. Starkova and A. Aniskevich, "Limits of linear viscoelastic behavior of polymers," *Mechanics of Time-Dependent Materials*, vol. 11, pp. 111–126, 2 2007.

[78] E. M. Woo, "Moisture-temperature equivalency in creep analysis of a heterogeneous-matrix carbon fibre/epoxy composite," *Composites*, vol. 25, pp. 425–430, 6 1994, ISSN: 00104361. DOI: 10.1016/0010-4361(94)90098-1.

[79] K. Aniskevich, R. Krastev, and Y. Hristova, "Effect of long-term exposure to water on the viscoelastic properties of an epoxy-based composition," *Mechanics of Composite Materials*, vol. 45, pp. 137–144, 2 2009.

[80] X. J. Fan, S. W. Lee, and Q. Han, "Experimental investigations and model study of moisture behaviors in polymeric materials," *Microelectronics Reliability*, vol. 49, pp. 861–871, 8 2009.

[81] A. Valls-Lluch, W. Camacho, A. Ribes-Greus, and S. Karlsson, "Influence of water on the viscoelastic behavior of recycled nylon 6,6," *Journal of Applied Polymer Science*, vol. 85, pp. 2211–2218, 10 2002.

[82] F. Goldschmidt and S. Diebels, "Modelling and numerical investigations of the mechanical behavior of polyurethane under the influence of moisture," *Archive of Applied Mechanics*, vol. 85, pp. 1035–1042, 8 2015, ISSN: 14320681.

[83] W. D. Callister and D. G. Rethwisch, *Material Science and Engineering, An Introduction*, 8th ed. John Wiley and Sons, Inc., 2010, p. 1000.

[84] M. L. Williams, R. F. Landel, and J. D. Ferry, "The temperature dependence of relaxation mechanisms in amorphous polymers and other glass-forming liquids," *Journal of the American Chemical Society*, vol. 77, pp. 3701–3707, 14 1955.

[85] R. M. Christensen, *Theory of Viscoelasticity, An Introduction*, 2nd ed. Dover Publications Inc., 2003, p. 363.

[86] L. Sperling, *Introduction to Physical Polymer Science*. John Wiley and Sons, Inc, 2006.

[87] H. Ardebili, E. H. Wong, and M. Pecht, "Hygroscopic swelling and sorption characteristics of epoxy molding compounds used in electronic packaging," *IEEE Transactions on Components, Packaging and Manufacturing Technology*, vol. 26, pp. 206–214, 1 2003.

[88] Y. J. Chang, C. T. Chen, and A. V. Tobolsky, "Correlations between types of absorbed water molecules and water permeability in swollen polymer membranes," *Journal of Polymer Science Part B: Polymer Physics*, vol. 12, pp. 1–6, 1 1974.

[89] W.-I. Cha, S.-H. Hyon, and Y. Ikada, "Microstructure of poly(vinyl alcohol) hydrogels investigated with differential scanning calorimetry," *Die Makromolekulare Chemie*, vol. 194, pp. 2433–2441, 9 1993, ISSN: 0025-116X. DOI: 10.1002/macp.1993.021940902.

[90] A. Higuchi and T. Iijima, "D.s.c. investigation of the states of water in poly(vinyl alcohol) membranes," *Polymer*, vol. 26, pp. 1207–1211, 1985.

[91] W. N. Findley, *Creep and relaxation of nonlinear viscoelastic materials : with an introduction to linear viscoelasticity*, W. N. Findley, J. S. Lai, and K. Onaran, Eds. Dover Publications Inc., 1989, p. 380.

[92] B. Yang, W. M. Huang, C. Li, and L. Li, "Effects of moisture on the thermomechanical properties of a polyurethane shape memory polymer," *Polymer*, vol. 47, pp. 1348–1356, 4 2006, ISSN: 00323861. DOI: 10.1016/j.polymer.2005.12.051.

[93] M. Pannico and P. L. Manna, "Sorption of water vapor in poly (l-lactic acid): A time-resolved ftir spectroscopy investigation," *Frontiers in Chemistry*, vol. 7, pp. 1–10, April 2019. DOI: 10.3389/fchem.2019.00275.

[94] B. C. Hancock, S. D. Clas, and K. Christensen, "Micro-scale measurement of the mechanical properties of compressed pharmaceutical powders. 1: The elasticity and fracture behavior of microcrystalline cellulose," *International Journal of Pharmaceutics*, vol. 209, 2000. [Online]. Available: www.elsevier.com/locate/ijpharm.

[95] L. Mascia, Y. Kouparitsas, D. Nocita, and X. Bao, "Antiplasticization of polymer materials: Structural aspects and effects on mechanical and diffusion-controlled properties," *Polymers*, vol. 12, 4 Apr. 2020, ISSN: 20734360.

[96] N. Jain, A. Verma, and V. K. Singh, "Dynamic mechanical analysis and creep-recovery behaviour of polyvinyl alcohol based cross-linked biocomposite reinforced with basalt fiber," *Materials Research Express*, vol. 6, 10 2019.

[97] Y. Nakazato, S. Zhu, A. Usuki, and M. Kato, "Analysis and prediction of creep viscoelasticity in nylon 6 clay hybrid nanocomposites," *Journal of Solid Mechanics*, vol. 4, pp. 856–863, 6 2010.

[98] A. L. Simal and A. R. Martin, "Structure of heat-treated nylon 6 and 6.6 fibers. i. the shrinkage mechanism," *Journal of Applied Polymer Science*, vol. 68, 3 1998.

[99] L. A. D. G. Oriani and A. L. Simal, "Structure of heat-treated nylon 6 fibers. i. application of the arrhenius equation," *Journal of Polymer Science*, vol. 46, pp. 1973–1985, 11 1992, ISSN: 10974628. DOI: 10.1002/app.1992.070461110.

[100] M. Teodorescu, M. Bercea, and S. Morariu, "Biomaterials of pva and pvp in medical and pharmaceutical applications: Perspectives and challenges," *Biotechnology Advances*, vol. 37, pp. 109–131, 1 Jan. 2019, ISSN: 07349750. DOI: 10.1016/j.biotechadv.2018.11.008.

[101] T. Gaaz *et al.*, "Properties and applications of polyvinyl alcohol, halloysite nanotubes and their nanocomposites," *Molecules*, vol. 20, pp. 22 833–22 847, 12 Dec. 2015, ISSN: 14203049. DOI: 10.3390/molecules201219884.

[102] M. C. Lin, C. W. Lou, J. Y. Lin, T. A. Lin, Y. S. Chen, and J. H. Lin, "Biodegradable polyvinyl alcohol vascular stents: Structural model and mechanical and biological property evaluation," *Materials Science and Engineering: C*, vol. 91, pp. 404–413, Oct. 2018, ISSN: 09284931. DOI: 10.1016/j.msec.2018.05.030.

[103] D. Li *et al.*, "Preparation of plasticized poly (lactic acid) and its influence on the properties of composite materials," *PLoS ONE*, vol. 13, pp. 1–15, 3 2018, ISSN: 19326203. DOI: 10.1371/journal.pone.0193520.

[104] M. A. Rahman *et al.*, "Biocomposites based on lignin and plasticized poly (l -lactic acid)," *Journal of Applied Polymer Science*, pp. 202–214, 2013.

[105] G. Baschek, G. Hartwig, and F. Zahradnik, "Effect of water absorption in polymers at low and high temperatures," *Polymer*, vol. 40, pp. 3433–3441, 1999.

Chapter 3

Moisture-induced Anti-plasticization of Polylactic Acid: Experiments and Modeling

3.1 Introduction

Polylactic acid (PLA) is an environmental-friendly polymer derived from bio-renewable resources such as corn starch, potato and sugar cane [59]. According to a report produced by Grand View Research, the market size of PLA had a value of $525.47 million USD in 2020 and is expected to have an annual growth rate of 18.1% in the next 8 years [106]. The reason behind this large demand is the broad range of applications of PLA originating from the various advantages it offers. Firstly, PLA is biocompatible, in that, it is non-toxic, and does not cause immunological rejection when in contact with a living system [107]. Thus, PLA is a natural choice for biomedical applications such as cardiovascular stents or sutures [62]. Secondly, PLA has good melt-processability. Traditional melt-based thermoplastic processing technologies, such as extrusion, injection molding and compression molding, can be used for PLA based product manufacturing [59]. Perhaps, one of the most important advantages of PLA is its biodegradability. PLA can be degraded by first inducing hydrolysis reaction of its ester bonds, followed by exposure to moisture, oxygen and natural microorganisms which decompose it into water, carbon dioxide and a small amount of

other non-toxic substances [59, 62, 63]. All these advantages make PLA an ideal alternative to petroleum-based polymers that are conventionally used in thermoplastics industry [59]. PLA has already been commercially utilized in food packaging [108], bottles [109], biomedical devices [110] and products in textile, transport and agriculture industries [63].

The most important advantage of PLA also leads to a major challenge during its applications. The ester groups in the molecular structure of PLA can be hydrolyzed by water molecules even at room temperature, which eventually leads to the start of biodegradation [62]. Several studies reported that PLA has a water contact angle of around 75°, suggesting that PLA is hydrophilic in nature [43–46]. The polar ester groups contribute to the hydrophilicity of PLA, making it susceptible to moisture absorption throughout its service life [93]. It has been shown that moisture absorption can significantly affect the viscoelastic behavior of PLA [24, 110], which may result in potential catastrophic failure of PLA products such as biomedical scaffold in biomedical applications, fibers in textile industry and structural components in transportation industry [39, 63, 110]. Therefore, the effect of moisture on the viscoelastic properties of PLA should be carefully studied, documented and considered during the product design [39, 110].

A number of studies have assessed and outlined the mechanism of hydrolytic degradation of PLA [62, 63, 108, 110–115]. Various parameters that affect hydrolytic degradation, including temperature, humidity, pH, presences of infills, etc. have been reported [112, 115]. Holm et al. [108] and Niaounakis et al. [112] studied the effect of hydrolytic degradation on the tensile properties of PLA including Young's modulus, tensile strength and elongation at break. Both works reported that all three properties decreased with hydrolytic degradation. Singh et al. [110] modeled the viscoelastic constitutive relation of PLA under the influence of hydrolytic degradation. A nonlinear standard solid model proposed by Khan et al. [116] was used and the change of model parameters during degradation was provided [110]. The proposed

model was validated against tensile test results for PLA degraded for up to 150 days [110].

Prior to hydrolytic degradation, significant diffusion of moisture into the PLA has to occur first. Niaounakis et al. [112] found negligible degradation when PLA was placed under room temperature (20°C) and 80% relative humidity (RH) for 130 days. Similar conclusion was drawn by Siparsky et al. [117] from the observation that the time scale for hydrolytic degradation was four to six orders of magnitude larger than that of moisture diffusion. Schmitt et al. [118] reported that, similar to other hydrophilic polymers, the water molecules that diffused into the PLA also existed in two forms, free water and bound water. Free water means those water molecules that are not attached to the polymer chains and hence are able to move freely within the polymer network [36]. These molecules tend to form clusters, increasing the inter-chain distance and the free volume within the polymer network [27]. As a result, the molecular mobility of the polymer chains is enhanced, causing the material to be softened (i.e., plasticized). Bound water molecules are attached to the polymer chains through the formation of hydrogen bonds. Additionally, they can establish bridges between polymer chains and therefore restrain their molecular mobility [22, 37, 92]. This so-called water-bridge-anti-plasticization (WBAP) effect has been found indirectly in a variety of hydrophilic polymers [20, 22, 40, 72]. The two opposite effects, plasticization caused by free water and anti-plasticization caused by bridging water, were discussed and modeled in a recent work [72]. The model was validated against the experimental results of Onogi et al. [26] for four different hydrophilic polymers, namely, polyvinyl alcohol (PVA) with degree of polymerization (DP) 600, PVA with DP 2060, Nylon 6 and heat-treated Nylon 6.

Compared to the studies on hydrolytic degradation, the effect of diffused water molecules on the mechanical properties of PLA, before the onset of hydrolytic degradation, has been limited. Zakir et al. [39] conditioned melt-drawn PLA fibers in four different levels of RH (0%, 35%, 75% and 98%) for four weeks to obtain PLA fibers

with different moisture content. They discovered that both Young's modulus and tensile strength of PLA fibers only slightly decreased with increased moisture content [39]. Algarni et al. [119] conducted tensile tests on 3D-printed PLA samples. While the moisture content had little effect on the Young's modulus, the tensile strength slightly increased with moisture content which was in contrast to the results of Zakir et al. [39] In addition, Widiastuti et al. [23, 24] studied the viscoelastic properties of 10 wt% potato starch infilled PLA and proposed an empirical model, using polynomials and fractions, for how the viscoelastic parameters changed with moisture content. The error from the model prediction increased drastically (up to 25% discrepancy) when the moisture content increased from 2 wt% to 6 wt%. Therefore, to the best of our knowledge, the effect of diffused moisture on the viscoelastic behavior of PLA before hydrolytic degradation is poorly studied, and discrepancies remain among the existing literatures.

The objective of the present study is to fill the knowledge gap by proposing a methodology for comprehensive evaluation of the effect of diffused moisture on the viscoelastic constitutive relation of PLA, prior to hydrolytic degradation. We expect that the results can be applied to the design of PLA products for a variety of applications such as food packing, bio-medical devices, and structural components. In addition, the experimental methodology developed in this study can be applied to other hydrophilic polymers whose viscoelastic behavior is sensitive to moisture.

3.2 Methodology

3.2.1 Preparation of PLA fiber samples

PLA fibers were produced by melt-extrusion. PLA grade 4043D pellets were provided by NatureWorks LLC, USA, which has a number-average molecular weight (M_n) of 106,000 g/mol, polydispersity index of 1.6, and D-lactic acid content from 4.5 wt% to 5 wt% [120]. According to the manufacturer provided instructions, PLA pellets were

firstly dried under vacuum at 80°C for 8 hours (in a Lindberg/Blue M^{TM} vacuum oven - Thermo Fisher Scientific, USA). Then, a Brabender^{TM} single screw extruder attached to ATR Plasti-Corder drive system (C.W. Brabender Instruments, Inc., Germany), Filabot^{TM} FB00626 air path and Filabot^{TM} FB00073 filament spooler (Triex LLC, USA) were used for fiber production as shown in Figure 3.1. The dried PLA pellets were melted in the Brabender single screw extruder then pulled out of a circular die. Then the fibers were cooled with filabot air path, and finally winded with a filament spooler. The diameter of the nozzle of the single screw extruder was 3 mm. Based on manufacturer provided data, the temperature for heating zones 1 and 2 was set to 180°C while the temperature for heating zones 3 and 4 was set to 175°C. The extrusion speed was approximately 1.5 g/min. Fibers with 0.5 ± 0.02 mm diameter were produced. The control of the fiber diameter was achieved by adjusting both the spooler RPM and extruder RPM. Fiber diameter was chosen based on balancing the considerations of moisture conditioning (thick fibers require longer conditioning time) and creep tests (creep tests are difficult to conduct on thin fibers).

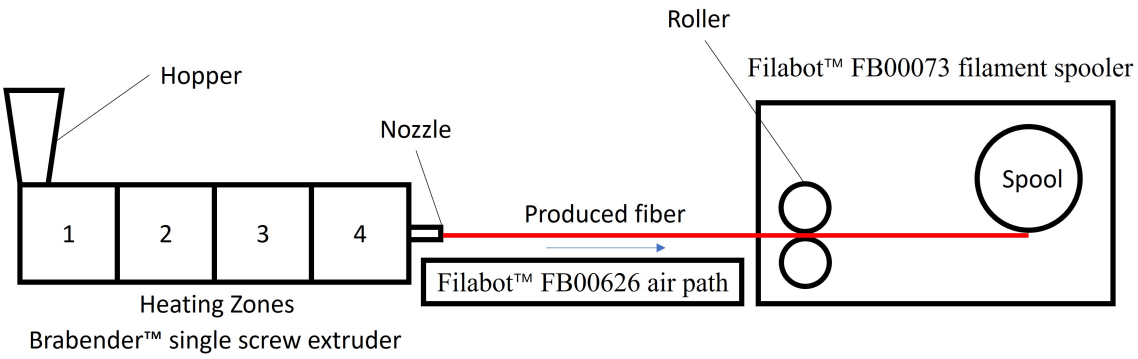

Figure 3.1: Schematic of the fiber extrusion process.

3.2.2 Sample conditioning and moisture absorption measurement

The produced PLA fibers were firstly placed in Lindberg/Blue M^{TM} vacuum oven at 60°C for 48 hours to release the moisture absorbed during extrusion. They were

then cut into approximately 80 mm in lengths for moisture absorption tests. The conditioning environments include chambers with different RH levels (33%, 75%, 98%) and immersion in distilled water, all at 20 °C. The different RH levels were achieved by placing saturated salt solutions ($MgCl_2 \cdot 6H_2O$ for 33%, NaCl for 75% and K_2SO_4 for 98%) within the conditioning chambers according to ASTM E104-20 [121]. Under each condition, moisture absorption was measured for seven identical samples using a scale with a precision of 0.1 mg. The samples were periodically removed from the conditioning chamber and weighed. Special attention was given during the removal of the samples from the chambers to minimize the impact of chamber environment due to the opening of the conditioning chambers.

The moisture content $C(t)$ at each measurement time t was calculated by the following equation [39, 108]

$$C(t) = \frac{m(t) - m(t=0)}{m(t=0)} \times 100\% \tag{3.1}$$

where $m(t)$ is the mass of the sample at time t, $m(t=0)$ is the weight of the dry sample. For a specific time t, statistics for $C(t)$ were collected from the seven identical samples and reported with average and standard deviation. The moisture absorption curves were reported as the moisture content C plotted against the square root of time ($\sqrt{t}$). Based on preliminary tests, the conditioning period was selected as 50 days since all the samples reached the saturation level, which is the equilibrium moisture content C_e, within that period. Assuming that the moisture diffusion in the PLA fibers follows Fick's law, the diffusivity D can be estimated by [39, 122, 123]:

$$D = \frac{\pi d^2}{16 C_e^2} \times k^2 \tag{3.2}$$

where d is the diameter of the fiber and k the slope of the initial linear portion of the moisture absorption curve (C with respect to $\sqrt{t}$).

3.2.3 Creep tests

After C_e is reached, tensile creep tests were conducted for 15 min to extract the creep compliance. To enhance the grip and minimize the stress concentration, at the two ends of the fiber, paper tabs shown in Figure 3.2 were used during the tensile creep tests according to ASTM D3822 [124]. Each fiber sample was glued by poly(ethylene-vinyl acetate) using a glue gun (Topelek, China), onto a paper tab with a gauge length of 40 mm as shown in Figure 3.2. All creep tests were conducted immediately after the fibers were taken from the conditioning chamber. During the tests, temperature was approximately 23°C and RH was around 20%. A universal tensile testing system (ElectroForce 3200 Series III, Bose Corporation, USA) equipped with a 10 N load cell and tensional clamp was used for all the creep tests.

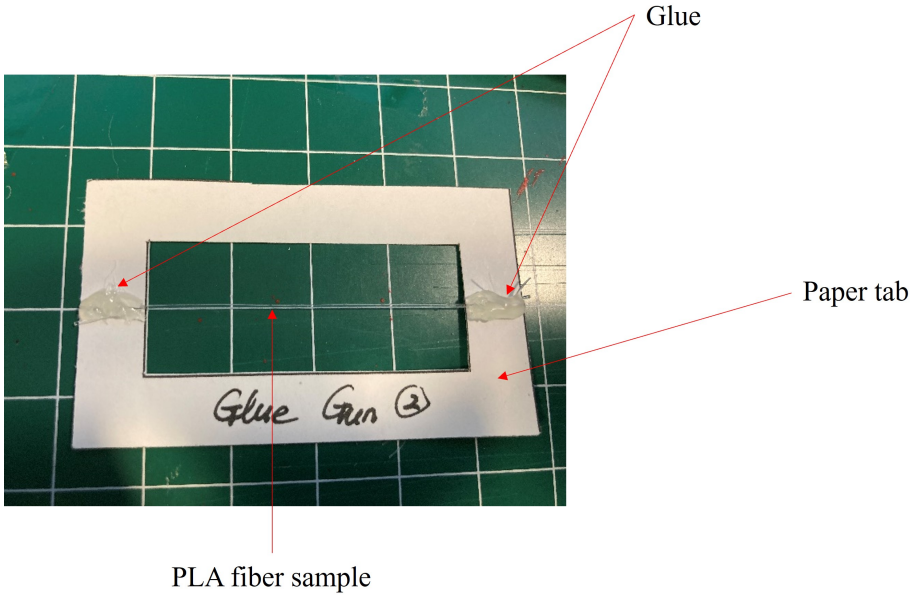

Figure 3.2: Mounting of the conditioned PLA fiber samples for tensile creep tests.

A series of creep tests were first conducted with different applied instantaneous stresses σ_0 in order to obtain the linear viscoelastic limits [77]. It was discovered that, regardless of C_e, the creep compliance did not change with σ_0 if $\sigma_0 \leq 8$ MPa. 8 MPa was therefore chosen as the applied stress for the remaining tests, so as to

limit the material to the linear viscoelastic regime. According to ASTM D2990 [125], the stress was programmed to be applied rapidly within 1 s. For each C_e, tests were performed on 5 replicas. The creep compliance was measured every 50 s during the test and the average values as well as the standard deviation over the 5 samples were reported.

3.2.4 Extracting moisture-dependent viscoelastic parameters

A modified Burgers-Reimschuessel model proposed in our previous work [72] was used to investigate the effect of diffused moisture on the viscoelastic properties of PLA. This model is briefly introduced here for the ease of access of the readers.

In this model, the constitutive relation of PLA is described by the Burgers model shown in Figure 3.3 [23, 126]. E_1 and E_2 are elastic parameters, μ_1 and μ_2 are viscous parameters, and $\varepsilon(t)$ and $\sigma(t)$ are time-dependent strain and stress, respectively. During a creep test, an instantaneous stress σ_0 is applied at time $t = 0$ and the strain response $\varepsilon(t)$ is measured. The creep compliance $J(t)$ is the ratio between $\varepsilon(t)$ and σ_0, which for the Burgers model is given by

$$J(t) = \frac{t}{\mu_2} + \frac{1}{E_2} + \frac{1}{E_1}\left[1 - \exp\left(-\frac{E_1}{\mu_1}t\right)\right], \qquad t \geq 0 \tag{3.3}$$

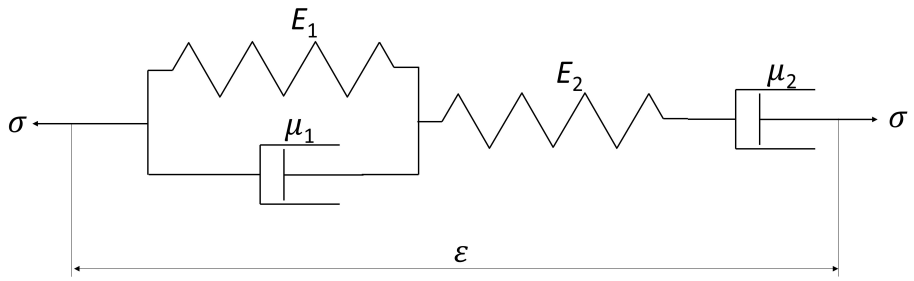

Figure 3.3: Schematic of Burgers model for viscoelasticity constitutive relation of the polymers

The effect of absorbed moisture is represented by the change of Burgers model parameters P (E_1, E_2, μ_1, or μ_2) with respect to C_e. The modified Burgers-Reimschuessel

model [72] proposed the following dependence of P on C_e

$$P(C_e) = P_s + (P_0 - P_s)\exp(-k_p C_e) + (k_A C_e)\exp(-k_D C_e) \tag{3.4}$$

where P_0 is value of the parameter for the dry polymer and P_s is the limiting value when C_e is large. k_p is a non-negative constant that describes the exponential decay due to the plasticization by free water; k_A and k_D are non-negative constants introduced to describe the WBAP effect by the last term in Equation 3.4. This term scales linearly with C_e when it is small, representing stiffening effect from water bridges, while decays at large C_e due to the breaking of water bridges caused by excessive water clusters.

3.3 Results and Discussion

3.3.1 Moisture absorption and diffusivity

The moisture absorption of the PLA fiber samples under different conditions are presented in Figure 3.4. The error bars are the standard deviation of the measurement by the 7 samples under the same condition. Under all conditions, rapid moisture uptake is observed within the first two weeks of conditioning, and the increasing trend is almost linear with $\sqrt{t}$. The rate of increase slows down after these two weeks, and the moisture content reaches the equilibrium values C_e after approximately 35 days. C_e increases with increasing RH level and samples immersed in distill-water has the maximum. These curves are typical Fickian absorption curves which describe the free diffusion of water molecules without other physical-chemical processes, such as hydrolytic degradation [36].

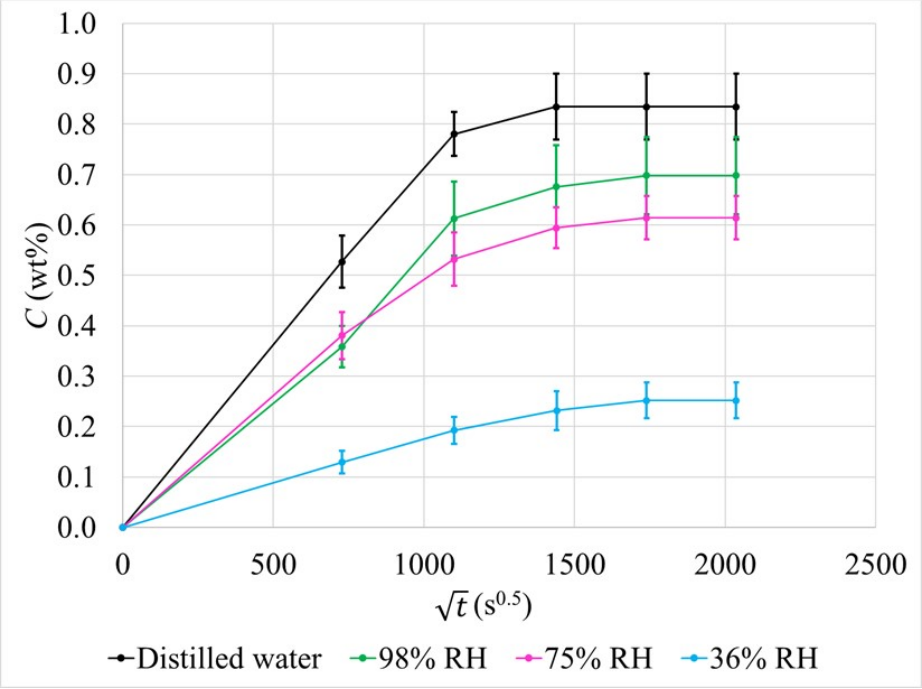

Figure 3.4: Moisture absorption of PLA fibers

Since the characteristics of diffusion follows the Fick's law, Equation 3.2 was used to calculate the diffusivity of water in PLA fibers [122]. The values of C_e and calculated diffusivity D are listed in Table 3.1. Due to the limited number of data points acquired in the initial linear part of the moisture absorption curves (Figure 3.4), the calculated diffusivity values vary slightly under different conditions. Also, the diffusivity is larger compared to the range reported by Zakir et al. [39], between 3.1×10^{-17} and 4.6×10^{-15} m^2/s. The difference might be attributed to the differences in manufacturing process, crystallinity, and grade of the PLA raw materials [127].

Table 3.1: Equilibrium moisture content and calculated diffusivity of PLA fibers

Condition	Equilibrium moisture content C_e (wt%)	Diffusivity D ($\times 10^{-14}$ m^2/s)
Distilled-water	0.835	3.59
98% RH	0.698	2.91
75% RH	0.614	3.20
36% RH	0.252	2.38
Average		**3.02**

3.3.2 Creep compliance

The creep compliances under different C_e are plotted in Figure 3.5, which exhibit the typical creep behavior of a semi-crystalline polymer [91]. The error bars are the standard deviation of the five replications. Equation 3.3 was used to fit the data in Figure 3.5, and the extracted Burgers model parameters are plotted against C_e in Figure 3.6 (red dots). Then, Equation 3.4 was used to fit the data in Figure 3.6 to capture the moisture dependence of Burgers model parameters. Due to the lack of data in the high C_e regime, the limiting values P_s were all assigned 0. The other parameters in Equation 3.4 obtained from the fitting and the adjusted R^2 values are shown in Table 3.2. P_0 of the four parameters are close to the results obtained by Widiastuti et al. [23], indicating that the fitting is physically reasonable. The initial increasing trend of P with respect to C_e confirmed the existence of the anti-plasticization effect. The results from the model fitting are presented by the blue curves in Figure 3.6, and the predictions of the creep compliance using parameters in Table 3.2 are shown in Figure 3.5 (solid curves). Clearly, the modified Burgers-Reimschuessel model [72] is able to predict the effect of absorbed moisture on the viscoelasticity of PLA.

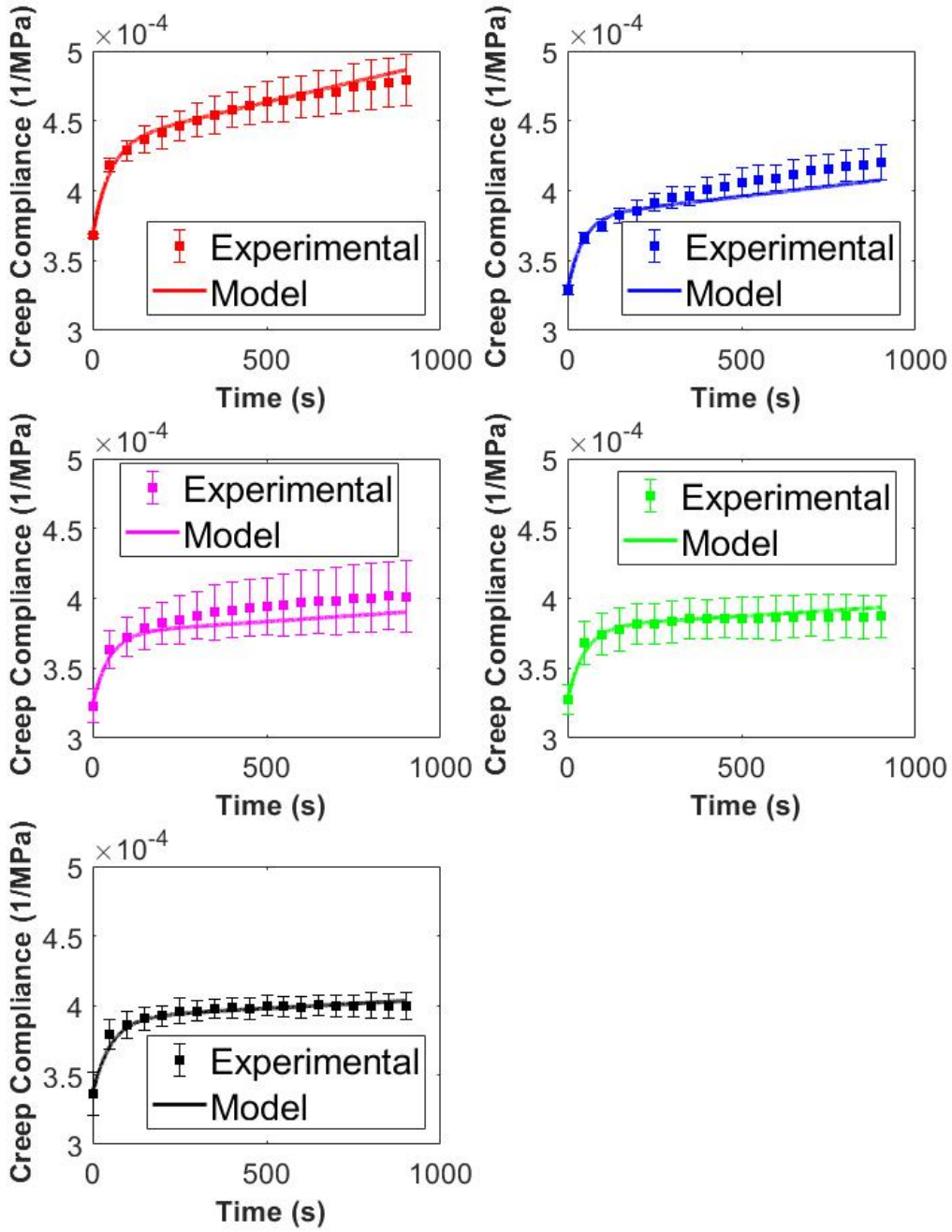

Figure 3.5: Creep compliance and modeling of PLA with different C_e: (a) dry samples; (b) samples conditioned in 36% RH, $C_e = 0.252$ wt%; (c) samples conditioned in 75% RH, $C_e = 0.614$ wt%; (d) samples conditioned in 98% RH, $C_e = 0.698$ wt%; (e) samples immersed in distilled water, $C_e = 0.835$ wt%.

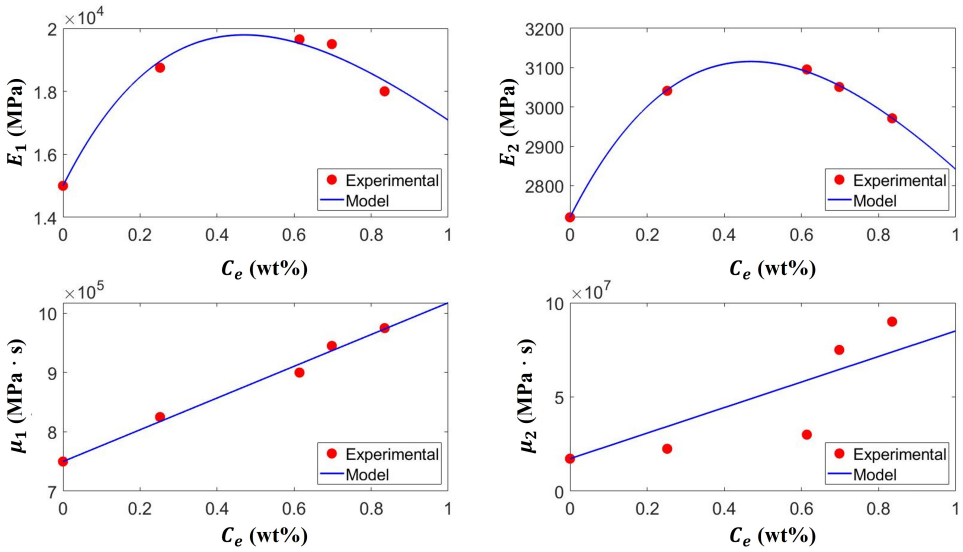

Figure 3.6: Change of Burgers model parameters with respect to C_e (red dots) as well as the fitting using the modified Burgers-Reimschuessel model (blue curves).

Table 3.2: Fitted modified Reimschuessel model parameters for PLA and quality of fitting

Parameter	P_0 (Unit)	P_s (Unit)	k_p (1/%)	k_A (Unit/%)	k_D (1/%)	Adjusted R^2
E_1 (MPa)	15000	0	1.214	42640	1.217	0.96014
E_2 (MPa)	2719.5	0	0.921	4449	0.928	0.99889
μ_1 (MPa·s)	7.5×10^5	0	0	2.677×10^5	0	0.99012
μ_2 (MPa·s)	1.725×10^7	0	0	6.782×10^7	0	0.69524

3.3.3 Discussion

As shown in Figure 3.5, the instantaneous elastic compliance (at $t = 0$) decreases from 3.7×10^{-4} MPa^{-1} to 3.3×10^{-4} MPa^{-1} when C_e increases from 0 to 0.252 wt%. In addition, with the increase of C_e, the creep compliance curves are more flattened in the last stage of the creep test. Both phenomena indicate that with more ab-

sorbed moisture the material is more resistive to external load, which can be explained by the WBAP effect [72]. Using Equation 3.4 and the parameters in Table 3.2, it can be calculated that for $C_e < 1$ wt%, the term that corresponds to plasticization $P_s + (P_0 - P_s)\exp(-k_p C_e)$ is significantly smaller than the anti-plasticization term $(k_A C_e)\exp(-k_D C_e)$. This further confirms that a significant portion of water molecules were forming water bridges which stiffened the material. The viscoelasticity of hydrophilic polymers with moisture content less than 1 wt% was never characterized in the literature. Onogi et al. [26] and Widiastuti et al. [23] only characterized viscoelasticity of PVA, Nylon 6 and 10 wt% potato starch reinforced PLA with moisture content more than 1.4 wt%. Thus, to the best of our knowledge, the anti-plasticization effect of water molecules on PLA was firstly characterized and modeled in this work.

Comparing Figure 3.5d and Figure 3.5e, the creep compliance of the samples immersed in distilled water is slightly higher than those conditioned under 98% RH, although C_e is higher for samples immersed in distilled water. The additional moisture in the samples immersed in distilled water did not stiffen the material, instead, it slightly plasticized the material. The reason is believed to be the different forms of water molecules on the boundary of the polymers during conditioning. According to Fan [36], the difference between water immersion and conditioning in a high RH environment is the state of water on the boundary between hydrophilic polymers and the environment. For polymers immersed in water, the water molecules enter as clusters while for polymers conditioned in a high RH environment, water molecules enter as individual molecules. Therefore, it is easier for water-bridges to be formed in the samples conditioned under high humidity, whereas water clusters tend to cause plasticization and soften the material.

Tsuji and Muramatsu [128] also characterized the tensile properties of pure PLA films before and after water immersion. In their work, the tensile strength and Young's modulus both decreased slightly after water immersion while the elongation at break

slightly increased. In other words, the PLA films were slightly plasticized by water absorption, and no anti-plasticization was observed. The difference from the present study is likely caused by the larger amount of water absorbed by PLA in Tsuji and Muramatsu (around 4 wt%), as compared to 0.835 wt% in this work after immersing PLA in distilled water. The different C_e achieved by water immersion might be caused by the different PLA raw materials (LACTY^{TM}5000 in Tsuji and Muramatsu vs. NatureWorks 4043D in this work), as well as the different sample preparation techniques (solution casting and melt-quenching in Tsuji and Muramatsu vs. melt-extrusion in this work).

In Figure 3.6, within the range of C_e obtained in this work, the elastic parameters (E_1 and E_2) firstly increase and then slightly decrease as C_e is increasing. The transition between the increasing and decreasing trends occurs at approximately 0.4 wt% of moisture content. However, the viscous parameters (μ_1 and μ_2) increase monotonically with C_e. One possible explanation is that when $C_e \geq 0.4$ wt%, small free water clusters might have already formed, which could break the existing water bridges and weaken the WBAP effect. The weakening appears to be more strongly reflected in the elastic parameters. These parameters represent the recoverability of the polymer chains from a deformed state and are affected by the interactions between polymer chain coils, including those arising from the water bridges [34, 72, 83, 86]. Breaking of the water bridges by the small water clusters could weaken the recoverability, thus causing a decrease in the elastic parameters. The viscous parameters capture the resistance when polymer chains slide past one another [7, 83]. They tend to increase with the amount of inter-chain non-covalent bonds, including water bridges while decrease with the free volume within the material [7, 34, 72]. While the small water clusters could reduce the interaction established by water bridges, they might also fill the existing free volumes and provide extra barriers for molecular chains to slide under external load [20]. These two competing factors could then reduce the impact of small water clusters on the viscous parameters.

The results presented in this paper provide strong evidence of water's anti-plasticization effect and the model is a useful tool for the prediction of change in the PLA's mechanical behaviors due to this effect. PLA has been used as micro-actuators [129] and substrates for sensors [130] in micro-electromechanical systems (MEMS). In these applications, a minor change in the mechanical behavior of the materials can significantly change the deformation of the components, which in turn changes the performances of these MEMs products [20, 131–133]. Therefore, during the design of these products, it is essential to evaluate and predict the mechanical behavior of the PLA components. The experimental methodology and model presented in this paper provide a useful tool for this purpose.

3.4 Conclusion

In this work, the effect of diffused moisture on the viscoelastic behavior of PLA was evaluated. Different equilibrium moisture content C_e was achieved by conditioning PLA samples under different RH or immersing them in distilled water. The modified Burgers-Reimschuessel model proposed by our group [72] was shown to be able to predict the creep compliance of the conditioned PLA samples with good accuracy. The experimental results here provided evidence on the stiffening effect of water molecules where they form bridges between the molecular chains. The present work highlights the importance of considering the water's anti-plasticization effect when evaluating the effect of moisture on the mechanical properties of hydrophilic polymers. The methodology used in this paper can also be adopted to evaluate the effect of moisture on the viscoelasticity of other hydrophilic polymers in different applications.

References

[7] M. T. Shaw and W. J. MacKnight, *Introduction to Polymer Viscoelasticity*, 3rd ed. John Wiley and Sons, Inc., 2005, p. 327.

[20] S. Schmid, S. Kühne, and C. Hierold, "Influence of air humidity on polymeric microresonators," *Journal of Micromechanics and Microengineering*, vol. 19, 6 2009.

[22] H. K. Reimschuessel, "Relationships on the effect of water on glass transition temperature and young's modulus of nylon 6," *Journal of Polymer Science Part A: Polymer Chemistry*, vol. 16, pp. 1229–1236, 6 1978.

[23] I. Widiastuti, I. Sbarski, and S. H. Masood, "Mechanical behavior of a fluid-sensitive material during liquid diffusion," *Mechanics of Time-Dependent Materials*, vol. 18, pp. 387–406, 2 2014, ISSN: 13852000. DOI: 10.1007/s11043-014-9233-9.

[24] I. Widiastuti, I. Sbarski, and S. H. Masood, "Mechanical response of poly(lactic acid)-based packaging under liquid exposure," *Journal of Applied Polymer Science*, vol. 131, pp. 1–10, 16 2014.

[26] S. Onogi, K. Sasaguri, T. Adachi, and S. Ogihara, "Time–humidity superposition in some crystalline polymers," *Journal of Polymer Science*, vol. 58, pp. 1–17, 166 1962.

[27] H. Fujita and A. Kishimoto, "Diffusion-controlled stress relaxation in polymers. iii. stress relaxation in a swelling polymer," *Journal of Polymer Science*, vol. 28, pp. 569–585, 118 1958.

[34] U. W. Gedde, *Polymer Physics*. Springer, 1999, p. 301.

[36] X. Fan, "Mechanics of moisture for polymers: Fundamental concepts and model study," 2008.

[37] R. M. Hodge, G. H. Edward, and G. P. Simon, "Water absorption and states of water in semicrystalline poly(vinyl alcohol) films," *Polymer*, vol. 37, pp. 1371–1376, 8 1996, ISSN: 00323861. DOI: 10.1016/0032-3861(96)81134-7.

[39] K. M. Zakir, A. J. Parsons, C. D. Rudd, I. Ahmed, and W. Thielemans, "Mechanical , crystallisation and moisture absorption properties of melt drawn polylactic acid fibres," *European Polymer Journal*, vol. 53, pp. 270–281, 2014, ISSN: 0014-3057. DOI: 10.1016/j.eurpolymj.2014.02.001. [Online]. Available: http://dx.doi.org/10.1016/j.eurpolymj.2014.02.001.

[40] A. Ishisaka and M. Kawagoe, "Examination of the time-water content superposition on the dynamic viscoelasticity of moistened polyamide 6 and epoxy," *Journal of Applied Polymer Science*, vol. 93, pp. 560–567, 2 2004.

[43] S. M. Bhasney, R. Patwa, A. Kumar, and V. Katiyar, "Plasticizing effect of coconut oil on morphological, mechanical, thermal, rheological, barrier, and optical properties of poly(lactic acid): A promising candidate for food packaging," *Journal of Applied Polymer Science*, vol. 134, p. 45 390, 41 Nov. 2017.

[44] V. Marturano *et al.*, "Light-responsive nanocapsule-coated polymer films for antimicrobial active packaging," *Polymers*, vol. 11, p. 68, 1 Jan. 2019.

[45] A. Orue, A. Eceiza, C. Peña-Rodriguez, and A. Arbelaiz, "Water uptake behavior and young modulus prediction of composites based on treated sisal fibers and poly(lactic acid)," *Materials*, vol. 9, p. 400, 5 2016.

[46] M. Esmaeili, G. Pircheraghi, R. Bagheri, and V. Altstädt, "Poly(lactic acid)/coplasticized thermoplastic starch blend: Effect of plasticizer migration on rheological and mechanical properties," *Polymers for Advanced Technologies*, vol. 30, pp. 839–851, 4 Apr. 2019.

[59] E Castro-aguirre, F Iñiguez-franco, H Samsudin, X Fang, and R Auras, "Poly (lactic acid) — mass production , processing , industrial applications , and end of life," *Advanced Drug Delivery Reviews*, vol. 107, pp. 333–366, 2016, ISSN: 0169-409X. DOI: 10.1016/j.addr.2016.03.010. [Online]. Available: http://dx.doi.org/10.1016/j.addr.2016.03.010.

[62] R. Auras, L. Lim, S. M. Selke, and H. Tsuji, *Polylactic Acid, Synthesis, Structures, Properties, Processing, and Applications*. John Wiley and Sons, 2010.

[63] N. F. Zaaba and M. Jaafar, "A review on degradation mechanisms of polylactic acid: Hydrolytic, photodegradative, microbial, and enzymatic degradation," *Polymer Engineering and Science*, vol. 60, pp. 2061–2075, 9 2020, ISSN: 15482634. DOI: 10.1002/pen.25511.

[72] Y. Chen, C. Ayranci, and T. Tang, "Modified burgers-reimschuessel model for moisture-sensitive polymers," *Journal of Polymer Science*, vol. 60, pp. 1539–1549, 9 Oct. 2021.

[77] O. Starkova and A. Aniskevich, "Limits of linear viscoelastic behavior of polymers," *Mechanics of Time-Dependent Materials*, vol. 11, pp. 111–126, 2 2007.

[83] W. D. Callister and D. G. Rethwisch, *Material Science and Engineering, An Introduction*, 8th ed. John Wiley and Sons, Inc., 2010, p. 1000.

[86] L. Sperling, *Introduction to Physical Polymer Science*. John Wiley and Sons, Inc, 2006.

[91] W. N. Findley, *Creep and relaxation of nonlinear viscoelastic materials : with an introduction to linear viscoelasticity*, W. N. Findley, J. S. Lai, and K. Onaran, Eds. Dover Publications Inc., 1989, p. 380.

[92] B. Yang, W. M. Huang, C. Li, and L. Li, "Effects of moisture on the thermomechanical properties of a polyurethane shape memory polymer," *Polymer*, vol. 47, pp. 1348–1356, 4 2006, ISSN: 00323861. DOI: 10.1016/j.polymer.2005.12.051.

[93] M. Pannico and P. L. Manna, "Sorption of water vapor in poly (l-lactic acid): A time-resolved ftir spectroscopy investigation," *Frontiers in Chemistry*, vol. 7, pp. 1–10, April 2019. DOI: 10.3389/fchem.2019.00275.

[106] "Polylactic acid market size, share and trends analysis report by end-use (packaging, textile, agriculture, automotive and transport, electronics), by region (north america, apac, europe), and segment forecasts, 2021 - 2028," Grand View Research, 2021, p. 130. [Online]. Available: https://www.grandviewresearch.com/industry-analysis/polylactic-acid-pla-market.

[107] Y. Ramot, M. Haim-Zada, A. J. Domb, and A. Nyska, "Biocompatibility and safety of pla and its copolymers," *Advanced Drug Delivery Reviews*, vol. 107, pp. 153–162, 2016, ISSN: 18728294. DOI: 10.1016/j.addr.2016.03.012. [Online]. Available: http://dx.doi.org/10.1016/j.addr.2016.03.012.

[108] V. K. Holm, S. Ndoni, and J. Risbo, "The stability of poly(lactic acid) packaging films as influenced by humidity and temperature," *Journal of Food Science*, vol. 71, pp. 40–44, 2 2006.

[109] R. A. Cairncross, J. G. Becker, S. Ramaswamy, and R. O'Connor, "Moisture sorption, transport, and hydrolytic degradation in polylactide," *Applied Biochemistry and Biotechnology*, vol. 131, pp. 774–785, 1-3 2006, ISSN: 02732289. DOI: 10.1385/ABAB:131:1:774.

[110] A. Singh, R. M. Guedes, D. Paiva, and F. D. Magalhães, "Experiment and modelling of the strain-rate-dependent response during in vitro degradation of pla fibres," *SN Applied Sciences*, vol. 2, pp. 1–18, 2 2020, ISSN: 25233971. DOI: 10.1007/s42452-020-1964-4. [Online]. Available: https://doi.org/10.1007/s42452-020-1964-4.

[111] E. C. L. A. M. Harris, "Improving mechanical performance of injection molded pla by controlling crystallinity," *Journal of Applied Polymer Science*, vol. 107, pp. 2246–2255, 2008.

[112] M. Niaounakis, E. Kontou, and M. Xanthis, "Effects of aging on the thermomechanical properties of poly(lactic acid)," *Journal of Applied Polymer Science*, vol. 119, pp. 472–481, 2011, ISSN: 00218995. DOI: 10.1002/app.

[113] D. M. Nieto, M. Alonso-García, M.-A. Pardo-Vicente, and L. Rodríguez-Parada, "Product design by additive manufacturing for water environments: Study of degradation and absorption behavior of pla and petg," *Polymers*, vol. 13, p. 1036, 7 2021, ISSN: 20734360. DOI: 10.3390/polym13071036.

[114] P. Kakanuru and K. Pochiraju, "Moisture ingress and degradation of additively manufactured pla, abs and pla/sic composite parts," *Additive Manufacturing*, vol. 36, p. 101 529, June 2020, ISSN: 22148604. DOI: 10.1016/j.addma.2020.101529. [Online]. Available: https://doi.org/10.1016/j.addma.2020.101529.

[115] S. Farah, D. G. Anderson, and R. Langer, "Physical and mechanical properties of pla , and their functions in widespread applications — a comprehensive review," *Advanced Drug Delivery Reviews*, vol. 107, pp. 367–392, 2016, ISSN: 0169-409X. DOI: 10.1016/j.addr.2016.06.012. [Online]. Available: http://dx.doi.org/10.1016/j.addr.2016.06.012.

[116] A. S. Khan, O. Lopez-Pamies, and R. Kazmi, "Thermo-mechanical large deformation response and constitutive modeling of viscoelastic polymers over a wide range of strain rates and temperatures," *International Journal of Plasticity*, vol. 22, pp. 581–601, 4 2006, ISSN: 07496419. DOI: 10.1016/j.ijplas.2005.08.001.

[117] G. L. Siparsky, K. J. Voorhees, J. R. Dorgan, and K. Schilling, "Water transport in polylactic acid (pla), pla/polycaprolactone copolymers, and pla/polyethylene glycol blends," *Journal of Polymers and the Environment*, vol. 5, pp. 125–136, 3 1997, ISSN: 10647546. DOI: 10.1007/BF02763656.

[118] E. A. Schmitt, D. R. Flanagan, and R. J. Linhardt, "Importance of distinct water environments in the hydrolysis of poly(dl-lactide-co-glycolide)," *Macromolecules*, vol. 27, pp. 743–748, 1994.

[119] M. Algarni, "The influence of raster angle and moisture content on the mechanical properties of pla parts produced by fused deposition modeling," *Polymers*, vol. 13, pp. 1–12, 2 2021, ISSN: 20734360. DOI: 10.3390/polym13020237.

[120] E. H. Backes, L. de N. Pires, L. C. Costa, F. R. Passador, and L. A. Pessan, "Analysis of the degradation during melt processing of pla/biosilicate® composites," *Journal of Composites Science*, vol. 3, p. 52, 2 2019.

[121] "Astm e104-20 standard practice for maintaining constant relative humidity by means of aqueous solutions," American Society for Testing and Materials, Tech. Rep., 2020, p. 5.

[122] J. Crank, *The Mathematics of Diffusion*. Oxford University Press, 1975, p. 421.

[123] Y. Y. Leu and W. S. Chow, "Kinetics of water absorption and thermal properties of poly(lactic acid)/organomontmorillonite/poly(ethylene glycol) nanocomposites," *Journal of Vinyl and Additive Technology*, vol. 17, pp. 40–47, 1 2011, ISSN: 10835601. DOI: 10.1002/vnl.20259.

[124] "Astm d3822-14 (2020) standard test method for tensile properties of single textile fibers," Tech. Rep., 2020.

[125] "Astm d2990-17 standard test methods for tensile, compressive, and flexureal creep and creep-rupture of plastics," Tech. Rep., 2017.

[126] J. Dong, C. Mei, J. Han, S. Lee, and Q. Wu, "3d printed poly(lactic acid) composites with grafted cellulose nanofibers: Effect of nanofiber and post-fabrication annealing treatment on composite flexural properties," *Additive Manufacturing*, vol. 28, pp. 621–628, May 2019, ISSN: 22148604. DOI: 10.1016/j.addma.2019.06.004. [Online]. Available: https://doi.org/10.1016/j.addma.2019.06.004.

[127] M. Drieskens, R. Peeters, J. Mullens, D. Franco, P. J. Lemstra, and D. G. Hristova-Bogaerds, "Structure versus properties relationship of poly(lactic acid). i. effect of crystallinity on barrier properties," *Journal of Polymer Science Part B: Polymer Physics*, vol. 47, pp. 2247–2258, 2009. DOI: 10.1002/polb. [Online]. Available: http://arxiv.org/abs/cond-mat/0406218%0Ahttp://dx.doi.org/10.1002/polb.

[128] H. Tsuji and H. Muramatsu, "Blends of aliphatic polyesters. iv. morphology, swelling behavior, and surface and bulk properties of blends from hydrophobic poly(l-lactide) and hydrophilic poly(vinyl alcohol)," *Journal of Applied Polymer Science*, vol. 81, pp. 2151–2160, 2001.

[129] S Amaya and S Sugiyama, "Development of mems using biodegradable polymer material," 2013, ISBN: 9781467359832.

[130] A. V. Quintero *et al.*, "Printing and encapsulation of electrical conductors on polylactic acid (pla) for sensing applications," 2014, pp. 532–535, ISBN: 9781479935086. DOI: 10.1109/MEMSYS.2014.6765695.

[131] C. J. Robin and K. N. Jonnalagadda, "Effect of size and moisture on the mechanical behavior of su-8 thin films," *Journal of Micromechanics and Microengineering*, vol. 26, 2 Jan. 2016, ISSN: 13616439. DOI: 10.1088/0960-1317/26/2/025020.

[132] K. B. Lee, *Principles of microelectromechanical systems*. WILEY, 2010.

[133] C. C. Nguyen, V. K. T. Ngo, H. Q. Le, and W. L. Li, "Influences of relative humidity on the quality factors of mems cantilever resonators in gas rarefaction," *Microsystem Technologies*, vol. 25, pp. 2767–2782, 7 Jul. 2019, ISSN: 09467076. DOI: 10.1007/s00542-018-4239-x.

Chapter 4

Linear viscoelasticity of bio-based composites of polylactic acid and regenerated cellulose fibers: modeling and experimental validation

4.1 Introduction

Since the 1990s, the use of traditional petroleum-based fiber-reinforced polymeric composites have been critically discussed mainly due to increased environmental concerns [2, 3, 68]. Examples include polymers such as polystyrene (PS) and polyethylene terephthalate (PET) reinforced by fibers such as glass, aramid or carbon. The concept of bio-based composites has been proposed as an alternative [4, 134, 135]. Bio-based composites are composites made from bio-renewable and bio-degradable constituents [4, 68]. In recent years, these bio-based composites have started to be widely used in large-volume industries, such as automotive and construction. For example, the major car manufacturers in Germany (Mercedes, BMW, Volkswagen Audi groups) are now making interior trim components such as dashboards and door panels, using bio-based composites [4, 136]. In the construction industry, bio-based composites have been used to manufacture doors, side panels, roofing sheets, etc. [4]

For the matrix phase of bio-based composites, such as polylactic acid (PLA), polyg-

lycolic acid (PGA), poly(3-hydroxybutyrate-co-3-hydroxyvalerate) (PHBV), poly(butylene succinate) (PBS) and thermoplastic starch have been reported to become serious alternatives to petroleum-based polymers [62, 137]. Among these, PLA is becoming increasingly popular due to a variety of reasons [65–67, 69, 138–142]. Firstly, PLA can be derived from some of the abundant types of bio-renewable resources such as corn starch and sugar cane and that leads to large-scale production capacity [59]. Secondly, the stiffness of PLA is comparable to petroleum-based polymers such as PS and PET [60–62]. Thirdly, PLA is a semi-crystalline thermoplastic which can be processed using well-established melt-processing techniques such as extrusion, injection molding and compression molding [59, 62]. Finally, PLA is environment-friendly [59], and can be reused, recycled or biodegraded under both natural and controlled environments [63, 64].

For the reinforcement phase of bio-based composites, natural fibers have various advantages over synthetic fibers [143]. Their advantages include renewability, biodegradability, cost effectiveness, low density, etc. [2, 4, 143] Cellulose-based plant fibers such as jute, flax, hemp and kenaf are frequently used natural fibers, due to their moderate price, high availability, and good mechanical properties [4, 143, 144]. Studies have shown that the incorporation of these cellulose-based plant fibers into PLA can increase its modulus, enhance the toughness, and improve the thermal stability [62, 145–148]. The reinforcements can even promote the biodegradation of PLA due to their high hydrophilicity, which enhances moisture adsorption and hydrolytic degradation of PLA [62, 149]. However, the major drawbacks of natural fibers are their inconsistency and the impurities on the fiber surface [15, 65, 67, 150]. Mechanical properties of natural fibers can vary significantly among different batches, and surface impurities such as wax, pectin, hemicellulose and lignin can greatly affect the adhesion between the natural fibers and PLA matrix [67, 145, 151]. For this reason, emerging studies have shown interests in reinforcing PLA with regenerated cellulose fibers (RCF) [13, 15, 71, 152–154]. RCF are generated from cellulose separated from

bio-feedstock using various chemical processes [155]. For instance, lyocell fibers are extracted from wood chips by dissolving them in non-toxic N-Methyl morpholine N-oxide (NMMO) and pumping them through the spinnerets into coagulation baths where regeneration of the cellulose takes place [155, 156]. This is an environmentally friendly process since 99% of the NMMO solvent can be recovered and reused [156]. Compared with natural fibers, RCF have better consistency, improved mechanical properties and almost no surface impurities since the fiber surface have been cleaned during extraction [15, 65, 66, 138]. PLA/RCF bio-based composites have the potential to replace petroleum-based non-biodegradable polymer composites or offer excellent alternatives, in a wide range of applications such as boxes for packaging, beams for decking and door panels for automotives [12].

A number of investigations have been carried out to study the manufacturing and characterization of PLA/RCF bio-based composites. Melt-mixing is the most frequently used method for embedding RCF into PLA matrix, while injection molding and compression molding have also been used to manufacture samples with various geometries and dimensions [12, 65–67, 70, 71]. In characterizing the mechanical properties of PLA/RCF composites, Bledzki et al. [67] discovered that the addition of 30 wt% RCF increased the Young's modulus by approximately a factor of 1.7 in comparison to bare PLA. Besides Young's modulus, Bax and Mussig [68] reported a significant increase in tensile strength and Charpy impact strength with the addition of 10-30 wt% RCF. Thermo-mechanical properties characterized by dynamic mechanical analysis were also reported in the literature. Huda et al. [66, 69], Baghaei et al. [71], Zhang et al. [157] and Kurokawa et al. [61] all reported an increased storage modulus when RCF were added into PLA, regardless of the manufacturing method. These findings suggest good compatibility between RCF and PLA, which enables effective stress transfer on the fiber-matrix interface. Furthermore, Baghaei et al. [71], Zhang et al. [157] and Kurokawa et al. [61] reported a drastic increase in storage modulus above PLA's glass transition temperature, suggesting that the

thermal stability and heat resistance of PLA has been significantly enhanced by the reinforcement of RCF.

Despite the enthusiasms in manufacturing and charactering PLA/RCF bio-based composites, attempts to model their mechanical properties have been limited [12, 66, 144, 158]. Huda et al. [66] provided a linear fitting to describe the increasing tensile modulus of the composite with respect to RCF content. Ganster et al. [144] and Rozite et al. [12] applied modified rule of mixture to predict the Young's modulus E_c of PLA/RCF composites:

$$E_c = \eta_l \eta_\theta E_f V_f + E_m V_m \tag{4.1}$$

where E_f and E_m are the Young's moduli of RCF and PLA, respectively; and V_f and V_m are volume fraction of RCF and PLA, respectively. η_l and η_θ are two empirical parameters introduced to capture the effect of fiber length and orientation on E_c, which do not have direct physical meaning and need to be extracted from fitting to experimental data. Karakoc et al. [158] used high-resolution X-ray microcomputed tomography (Micro-CT) to characterize the internal structure of a PLA/RCF bio-based composite sample and incorporated it into a finite element solver to simulate its mechanical behavior under different loadings. Effective elastic properties were determined from the simulation results. However, the above-mentioned work by Karakoc et al. [158] still assumed the composite to be elastic while PLA has been discovered to exhibit viscoelasticity [24, 25, 73, 110]. Consequently, the PLA/RCF composites can show viscoelastic behaviors such as creep and stress relaxation [9], which may impact the performance of the composites under long-term loadings [9, 159]. To the best of the authors' knowledge, only Rozite et al. [12] conducted creep-recovery tests on PLA/RCF composites, with 5 wt% RCF reinforcement. The composites were found to exhibit creep behavior similar to conventional polymer-based composites [12]. To the best of authors' knowledge, predictive models capable of capturing the viscoelasticity of PLA/RCF composites was not found, indicating an important gap in the literature.

Consequently, the present work aims at developing a constitutive model that can accurately describe the viscoelastic behavior of PLA/RCF bio-based composites, while being simple enough for usage by a broad audience. In the literature, a variety of models has been proposed and validated to predict the elastic constitutive relation of fiber reinforced polymer composites with different assembly structures [1, 159, 160]. For instance, Vilaseca et al. [160] proposed a model that combines the Tsai-Pagano model [57] and Halpin-Tsai model [56], which predicts the Young's modulus of short fiber reinforced polymer composites based on fiber morphology, fiber distribution, as well as mechanical properties of the fiber and matrix. Mazzanti et al. [161] applied this model to PLA bio-based composites reinforced by alkali treated hemp fibers and found good agreement with experiments for hemp concentration up to 6 wt%. In this work, we go beyond the linear elastic regime and develop a model that predicts the creep compliance of PLA/RCF bio-based composites. Validated against experimental results, the developed model is expected to assist in the design of PLA/RCF bio-based composites and modulation of their mechanical properties. Potentially, this model may also be applied to predict the viscoelasticity of other types of short fiber reinforced bio-based composites.

4.2 Model

Consider a PLA/RCF composite where the RCF are homogeneously distributed with random orientation in the PLA matrix. The bonding between fiber and matrix is assumed to be perfect with no interfacial defects. Widely used in a variety of applications, this type of composites can be considered as a statistically homogeneous and isotropic material [162]. The focus of the modeling is to derive the time (t) dependent creep compliance $J_c(t)$ of the composite in the linear viscoelastic regime. Under one-dimensional loading, the stress $\sigma_c(t)$ and strain $\varepsilon_c(t)$ of the composite are related

through $J_c(t)$, given by [85]:

$$\varepsilon_c(t) = \int_0^t J_c(t-\tau) d\sigma_c(\tau) \tag{4.2}$$

In linear viscoelasticity, it is a common approach to determine creep compliance or stress relaxation function in one-dimensional form [91], which can then be extended to higher dimensions [1, 56]. Below we will first formulate the constitutive relations for the constituents (RCF, PLA), after which $J_c(t)$ will be derived based on a homogenization approach coupled with the correspondence principle.

4.2.1 Constitutive relation for the constituents

RCF are usually highly crystallized [163]; it is therefore reasonable to assume the RCF reinforcement in the composite to be linearly elastic, satisfying the following constitutive relation (stress-strain relation)

$$\sigma_f(t) = E_f \varepsilon_f(t) \quad or \quad \varepsilon_f(t) = S_f \sigma_f(t) \tag{4.3}$$

where $\sigma_f(t)$ and $\varepsilon_f(t)$ are the stress and strain of the RCF, respectively. E_f and S_f are the Young's modulus and elastic compliance of the fibers respectively, which are time-independent and related by $E_f S_f = 1$. A previous study by our group [73] showed that PLA exhibits linear viscoelasticity, which can be described by the Burgers model as schematically shown in Figure 4.1a. E_{m1} and E_{m2} are elastic constants of the linear Hookean springs, and μ_{m1} and μ_{m2} are viscosities of the linear viscous dashpots. $\sigma_m(t)$ and $\varepsilon_m(t)$ are the stress and strain of PLA, respectively [91]. The creep compliance for this model is given by [91]:

$$J_m(t) = \frac{t}{\mu_{m2}} + \frac{1}{E_{m2}} + \frac{1}{E_{m1}} \left[1 - \exp\left(-\frac{E_{m1}}{\mu_{m1}} t \right) \right], \qquad t \geq 0 \tag{4.4}$$

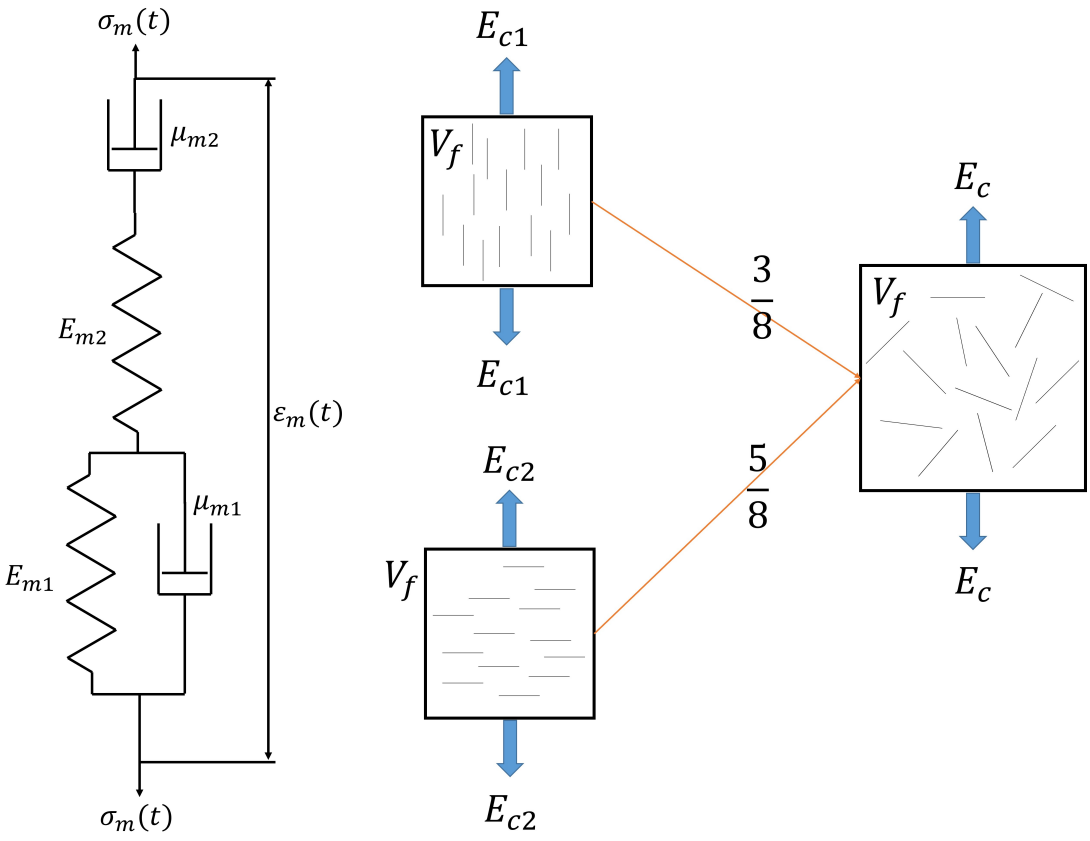

(a) (b)

Figure 4.1: Schematic representation of (a) linear Burgers model for PLA [91]; (b) Tsai-Pagano model for linear elastic composites [57].

4.2.2 Composite model

Since the constitutive relations of both constituents follow linearity, the correspondence principle can be used to extend a linear elastic model to the corresponding linear viscoelastic model in the Laplace transformed domain [9, 85, 164]. Tsai and Pagano [57] proposed a linear elastic model for composites reinforced by homogeneously distributed and randomly oriented fibers. The effective Young's modulus (E_c) of the composite is calculated by the weighted average of the longitudinal (E_{c1}) and transverse (E_{c2}) Young's moduli of composites reinforced by aligned short fibers with the same volume fraction (V_f). This relation is given by equation 4.5 and schematically depicted in Figure 4.1b.

$$E_c = \frac{3}{8}E_{c1} + \frac{5}{8}E_{c2} \tag{4.5}$$

E_{c1} and E_{c2} can be determined by the Halpin-Tsai model [56, 159, 165].

$$\frac{E_{ci}}{E_m} = \frac{1 + \xi_i \eta_i V_f}{1 - \eta_i V_f}, \quad \eta_i = \frac{E_f/E_m - 1}{E_f/E_m + \xi_i} \tag{4.6}$$

where E_m and E_f are the Young's moduli of matrix and fiber respectively; $i(= 1,\ 2)$ indicates the direction; ξ_i is a semi-empirical parameter related to the fiber aspect ratio and the direction i. Halpin and Kardos [56] provided the values of ξ_i for aligned short fiber reinforced composites. In the longitudinal direction ($i = 1$), $\xi_1 = 2L_f/d_f$, where L_f and d_f are respectively the length and diameter of the reinforcement fibers. In transverse direction ($i = 2$), $\xi_2 = 2$.

Defining the elastic compliance to be the reciprocal of Young's modulus ($S_m = 1/E_m,\ S_f = 1/E_f,\ S_c = 1/E_c,\ S_{c1} = 1/E_{c1},\ S_{c2} = 1/E_{c2}$), equations 4.5 can also be written into

$$\frac{1}{S_c} = \frac{3}{8}\frac{1}{S_{c1}} + \frac{5}{8}\frac{1}{S_{c2}} \tag{4.7}$$

where the elastic compliances in the longitudinal and transverse directions, S_{ci} ($i = 1, 2$), are obtained from equation 4.6 and given by

$$\frac{1}{S_{ci}} = \frac{1}{S_m}\frac{1 + \xi_i \eta_i V_f}{1 - \eta_i V_f}, \quad \eta_i = \frac{S_m/S_f - 1}{S_m/S_f + \xi_i} \tag{4.8}$$

The above elastic solution can now be extended into the linear viscoelastic regime using the correspondence principle. Denote the Laplace transformed creep compliances of the matrix, the fiber and the composite by $\hat{J_m}(s)$, $\hat{J_f}(s)$ and $\hat{J_c}(s)$ respectively, where s is the independent variable in the Laplace domain. $\hat{J_m}(s)$ and $\hat{J_f}(s)$ can be obtained by taking the Laplace transform $\mathcal{L}\{\cdot\}$ of equation 4.4 and the constant fiber compliance S_f, leading to

$$\hat{J_m}(s) = \mathcal{L}\{J_m(t)\} = \frac{1}{\mu_{m2}s^2} + \frac{1}{E_{m2}s} + \frac{1}{E_{m1}s + \mu_{m1}s^2} \tag{4.9}$$

$$\hat{J}_f(s) = \mathcal{L}\{J_f(t) = S_f\} = \frac{S_f}{s} \tag{4.10}$$

Based on the correspondence principle [9], the Laplace transformed creep compliances of the linear viscoelastic composite follow the relationship, equation 4.7, for the compliances of the linear elastic composite in that

$$\frac{1}{s\hat{J}_c(s)} = \frac{3}{8}\frac{1}{s\hat{J}_{c1}(s)} + \frac{5}{8}\frac{1}{s\hat{J}_{c2}(s)} \tag{4.11}$$

where

$$\frac{1}{s\hat{J}_{ci}(s)} = \frac{1}{s\hat{J}_m(s)}\frac{1+\xi_i\eta_i V_f}{1-\eta_i V_f}, \quad \eta_i = \frac{\left[s\hat{J}_m(s)\right] / \left[s\hat{J}_f(s)\right] - 1}{\left[s\hat{J}_m(s)\right] / \left[s\hat{J}_f(s)\right] + \xi_i} \tag{4.12}$$

are extended from the elastic solution, equation 4.8. Combining equations 4.9, 4.10, 4.11 and 4.12, $\hat{J}_c(s)$ is calculated to be

$$\hat{J}_c(s) = \frac{F_6 s^6 + F_5 s^5 + F_4 s^4 + F_3 s^3 + F_2 s^2 + F_1 s + F_0}{D_7 s^7 + D_6 s^6 + D_5 s^5 + D_4 s^4 + D_3 s^3 + D_2 s^2} \tag{4.13}$$

where F_p (p = 0 to 6) and D_q, (q = 2 to 7) are constants related to E_{m1}, E_{m2}, μ_{m1}, μ_{m2}, E_f, ξ_1 and ξ_2, as given in the Appendix A. The creep compliance of the composite in the time domain, $J_c(t)$, is finally obtained by taking the inverse Laplace transform of $\hat{J}_c(s)$

$$J_c(t) = \mathcal{L}^{-1}\Big\{\hat{J}_c(s)\Big\} \tag{4.14}$$

The full expression of $J_c(t)$ was obtained using the symbolic core of Mathematica™ (Wolfram Research, USA). It is lengthy (involving over 3000 terms) and therefore not presented here.

4.3 Experiments

4.3.1 Materials

Extrusion grade PLA (4043D) was obtained from NatureWorks LLC, USA. The number-average molecular weight (M_n) is 106,000 g/mol, and it has a D-lactic acid content from 4.5 to 5 wt% [120]. The RCF used in this work was BioMid^{TM}, which was obtained from Gordon Shank Consulting and Engineered Natural Composites, Inc., Canada. These BioMid^{TM} fibers are continues strands of RCF made from the wastes generated during lumber production in western Canada [166]. It has been reported that BioMid^{TM} fibers has a crystallinity of 95% and it can sustain a processing temperature of 360°C, which is higher than the majority of the natural fibers [167, 168].

4.3.2 Composite Manufacturing

Attempts were made to chop the long continuous RCF into short fibers and melt-mix it with PLA. However, good dispersion of RCF in PLA was not possible in our first attempt due to the limitation of the single screw extruder in our laboratory. Thus, the following unconventional two-step extrusion technique was utilized to produce PLA/RCF composites. The authors acknowledge that the dispersion of the RCF in the composite samples produced with this method are still not ideal.

Preparation of the masterbatch

Both PLA and RCF fibers were dried under vacuum at 80°C for 8 h in a Lindberg/Blue M^{TM} vacuum oven (Thermo Fisher Scientific, USA) to remove the residual moisture that may cause air bubbles during extrusion. Then, a Brabender^{TM} single screw extruder equipped with a core-shell die (a.k.a. crosshead die), attached to an ATR Plasti-Corder drive system (C.W. Brabender Instruments, Inc., Germany), was used to manufacture the masterbatch of the PLA/RCF composites containing 5.6 wt% RCF. The extrusion process is schematically shown in Figure 4.2a and the cross-

sectional view of the core-shell die is shown in Figure 4.2b. In this process, the long continuous RCF strand went through the core part of the die while the PLA pellets were melted in the extruder and flow through the shell part of the die, as shown by Figure 4.2b. The processing temperature and screw RPM for the masterbatch composite pellet preparation are shown in Table 4.1, which were selected based on the manufacturer provided data for 4043D PLA pellets. Finally, the extrudate was cooled by Filabot^{TM} FB00626 cooling fan (Triex LLC, USA) with 100% fan level and Filabot^{TM} FB00073 filament spooler (Triex LLC, USA) was used to pull the PLA/RCF composite masterbatch. The pulling speed of the spooler were carefully adjusted to ensure a uniform and consistent wrapping of PLA on the outside of RCF. Pure PLA masterbatch filaments without RCF reinforcement were also produced using the same extrusion setup and processing parameters.

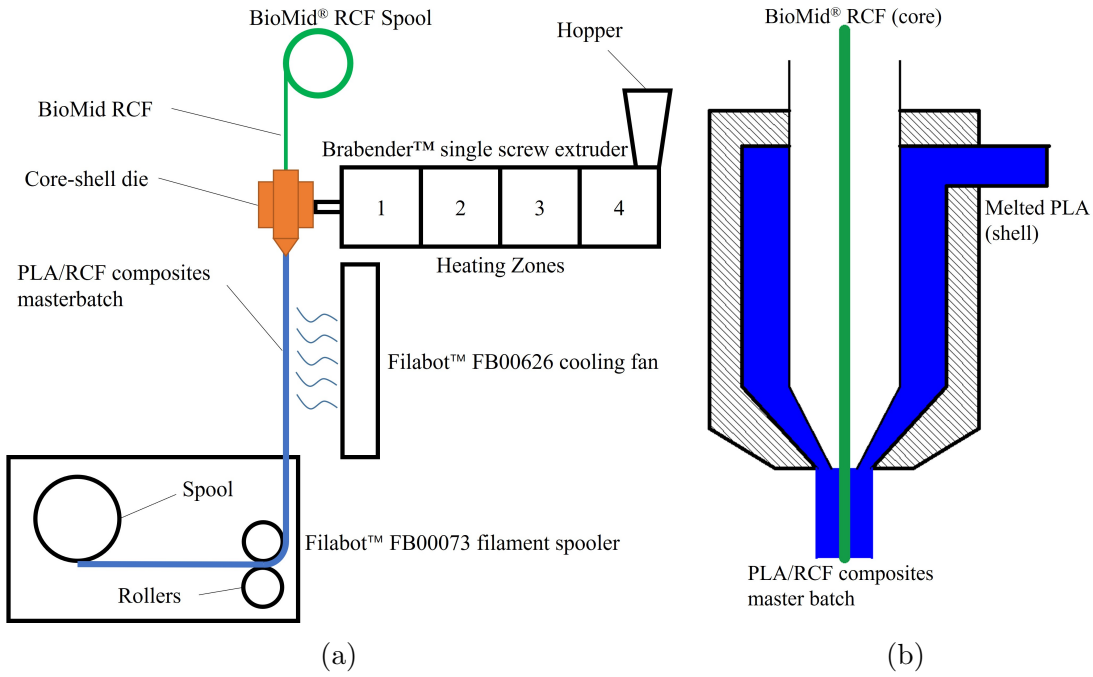

Figure 4.2: (a) Schematic representation of the core-shell extrusion process. (b) Schematics for the cross-section of the core-shell die shown with orange in (a).

Table 4.1: Extrusion processing parameters

Process	Zone 1 temperature (°C)	Zone 2 temperature (°C)	Zone 3 temperature (°C)	Zone 4 temperature (°C)	Screw speed (RPM)
Masterbatch composite pellet extrusion	200	200	190	180	15
Sheet extrusion	180	180	175	170	20

Sample preparation

Both masterbatches (pure PLA and 5.6 wt% PLA/RCF composite) were chopped into pellets using a sewing scissors since the pellitizer was not strong enough the cut the composite pellets. Prepared composite pellets are shown in Figure 4.3a. These pellets were again dried under vacuum at 80°C for 8 h in the Lindberg/Blue M^{TM} vacuum oven to remove the residual moisture that possibly absorbed during chopping and handling. Then, the Brabender^{TM} single screw extruder was used with a fixed sheet die (100 mm in width and 0.5 mm in thickness) to produce sheet samples. The processing parameters for this sheet preparation stage were slightly altered (Table 4.1) to minimize excessive shrinkage during cooling. The pulling of the sheet extrudate was done by the sheet puller in our lab. The pulling speed was then carefully adjusted to avoid both wrapping and breaking of the extrudates. In this stage, the fan speed was still 100%.

Samples with three different RCF concentrations were produced. Pure PLA samples (0.0RCF/PLA) were produced using pure PLA masterbatch; 2.8 wt% RCF reinforced PLA composites (2.8RCF/PLA) were produced by diluting the 5.6 wt% PLA/RCF masterbatch with pure PLA masterbatch at 1:1 ratio; 5.6 wt% RCF reinforced PLA/RCF composites (5.6RCF/PLA) were produced using 5.6 wt% PLA/RCF masterbatch. Due to the shear force provided during the extrusion, the fibers were ap-

proximately homogeneously distributed and randomly oriented in the sheet samples, as shown by Figure 4.3b. In order to confirm the dispersion of RCF, the Micro-CT characterization were performed on a triangular section of a 5.6RCF/PLA sample and one of the cross-sections of the triangular section is shown in Figure 4.3c.

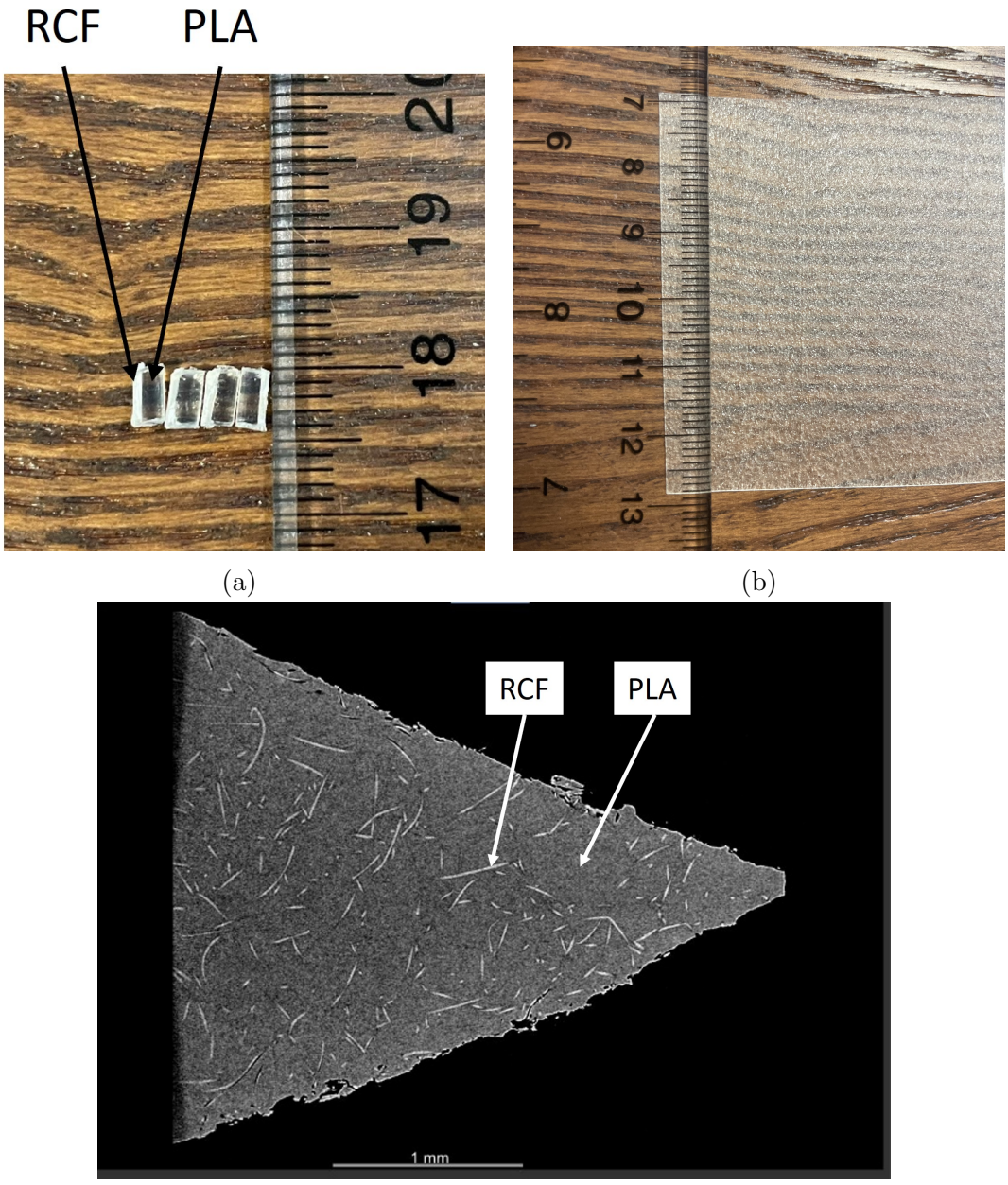

Figure 4.3: Samples of 5.6RCF/PLA: (a) Chopped masterbatch pellets after the first extrusion process; the gaps on the ruler are 1 mm; (b) A sheet sample of 5.6RCF/PLA; (c) Micro-CT image of a triangular section of a sheet sample of 5.6RCF/PLA

4.3.3 Characterization

The samples were dried under vacuum at 80°C for 8 h in the Lindberg/Blue M^{TM} vacuum oven to remove the moisture and release the residual stress that might have been generated during the extrusion process. Following this drying, the characterizations listed below were performed.

Parameter of RCF

Single RCF samples were hand separated and their diameters were measured with Olympus IX-83 confocal microscope (Olympus Corporation, Japan). A total of 80 measurements were taken for the fiber diameter (d_f).

Assuming that the length of the fibers did not change during the sheet sample extrusion, it was obtained by measuring the length of the chopped pellets of PLA/RCF composite masterbatch by a caliper, before the sample preparation process, and 100 measurements were taken for the fiber length (L_f).

Tensile tests were conducted to measure the Young's modulus (E_f) of single RCF according to ASTM D3379 [169]. As shown in Figure 4.4, the single RCF was hand separated and mounted on a paper tab by poly(ethylene-vinyl acetate) (PEVA, marked as "glue" in the figure) using a glue gun (Topelek, China). The gauge length of the paper tab was 20 mm.

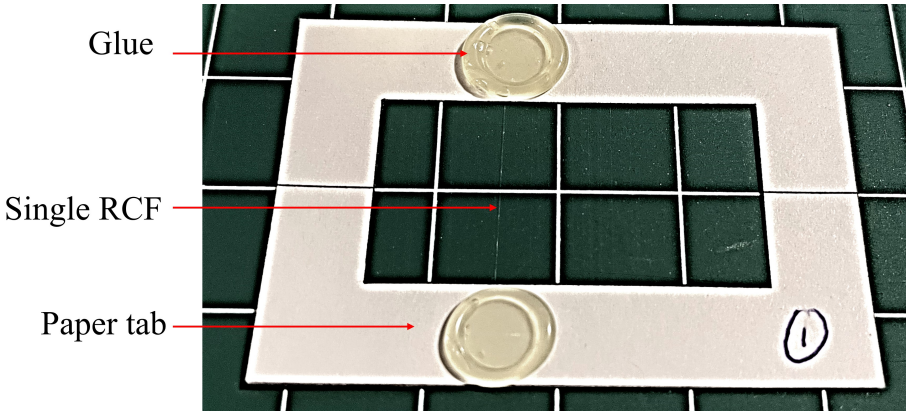

Figure 4.4: Mounting of the single RCF for tensile tests (sharpness was tuned to better visualize the sample).

Tensile tests of the prepared single RCF samples were conducted on a universal tensile testing system (ElectroForce 3200 Series III, Bose Corporation, USA) equipped with a 250 g load cell. After mounting the sample on the tensile clamps, the paper tab was cut, and a constant displacement rate of 0.6 mm/min was applied based on ASTM D3379 [169]. The ambient environment during the tests was 18% RH and around 22°C. To calculate the nominal stress, the diameter of the samples was measured with the Olympus IX-83 confocal microscope mentioned above. Young's modulus of the fiber was determined by linear fitting of the initial part of the stress-strain curve. The tensile tests were performed on ten RCF samples to obtain the averaged Young's modulus as well as its standard deviation.

Creep tests

Tensile creep tests were conducted on sheet samples of 0.0PLA/RCF, 2.8PLA/RCF and 5.6PLA/RCF for 15 min. The extruded sheet samples were cut into rectangle samples 60 mm long and 10 mm wide to be mounted onto the tensile clamps of the aforementioned universal tensile testing system.

The creep tests were performed according to ASTM D2990 [125], where the creep stress was programmed to be applied within 1 s and the strain was recorded every 50 s. A series of pre-tests were first conducted with different creep stresses σ_0 to identify the linear viscoelastic limit. The measured strain was normalized by the creep stress σ_0 to obtain the creep compliance. According to the results of these pre-tests, the creep compliance did not change with σ_0 when $\sigma_0 \leq 6.8$ MPa, regardless of the RCF concentration. Thus, 6.8 MPa was used as the stress for all creep tests. Five replications were performed at each RCF concentration. The ambient environment during creep tests was around 22% RH and 23°C.

Crystallinity of PLA matrix

Differential scanning calorimetry (DSC) measurements were conducted on DSC Q100 (TA instruments, USA) in the temperature range of 20-180°C for all types of samples to measure the crystallinity of the PLA matrix [148]. The heating scan was performed with a heating rate of 5°C/min. The crystallinity X_c of PLA in the samples were calculated with equation 4.15 [170].

$$X_c = \frac{\Delta H_m - \Delta H_c}{\Delta H_{mf}} \times 100\% \tag{4.15}$$

where ΔH_m is the heat of fusion; ΔH_c is the heat of crystallization during the DSC scan; $\Delta H_{mf} = 93.1$ J/g is the heat of fusion of fully crystallized PLA [62, 170, 171].

4.4 Results and Discussion

4.4.1 Material parameters for the constituents

The geometrical information required by the model includes fiber length L_f and fiber diameter d_f. The statistics of measured L_f and d_f values are 4.71 ± 0.53 mm and 12.50 ± 0.87 μm respectively. The small standard deviations indicate that fiber geometry in the composite is consistent, and thus the averages were used in the model (Table 4.2).

Table 4.2: Parameters of RCF and PLA for the model given by Figure 4.1 and equation 4.13

Parameter	L_f (mm)	d_f (μm)	E_f (GPa)	E_{m1} (GPa)	E_m2 (GPa)	μ_{m1} (GPa·s)	μ_{m2} (GPa·s)
Value	4.71	12.50	49.68	8.79	2.46	632.2	8892

The stress-strain curves of single RCF samples were all approximately linear within the strain of 0.3%, which validates the linear elastic assumption of RCF. The measured Young's modulus E_f of the RCF was 49.68 ± 5.06 GPa (Table 4.2).

The measured creep compliance of pure PLA, i.e., 0.0PLA/RCF, is shown by the blue squares in Figure 4.5. The error bars are the standard deviation of the 5 replicated experiments. The data exhibits the typical creep behavior of semi-crystalline polymers: an instantaneous elastic compliance followed by a delayed creep compliance (Figure 4.5) [7, 85]. Equation 4.4 was used to fit the experimental results of 0.0PLA/RCF and extract the Burgers model parameters of PLA [23, 73]. As shown in Figure 4.5, a good match was achieved between the experimental data and the model fitting (blue curve), with adjusted $R^2 = 0.99302$. The Burgers model parameters obtained from the fitting are given in Table 4.2 as well, which are close to what was reported in the literature [23, 73].

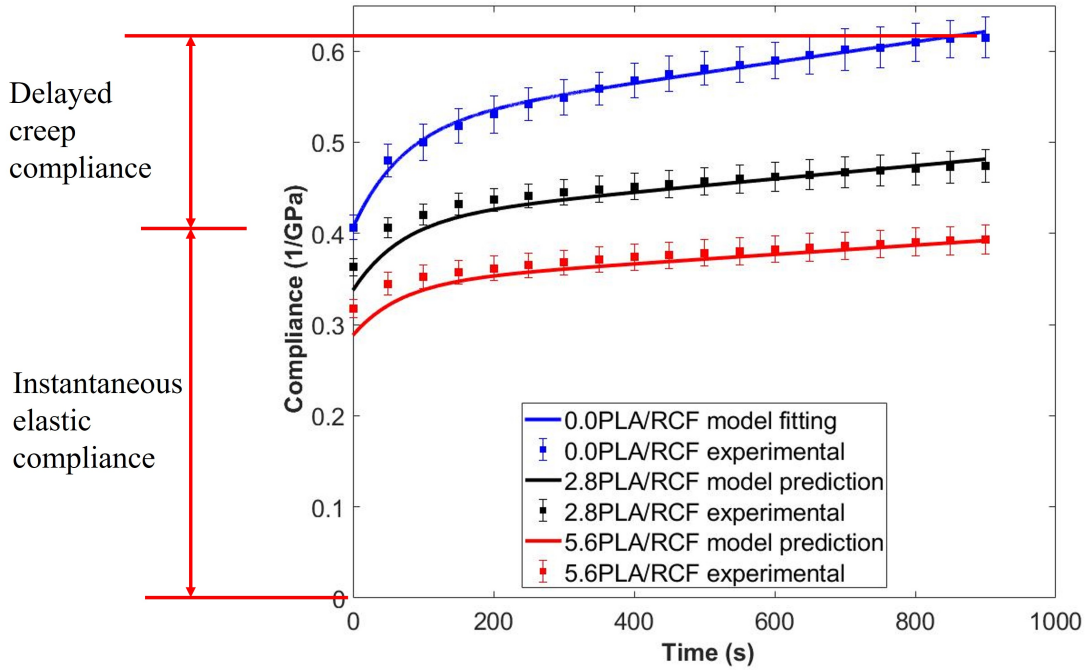

Figure 4.5: Measured creep compliance and corresponding model prediction for PLA and PLA/RCF composites

4.4.2 Model prediction for the composites

With the material parameters for the constituents determined, the creep compliance of the PLA/RCF composites can be directly predicted using the developed model. The

predicted compliances are plotted in Figure 4.5 for 2.8PLA/RCF and 5.6PLA/RCF based on equation 4.14 and the parameters in Table 4.2, with no additional fittings. Comparisons are made in the same figure with experimentally measured compliances, which shows good agreement. This confirms that the model developed in this work is capable of predicting the linear viscoelastic behavior of PLA/RCF composites.

From Figure 4.5, the addition of RCF decreased the instantaneous elastic compliance, indicating that the stiffness of the composites (2.8PLA/RCF and 5.6 PLA/RCF) were higher than that of pure PLA (0.0PLA/RCF). There are two potential reasons for the observed increase. Firstly, the RCF is significantly stiffer than PLA. The measured Young's modulus of RCF was 49.68 GPa, which is one order of magnitude larger than the elastic parameters (E_{m1} and E_{m2}) of PLA. Secondly, it has been reported that regenerated cellulose can serve as nucleation agents and increase the crystallinity X_c of PLA [157, 172]. As such, higher stiffness was reported for PLA/RCF composites by Suryanegara et al. [173] and Zakir et al. [39], when compared to bare PLA. To confirm this for our study, DSC characterization was conducted to determine X_c. The change of heat flow with respect to temperature for all three types of samples are shown in Figure 4.6. Crystallization peak was not observed in temperature between 80°C and 120°C, indicating that PLA matrix in the samples is all fully crystallized [148]. The X_c of PLA in the samples were evaluated using equation 4.15 with temperature from 80°C to 160°C and the results are shown in Figure 4.6 as well. As suspected, X_c of pure PLA was lower than that in the composite samples and X_c increased with RCF concentration.

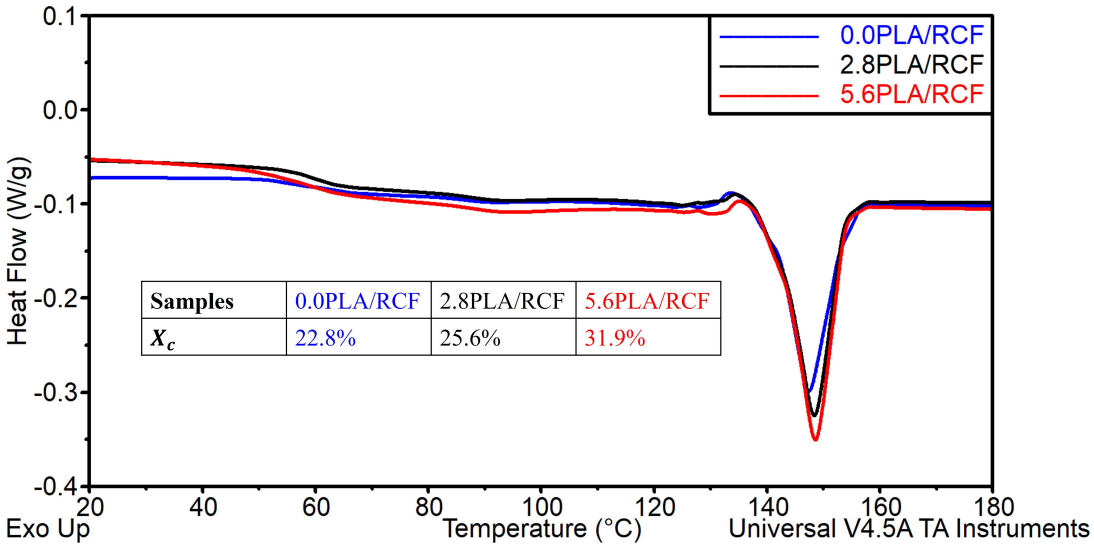

Figure 4.6: DSC thermograms and crystallinity of PLA and PLA/RCF composites with different RCF concentrations.

Another observation made from Figure 4.5 is that the delayed creep compliance decreased with increasing RCF concentration. For 0.0PLA/RCF samples, the compliance increased from 0.406 GPa^{-1} at $t = 0$ to 0.615 GPa^{-1} at $t = 900$ s, corresponding to an increment of 0.209 GPa^{-1}. During the same time frame, the delayed creep compliances were only 0.111 GPa^{-1} for 2.8PLA/RCF and 0.076 GPa^{-1} for 5.6PLA/RCF. In addition to the enhanced elasticity caused by RCF [69, 167], the hydrogen bonds formed between PLA and RCF acted as extra hinderance that reduced the mobility of PLA chains during creep [66, 69, 71, 173, 174].

4.4.3 Discussion

The model developed in this work only requires information on the constitutive relation of the constituents, concentration of the RCF and geometry of the RCF. No other fitting parameters are involved. A parametric study was conducted to demonstrate how this model may be applied to tailor the property of PLA/RCF composite (Figure 4.7).

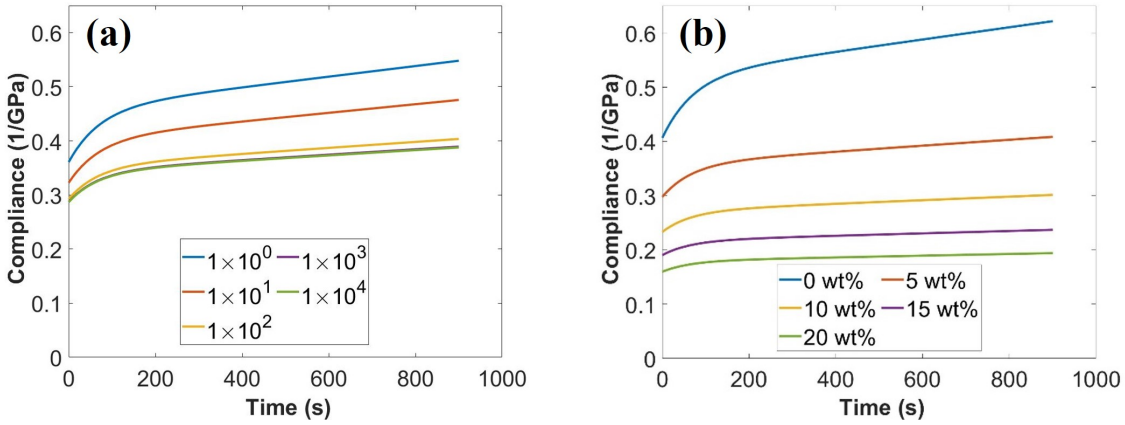

Figure 4.7: Parametric study on PLA/RCF composites using the developed model: (a) Varying fiber aspect ratio L_f/d_f for 5.6RCF/PLA; the other parameters in the model are fixed at the values shown in Table 4.2 (b) Varying fiber concentration, the other parameters in the model are fixed at the values shown in Table 4.2.

Figure 4.7a shows the effect of varying fiber aspect ratio L_f/d_f on the compliance of the composite. While increasing L_f/d_f causes decrease in compliance (increase in stiffness), the change starts to saturate when L_f/d_f reaches 10^2. This saturation point is known as the critical fiber aspect ratio and has been observe experimentally by different studies [175–177]. Since longer fibers usually require higher manufacturing costs, it is beneficial to determine the critical aspect ratio in order to produce cost-effective composites while maintaining desired mechanical properties [175]. The model developed here provides a tool to calculate this critical aspect ratio without extensive experimental testing. The effect of fiber concentration is shown in Figure 4.7b. Increasing fiber concentration not only increases the composite's stiffness, but also gradually converts the composite from a viscoelastic material to an elastic material, with an almost time-independent compliance when RCF concentration reaches 20 wt%. This is beneficial to applications that require constant load bearing capacity and small creep deformation, such as structural components in houses. Since excessive fiber embedment will cause discontinuity in the matrix phase and possible fiber entanglement [178], the model can be used to determine the minimum RCF concentration that will render acceptable level of time-dependency for the creep compliance.

Re-examination of Figure 4.5 reveals that compared with experimental data for 2.8PLA/RCF and 5.6PLA/RCF, the model slightly underestimated the initial elastic compliance and overestimated the delayed creep compliance. The material parameters used for 2.8PLA/RCF and 5.6PLA/RCF were extracted from pure RCF and PLA without modification (Table 4.2), while Figure 4.6 shows that the crystallinity of PLA was increased by the addition of RCF. This might explain the overestimated delayed creep compliance since the additional crystals formed can increase the elasticity as well as providing extra hinderance when polymer chains slip past each other under external load [86]. As a result, the material parameters of PLA (E_{m1}, E_{m2}, μ_{m1} and μ_{m2}) may increase as X_c increases, causing the delayed creep compliance to decrease [86]. For the underestimated instantaneous elastic compliance, we hypothesize that it might be due to the minor amount of moisture absorbed during the creep tests, which were conducted under 22% RH. Rozite et al. [12] discovered that the compliance of PLA/RCF composites increased as the RH level of the testing environment increased from 34% to 66%. The strong hydrophilicity of cellulose makes it susceptible to moisture adsorption, for example, Sahputra et al. [179] reported a drastic decrease of cellulose Young's modulus with increasing moisture content by both experiment and molecular dynamics simulation. To test the above hypotheses, the material parameters in the model were slightly modified, with the PLA parameters increased to reflect the increasing crystallinity and RCF Young's modulus slightly decreased to capture the effect of absorbed moisture. The predictions using the modified parameters are shown in Figure 4.8, which shows better comparison with experimental data. Future work can be done to model the effect of crystallinity and moisture more explicitly.

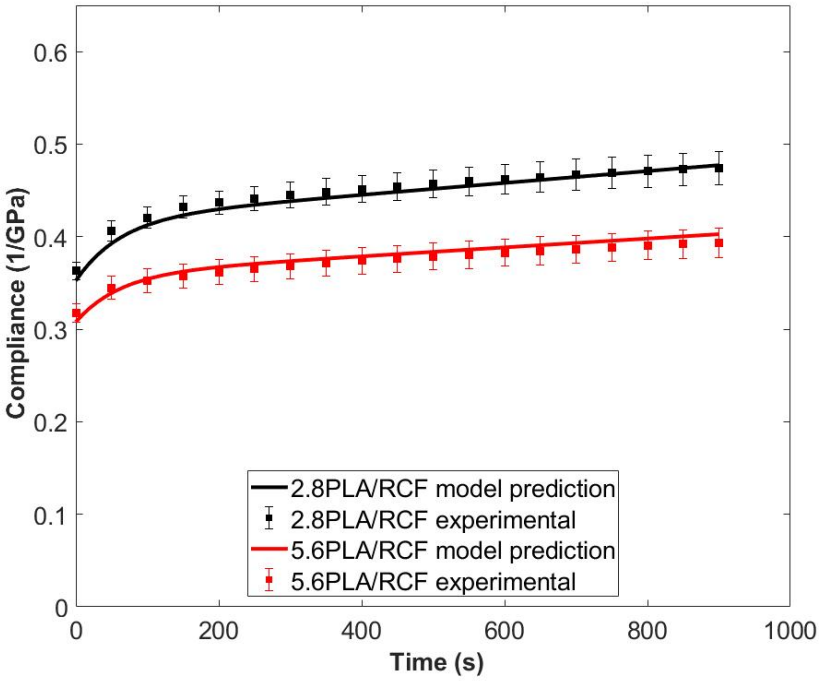

Figure 4.8: Demonstration of better comparison with experiments when accounting for increased PLA crystallinity caused by RCF and decreased RCF Young's modulus due to moisture absorption. The model prediction was generated using modified parameters of E_f = 39 GPa, E_{m1} = 11 GPa, μ_{m1} = 700 GPa·s, μ_{m2}=11000 GPa·s, other parameters of the model remain the same as those in Table 4.2.

4.5 Conclusion

The Halpin-Tsai-Pagano model for linear elastic composites was extended to the linear viscoelastic regime to describe the mechanical response of PLA/RCF bio-based composites. Based on the correspondence principle, the model only requires information on the constitutive relation of the constituents, concentration of the RCF and geometry of the RCF. Good agreement was found between model prediction and creep compliance measured experimentally for PLA/RCF composites with different RCF concentration. The addition of RCF reduced not only the instantaneous elastic compliance, but also the delayed creep compliance. A parametric study was performed to demonstrate the application of this model in modulating the composite properties and hence guiding the design and manufacturing of this bio-based composite. In addi-

tion, the model has the potential to predict other viscoelastic properties such as stress relaxation modulus for different types of short fiber reinforced bio-based composites.

References

[1] A. K. Kaw, *Mechanics of Composite Materials*, 2nd ed. CRC Press, 2006, p. 491.

[2] A. K. Mohanty, M Misra, and G Hinrichsen, "Biofibres, biodegradable polymers and biocomposites: An overview," *Macromolecular Materials and Engineering*, vol. 277, pp. 1–24, 2000.

[3] D. Bondeson and K. Oksman, "Dispersion and characteristics of surfactant modified cellulose whiskers nanocomposites," *Composite Interfaces*, vol. 14, pp. 617–630, 7-9 Sep. 2007, ISSN: 09276440. DOI: 10.1163/156855407782106519.

[4] A. K. Mohanty, M. Misra, and L. T. Drzal, *Natural fibers, biopolymers, and biocomposites*. Taylor and Francis, 2005.

[7] M. T. Shaw and W. J. MacKnight, *Introduction to Polymer Viscoelasticity*, 3rd ed. John Wiley and Sons, Inc., 2005, p. 327.

[9] R. A. Schapery, *Viscoelastic Behavior and Analysis of Composite Materials*, 1st ed., G. P. Sendeckyj, Ed. Academic Press, 1974, pp. 85–168.

[12] L. Rozite, J. Varna, R. Joffe, and A. Pupurs, "Nonlinear behavior of pla and lignin-based flax composites subjected to tensile loading," *Journal of Thermoplastic Composite Materials*, vol. 26, pp. 476–496, 4 May 2013, ISSN: 08927057. DOI: 10.1177/0892705711425846.

[13] B. Baghaei and M. Skrifvars, "Characterisation of polylactic acid biocomposites made from prepregs composed of woven polylactic acid/hemp-lyocell hybrid yarn fabrics," *Composites Part A: Applied Science and Manufacturing*, vol. 81, pp. 139–144, Feb. 2016, ISSN: 1359835X. DOI: 10.1016/j.compositesa.2015.10.042.

[15] J. W. Park, T. H. Lee, J. H. Back, S. W. Jang, H. J. Kim, and M. Skrifvars, "Phenyl silane treatment and carding process to improve the mechanical, thermal, and water-absorption properties of regenerated cellulose lyocell/polylactic acid bio-composites," *Composites Part B: Engineering*, vol. 167, pp. 387–395, Jun. 2019, ISSN: 13598368. DOI: 10.1016/j.compositesb.2019.02.064.

[23] I. Widiastuti, I. Sbarski, and S. H. Masood, "Mechanical behavior of a fluid-sensitive material during liquid diffusion," *Mechanics of Time-Dependent Materials*, vol. 18, pp. 387–406, 2 2014, ISSN: 13852000. DOI: 10.1007/s11043-014-9233-9.

[24] I. Widiastuti, I. Sbarski, and S. H. Masood, "Mechanical response of poly(lactic acid)-based packaging under liquid exposure," *Journal of Applied Polymer Science*, vol. 131, pp. 1–10, 16 2014.

[25] I. Widiastuti, I. Sbarski, and S. H. Masood, "Creep behavior of pla-based biodegradable plastic exposed to a hydrocarbon liquid," *Journal of Applied Polymer Science*, vol. 127, pp. 2654–2660, 4 2013, ISSN: 00218995. DOI: 10.1002/app.37575.

[39] K. M. Zakir, A. J. Parsons, C. D. Rudd, I. Ahmed, and W. Thielemans, "Mechanical , crystallisation and moisture absorption properties of melt drawn polylactic acid fibres," *European Polymer Journal*, vol. 53, pp. 270–281, 2014, ISSN: 0014-3057. DOI: 10.1016/j.eurpolymj.2014.02.001. [Online]. Available: http://dx.doi.org/10.1016/j.eurpolymj.2014.02.001.

[56] J. C. Halpin and J. L. Kardos, "The halpin-tsai equations: A review," *Polymer Engineering and Science*, vol. 16, pp. 345–352, 5 1976.

[57] S. W. Tsai and N. J. Pagano, "Invarient properties of composite materials," Air Force Materials Laboratory, May 1968.

[59] E Castro-aguirre, F Iñiguez-franco, H Samsudin, X Fang, and R Auras, "Poly (lactic acid) — mass production , processing , industrial applications , and end of life," *Advanced Drug Delivery Reviews*, vol. 107, pp. 333–366, 2016, ISSN: 0169-409X. DOI: 10.1016/j.addr.2016.03.010. [Online]. Available: http://dx.doi.org/10.1016/j.addr.2016.03.010.

[60] D. Tzetzis, K. Tsongas, and G. Mansour, "Determination of the mechanical properties of epoxy silica nanocomposites through fea-supported evaluation of ball indentation test results," *Journal of Materials Research*, vol. 20, pp. 1571–1578, 6 Nov. 2017, ISSN: 15161439. DOI: 10.1590/1980-5373-MR-2017-0454.

[61] N. Kurokawa and A. Hotta, "Regenerated cellulose nanofibers fabricated through electrospinning and saponification of cellulose acetate as reinforcement of polylactide composites," *Cellulose*, vol. 26, pp. 7797–7808, 13-14 Sep. 2019, ISSN: 1572882X. DOI: 10.1007/s10570-019-02623-6.

[62] R. Auras, L. Lim, S. M. Selke, and H. Tsuji, *Polylactic Acid, Synthesis, Structures, Properties, Processing, and Applications*. John Wiley and Sons, 2010.

[63] N. F. Zaaba and M. Jaafar, "A review on degradation mechanisms of polylactic acid: Hydrolytic, photodegradative, microbial, and enzymatic degradation," *Polymer Engineering and Science*, vol. 60, pp. 2061–2075, 9 2020, ISSN: 15482634. DOI: 10.1002/pen.25511.

[64] M. Funabashi, F. Ninomiya, and M. Kunioka, "Biodegradability evaluation of polymers by iso 14855-2," *International Journal of Molecular Sciences*, vol. 10, pp. 3635–3654, 8 Aug. 2009, ISSN: 14220067. DOI: 10.3390/ijms10083635.

[65] M. Shibata, S. Oyamada, S.-I. Kobayashi, and D. Yaginuma, "Mechanical properties and biodegradability of green composites based on biodegradable polyesters and lyocell fabric," *Journal of Applied Polymer Science*, vol. 92, pp. 3857–3863, 2004.

[66] M. S. Huda, A. K. Mohanty, L. T. Drzal, E Schut, and M Misra, "Green composites from recycled cellulose and poly(lactic acid): Physico-mechanical and morphological properties evaluation," *Journal of Materials Science*, vol. 40, pp. 4221–4229, 2005.

[67] A. K. Bledzki, A. Jaszkiewicz, and D. Scherzer, "Mechanical properties of pla composites with man-made cellulose and abaca fibres," *Composites Part A: Applied Science and Manufacturing*, vol. 40, pp. 404–412, 4 Apr. 2009, ISSN: 1359835X. DOI: 10.1016/j.compositesa.2009.01.002.

[68] B. Bax and J. Müssig, "Impact and tensile properties of pla/cordenka and pla/flax composites," *Composites Science and Technology*, vol. 68, pp. 1601–1607, 7-8 Jun. 2008, ISSN: 02663538. DOI: 10.1016/j.compscitech.2008.01.004.

[69] M. S. Huda, L. T. Drzal, A. K. Mohanty, and M. Misra, "Chopped glass and recycled newspaper as reinforcement fibers in injection molded poly(lactic acid) (pla) composites: A comparative study," *Composites Science and Technology*, vol. 66, pp. 1813–1824, 11-12 Sep. 2006, ISSN: 02663538. DOI: 10.1016/j.compscitech.2005.10.015.

[70] B. Geissler, M. Feuchter, S. Laske, M. Fasching, C. Holzer, and G. R. Langecker, "Strategies to improve the mechanical properties of high-density polylactic acid foams," *Journal of Cellular Plastics*, vol. 52, pp. 15–35, 1 Jan. 2016, ISSN: 15307999. DOI: 10.1177/0021955X14538274.

[71] B. Baghaei, M. Skrifvars, M. Rissanen, and S. K. Ramamoorthy, "Mechanical and thermal characterization of compression moulded polylactic acid natural fiber composites reinforced with hemp and lyocell fibers," *Journal of Applied Polymer Science*, vol. 131, 15 Aug. 2014, ISSN: 10974628. DOI: 10.1002/app.40534.

[73] Y. Chen, T. Tang, and C. Ayranci, "Moisture-induced anti-plasticization of polylactic acid: Experiments and modeling," *Journal of Applied Polymer Science*, vol. 139, 24 Jun. 2022, ISSN: 10974628. DOI: 10.1002/app.52369.

[85] R. M. Christensen, *Theory of Viscoelasticity, An Introduction*, 2nd ed. Dover Publications Inc., 2003, p. 363.

[86] L. Sperling, *Introduction to Physical Polymer Science*. John Wiley and Sons, Inc, 2006.

[91] W. N. Findley, *Creep and relaxation of nonlinear viscoelastic materials : with an introduction to linear viscoelasticity*, W. N. Findley, J. S. Lai, and K. Onaran, Eds. Dover Publications Inc., 1989, p. 380.

[110] A. Singh, R. M. Guedes, D. Paiva, and F. D. Magalhães, "Experiment and modelling of the strain-rate-dependent response during in vitro degradation of pla fibres," *SN Applied Sciences*, vol. 2, pp. 1–18, 2 2020, ISSN: 25233971. DOI: 10.1007/s42452-020-1964-4. [Online]. Available: https://doi.org/10.1007/s42452-020-1964-4.

[120] E. H. Backes, L. de N. Pires, L. C. Costa, F. R. Passador, and L. A. Pessan, "Analysis of the degradation during melt processing of pla/biosilicate® composites," *Journal of Composites Science*, vol. 3, p. 52, 2 2019.

[125] "Astm d2990-17 standard test methods for tensile, compressive, and flexureal creep and creep-rupture of plastics," Tech. Rep., 2017.

[134] P. K. Bajpai, I. Singh, and J. Madaan, "Development and characterization of pla-based green composites: A review," *Journal of Thermoplastic Composite Materials*, vol. 27, pp. 52–81, 1 2014, ISSN: 08927057. DOI: 10.1177/0892705712439571.

[135] V. K. Thakur, M. K. Thakur, P. Raghavan, and M. R. Kessler, "Progress in green polymer composites from lignin for multifunctional applications: A review," *ACS Sustainable Chemistry and Engineering*, vol. 2, pp. 1072–1092, 5 2014, ISSN: 21680485. DOI: 10.1021/sc500087z.

[136] G. Koronis and A. Silva, *Green Composites for Automotive Applications*. Woodhead Publishing, 2019.

[137] K. Jha, R. Kataria, J. Verma, and S. Pradhan, "Potential biodegradable matrices and fiber treatment for green composites: A review," *AIMS Materials Science*, vol. 6, pp. 119–138, 1 2019, ISSN: 23720468. DOI: 10.3934/matersci.2019.1.119.

[138] A. K. Bledzki and A. Jaszkiewicz, "Mechanical performance of biocomposites based on pla and phbv reinforced with natural fibres - a comparative study to pp," *Composites Science and Technology*, vol. 70, pp. 1687–1696, 12 2010, ISSN: 02663538. DOI: 10.1016/j.compscitech.2010.06.005. [Online]. Available: http://dx.doi.org/10.1016/j.compscitech.2010.06.005.

[139] A. K. Bledzki and J Gassan, "Composites reinforced with cellulose based fibres," *Progress in Polymer Science*, vol. 24, pp. 221–274, 1999.

[140] V. Placet, O. Cisse, V. Guicheret-Retel, F. Trivaudey, and L. Boubakar, "Viscoelastic behaviour of single hemp fibre under constant and cyclic humidity environment - experiment and modelling," *ICCM International Conferences on Composite Materials*, vol. 2015-July, July 2015.

[141] S. Oza, H. Ning, I. Ferguson, and N. Lu, "Effect of surface treatment on thermal stability of the hemp-pla composites: Correlation of activation energy with thermal degradation," *Composites Part B: Engineering*, vol. 67, pp. 227–232, 2014, ISSN: 13598368. DOI: 10.1016/j.compositesb.2014.06.033.

[142] A. Jabbar, M. Tausif, H. R. Tahir, A. Basit, M. R. A. Bhatti, and G. Abbas, "Polylactic acid/lyocell fibre as an eco-friendly alternative to polyethylene terephthalate/cotton fibre blended yarns and knitted fabrics," *Journal of The Textile Institute*, vol. 111, pp. 129–138, 1 Jan. 2020, ISSN: 17542340. DOI: 10.1080/00405000.2019.1624070.

[143] G. Rajeshkumar *et al.*, "Environment friendly, renewable and sustainable poly lactic acid (pla) based natural fiber reinforced composites – a comprehensive review," *Journal of Cleaner Production*, vol. 310, p. 127 483, May 2021, ISSN: 09596526. DOI: 10.1016/j.jclepro.2021.127483. [Online]. Available: https://doi.org/10.1016/j.jclepro.2021.127483.

[144] J. Ganster and H. P. Fink, "Novel cellulose fibre reinforced thermoplastic materials," *Cellulose*, vol. 13, pp. 271–280, 3 Jun. 2006, ISSN: 09690239. DOI: 10.1007/s10570-005-9045-9.

[145] M. Sawpan, K. Pickering, and A. Fernyhough, "Hemp fibre reinforced poly(lactic acid) composites," *Advanced Materials and Processes*, vol. 29-30, pp. 337–340, 2007, ISSN: 1662-8985. [Online]. Available: http://www.scientific.net/AMR.29-30.337.

[146] N. Graupner, "Improvement of the mechanical properties of biodegradable hemp fiber reinforced poly(lactic acid) (pla) composites by the admixture of man-made cellulose fibers," *Journal of Composite Materials*, vol. 43, pp. 689–702, 6 2009, ISSN: 00219983. DOI: 10.1177/0021998308100688.

[147] B. Baghaei, M. Skrifvars, and L. Berglin, "Manufacture and characterisation of thermoplastic composites made from pla/hemp co-wrapped hybrid yarn prepregs," *Composites Part A: Applied Science and Manufacturing*, vol. 50, pp. 93–101, 2013, ISSN: 1359835X. DOI: 10.1016/j.compositesa.2013.03.012. [Online]. Available: http://dx.doi.org/10.1016/j.compositesa.2013.03.012.

[148] L. Suryanegara, A. N. Nakagaito, and H. Yano, "The effect of crystallization of pla on the thermal and mechanical properties of microfibrillated cellulose-reinforced pla composites," *Composites Science and Technology*, vol. 69, pp. 1187–1192, 7-8 Jun. 2009, ISSN: 02663538. DOI: 10.1016/j.compscitech.2009.02.022.

[149] M. A. Elsawy, K. H. Kim, J. W. Park, and A. Deep, "Hydrolytic degradation of polylactic acid (pla) and its composites," *Renewable and Sustainable Energy Reviews*, vol. 79, pp. 1346–1352, November 2017, ISSN: 18790690. DOI: 10.1016/j.rser.2017.05.143. [Online]. Available: http://dx.doi.org/10.1016/j.rser.2017.05.143.

[150] M. Bulota, S. Tanpichai, M. Hughes, and S. J. Eichhorn, "Micromechanics of tempo-oxidized fibrillated cellulose composites," *ACS Applied Materials and Interfaces*, vol. 4, pp. 331–337, 1 Jan. 2012, ISSN: 19448244. DOI: 10.1021/am201399q.

[151] M. A. Sawpan, K. L. Pickering, and A. Fernyhough, "Improvement of mechanical performance of industrial hemp fibre reinforced polylactide biocomposites," *Composites Part A: Applied Science and Manufacturing*, vol. 42, pp. 310–319, 3 2011, ISSN: 1359835X. DOI: 10.1016/j.compositesa.2010.12.004. [Online]. Available: http://dx.doi.org/10.1016/j.compositesa.2010.12.004.

[152] S. H. Lee, S. Wang, and Y. Teramoto, "Isothermal crystallization behavior of hybrid biocomposite consisting of regenerated cellulose fiber, clay, and poly(lactic acid)," *Journal of Applied Polymer Science*, vol. 108, pp. 870–875, 2 Apr. 2008, ISSN: 00218995. DOI: 10.1002/app.26853.

[153] M. M. Kim, B. S. Kim, J. R. Ha, S. K. Kim, J. W. Yi, and J. Y. Lim, "Interfacial optimization of lyocell fabric/pla with silane treatments," *Advanced Materials Research*, vol. 123-125, pp. 1155–1158, 2010, ISSN: 10226680. DOI: 10.4028/www.scientific.net/amr.123-125.1155.

[154] J. H. Lin, A. P. Chen, J. Y. Lin, T. A. Lin, and C. W. Lou, "Manufacturing technique and mechanical properties of environment-protective composite nonwoven fabrics," *Advanced Materials Research*, vol. 287-290, pp. 2673–2676, 2011, ISSN: 10226680. DOI: 10.4028/www.scientific.net/AMR.287-290.2673.

[155] C. Woodings, *Regenerated cellulose fibers*. CRC Press LLC, 2001.

[156] S. Zhang *et al.*, "Regenerated cellulose by the lyocell process, a brief review of the process and properties," *BioResources*, vol. 13, pp. 4577–4592, 2 2018.

[157] Y. Zhang *et al.*, "Biodegradable regenerated cellulose-dispersed composites with improved properties via a pickering emulsion process," *Carbohydrate Polymers*, vol. 179, pp. 86–92, Jan. 2018, ISSN: 01448617. DOI: 10.1016/j.carbpol.2017.09.065.

[158] A. Karakoç, A. Miettinen, J. Virkajarvi, and R. Joffe, "Effective elastic properties of biocomposites using 3d computational homogenization and x-ray microcomputed tomography," *Composite Structures*, vol. 273, Oct. 2021, ISSN: 02638223. DOI: 10.1016/j.compstruct.2021.114302.

[159] B. Raju, S. R. Hiremath, and D. R. Mahapatra, "A review of micromechanics based models for effective elastic properties of reinforced polymer matrix composites," *Composite Structures*, vol. 204, pp. 607–619, Nov. 2018, ISSN: 02638223. DOI: 10.1016/j.compstruct.2018.07.125.

[160] F. Vilaseca, R. D. Rey, R. Serrat, J. Alba, P. Mutje, and F. X. Espinach, "Macro and micro-mechanics behavior of stifness in alkaline treated hemp core fibres polypropylene-based composites," *Composites Part B: Engineering*, vol. 144, pp. 118–125, Jul. 2018, ISSN: 13598368. DOI: 10.1016/j.compositesb.2018.02.029.

[161] V. Mazzanti, R. Pariante, A. Bonanno, O. R. de Ballesteros, F. Mollica, and G. Filippone, "Reinforcing mechanisms of natural fibers in green composites: Role of fibers morphology in a pla/hemp model system," *Composites Science and Technology*, vol. 180, pp. 51–59, May 2019, ISSN: 02663538. DOI: 10.1016/j.compscitech.2019.05.015. [Online]. Available: https://doi.org/10.1016/j.compscitech.2019.05.015.

[162] N. Pan, "The elastic constants of randomly oriented fiber composites: A new approach to prediction," *Science and Engineering of Composite Materials*, vol. 5, pp. 63–72, 2 1996.

[163] G. Jiang *et al.*, "Structure and properties of regenerated cellulose fibers from different technology processes," *Carbohydrate Polymers*, vol. 87, pp. 2012–2018, 3 Feb. 2012, ISSN: 01448617. DOI: 10.1016/j.carbpol.2011.10.022.

[164] Z. Hashin, "Complex moduli of viscoelastic composites-ii. fiber reinforced materials," *International Journal of Solids and Structures*, vol. 6, pp. 797–807, 6 1970, ISSN: 00207683. DOI: 10.1016/0020-7683(70)90018-1. [Online]. Available: http://dx.doi.org/10.1016/0020-7683(70)90018-1.

[165] J. C. Halpin, *Primer on Composite Materials Analysis*, 1st ed. CRC Press, 1992, p. 240.

[166] *How is biomid fiber made*, 2018. [Online]. Available: https://biomidfiber.com/.

[167] I. I. Qamhia, "Experimental and analytical characterization of regenerated/-nano cellulose composites," University of Wisconsin-Milwaukee, 2014. [Online]. Available: http://dc.uwm.edu/etd.

[168] M. Legault, *Bio-composites update: Beyong eco-branding*, Jun. 2013. [Online]. Available: https://www.compositesworld.com/articles/biocomposites-update-beyond-eco-branding.

[169] "Astm d3379-75 standard test method for tensile strength and young's modulus for high-modulus single-filament materials," Tech. Rep., 1989.

[170] L Lim, R Auras, and M Rubino, "Processing technologies for poly (lactic acid)," *Progress in Polymer Science*, vol. 33, pp. 820–852, 2008. DOI: 10.1016/j.progpolymsci.2008.05.004.

[171] F. EW, S. HJ, and W. G, "Investigation of the structure of solution grown crystals of lactide copolymers by means of chemical reactions," *Kolloid-Zeitschrift und Zeitschrift für Polymere*, pp. 980–990, 251 1973.

[172] A. Pei, Q. Zhou, and L. A. Berglund, "Functionalized cellulose nanocrystals as biobased nucleation agents in poly(l-lactide) (plla) - crystallization and mechanical property effects," *Composites Science and Technology*, vol. 70, pp. 815–821, 5 May 2010, ISSN: 02663538. DOI: 10.1016/j.compscitech.2010.01.018.

[173] L. Suryanegara, A. N. Nakagaito, and H. Yano, "Thermo-mechanical properties of microfibrillated cellulose-reinforced partially crystallized pla composites," *Cellulose*, vol. 17, pp. 771–778, 4 2010, ISSN: 09690239. DOI: 10.1007/s10570-010-9419-5.

[174] Z. Ren, R. Guo, H. Bi, X. Jia, M. Xu, and L. Cai, "Interfacial adhesion of polylactic acid on cellulose surface: A molecular dynamics study," *ACS Applied Materials and Interfaces*, vol. 12, pp. 3236–3244, 2 Jan. 2020, ISSN: 19448252. DOI: 10.1021/acsami.9b20101.

[175] L. Monette, M. P. Anderson, and G. S. Grest, "The meaning of the critical length concept in composites: Study of matrix viscosity and strain rate on the average fiber fragmentation length in short-fiber polymer composites," *Polymer Composites*, vol. 14, pp. 101–115, 2 1993, ISSN: 15480569. DOI: 10.1002/pc.750140204.

[176] S. R. Ryu and D. J. Lee, "Effects of fiber aspect ratio, fiber content, and bonding agent on tensile and tear properties of short-fiber reinforced rubber," *KSME International Journal*, vol. 15, pp. 35–43, 1 2001, ISSN: 12264865. DOI: 10.1007/BF03184796.

[177] I. Robinson and J. Robinson, "The effect of fibre aspect ratio on the stiffness of discontinuous fibre-reinforced composites," *Composites*, vol. 25, p. 499, 7 1994.

[178] S. Houshyar, R. A. Shanks, and A. Hodzic, "The effect of fiber concentration on mechanical and thermal properties of fiber-reinforced polypropylene composites," *Journal of Applied Polymer Science*, vol. 96, pp. 2260–2272, 6 Jun. 2005, ISSN: 00218995. DOI: 10.1002/app.20874.

[179] I. H. Sahputra, A. Alexiadis, and M. J. Adams, "Effects of moisture on the mechanical properties of microcrystalline cellulose and the mobility of the water molecules as studied by the hybrid molecular mechanics–molecular dynamics simulation method," *Journal of Polymer Science, Part B: Polymer Physics*, vol. 57, pp. 454–464, 8 Apr. 2019, ISSN: 10990488. DOI: 10.1002/polb.24801.

Chapter 5

Modeling creep compliance of bio-based composites subjected to moisture diffusion

5.1 Introduction

With increasing environmental concerns associated with using non-degradable materials, the development of bio-based composites has drawn much interest in research and engineering [6, 66]. Bio-based composites are defined as composites made from biorenewable and biodegradable constituents [4, 68]. Cellulosic natural fibers and regenerated cellulose fibers (RCF) have become promising candidates to replace conventional synthetic fibers as reinforcements [6, 13, 15, 71, 152, 153, 180]. Biodegradable polymers such as poly(lactic) acid (PLA) and poly(3-hydroxybutyrate-co-3-hydroxyvalerate) (PHBV) are commonly used as alternatives for petroleum-based matrices of composites [55, 139, 181, 182]. In the past decade, these bio-based composites have been used in a variety of industries such as automotive, aerospace, sports, packaging, construction, etc. [6, 48, 52, 180, 181, 183, 184].

In the development and application of bio-based composites, understanding and predicting the mechanical behavior is one of the most important aspects [1]. Humid working conditions have discovered to possess detrimental effects on the mechanical properties of bio-based composites. For example, Panthapulakkal et al. [185], Al-

varez et al. [186], Chow et al. [187] and Lu et al. [188] all reported a decreased Young's modulus with respect to increasing moisture content for various bio-based composites. Rozite et al. [12] discovered that, under the same creep stress, the creep strain of both PLA/flax composites and PLA/RCF bio-based composites increased significantly when the relative humidity (RH) of the creep tests increased from 34% to 66%. Chapter 4 also highlighted that using the mechanical properties of PLA and RCF without moisture content will underestimate the creep compliance of PLA/RCF tested under 22% RH environment. It is worth noting that, in applications such as dashboards and door panels in automotive industry, as well as doors and roofing sheets in construction industry, bio-based composites are frequently subjected drastic humidity changes during their entire service lives [4, 136]. Thus, the moisture-dependent mechanical properties may affect the functioning of the products made from these bio-based composites.

The moisture-dependent mechanical properties originate from the hydrophilicity of the constituents [32]. The different chemical potential of water between the inside and outside of these composites provides driving force for the water molecules to diffuse into or out of the composites [122]. As such, water molecules will interact with the molecular chains affect its mechanical behavior [22]. Complex phenomena including hydrolysis, plasticization, anti-plasticization, swelling mismatch and fiber/-matrix interfacial debonding may occur during moisture diffusion process [29, 30, 63, 72]. Both matrix and fiber reinforcement may be hydrolyzed by water molecules, and this is the initial step for its biodegradation process [63, 189]. However, the time scale for hydrolysis reaction to impose any significant effect on mechanical properties could be years under room temperature and mild ambient humidity level [31], thus it is usually not considered during modeling. According to Chen et al. [72], water molecules may attach to the molecular chains of hydrophilic fiber and matrix materials or form water clusters within them, which could cause anti-plasticization and plasticization effect, respectively. The combination of these two effects may lead to a

non-monotonical change of mechanical properties of the material with respect to its moisture content [72, 73]. Swelling mismatch and fiber/matrix interface debonding caused by diffused water molecules will impair the mechanical properties of the bio-based composites [29, 48, 49, 53, 55]. More specifically, in most cases, the fibers are more hydrophilic and will absorb significantly more moisture than the matrix [190]. Thus, the larger fiber swelling will create an internal stress within the composites and damage the overall stiffness of the composites [29, 50]. Fiber/matrix interfacial debonding originates from the widely existed hydrogen bonds between the surfaces of fiber and matrix in bio-based composites [174, 191]. The strength of hydrogen bonds will be weakened by those diffused water molecules and delamination between the fiber/matrix interface may happen under the external load [92, 174, 192]. In summary, the moisture-dependent mechanical properties of these bio-based composites have become one of the major challenges in the wide-spread application of these bio-based composites. It is important to be able to model and predict the moisture-dependence of the mechanical properties of these bio-based composites.

In the literature, efforts have been devoted to model the effect of moisture on the mechanical properties of bio-based composites. Under the framework of Mori-Tanaka model, Pan and Zhong [29, 50] proposed to use damage coefficients to consider the swelling mismatch between fiber and matrix. The model was then extended by Kamau et al. [55] to account for the fiber/matrix interface debonding caused by absorbed moisture and the model prediction was validated with the results of wood fiber reinforced PLA bio-based composites. However, both models assumed the state of equilibrium moisture content. To account for the moisture diffusion process, Pan and Zhong [47–49, 51, 53] formulated a Helmholtz free energy of the composite system and considered the moisture diffusion process as a thermodynamically irreversible process involving energy dissipation. The composites' mechanical properties change due to the change of fiber mechanical properties, fiber/matrix interface debonding and hygroscopic mismatch of the swollen fiber and matrix were all considered the in

their model by introducing different empirical parameters [48, 49, 53]. The model has been validated with experimental results of unidirectional long natural fiber reinforced bio-based composites [48], randomly oriented short natural fiber reinforced bio-based composites [53], wood cell wall [49], and hybridized fiber reinforced composites consists of natural fibers and synthetic fibers [54]. Wang et al. [52] further attempted this model to predict the mechanical behavior of bidirectional natural fiber reinforced bio-based composites under buckling and vibration. Despite the success of the model in elasticity, application of this model in the viscoelastic regime was not investigated and reported in the literature. In fact, a variety of studies have demonstrated the importance to consider the viscoelasticity of bio-based composites because almost all biopolymer matrices exhibit viscoelastic behavior such as creep and stress relaxation [7, 12, 182, 193]. To the best of the authors' knowledge, only Sun et al. [183] used Schapery's nonlinear creep model to describe the creep behavior, and the effect of moisture is represented by a linear relation between the model parameters and moisture content. However, the limitation of their work is that the physics of moisture diffusion and the mechanism of how moisture affect the mechanical properties were not considered during the development of the models. Therefore, the existing studies lack a model that can predict the viscoelasticity of bio-based composites during moisture diffusion based on the considerations of the fundamental of physics.

For the broader application and adaptation of these bio-based composites, a predictive model that can accurately account for the viscoelasticity of bio-based composites with respect to moisture diffusion is necessary. Therefore, the objective of this article is to develop a simple yet useful semi-empirical model to describe the viscoelastic properties of bio-based composites during moisture diffusion. The proposed model is validated with experimental results of PLA/RCF bio-based composites. Although the model is semi-empirical, its success in describing the creep behavior of this PLA/RCF bio-composites during moisture diffusion has been demonstrated.

5.2 Model

The physical phenomena that need to be considered includes moisture-dependent mechanical properties of the constituents, swelling mismatch and interfacial debonding. Also, the diffusion process leads to a spatially non-uniform moisture content within the bio-based composites, which also needs to be considered. These will be discussed and modeled in this section.

5.2.1 Moisture-dependent mechanical properties of the constituents

Among the existing studies, only Pan and Zhong [47] considered the moisture-dependent mechanical properties of fiber reinforcements, which in turn affect the overall mechanical properties of the bio-based composites. Their consideration was only limited to plasticization effect of moisture while existing studies have shown the existence of anti-plasticization effect especially at relatively low moisture content [20, 22, 72]. Thus, our group's previous work [72] proposed modified Reimschuessel model shown in equation 5.1 to describe the effect of moisture on the constitutive relation of hydrophilic polymers by considering both plasticization and anti-plasticization. In short, any material's parameters P with respect to equilibrium moisture content C_e can be given by:

$$P(C_e) = P_s + (P_0 - P_s)\exp(-k_p C_e) + (k_A C_e)\exp(-k_D C_e) \tag{5.1}$$

where P_s is the saturation level of the parameter at large C_e; P_0 is the value of this parameter when $C_e = 0$; k_p is a positive constant that describes the exponential decay of this parameter due to plasticization; k_A is a positive constant that describes the magnitude of the anti-plasticization effect and k_d is also a positive constant that describes the exponential decay of anti-plasticization effect.

For bio-based composites, the reinforcement fibers usually exhibit linear elasticity [182], thus the modified Hookean-Reimschuessel model given by equation 5.2 is

proposed here to describe the moisture-dependent constitutive relation of the fibers.

$$\sigma_f = E_f(C_{fe})\varepsilon_f \tag{5.2}$$

where σ_f and ε_f are stress and strain of the material, respectively; $E\left(C_{fe}\right)$ is the moisture dependent Young's modulus which is given by the modified Reimschuessel model shown in equation 5.1.

In terms of matrix materials, Burgers model has demonstrated success in describing the constitutive relation since it can capture the essential features of polymer viscoelasticity, which is given by equation 5.3 [86, 91].

$$\frac{\mu_{m1}\mu_{m2}}{E_{m1}}\frac{d^2\varepsilon_m}{dt^2} + \mu_{m2}\frac{d\varepsilon_m}{dt} = \frac{\mu_{m1}\mu_{m2}}{E_{m1}E_{m2}}\frac{d^2\sigma_m}{dt^2} + \left(\frac{\mu_{m1}}{E_{m1}} + \frac{\mu_{m2}}{E_{m1}} + \frac{\mu_{m2}}{E_{m2}}\right)\frac{d\sigma_m}{dt} + \sigma_m \tag{5.3}$$

where E_{m1}, E_{m2}, μ_{m1} and μ_{m2} are moisture-dependent material parameters given by equation 5.1. σ_m and ε_m are stress and strain of the matrix, respectively.

5.2.2 Fiber/matrix swelling mismatch and interfacial debonding

The phenomena of swelling and fiber/matrix interfacial debonding can be described by an equvalent composite reinforced by a weaker effective fiber with no swelling mismatch and interfacial debonding. The Young's modulus of the effective fiber is related to the Young's modulus E_f of the original fiber and the moisture content of the composites C_c. A single damage coefficient C_{da}, which depends on the overall moisture content of composites C_c is proposed here and the Young's modulus of the effective fiber reinforcement E_{f-eff} is given by equation 5.4.

$$E_{f-eff} = C_{da}\left(C_c\right)E_f\left(C_{fe}\right) \tag{5.4}$$

Previous studies discovered that both the decreasing trend of mechanical properties caused by swelling mismatch and interface debonding are more significant at low moisture content and slow down as moisture content is high, which is similar to the plasticization effect caused by moisture absorption [50, 194]. Thus, to properly

described this phenomenon while maintaining simplicity of the model, we propose the following relation between the damage coefficient C_{da} and moisture content of the composites C_c.

$$C_{da} \equiv \exp\left(-k_{da} C_c\right) \tag{5.5}$$

where k_{da} is a positive constant and can be fitted by experimental results.

5.2.3 Moisture diffusion

The moisture concentration within the composites would be a smooth distribution from boundary to the center of the material at any given time t [122]. Studying the coupled effect of time-dependent moisture diffusion and time-dependent viscoelastic mechanical behavior could be a difficult task since there is a continuous variation of mechanical properties within the material due to the continuous spatial change in moisture concentration. Thus, to simplify the model while maintaining reasonable accuracy, this work proposes a two-layer layer model that consists of a surface layer near the boundary of the samples while inner layer at the center of the material to describe both the moisture concentration and the moisture-dependent mechanical properties. The moisture diffusion process is captured by a time-dependent areal fraction of the inner layer. To demonstrate this, considering a sheet sample shown by Figure 5.1a acquired equilibrium state of moisture content in a higher RH environment and placed in a lower RH environment, the moisture content at the surface layer is assumed to be the equilibrium moisture content for this sample placed in the lower RH environment, the moisture content at the inner layer will be the equilibrium moisture content for this sample placed in the higher RH environment. As an example, a typical one-dimensional diffusion pattern is shown in Figure 5.1b based on Fick's law of diffusion [122] and the corresponding two-layer model is shown by Figure 5.1c. With this two-layer model, the time-dependent moisture concentration change is represented by the change of the areal fraction $f(t)$ of the inner layer, as demonstrated by Figure 5.1c.

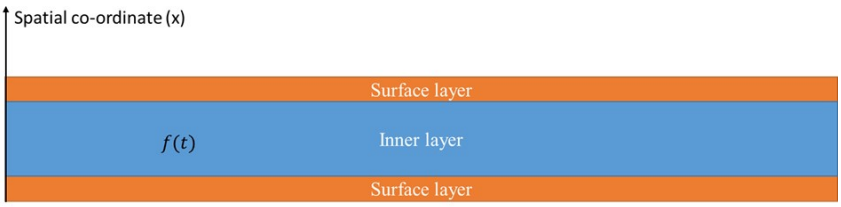

(a)

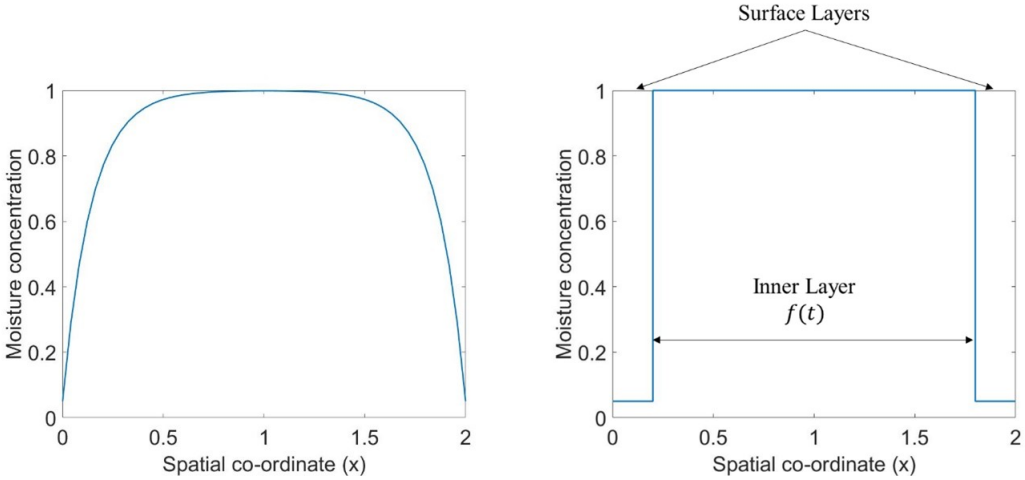

(b) (c)

Figure 5.1: Demonstration two-layer model (a) the schematic drawing of the cross section of the proposed two-layer model (b) actual diffusion pattern at time t in one-dimensional case; (c) the approximated two-layer model at time t for this one-dimensional case.

Based on the observation of diffusion pattern shown in Figure 5.1b, we propose that in this one-dimensional case, areal fraction of inner layer $f(t)$ (area of the inner lay divided by the overall area of the cross-section) varies with time t according to equation 5.6.

$$f(t) \equiv \exp(-k_w t) \tag{5.6}$$

where k_w is a positive constant that describes the shrinkage of inner layer thickness.

5.2.4 Model application to a sheet sample as a case study

To demonstrate the application of this model, consider a sheet sample shown in Figure 5.2a with fiber reinforcements homogeneously distributed and randomly oriented. This type of samples has been widely used in a variety of applications such as door

panels and roofing sheets due to its statistical homogeneity, isotropy and ease in manufacturing process [162]. Also, the samples acquired equilibrium state of moisture content in a higher level of RH environment and placed in a lower level of RH environment as the load applies. Since the surface area on the two large surfaces is significantly larger than the areas on the four edges of the samples, the distribution of moisture concentration within the sample can be considered as a one-dimensional diffusion along the thickness of the sample. The proposed two-layer model in this case is demonstrated in Figure 5.2b, in which the surface layers possess equilibrium moisture content of this composites at the lower level of RH (indicated by orange) and inner layer possesses equilibrium moisture content of this composites at the higher level of RH (indicated by blue). The thickness of the inner layer is time dependent and can be given by the product of the overall thickness w and thickness proportion function $f(t)$ given by equation 5.6.

For the loading of the sample, a simple tensional creep loading condition is considered here, i.e., upon placing the samples in the lower RH environment, an instantaneous tensional stress σ_0 is applied to the samples at time $t = 0$. In this case, the coupling effect of external load and moisture diffusion can be neglected since existing studies have shown that the diffusivity of a material is a function of its applied stress [195]. Finally, similar to Chapter 4, the example here only considers relatively small load, thus linear viscoelastic assumption shall be made.

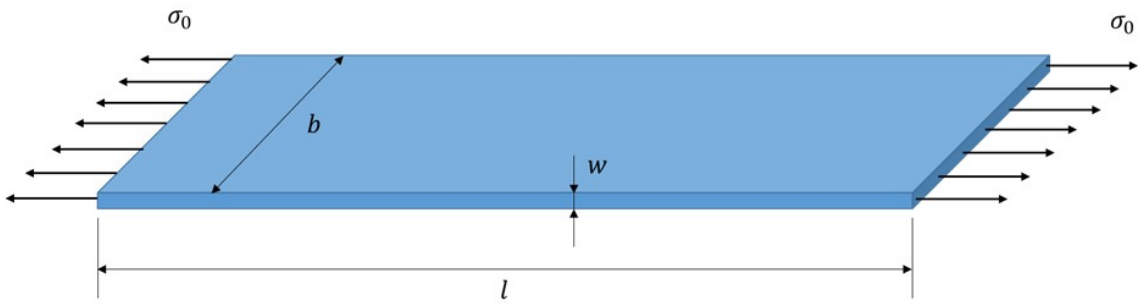

(a)

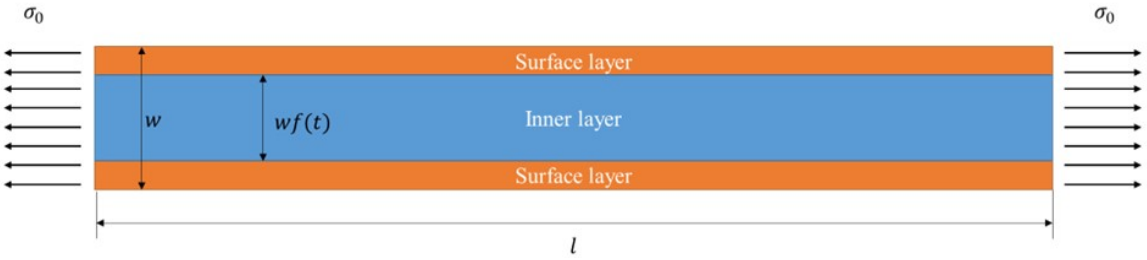

(b)

Figure 5.2: (a) Sheet sample with length l, width b and thickness w, under one-dimensional tensional load (σ_0); (b) Demonstration of the two-layer model at the longitudinal cross-section of the sheet sample

Assembly of the layers

The bonding between surface layer and inner layer is assumed to be perfect thus this two-layer model shall be considered as a Voight parallel model [159]. Since the samples are subjected to a constant stress σ_0, based on Figure 5.2b, this one-dimensional Voight parallel model can be described by equation 5.7.

$$[1 - f(t)]\,\sigma_S(t) + f(t)\,\sigma_I(t) = \sigma_0 \tag{5.7}$$

where $\sigma_S(t)$ and $\sigma_I(t)$ are the stress in the surface and inner layers, respectively. Since both layers are linear viscoelastic materials, their constitutive relations can be given by equation 5.8 and equation 5.9.

$$\sigma_S(t) = \int_0^t G_{CS}(t-\tau)\,d\varepsilon_s(\tau) \tag{5.8}$$

$$\sigma_I(t) = \int_0^t G_{CI}(t-\tau)\,d\varepsilon_I(\tau) \tag{5.9}$$

where τ is the integration variable; $\varepsilon_S(t)$ and $\varepsilon_I(t)$ are strain of surface and inner layers, respectively. For this parallel model, the relation between the strains is shown in equation 5.10

$$\varepsilon_I(t) = \varepsilon_S(t) = \varepsilon_C(t) \tag{5.10}$$

where $\varepsilon_C(t)$ is the strain of the composites. Thus, substitute equation 5.8 5.9 and 5.10 into 5.7,

$$[1 - f(t)] \int_0^t G_{CS}(t-\tau)\, d\varepsilon_C(\tau) + f(t) \int_0^t G_{CI}(t-\tau)\, d\varepsilon_C(\tau) = \sigma_0 \tag{5.11}$$

Linear viscoelasticity of the layers

Since the moisture diffusion process has been captured by the time-dependent areal fraction of the surface and inner layers, the moisture content within the layers is assumed to be uniform and at equilibrium state. Thus, the model proposed in Chapter 4 can be used here to predict the effective viscoelastic properties of composites under equilibrium moisture content for each layer. This model is briefly described here.

Based on Tsai-Pagano's work [57], effective Young's modulus E_c of randomly oriented, uniformly distributed fiber reinforced composites can be estimated by equation 5.12.

$$E_c = \frac{3}{8}E_{c1} + \frac{5}{8}E_{c2} \tag{5.12}$$

where E_{c1} and E_{c2} are longitudinal and transverse Young's moduli of the aligned short fiber reinforced composites with the same fiber volume fraction V_f, which are both given by Halpin-Tsai model shown in equation 5.13.

$$E_{ci} = E_m \frac{1 + \xi_i \eta_i V_f}{1 - \eta_i V_f}, \qquad \eta_i = \frac{\frac{E_{f-eff}}{E_m} - 1}{\frac{E_{f-eff}}{E_m} + \xi_i} \tag{5.13}$$

where E_m is the Young's modulus of matrix; E_{f-eff} is the Young's modulus of the effective fiber that considered swelling and interfacial debonding given by equation 5.4; ξ_i is a semi-empirical parameter that considers the fiber geometry and the direction i in which E_{ci} is estimated. According to Halpin and Kardos' work [56], $\xi_1 = 2L_f/d_f$,

where L_f is the fiber length, d_f is the fiber diameter; $\xi_2 = 2$. Same as Chapter 4, correspondence principle can be applied here to extend equation 5.12 and 5.13 to linear viscoelastic domain, as shown in equation 5.14 and 5.15

$$\hat{G}_C(s) = \frac{3}{8}\hat{G}_{c1}(s) + \frac{5}{8}\hat{G}_{c2}(s) \tag{5.14}$$

where $\hat{G}_C(s)$, is the Laplace transformed stress relaxation modulus of randomly oriented, uniformly distributed fiber reinforced composites; Note that for surface layers, it is denoted as $\hat{G}_{CS}(s)$ while for inner layer, it is denoted as $\hat{G}_{CI}(s)$; $\hat{G}_{c1}(s)$, $\hat{G}_{c2}(s)$ are given by equation 5.15.

$$\hat{G}_{ci}(s) = \hat{G}_m(s)\frac{1+\xi_i\eta_i V_f}{1-\eta_i V_f}, \qquad \eta_i = \frac{\frac{\hat{G}_{f-eff}(s)}{\hat{G}_m(s)} - 1}{\frac{\hat{G}_{f-eff}(s)}{\hat{G}_m(s)} + \xi_i} \tag{5.15}$$

where $\hat{G}_{f-eff}(s)$ and $\hat{G}_m(s)$ are Laplace transformed stress relaxation modulus of fiber and matrix, respectively. Under equilibrium moisture content, the effective fiber Young's modulus given by equation 5.4 is a constant. Thus, $\hat{G}_{f-eff}(s)$ is given by equation 5.16.

$$\hat{G}_{f-eff}(s) = \mathcal{L}\{G_{f-eff}(t) = E_{f-eff}\} = \frac{E_{f-eff}}{s} \tag{5.16}$$

For the matrix phase, the stress relaxation modulus solution of equation 5.5 is given by equation 5.17 [91].

$$G_m(t) = \frac{1}{\sqrt{p_1^2 - 4p_2}}\left[(q_1 - q_2 r_1)\exp(-r_1 t) - (q_1 - q_2 r_2)\exp(-r_2 t)\right] \tag{5.17}$$

where

$$\begin{aligned} p_1 &= \frac{\mu_1}{E_1} + \frac{\mu_2}{E_1} + \frac{\mu_2}{E_2} \\ p_2 &= \frac{\mu_1\mu_2}{E_1 E_2} \\ q_1 &= \mu_2 \\ q_2 &= \frac{\mu_1\mu_2}{E_1} \\ r_1 &= \frac{p_1 - \sqrt{p_1^2 - 4p_2}}{2p_2} \\ r_2 &= \frac{p_1 + \sqrt{p_1^2 - 4p_2}}{2p_2} \end{aligned} \tag{5.18}$$

Thus, $\hat{G}_m(s)$ is given by equation 5.19.

$$\hat{G}_m(s) = \mathcal{L}\{G_m(t)\} = \frac{1}{\sqrt{p_1^2 - 4p_2}} \left[\frac{q_1 - q_2 r_1}{s + r_1} - \frac{q_1 - q_2 r_2}{s + r_2} \right] \tag{5.19}$$

Finally, the t dependent stress relaxation modulus of surface layers (G_{CS}) and inner lay (G_{CI}) can be obtained by performing inverse Laplace transform of the corresponding stress relaxation modulus in Laplace transformed domain calculated by equation 5.14.

$$G_{CS}(t) = \mathcal{L}^{-1}\left\{\hat{G}_{CS}(s)\right\} \tag{5.20}$$

$$G_{CI}(t) = \mathcal{L}^{-1}\left\{\hat{G}_{CI}(s)\right\} \tag{5.21}$$

Numerical method

Unfortunately, equation 5.11 cannot be solved analytically. Thus, a numerical solution is derived here. Firstly, for calculation purposes, equation 5.11 is converted to equation 5.22 according to integration by part and change of variables [85].

$$\begin{aligned} &[1 - f(t)] \left[G_{CS}(0)\, \varepsilon_C(t) + \int_0^t \varepsilon_C(t - \tau) \frac{dG_{CS}(\tau)}{d\tau} d\tau \right] \\ &+ f(t) \left[G_{CI}(0)\, \varepsilon_C(t) + \int_0^t \varepsilon_C(t - \tau) \frac{dG_{CI}(\tau)}{d\tau} d\tau \right] = \sigma_0 \end{aligned} \tag{5.22}$$

By definition, creep compliance $J_c(t)$ is given by equation 5.23 [85].

$$J_C(t) = \frac{\varepsilon_C(t)}{\sigma_0} \tag{5.23}$$

Thus, dividing both sides of equation 5.22 by σ_0, it can be converted to equation 5.24.

$$\begin{aligned} &[1 - f(t)] \left[G_{CS}(0)\, J_C(t) + \int_0^t J_C(t - \tau) \frac{dG_{CS}(\tau)}{d\tau} d\tau \right] \\ &+ f(t) \left[G_{CI}(0)\, J_C(t) + \int_0^t J_C(t - \tau) \frac{dG_{CI}(\tau)}{d\tau} d\tau \right] = 1 \end{aligned} \tag{5.24}$$

For time discretization, the numerical integration evaluation and the solution of the integral function share the same time discretization scheme, i.e., $t_0 = \tau_0 = 0$ and $\Delta t = \Delta\tau$. Based on trapezoidal rule of numerical integration, equation 5.24 can be

discretized that leads to equation 5.25 when $t = t_n = n\Delta t$.

$$[1 - f_n]\left[G_{CS}(0)\,J_n + \frac{\Delta\tau}{2}\left[J_{n,0}G'_{CS(0)} + 2J_{n,1}G'_{CS(1)} + \cdots + 2J_{n,n-1}G'_{CS(n-1)} + J_{n,n}G'_{CS(n)}\right]\right]$$
$$+ f_n\left[G_{CI}(0)\,J_n + \frac{\Delta\tau}{2}\left[J_{n,0}G'_{CI(0)} + 2J_{n,1}G'_{CI(1)} + \cdots + 2J_{n,n-1}G'_{CI(n-1)} + J_{n,n}G'_{CI(n)}\right]\right] = 1 \tag{5.25}$$

where, for simplicity purpose,

$$\begin{aligned} G'_{CS(i)} &= \left.\frac{dG_{CS}}{d\tau}\right|_{\tau=\tau_i}, \\ G'_{CI(i)} &= \left.\frac{dG_{CI}}{d\tau}\right|_{\tau=\tau_i} \\ f_i &= f(t_i) \\ J_{i,j} &= J_c(t_i - \tau_j) \end{aligned} \tag{5.26}$$

Since both t and τ share the same discretization scheme, i.e., $\Delta t = \Delta\tau$, $t_0 = \tau_0 = 0$, $J_{i,j}$ can be simplified as equation 5.27.

$$J_{i,j} = J_c(t_i - \tau_j) = J_c((i-j)\,\Delta t) = J_c(t_{i-j}) = J_{i-j} \tag{5.27}$$

Thus, equation 5.25 can be re-written as equation 5.28.

$$[1 - f_n]\left[G_{CS}(0)\,J_n + \frac{\Delta t}{2}\left[J_nG'_{CS(0)} + 2J_{n-1}G'_{CS(1)} + \cdots + 2J_1G'_{CS(n-1)} + J_0G'_{CS(n)}\right]\right]$$
$$+ f_n\left[G_{CI}(0)\,J_n + \frac{\Delta t}{2}\left[J_nG'_{CI(0)} + 2J_{n-1}G'_{CI(1)} + \cdots + 2J_1G'_{CI(n-1)} + J_0G'_{CI(n)}\right]\right] = 1 \tag{5.28}$$

In fact, equation 5.28 is a system of $n+1$ equations with J_0, J_1, $\cdots$, J_n as unknowns. Solving this system of equation will give us the creep compliance J_c with respect to discretized time domain,

5.3 Experiment

5.3.1 Materials and sample preparation

To validate the model, extruded sheet samples of 5.6 wt% regenerated cellulose fibers (RCF) reinforced polylactic acid (PLA) biocomposites (5.6RCF/PLA) were produced.

Samples were manufactured by two-step extrusion method described in detail in Chapter 4. The materials used in the process were 4043D PLA pellets produced by NatureWorks LLC, USA that forms the matrix, and BioMid^{TM} RCF produced by Gordon Shank Consulting and Engineered Natural Composites, Inc., Burnaby, Canada that forms the fiber reinforcement, respectively.

5.3.2 Moisture-dependent mechanical properties of the constituents

The methodology proposed in our group's previous work [73] to obtained moisture-dependent mechanical properties of hydrophilic polymers was used here to characterize the moisture-dependent mechanical properties of PLA and RCF.

Moisture conditioning

Moisture conditioning were achieved by placing the samples in humidity chambers with 59%, 75%, 85% and 98% RH under room temperature (22-24°C). The humidity chambers were prepared according to ASTM E104 [121]. Extruded PLA sheet samples with thickness of 0.07 mm were cut into rectangular shape with 120 mm in length and 55 mm in width while RCF fiber bundles were cut into approximately 200 mm in length. Both PLA and RCF samples were placed in a Lindberg/Blue M^{TM} vacuum oven (Thermo Fisher Scientific, USA) under 80°C for 24 h to remove the residual moisture content.

Based on preliminary tests, regardless of the humidity levels, the RCF reached equilibrium within 2 h while PLA sheet samples will reach equilibrium within 48 h. Thus, before any further characterizations, RCF samples were placed in the chambers for more than 24 h while PLA sheet samples were placed in the chambers for at least 168 h. This is to ensure the samples have acquired equilibrium moisture content.

The equilibrium moisture content C_e of the samples under different RH levels were

measured using equation 5.29 [26].

$$C_e = \frac{m_{wet} - m_{dry}}{m_{dry}} \times 100\% \tag{5.29}$$

where m_{dry} is the initial dry mass of the samples while m_{wet} is the sample mass at equilibrium state. Shen and Springer [196] proposed that, for a hydrophilic polymer conditioned under a constant RH, the relation between equilibrium moisture content C_e and the RH level ϕ can be given by equation 5.30.

$$C_e = S_a \phi^{S_b} \tag{5.30}$$

where S_a and S_b are empirical parameters to be fitted with experimental data.

Tensile tests on RCF reinforcement

Tensile tests of the RCF fibers with different C_{fe} were conducted based on the methodology used in [73] to measure the E_f with respect to C_{fe}. The conditioned fibers were hand-separated and glued onto a paper tab for tensile tests according to ASTM D3379 [169]. The gauge length of the tests was 20 mm. After gluing onto the paper tab, the samples were placed back to the humidity chambers for more than 1 h to eliminate the moisture content loss during the sample preparation process. Finally, tensile tests of the RCF samples were conducted on ElectroForce 3200 Series III, Bose Corporation, USA, which is a universal tensile testing system. After mounting the samples on to the tensile clamps, the paper tab was cut. The constant displacement rate was set as 0.6 mm/min according to ASTM D3379 [169]. The testing environment was around 18% RH and 22°C. For each test, the time from taking the samples out of the chamber to the end of tests is less than 30 s, which was significantly smaller than the time to reach C_{fe} for RCF fibers (2 h). Thus, the moisture loss during the tensile tests were neglected. The value of E_f of the samples under each humidity level was averaged by 10 replications of experiments and the value was also reported with the standard deviation of the 10 replications.

Tensile creep tests on PLA matrix

Conditioned PLA sheet samples were then cut into tensile test samples with 60 mm in length and 10 mm in width for 15 min tensile creep tests. The testing methodology used by [73] were also used here. Similarly, sheet samples were mounted on the tensile clamps of ElectroForce 3200 Series III and the tests were conducted according to ASTM D2290 [125]. Preliminary tests discovered that, regardless of moisture content, with creep stress $\sigma_0 \leq 6.8$ MPa, the creep compliance will not change with respect to σ_0. Thus, 6.8 MPa was used as the applied creep stress for all the creep tests. The ambient environment during creep tests was around 20% RH and 22°C. The moisture loss during the 15 min were neglected since it takes 48 h for PLA samples to reach equilibrium moisture content. The testing time (15 min) is significantly smaller than that. The measured displacement was firstly normalized by gauge length (40 mm) to obtain the creep strain and then creep stress were further used to obtain the creep compliance of the samples. Same as [73], the reported creep compliance was measured every 50 s during the tests and the average and standard deviation of 5 replications of experiments were reported.

5.3.3 Mechanical properties of 5.6PLA/RCF composites under moisture diffusion

Moisture conditioning

To validate the model, 5.6RCF/PLA samples were conditioned under 98% RH and creeped under room environment. Similar to PLA matrix samples, 5.6RCF/PLA samples with average thickness of 0.42 mm were vacuum dried under 80°C for 24 h and cut into rectangular samples with 120 mm in length and 55 mm in width. It takes about 24 h for 5.6RCF/PLA composite samples to reach equilibrium moisture content. Thus, same as PLA samples, the wet sample mass was measured after 7 days of conditioning and the equilibrium moisture content of composite samples were also calculated using equation 5.29.

Tensile creep tests on 5.6RCF/PLA composites

Tensile creep tests were also conducted on 5.6RCF/PLA composite samples. The average thickness of the samples was 0.42 mm while the average length and width were 60.28 mm and 10.03 mm, respectively. The creep stress was also 6.8 MPa and creep time was also 15 min. The testing environment was around 24% RH and 22°C. The creep compliance was also reported every 50 s and the average and standard deviation of the 5 replications were also reported.

Desorption test

The moisture loss of the 5.6RCF/PLA within 15 min were also measured by desorption tests. More specifically, the sheet samples were conditioned until fully equilibrium in 98% RH and placed in a precision scale under room environment (around 24% RH and 22°C). The sample mass was measured every 50 s and the moisture content $C(t)$ of the samples were calculated with equation 5.31 [122].

$$C(t) = \frac{m(t) - m_{dry}}{m_{dry}} \times 100\% \tag{5.31}$$

where $m\,(t)$ is the mass of the sample at time t.

5.4 Results and Discussion

5.4.1 Moisture content

Both PLA matrix and RCF reinforcement were conditioned under the 4 different RH levels as mentioned previously. The relation between their C_e and the conditioning RH levels are shown in Figure 5.3. The error bars are the standard deviation of 5 replications. Under the same conditioning level, C_{fe} is almost one order of magnitude larger than C_{me}, indicating the stronger hydrophilicity of RCF over PLA. Shen and Springer model given by equation 5.30 was used to fit the experimental results, and the fitted parameters are shown in Table 5.1. Fitting of both materials' experimental results gives adjusted R^2 values larger than 0.9, which means that the empirical model

proposed by Shen and Springer [196] can describe the C_e with respect to conditioning RH levels for both of the materials.

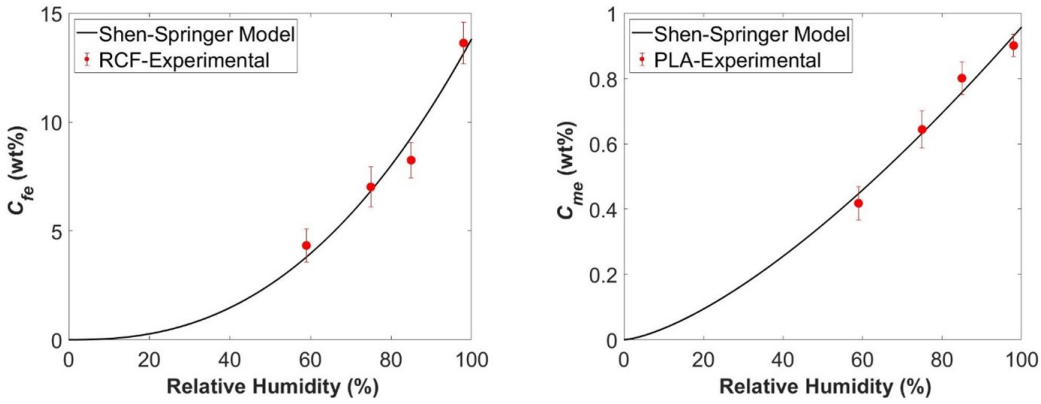

(a) (b)

Figure 5.3: Relation between conditioning RH and C_e including experimental results (red dots) and Shen-Springer model fitting (black curves): (a) RCF reinforcement; (b) PLA matrix

Table 5.1: Shen-Springer model parameters and goodness of fit

Material	S_a	S_b	Adjusted R^2
RCF	0.000176	2.447	0.94716
PLA	0.001246	1.443	0.95783

For 5.6PLA/RCF composites conditioned under 98% RH, its equilibrium moisture content C_C was measured as 1.313 wt%. As can be seen from the experimental results in Figure 5.3, under 98% RH, $C_{fe} = 13.63$ wt% while $C_{me} = 0.901$ wt%. If assuming both constituents absorb same amount of moisture under the same conditioning RH level, the composites moisture content shall be calculated by the weighted average of its constituents as shown by equation 5.32.

$$C_{C-p} = W_f C_{fe} + W_m C_{me} \tag{5.32}$$

where C_{C-p} is the predicted equilibrium moisture content of the composites under the same conditioning RH level of C_{fe} and C_{me}; W_f and W_m are the weight fraction of reinforcement fiber and matrix, respectively.

However, when calculated by equation 5.32, the 5.6PLA/RCF composites should absorb 1.614 wt% of moisture content under 98% RH, which is different from the measured value. It is possible that the lower amount of moisture absorbed is due to the restricted swelling of the reinforcement fibers since the fibers are embedded within the matrix material. Thus, in the following work of modeling, C_{fe} is calculated with equation 5.33 by assuming PLA matrix absorbs same amount of moisture content in the same environment while RCF absorbs less moisture due to restricted swelling [196].

$$C_{fe} = \frac{C_{C-a} - W_m C_{me}}{W_f} \tag{5.33}$$

where C_{C-a} is the actual composites moisture content measured by experiments, which is 1.313 wt% in this case.

5.4.2 Moisture-dependent constitutive relation of RCF reinforcement and PLA matrix

The experimental results of E_f with respect to C_{fe} is shown by the red dots in Figure 5.4 and modified Reimschuessel model given by equation 5.1 is fitted with this experimental data. The error bars are the standard deviation of the 10 replications. The fitted parameters are presented in Table 5.2. The fitting had an adjusted R^2 of 0.99281, indicating that the model can properly describe the trend. As can be seen from Table 5.2, the anti-plasticization effect is rather minor since $k_A = 4.615$ GPa/% and $k_D = 15.46$ 1/%. The small k_A indicates a small magnitude of anti-plasticization effect and larger k_D indicates a faster decay of the effect with increasing C_{fe}. This is due to the hydrophilic and hygroscopic nature of cellulose since it possesses many hydroxyls (-OH) groups on its molecular structure [197]. Large amount of diffused water molecules will easily form water clusters and causing plasticization effect instead of anti-plasticization effect [72]. In addition, the saturation level P_s of E_f is 26.70 GPa, which is about 53.7% of its dry value P_0. This means that even if a significant amount of moisture (more than 13 wt%) is absorbed, cellulose fibers can still retain

more than 50% of its stiffness. This can be explained by the high crystallinity of RCF since the water molecules cannot penetrate the crystalline regions due to its closely compacted nature [22].

Table 5.2: Modified Reimschuessel model fitted parameters and quality of fitting for both RCF reinforcement (E_f) and PLA matrix (E_1, E_2, μ_1, μ_2)

Parameter	P_0 (Unit)	P_s (Unit)	k_p (1/%)	k_A (Unit/%)	k_D (1/%)	Adjusted R^2
E_f (GPa)	49.68	26.70	0.2092	4.74	10.17	0.99281
E_{m1} (GPa)	8.794	0	0.7070	12.88	0.7257	0.86599
E_{m2} (GPa)	2.460	0	0.1768	5.032	4.058	0.94085
μ_{m1} (GPa·s)	632.16	0	0.4889	4125	4.337	0.70940
μ_{m2} (GPa·s)	8892	0	1.461	45530	1.462	0.97717

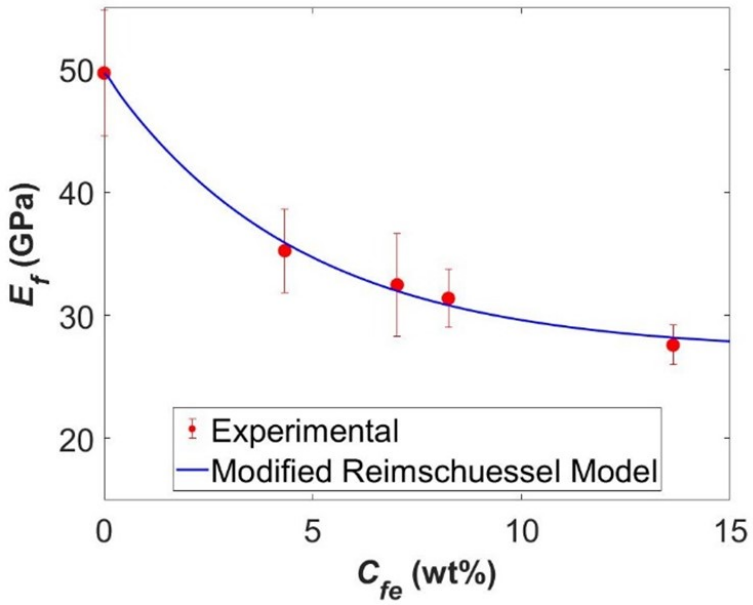

Figure 5.4: Experimental results of E_f with respect to C_{fe} (red dots) and the fitting of modified Reimschuessel model (blue curve)

The creep compliance of PLA matrix under different RH conditions are shown in Figure 5.5 and the dependence of Burgers model parameters on C_{me} is shown in Figure 5.6. The error bars are the standard deviation of 5 replications. Similar to the previous work [73], modified Burgers-Reimschuessel model given by equation 5.1 and 5.3 was used to fit the experimental results and the fitted parameters as well as the goodness of fitting is shown in Table 5.2 as well. Due to the lack of information in high C_{me} region, the saturation levels P_s of the parameters were all assigned to be 0 in this case. All the fitted parameters are in the similar order of magnitude as [73]. The difference on the absolute values may be caused by the difference in sample morphology (fibers vs. sheet) and the potential thermal degradation since the PLA in [73] was experiencing longer dwelling time within the high temperature zones of the extruder. Based on the fitted curves shown in Figure 5.5 and Figure 5.6, as well as the adjusted R^2 values shown in Table 5.2, a conclusion same as [73] can be drawn: Modified Burger-Reimschuessel can properly capture the anti-plasticization effect and this model is able to predict the effect of absorbed water on the viscoelasticity of PLA matrix.

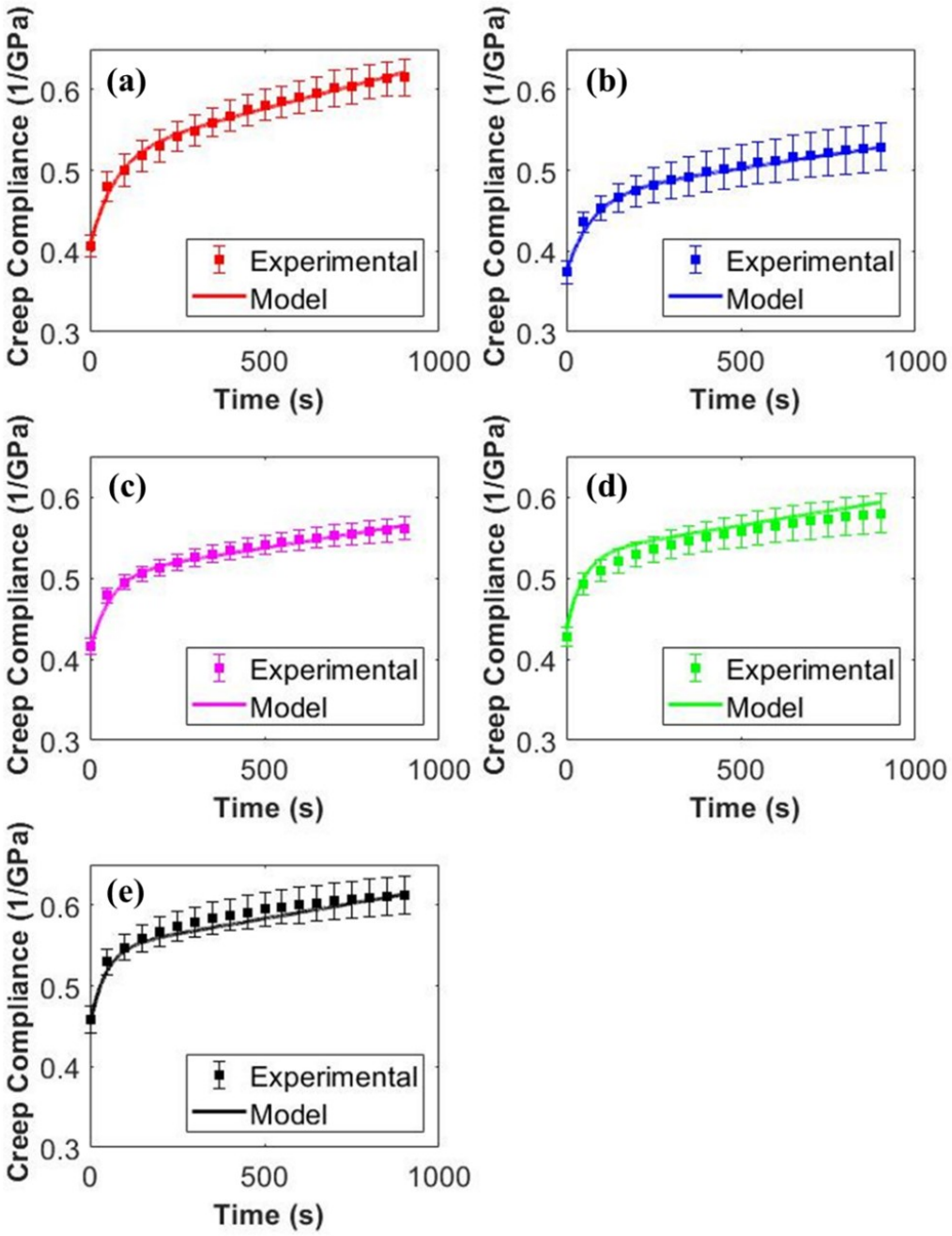

Figure 5.5: Creep compliance of PLA matrix with different RH conditions, as well as modified Burgers-Reimschuessel model fitting: (a) dry samples; (b) samples conditioned in 59% RH; (c) samples conditioned in 75% RH; (d) samples conditioned in 85% RH; (e) samples conditioned in 98% RH.

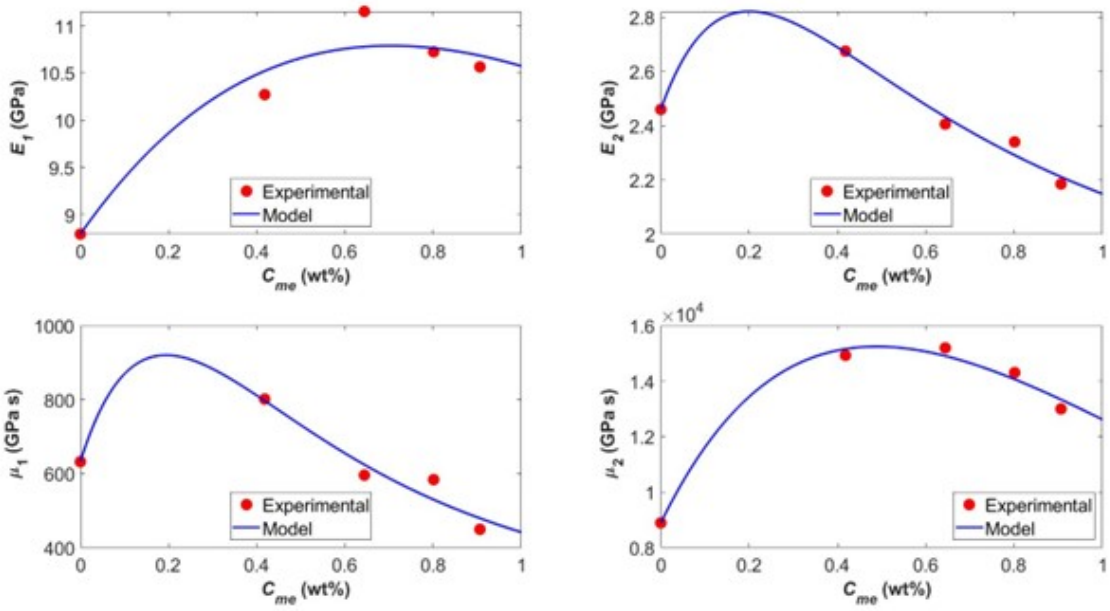

Figure 5.6: Experimental results of relation between Burgers model parameters C_{me} (red dots) and modified Reimschuessel model fitting (blue curves)

5.4.3 Creep compliance of 5.6RCF/PLA composites and model

In Figure 5.7, the experimental creep compliance and the model is shown by the black-color dots and black-color dashed lines, respectively. The error bars are the standard deviation of the 5 replications. Firstly, the instantaneous creep compliance of the samples conditioned under 98% RH is significantly higher than that of dry composites shown in Figure 4.5 in Chapter 4, which means that the stiffness of the composites is weakened by moisture absorption as expected. This is partially because of the reduced stiffness of both RCF and PLA, as shown by Figure 5.4 and Figure 5.5. It is also because of the fiber/matrix swelling mismatch and interface debonding as previously mentioned. Secondly, normally, without moisture diffusion, the creep compliance increases as time increases. However, for the wet composites, the creep compliance only increased from 0.414 1/GPa from the beginning to 0.458 1/GPa at 150 s, after which the increasing trend disappear and even shown a slight decreasing trend after 300 s. This is due to the moisture loss during the test since the conditioning

environment is 98% RH, which is significantly higher than the humidity of the testing environment (24% RH). Since lower moisture results in stiffer mechanical properties for both RCF and PLA, the increasing stiffness compensated for the increasing creep compliance.

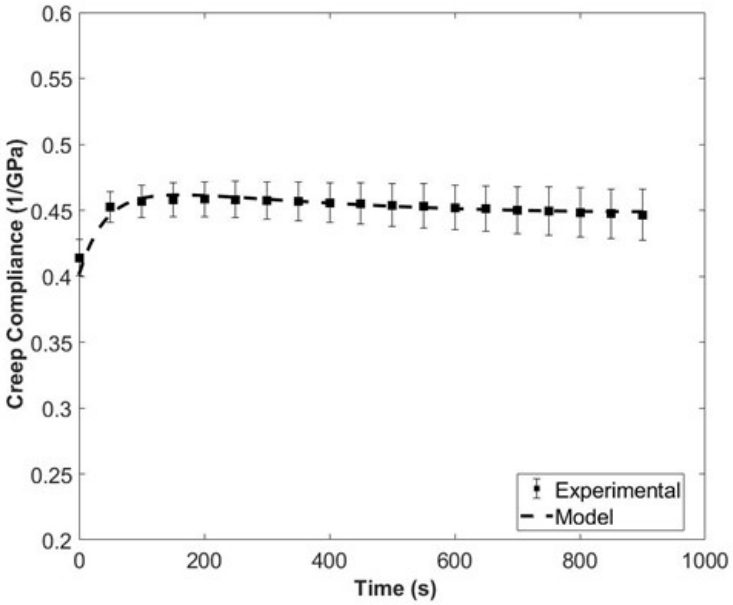

Figure 5.7: Experimental results of creep compliance of the composites conditioned under 98% RH and creeped under 24% RH (black dots), as well as the model fitting (dash line)

The proposed two-layer model was fitted with the experimental data and the fitted parameters are shown in Table 5.3. The adjusted R^2 value and the black dashed line in Figure 5.7 indicate that the model can properly describe the creep compliance of the composites during moisture diffusion.

Table 5.3: Two-layer model parameters and goodness of fit

Parameter	Value	Adjusted R^2
k_{ad} (1/%)	0.73855	0.83989
k_w (1/s)	6.3408×10^{-4}	

Since the two-layer model shown in Figure 5.1 only consists of the surface layers

and inner layer, the moisture content of the composites $C_c(t)$ during the non-steady state process can also be predicted using equation 5.34.

$$C_c(t) = f(t) C_{Ie} + [1 - f(t)] C_{Se} \tag{5.34}$$

where C_{Ie} and C_{Se} are the equilibrium moisture content of the inner layer and surface layers, calculated by equation 5.32 and experimental result C_{c-a}, respectively. The model prediction is shown in Figure 5.8 by the blue solid line.

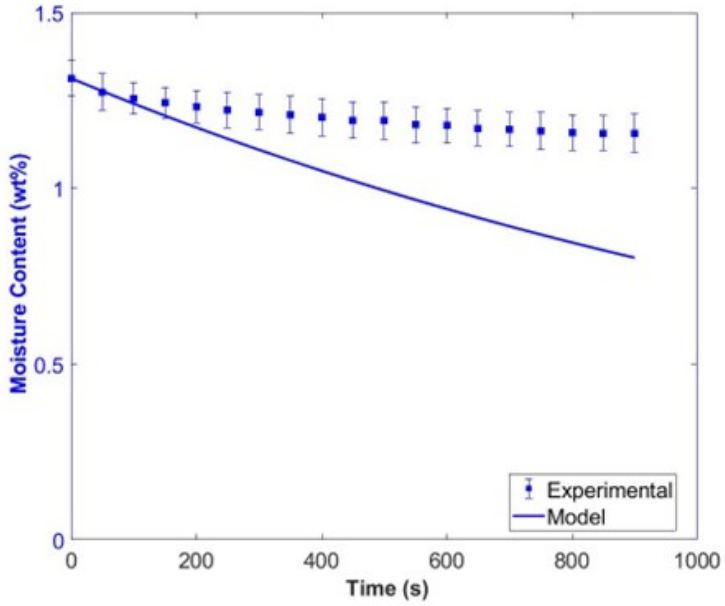

Figure 5.8: Experimental results of moisture desorption of the samples conditioned under 98% RH and placed under 24% RH (blue dots), as well as the desorption predicted by the proposed two-layer model (blue solid line).

5.4.4 Discussion

As can be seen in Figure 5.7 and Figure 5.8, although the proposed two-layer model can predict the creep compliance, large deviations between experiments and model prediction of moisture content is observed. The deviation on moisture content is due to the external stresses applied on the samples during the tensile creep test. Neumann and Marom [195] discovered that the diffusion coefficient of composites is dependent on the composites stress state and according to their study, external stress

will increase the diffusivity of the materials. Therefore, the moisture diffusion will be faster under stressed state. During the desorption test, the samples were placed in a beaker on the scale with two largest surfaces fully exposed to the environment. Therefore, except gravity, no external load was applied. The diffusion of the samples during the desorption test is expected to be smaller compared to the creep samples.

The advantage of this model is its simplicity with only two fitting parameters were involved. Instead of evaluating complicated diffusion equation or solving a boundary value problem with time-dependent mechanical properties caused by moisture desorption, this model makes prediction by simply combined the mechanical properties of the two components, which is an ideal tool for industrial design and evaluation. Also, although only moisture desorption was demonstrated in this work, this model can be easily used in moisture absorption with surface layers have higher moisture content while inner lay possesses lower moisture content.

In this model, two parameters were fitted with experimental results, which are the fiber damage constant k_{da} and inner layer shrinkage constant k_w. However, potentially, both parameters can be determined experimentally. k_{da} described the weakening of the fiber/matrix interface and swelling mismatch. Single-fiber-pull-out test has been used in the literature to characterize the adhesion between the fiber and matrix, which could be further utilized to determine k_{ad} experimentally rather than fitting. As mentioned in Figure 5.1, the two-layer model approximates the actual diffusion pattern of the material. Thus, k_w can be determined with the simulation of the diffusion pattern [122]. Also, if permitted, multiple layers can be introduced as shown in Figure 5.9. For each layer in the model shown in Figure 5.9b, the layer thickness and moisture content can be determined with the help of the actual diffusion pattern shown in Figure 5.9a.

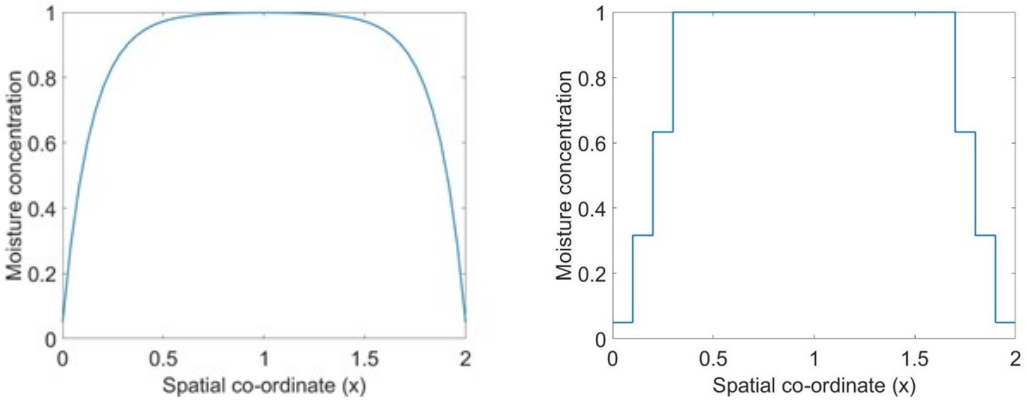

(a) (b)

Figure 5.9: Demonstration of multiple-layer model: (a) actual diffusion pattern at time t; (b) the multiple-layer model at time t

5.5 Conclusion

In this work, a two-layer model was proposed to describe the effect of moisture diffusion. The effect of weakened interface bonding and swelling mismatch was represented by a fiber damaging coefficient and the effect of moisture loss during moisture diffusion was represented by the change of areal fractions of surface layers and the inner layer. The proposed model was validated by experimental results of 5.6 wt% RCF reinforced PLA biocomposites, which was conditioned under 98% RH to acquire equilibrium moisture content and creeped under 24% RH. The proposed model can also be used to estimate the mechanical behavior of products made by these hydrophilic materials under constant load and varying humidity environment.

References

[1] A. K. Kaw, *Mechanics of Composite Materials*, 2nd ed. CRC Press, 2006, p. 491.

[4] A. K. Mohanty, M. Misra, and L. T. Drzal, *Natural fibers, biopolymers, and biocomposites*. Taylor and Francis, 2005.

[6] J. K. Pandey, S. H. Ahn, C. S. Lee, A. K. Mohanty, and M. Misra, "Recent advances in the application of natural fiber based composites," *Macromolecular Materials and Engineering*, vol. 295, pp. 975–989, 11 Nov. 2010, ISSN: 14387492. DOI: 10.1002/mame.201000095.

[7] M. T. Shaw and W. J. MacKnight, *Introduction to Polymer Viscoelasticity*, 3rd ed. John Wiley and Sons, Inc., 2005, p. 327.

[12] L. Rozite, J. Varna, R. Joffe, and A. Pupurs, "Nonlinear behavior of pla and lignin-based flax composites subjected to tensile loading," *Journal of Thermoplastic Composite Materials*, vol. 26, pp. 476–496, 4 May 2013, ISSN: 08927057. DOI: 10.1177/0892705711425846.

[13] B. Baghaei and M. Skrifvars, "Characterisation of polylactic acid biocomposites made from prepregs composed of woven polylactic acid/hemp-lyocell hybrid yarn fabrics," *Composites Part A: Applied Science and Manufacturing*, vol. 81, pp. 139–144, Feb. 2016, ISSN: 1359835X. DOI: 10.1016/j.compositesa.2015.10.042.

[15] J. W. Park, T. H. Lee, J. H. Back, S. W. Jang, H. J. Kim, and M. Skrifvars, "Phenyl silane treatment and carding process to improve the mechanical, thermal, and water-absorption properties of regenerated cellulose lyocell/polylactic acid bio-composites," *Composites Part B: Engineering*, vol. 167, pp. 387–395, Jun. 2019, ISSN: 13598368. DOI: 10.1016/j.compositesb.2019.02.064.

[20] S. Schmid, S. Kühne, and C. Hierold, "Influence of air humidity on polymeric microresonators," *Journal of Micromechanics and Microengineering*, vol. 19, 6 2009.

[22] H. K. Reimschuessel, "Relationships on the effect of water on glass transition temperature and young's modulus of nylon 6," *Journal of Polymer Science Part A: Polymer Chemistry*, vol. 16, pp. 1229–1236, 6 1978.

[26] S. Onogi, K. Sasaguri, T. Adachi, and S. Ogihara, "Time–humidity superposition in some crystalline polymers," *Journal of Polymer Science*, vol. 58, pp. 1–17, 166 1962.

[29] Y. Pan and Z. Zhong, "A micromechanical model for the mechanical degradation of natural fiber reinforced composites induced by moisture absorption," *Mechanics of Materials*, vol. 85, pp. 7–15, Aug. 2015, ISSN: 01676636. DOI: 10.1016/j.mechmat.2015.02.001.

[30] Z. Huo, "Modeling and evaluation of moisture diffusion in polymer composite materials," Missouri University of Science and Technology, 2016.

[31] D. Roy, *Biocomposites for high-performance applications: current barriers and future needs towards industrial development*. Woodhead Publishing, 2017.

[32] S. Koltzenburg, M. Maskos, and O. Nuyken, *Polymer chemistry*. Springer, 2017.

[47] Y. Pan and Z. Zhong, "Modeling of the mechanical degradation induced by moisture absorption in short natural fiber reinforced composites," *Composites Science and Technology*, vol. 103, pp. 22–27, Oct. 2014, ISSN: 02663538. DOI: 10.1016/j.compscitech.2014.08.010.

[48] Y. Pan and Z. Zhong, "A nonlinear constitutive model of unidirectional natural fiber reinforced composites considering moisture absorption," *Journal of the Mechanics and Physics of Solids*, vol. 69, pp. 132–142, 1 2014, ISSN: 00225096. DOI: 10.1016/j.jmps.2014.04.007.

[49] Y. Pan and Z. Zhong, "Analysis of creep and modulus loss of the wood cell wall," *Acta Mechanica*, vol. 227, pp. 3191–3203, 11 Nov. 2016, ISSN: 00015970. DOI: 10.1007/s00707-015-1532-y.

[50] Y. Pan and Z. Zhong, "Micromechanical modeling of the wood cell wall considering moisture absorption," *Composites Part B: Engineering*, vol. 91, pp. 27–35, Apr. 2016, ISSN: 13598368. DOI: 10.1016/j.compositesb.2015.12.038.

[51] Z. Zhong and F. Tian, "Modeling of mechanical behaviors for natural fiber reinforced composites under hygrothermal ageing," *Science China: Physics, Mechanics and Astronomy*, vol. 60, 12 Dec. 2017, ISSN: 18691927. DOI: 10.1007/s11433-017-9103-3.

[52] K. F. Wang and B. L. Wang, "A mechanical degradation model for bidirectional natural fiber reinforced composites under hydrothermal ageing and applying in buckling and vibration analysis," *Composite Structures*, vol. 206, pp. 594–600, Dec. 2018, ISSN: 02638223. DOI: 10.1016/j.compstruct.2018.08.063.

[53] Y. H. Pan and Z. Zhong, "Relative humidity and temperature dependence of mechanical degradation of natural fiber composites," *Science China: Physics, Mechanics and Astronomy*, vol. 59, 6 Jun. 2016, ISSN: 16747348. DOI: 10.1007/s11433-015-0520-0.

[54] Y. Pan and Z. Zhong, "The effect of hybridization on moisture absorption and mechanical degradation of natural fiber composites: An analytical approach," *Composites Science and Technology*, vol. 110, pp. 132–137, Apr. 2015, ISSN: 02663538. DOI: 10.1016/j.compscitech.2015.02.005.

[55] K. Kamau-Devers and S. A. Miller, "Using a micromechanical viscoelastic creep model to capture multi-phase deterioration in bio-based wood polymer composites exposed to moisture," *Construction and Building Materials*, vol. 314, Jan. 2022, ISSN: 09500618. DOI: 10.1016/j.conbuildmat.2021.125252.

[56] J. C. Halpin and J. L. Kardos, "The halpin-tsai equations: A review," *Polymer Engineering and Science*, vol. 16, pp. 345–352, 5 1976.

[57] S. W. Tsai and N. J. Pagano, "Invarient properties of composite materials," Air Force Materials Laboratory, May 1968.

[63] N. F. Zaaba and M. Jaafar, "A review on degradation mechanisms of polylactic acid: Hydrolytic, photodegradative, microbial, and enzymatic degradation," *Polymer Engineering and Science*, vol. 60, pp. 2061–2075, 9 2020, ISSN: 15482634. DOI: 10.1002/pen.25511.

[66] M. S. Huda, A. K. Mohanty, L. T. Drzal, E Schut, and M Misra, "Green composites from recycled cellulose and poly(lactic acid): Physico-mechanical and morphological properties evaluation," *Journal of Materials Science*, vol. 40, pp. 4221–4229, 2005.

[68] B. Bax and J. Müssig, "Impact and tensile properties of pla/cordenka and pla/flax composites," *Composites Science and Technology*, vol. 68, pp. 1601–1607, 7-8 Jun. 2008, ISSN: 02663538. DOI: 10.1016/j.compscitech.2008.01.004.

[71] B. Baghaei, M. Skrifvars, M. Rissanen, and S. K. Ramamoorthy, "Mechanical and thermal characterization of compression moulded polylactic acid natural fiber composites reinforced with hemp and lyocell fibers," *Journal of Applied Polymer Science*, vol. 131, 15 Aug. 2014, ISSN: 10974628. DOI: 10.1002/app.40534.

[72] Y. Chen, C. Ayranci, and T. Tang, "Modified burgers-reimschuessel model for moisture-sensitive polymers," *Journal of Polymer Science*, vol. 60, pp. 1539–1549, 9 Oct. 2021.

[73] Y. Chen, T. Tang, and C. Ayranci, "Moisture-induced anti-plasticization of polylactic acid: Experiments and modeling," *Journal of Applied Polymer Science*, vol. 139, 24 Jun. 2022, ISSN: 10974628. DOI: 10.1002/app.52369.

[85] R. M. Christensen, *Theory of Viscoelasticity, An Introduction*, 2nd ed. Dover Publications Inc., 2003, p. 363.

[86] L. Sperling, *Introduction to Physical Polymer Science*. John Wiley and Sons, Inc, 2006.

[91] W. N. Findley, *Creep and relaxation of nonlinear viscoelastic materials : with an introduction to linear viscoelasticity*, W. N. Findley, J. S. Lai, and K. Onaran, Eds. Dover Publications Inc., 1989, p. 380.

[92] B. Yang, W. M. Huang, C. Li, and L. Li, "Effects of moisture on the thermomechanical properties of a polyurethane shape memory polymer," *Polymer*, vol. 47, pp. 1348–1356, 4 2006, ISSN: 00323861. DOI: 10.1016/j.polymer.2005.12.051.

[121] "Astm e104-20 standard practice for maintaining constant relative humidity by means of aqueous solutions," American Society for Testing and Materials, Tech. Rep., 2020, p. 5.

[122] J. Crank, *The Mathematics of Diffusion*. Oxford University Press, 1975, p. 421.

[125] "Astm d2990-17 standard test methods for tensile, compressive, and flexureal creep and creep-rupture of plastics," Tech. Rep., 2017.

[136] G. Koronis and A. Silva, *Green Composites for Automotive Applications*. Woodhead Publishing, 2019.

[139] A. K. Bledzki and J Gassan, "Composites reinforced with cellulose based fibres," *Progress in Polymer Science*, vol. 24, pp. 221–274, 1999.

[152] S. H. Lee, S. Wang, and Y. Teramoto, "Isothermal crystallization behavior of hybrid biocomposite consisting of regenerated cellulose fiber, clay, and poly(lactic acid)," *Journal of Applied Polymer Science*, vol. 108, pp. 870–875, 2 Apr. 2008, ISSN: 00218995. DOI: 10.1002/app.26853.

[153] M. M. Kim, B. S. Kim, J. R. Ha, S. K. Kim, J. W. Yi, and J. Y. Lim, "Interfacial optimization of lyocell fabric/pla with silane treatments," *Advanced Materials Research*, vol. 123-125, pp. 1155–1158, 2010, ISSN: 10226680. DOI: 10.4028/www.scientific.net/amr.123-125.1155.

[159] B. Raju, S. R. Hiremath, and D. R. Mahapatra, "A review of micromechanics based models for effective elastic properties of reinforced polymer matrix composites," *Composite Structures*, vol. 204, pp. 607–619, Nov. 2018, ISSN: 02638223. DOI: 10.1016/j.compstruct.2018.07.125.

[162] N. Pan, "The elastic constants of randomly oriented fiber composites: A new approach to prediction," *Science and Engineering of Composite Materials*, vol. 5, pp. 63–72, 2 1996.

[169] "Astm d3379-75 standard test method for tensile strength and young's modulus for high-modulus single-filament materials," Tech. Rep., 1989.

[174] Z. Ren, R. Guo, H. Bi, X. Jia, M. Xu, and L. Cai, "Interfacial adhesion of polylactic acid on cellulose surface: A molecular dynamics study," *ACS Applied Materials and Interfaces*, vol. 12, pp. 3236–3244, 2 Jan. 2020, ISSN: 19448252. DOI: 10.1021/acsami.9b20101.

[180] H. Cheung, M. Ho, K. Lau, F. Cardona, and D. Hui, "Natural fibre-reinforced composites for bioengineering and environmental engineering applications," *Composites Part B: Engineering*, vol. 40, pp. 655–663, 7 Oct. 2009, ISSN: 13598368. DOI: 10.1016/j.compositesb.2009.04.014.

[181] Y. K. Dasan, A. H. Bhat, and F. Ahmad, "Polymer blend of pla/phbv based bionanocomposites reinforced with nanocrystalline cellulose for potential application as packaging material," *Carbohydrate Polymers*, vol. 157, pp. 1323–1332, Feb. 2017, ISSN: 01448617. DOI: 10.1016/j.carbpol.2016.11.012.

[182] Y. Chen, T. Tang, and C. Ayranci, "Linear viscoelasticity of bio-based composites of polylactic acid and regenerated cellulose fibers: Modeling and experimental validation," 2022.

[183] T. Sun, C. Yu, W. Yang, J. Zhong, and Q. Xu, "Experimental and numerical research on the nonlinear creep response of polymeric composites under humid environments," *Composite Structures*, vol. 251, Nov. 2020, ISSN: 02638223. DOI: 10.1016/j.compstruct.2020.112673.

[184] A. Moudood, A. Rahman, N. M. L. Huq, A. Öchsner, M. M. Islam, and G. Francucci, "Mechanical properties of flax fiber-reinforced composites at different relative humidities: Experimental, geometric, and displacement potential function approaches," *Polymer Composites*, vol. 41, pp. 4963–4973, 12 Dec. 2020, ISSN: 15480569. DOI: 10.1002/pc.25766.

[185] S. Panthapulakkal and M. Sain, "Injection-molded short hemp fiber/glass fiber-reinforced polypropylene hybrid composites -mechanical, water absorption and thermal properties," *Journal of Applied Polymer Science*, vol. 103, pp. 2432–2441, 4 Feb. 2007, ISSN: 00218995. DOI: 10.1002/app.25486.

[186] V. A. Alvarez, A. N. Fraga, and A. Vázquez, "Effects of the moisture and fiber content on the mechanical properties of biodegradable polymer-sisal fiber biocomposites," *Journal of Applied Polymer Science*, vol. 91, pp. 4007–4016, 6 Mar. 2004, ISSN: 00218995. DOI: 10.1002/app.13561.

[187] C. P. Chow, X. S. Xing, and R. K. Li, "Moisture absorption studies of sisal fibre reinforced polypropylene composites," *Composites Science and Technology*, vol. 67, pp. 306–313, 2 Feb. 2007, ISSN: 02663538. DOI: 10.1016/j.compscitech.2006.08.005.

[188] X. Lu, M. Q. Zhang, M. Z. Rong, G. Shi, and G. C. Yang, "All-plant fiber composites. ii: Water absorption behavior and biodegradability of unidirectional sisal fiber reinforced benzylated wood," *Polymer Composites*, vol. 24, pp. 367–379, 3 2003, ISSN: 15480569. DOI: 10.1002/pc.10036.

[189] T. Bechtold and C. B. Schimper, "Hydrolysis of regenerated cellulose fibres for textile and other applications," *Advances in Textile Biotechnology*, pp. 312–327, Jan. 2010. DOI: 10.1533/9780857090232.2.312.

[190] M. M. Lu, C. A. Fuentes, and A. W. V. Vuure, "Moisture sorption and swelling of flax fibre and flax fibre composites," *Composites Part B: Engineering*, vol. 231, Feb. 2022, ISSN: 13598368. DOI: 10.1016/j.compositesb.2021.109538.

[191] Y. Zhou, M. Fan, and L. Chen, "Interface and bonding mechanisms of plant fibre composites: An overview," *Composites Part B: Engineering*, vol. 101, pp. 31–45, Sep. 2016, ISSN: 13598368. DOI: 10.1016/j.compositesb.2016.06.055.

[192] L. T. Lim, I. J. Britt, and M. A. Tung, "Sorption and transport of water vapor in nylon 6,6 film," *Journal of Applied Polymer Science*, vol. 71, pp. 197–206, 2 Jan. 1999, ISSN: 00218995. DOI: 10.1002/(SICI)1097-4628(19990110)71:2⟨197::AID-APP2⟩3.0.CO;2-J.

[193] S. M. K. Thiagamani, M. E. Hoque, S. Krishnasamy, C. Muthukumar, and S. Siengchin, *Vibration and Damping Behavior of Biocomposites*, 1st ed. CRC Press, 2022.

[194] F. Tian, Y. Pan, and Z. Zhong, "A long-term mechanical degradation model of unidirectional natural fiber reinforced composites under hydrothermal ageing," *Composites Science and Technology*, vol. 142, pp. 156–162, Apr. 2017, ISSN: 02663538. DOI: 10.1016/j.compscitech.2017.01.021.

[195] S. Neumann and G. Marom, "Stress dependence of the coefficient of moisture diffusion in composite materials," *Polymer Composites*, vol. 6, pp. 9–12, 1 1985.

[196] C. H. Shen and G. S. Springer, "Moisture absorption and desorption of composite materials," *Journal of Composite Materials*, vol. 10, pp. 2–20, 1 1976, ISSN: 1530793x. DOI: 10.1177/002199837601000101.

[197] D. W. Wei, H. Wei, A. C. Gauthier, J. Song, Y. Jin, and H. Xiao, "Superhydrophobic modification of cellulose and cotton textiles: Methodologies and applications," *Journal of Bioresources and Bioproducts*, vol. 5, pp. 1–15, 1 Feb. 2020, ISSN: 23699698. DOI: 10.1016/j.jobab.2020.03.001.

Chapter 6

Conclusions, and Future Works

6.1 Conclusions

Bio-based composites that consist of bio-renewable and bio-degradable constituents present serious alternatives to those non-degradable, petroleum-based composites in a broad range of industries. To promote their wide-spread use, a fundamental understanding of their mechanical behavior and properties is crucial. These bio-based composites can show viscoelastic behaviors and, due to the hydrophilic nature of these composites, their viscoelasticity is substantially affected by ambient humidity and moisture content. Thus, a predictive model to evaluate the moisture-dependent mechanical properties of these composites is necessary. This can be achieved in four steps: 1) developing a model that can describe the effect of moisture on viscoelasticity of hydrophilic polymers; 2) conducting an experimental study that can comprehensively evaluate the moisture-dependent viscoelasticity of hydrophilic polymers; 3) developing a model that can predict the viscoelasticity of bio-based composites with the knowledge of the mechanical properties of their constituents; 4) developing a model that can predict the moisture-dependent viscoelasticity of bio-based composites based on the evaluated moisture-dependent mechanical properties of their constituents. As such, these four steps are the four main objectives of this thesis.

Firstly, a model is developed to describe the effect of moisture on the viscoelasticity of hydrophilic polymers in Chapter 2. Similar to other small molecules, water

molecules penetrating the hydrophilic polymers' molecular chains can cause plasticization and anti-plasticization effect. The existing Reimschuessel model in the literature only considered the plasticization effect and lack of consideration on the anti-plasticization effect results in an underestimation of the stiffness of the hydrophilic polymers at intermediate moisture level. Therefore, in this study, a simple yet important modification to the Reimschuessel model is introduced to consider both plasticization and anti-plasticization effect. Together with Burgers model, the proposed modified Reimschuessel model was validated against the stress relaxation results of four different hydrophilic polymers in the literature. Good agreement was achieved, and the proposed model revealed the possible stiffening effect of small amount of diffused moisture. Since the developed model established a relation between the viscoelasticity and moisture content of the polymer, it can be used to estimate the performance and service life of the products made from these hydrophilic polymers under given working environment.

Based on the developed modified Burgers-Reimschuessel model, an experimental methodology that can comprehensively evaluate the effect of moisture on the viscoelasticity of hydrophilic polymers is proposed in Chapter 3. Polylactic acid (PLA), which is the most frequently used biopolymer, was studied using the proposed methodology. The melt-extruded PLA fibers were conditioned under constant humidity environment (36%, 75%, and 98%), as well as immersed in distilled water, to acquire different levels of equilibrium moisture content. After conditioning, creep tests were conducted and the modified Burgers-Reimschuessel model was fitted to the moisture-dependent creep compliance data. Good agreement was found, and the experimental results provided direct evidence on the stiffening effect of water molecules at low moisture levels, which was predicted by the proposed modified Burgers-Reimschuessel model. The experimental results obtained in this work highlighted the importance of considering anti-plasticization effect of moisture. Also, the developed methodology can be used to evaluate the effect of moisture on the mechanical properties of other

hydrophilic polymers in different applications.

Thirdly, a model that can predict the viscoelasticity of homogeneously distributed and randomly oriented short fiber reinforced bio-based composites is provided in Chapter 4. The model extends on the Halpin-Tsai-Pagano model for linear elastic composites in the linear viscoelastic regime based on correspondence principle. Then, the model was applied to calculate the creep compliance of bio-based composites from PLA and regenerated cellulose fibers (RCF). In order to validate the model, sheet samples of PLA/RCF bio-based composites with RCF concentration up to 5.6 wt% were produced using a two-step extrusion technique and creep tests were conducted. The model showed good agreement with the experimental data for different RCF concentrations, which provided a strong and solid basic for the study of moisture-dependent viscoelasticity of bio-based composites in Chapter 5. In addition, Chapter 4 also demonstrated the application of the developed model in modulating the properties of this bio-based composites by a parametric study. The results from the parametric study can guide the design and manufacturing of this bio-based composites.

Finally, in Chapter 5, a simple yet useful semi-empirical model is developed to describe the materials' viscoelasticity with moisture diffusion based on physical considerations. The model is based on the micromechanical framework developed in Chapter 4. Two empirical parameters were introduced. One of them described the time-dependent moisture diffusion while the other one described the weakening effect due to interface debonding and the hygroscopic swelling mismatch between the matrix and reinforcement. The proposed model is validated against the experimental results of 5.6 wt% RCF reinforced PLA bio-based composites conditioned in 98% RH and creeped under 22% RH. A good agreement was achieved after fitting the two empirical parameters.

In summary, this thesis investigates the physics behind the moisture-dependent viscoelasticity of hydrophilic bio-based polymer composites, and lead to development of a semi-empirical model based on the considerations of these physics. Validated

against the experimental results, the developed model is able to describe the moisture-dependent viscoelasticity of these bio-based composites under different humidity levels with limited amount of fitting parameters. In the design of products made by these bio-based composites, the effect of moisture on their viscoelasticity can be predicted and considered. This will promote further and broader usage of these bio-based composites. In addition, the developed model can provide guidance to the design and optimization of the products made from these bio-based composites.

6.2 Future Works

This thesis identified several limitations and recommendations for future investigations that are listed below:

- The proposed modified Burgers-Reimschuessel model is empirical, and all the model parameters need to be fitted against the experimental results. Thus, additional efforts can be devoted to study the relation between the parameters with physical properties of polymers such as molecular weight, free volume, crystallinity, and density of those polar groups on the molecular chains.

- The proposed Burger-Reimschuessel model is based on an isothermal assumption. However, in practical applications, especially in outdoor conditions, coupled effects of temperature and moisture on polymers' viscoelasticity are usually observed. Future works can be done to describe the coupled effect of temperature and moisture, which could further promote the use of these hydrophilic polymers in different applications.

- The experimental methodology proposed in Chapter 3 of this thesis was also based on isothermal condition, in which all the conditioning and creep tests were conducted under room temperature. Thus, with the development of the above-mentioned model that captures the coupled effect of temperature and

moisture, the experimental methodology shall also be modified to evaluate the coupled effect.

- In Chapter 4, with the data from DSC characterization, it has been discovered that the reinforcement of RCF will increase the crystallinity of PLA matrix. However, the developed model did not consider the crystallinity change. Thus, a slight overestimation was observed on the delayed creep compliance. To demonstrate this hypothesis, the PLA parameters were slightly modified to reflect the increasing crystallinity and a better agreement with the experimental results was shown. Future works can be done to explicitly model the effect of changing crystallinity on the viscoelasticity of the composites.

- The two fitting parameters introduced in Chapter 5 both have physical considerations, thus, potentially, they can be determined experimentally. The fiber damage constant k_{da} can be determined using single-fiber-pull-out test and the inner lay shrinkage constant k_w can be determined with the simulation of moisture diffusion based on Fick's law of diffusion.

- If calculation power is permitted, multiple layers can be introduced to have a better and more accurate prediction of viscoelasticity under moisture diffusion.

- All the models developed in this work only considered the case under a simple one-dimensional tensional load. More complicated cases such as bending shall be attempted in the future to further validate the general applicability of this model.

Bibliography

[1] A. K. Kaw, *Mechanics of Composite Materials*, 2nd ed. CRC Press, 2006, p. 491.

[2] A. K. Mohanty, M Misra, and G Hinrichsen, "Biofibres, biodegradable polymers and biocomposites: An overview," *Macromolecular Materials and Engineering*, vol. 277, pp. 1–24, 2000.

[3] D. Bondeson and K. Oksman, "Dispersion and characteristics of surfactant modified cellulose whiskers nanocomposites," *Composite Interfaces*, vol. 14, pp. 617–630, 7-9 Sep. 2007, ISSN: 09276440. DOI: 10.1163/156855407782106519.

[4] A. K. Mohanty, M. Misra, and L. T. Drzal, *Natural fibers, biopolymers, and biocomposites*. Taylor and Francis, 2005.

[5] T. Gurunathan, S. Mohanty, and S. K. Nayak, "A review of the recent developments in biocomposites based on natural fibres and their application perspectives," *Composites Part A: Applied Science and Manufacturing*, vol. 77, pp. 1–25, Jun. 2015, ISSN: 1359835X. DOI: 10.1016/j.compositesa.2015.06.007.

[6] J. K. Pandey, S. H. Ahn, C. S. Lee, A. K. Mohanty, and M. Misra, "Recent advances in the application of natural fiber based composites," *Macromolecular Materials and Engineering*, vol. 295, pp. 975–989, 11 Nov. 2010, ISSN: 14387492. DOI: 10.1002/mame.201000095.

[7] M. T. Shaw and W. J. MacKnight, *Introduction to Polymer Viscoelasticity*, 3rd ed. John Wiley and Sons, Inc., 2005, p. 327.

[8] D. Gutierrez-Lemini, *Engineering Viscoelasticity*. Springer, 2014, p. 353.

[9] R. A. Schapery, *Viscoelastic Behavior and Analysis of Composite Materials*, 1st ed., G. P. Sendeckyj, Ed. Academic Press, 1974, pp. 85–168.

[10] A. Atmakuri, A. Palevicius, M. Siddabathula, A. Vilkauskas, and G. Janusas, "Analysis of mechanical and wettability properties of natural fiber-reinforced epoxy hybrid composites," *Polymers*, vol. 12, pp. 1–15, 12 Dec. 2020, ISSN: 20734360. DOI: 10.3390/polym12122827.

[11] K. E. Mazur *et al.*, "Analysis of the effect of photo and hydrodegradation on the surface morphology and mechanical properties of composites based on pla and phi modified with natural particles," *Materials*, vol. 15, 3 Feb. 2022, ISSN: 19961944. DOI: 10.3390/ma15030878.

[12] L. Rozite, J. Varna, R. Joffe, and A. Pupurs, "Nonlinear behavior of pla and lignin-based flax composites subjected to tensile loading," *Journal of Thermoplastic Composite Materials*, vol. 26, pp. 476–496, 4 May 2013, ISSN: 08927057. DOI: 10.1177/0892705711425846.

[13] B. Baghaei and M. Skrifvars, "Characterisation of polylactic acid biocomposites made from prepregs composed of woven polylactic acid/hemp-lyocell hybrid yarn fabrics," *Composites Part A: Applied Science and Manufacturing*, vol. 81, pp. 139–144, Feb. 2016, ISSN: 1359835X. DOI: 10.1016/j.compositesa.2015.10.042.

[14] C. A. Murphy and M. N. Collins, "Microcrystalline cellulose reinforced polylactic acid biocomposite filaments for 3d printing," *Polymer Composites*, vol. 39, pp. 1311–1320, 4 Apr. 2018, ISSN: 15480569. DOI: 10.1002/pc.24069.

[15] J. W. Park, T. H. Lee, J. H. Back, S. W. Jang, H. J. Kim, and M. Skrifvars, "Phenyl silane treatment and carding process to improve the mechanical, thermal, and water-absorption properties of regenerated cellulose lyocell/polylactic acid bio-composites," *Composites Part B: Engineering*, vol. 167, pp. 387–395, Jun. 2019, ISSN: 13598368. DOI: 10.1016/j.compositesb.2019.02.064.

[16] A. Smoca, "Water absorption properties of hemp fibres reinforced pla biocomposites," *Engineering for Rural Development*, vol. 18, pp. 1079–1083, 2019, ISSN: 16915976. DOI: 10.22616/ERDev2019.18.N522.

[17] M. A. Sawpan, M. R. Islam, M. D. H. Beg, and K. Pickering, "Effect of accelerated weathering on physico-mechanical properties of polylactide biocomposites," *Journal of Polymers and the Environment*, vol. 27, pp. 942–955, 5 2019, ISSN: 15662543. DOI: 10.1007/s10924-019-01405-2. [Online]. Available: http://dx.doi.org/10.1007/s10924-019-01405-2.

[18] R. A. Jurf and J. R. Vinson, "Effect of moisture on the static and viscoelastic shear properties of epoxy adhesives," *Journal of Materials Science*, vol. 20, pp. 2979–2989, 8 1985, ISSN: 00222461. DOI: 10.1007/BF00553063.

[19] F. Huber, H. Etschmaier, H. Walter, G. Urstöger, and P. Hadley, "A time temperature moisture concentration superposition principle that describes the relaxation behavior of epoxide molding compounds for microelectronics packaging," *International Journal of Polymer Analysis and Characterization*, vol. 25, pp. 467–478, 6 2020, ISSN: 15635341. [Online]. Available: https://doi.org/10.1080/1023666X.2020.1807680.

[20] S. Schmid, S. Kühne, and C. Hierold, "Influence of air humidity on polymeric microresonators," *Journal of Micromechanics and Microengineering*, vol. 19, 6 2009.

[21] M. B. Satterfiield and J. B. Benziger, "Viscoelastic properties of nafion at elevated temperature and humidity," *Journal of Polymer Science Part B: Polymer Physics*, vol. 47, pp. 11–24, 2009. [Online]. Available: http://arxiv.org/abs/cond-mat/0406218%0Ahttp://dx.doi.org/10.1002/polb.

[22] H. K. Reimschuessel, "Relationships on the effect of water on glass transition temperature and young's modulus of nylon 6," *Journal of Polymer Science Part A: Polymer Chemistry*, vol. 16, pp. 1229–1236, 6 1978.

[23] I. Widiastuti, I. Sbarski, and S. H. Masood, "Mechanical behavior of a fluid-sensitive material during liquid diffusion," *Mechanics of Time-Dependent Materials*, vol. 18, pp. 387–406, 2 2014, ISSN: 13852000. DOI: 10.1007/s11043-014-9233-9.

[24] I. Widiastuti, I. Sbarski, and S. H. Masood, "Mechanical response of poly(lactic acid)-based packaging under liquid exposure," *Journal of Applied Polymer Science*, vol. 131, pp. 1–10, 16 2014.

[25] I. Widiastuti, I. Sbarski, and S. H. Masood, "Creep behavior of pla-based biodegradable plastic exposed to a hydrocarbon liquid," *Journal of Applied Polymer Science*, vol. 127, pp. 2654–2660, 4 2013, ISSN: 00218995. DOI: 10.1002/app.37575.

[26] S. Onogi, K. Sasaguri, T. Adachi, and S. Ogihara, "Time–humidity superposition in some crystalline polymers," *Journal of Polymer Science*, vol. 58, pp. 1–17, 166 1962.

[27] H. Fujita and A. Kishimoto, "Diffusion-controlled stress relaxation in polymers. iii. stress relaxation in a swelling polymer," *Journal of Polymer Science*, vol. 28, pp. 569–585, 118 1958.

[28] I. Emri and V. Pavsek, "On the influence of moisture on the mechanical properties of polymers," *Materials Forum*, vol. 16, pp. 123–131, 2 1992.

[29] Y. Pan and Z. Zhong, "A micromechanical model for the mechanical degradation of natural fiber reinforced composites induced by moisture absorption," *Mechanics of Materials*, vol. 85, pp. 7–15, Aug. 2015, ISSN: 01676636. DOI: 10.1016/j.mechmat.2015.02.001.

[30] Z. Huo, "Modeling and evaluation of moisture diffusion in polymer composite materials," Missouri University of Science and Technology, 2016.

[31] D. Roy, *Biocomposites for high-performance applications: current barriers and future needs towards industrial development*. Woodhead Publishing, 2017.

[32] S. Koltzenburg, M. Maskos, and O. Nuyken, *Polymer chemistry*. Springer, 2017.

[33] P. Gilormini and J. Verdu, "On the role of hydrogen bonding on water absorption in polymers," *Polymer*, vol. 142, pp. 164–169, 2018. DOI: 10.1016/j.polymer.2018.03.033. [Online]. Available: https://hal.archives-ouvertes.fr/hal-01743020.

[34] U. W. Gedde, *Polymer Physics*. Springer, 1999, p. 301.

[35] R. M. Hodge, T. J. Bastow, G. H. Edward, G. P. Simon, and A. J. Hill, "Free volume and the mechanism of plasticization in water-swollen poly(vinyl alcohol)," *Macromolecules*, vol. 29, pp. 8137–8143, 25 1996, ISSN: 00249297. DOI: 10.1021/ma951073j.

[36] X. Fan, "Mechanics of moisture for polymers: Fundamental concepts and model study," 2008.

[37] R. M. Hodge, G. H. Edward, and G. P. Simon, "Water absorption and states of water in semicrystalline poly(vinyl alcohol) films," *Polymer*, vol. 37, pp. 1371–1376, 8 1996, ISSN: 00323861. DOI: 10.1016/0032-3861(96)81134-7.

[38] K. Inoue and S. Hoshino, "Swelling of nylon 6 film due to water sorption.," *Journal of Polymer Science Part B: Polymer Physics*, vol. 14, pp. 1513–1526, 8 1976, ISSN: 00981273. DOI: 10.1002/pol.1976.180140812.

[39] K. M. Zakir, A. J. Parsons, C. D. Rudd, I. Ahmed, and W. Thielemans, "Mechanical , crystallisation and moisture absorption properties of melt drawn polylactic acid fibres," *European Polymer Journal*, vol. 53, pp. 270–281, 2014, ISSN: 0014-3057. DOI: 10.1016/j.eurpolymj.2014.02.001. [Online]. Available: http://dx.doi.org/10.1016/j.eurpolymj.2014.02.001.

[40] A. Ishisaka and M. Kawagoe, "Examination of the time-water content superposition on the dynamic viscoelasticity of moistened polyamide 6 and epoxy," *Journal of Applied Polymer Science*, vol. 93, pp. 560–567, 2 2004.

[41] R. D. Maksimov, E. A. Sokolov, and V. P. Mochalov, "Effect of temperature and moisture on the creep of polymeric materials 1. one-dimensional extension under stationary temperature-moisture conditions," *Mechanics of Composite Materials*, vol. 11, pp. 334–339, 3 1975.

[42] I. T. Garces, S. Aslanzadeh, Y. Boluk, and C. Ayranci, "Effect of moisture on shape memory polyurethane polymers for extrusion-based additive manufacturing," *Materials*, vol. 12, 2 2019, ISSN: 19961944.

[43] S. M. Bhasney, R. Patwa, A. Kumar, and V. Katiyar, "Plasticizing effect of coconut oil on morphological, mechanical, thermal, rheological, barrier, and optical properties of poly(lactic acid): A promising candidate for food packaging," *Journal of Applied Polymer Science*, vol. 134, p. 45 390, 41 Nov. 2017.

[44] V. Marturano *et al.*, "Light-responsive nanocapsule-coated polymer films for antimicrobial active packaging," *Polymers*, vol. 11, p. 68, 1 Jan. 2019.

[45] A. Orue, A. Eceiza, C. Peña-Rodriguez, and A. Arbelaiz, "Water uptake behavior and young modulus prediction of composites based on treated sisal fibers and poly(lactic acid)," *Materials*, vol. 9, p. 400, 5 2016.

[46] M. Esmaeili, G. Pircheraghi, R. Bagheri, and V. Altstädt, "Poly(lactic acid)/coplasticized thermoplastic starch blend: Effect of plasticizer migration on rheological and mechanical properties," *Polymers for Advanced Technologies*, vol. 30, pp. 839–851, 4 Apr. 2019.

[47] Y. Pan and Z. Zhong, "Modeling of the mechanical degradation induced by moisture absorption in short natural fiber reinforced composites," *Composites Science and Technology*, vol. 103, pp. 22–27, Oct. 2014, ISSN: 02663538. DOI: 10.1016/j.compscitech.2014.08.010.

[48] Y. Pan and Z. Zhong, "A nonlinear constitutive model of unidirectional natural fiber reinforced composites considering moisture absorption," *Journal of the Mechanics and Physics of Solids*, vol. 69, pp. 132–142, 1 2014, ISSN: 00225096. DOI: 10.1016/j.jmps.2014.04.007.

[49] Y. Pan and Z. Zhong, "Analysis of creep and modulus loss of the wood cell wall," *Acta Mechanica*, vol. 227, pp. 3191–3203, 11 Nov. 2016, ISSN: 00015970. DOI: 10.1007/s00707-015-1532-y.

[50] Y. Pan and Z. Zhong, "Micromechanical modeling of the wood cell wall considering moisture absorption," *Composites Part B: Engineering*, vol. 91, pp. 27–35, Apr. 2016, ISSN: 13598368. DOI: 10.1016/j.compositesb.2015.12.038.

[51] Z. Zhong and F. Tian, "Modeling of mechanical behaviors for natural fiber reinforced composites under hygrothermal ageing," *Science China: Physics, Mechanics and Astronomy*, vol. 60, 12 Dec. 2017, ISSN: 18691927. DOI: 10.1007/s11433-017-9103-3.

[52] K. F. Wang and B. L. Wang, "A mechanical degradation model for bidirectional natural fiber reinforced composites under hydrothermal ageing and applying in buckling and vibration analysis," *Composite Structures*, vol. 206, pp. 594–600, Dec. 2018, ISSN: 02638223. DOI: 10.1016/j.compstruct.2018.08.063.

[53] Y. H. Pan and Z. Zhong, "Relative humidity and temperature dependence of mechanical degradation of natural fiber composites," *Science China: Physics, Mechanics and Astronomy*, vol. 59, 6 Jun. 2016, ISSN: 16747348. DOI: 10.1007/s11433-015-0520-0.

[54] Y. Pan and Z. Zhong, "The effect of hybridization on moisture absorption and mechanical degradation of natural fiber composites: An analytical approach," *Composites Science and Technology*, vol. 110, pp. 132–137, Apr. 2015, ISSN: 02663538. DOI: 10.1016/j.compscitech.2015.02.005.

[55] K. Kamau-Devers and S. A. Miller, "Using a micromechanical viscoelastic creep model to capture multi-phase deterioration in bio-based wood polymer composites exposed to moisture," *Construction and Building Materials*, vol. 314, Jan. 2022, ISSN: 09500618. DOI: 10.1016/j.conbuildmat.2021.125252.

[56] J. C. Halpin and J. L. Kardos, "The halpin-tsai equations: A review," *Polymer Engineering and Science*, vol. 16, pp. 345–352, 5 1976.

[57] S. W. Tsai and N. J. Pagano, "Invarient properties of composite materials," Air Force Materials Laboratory, May 1968.

[58] R. A. Ilyas *et al.*, "Polylactic acid (pla) biocomposite: Processing, additive manufacturing and advanced applications," *Polymers*, vol. 13, 8 Apr. 2021, ISSN: 20734360. DOI: 10.3390/polym13081326.

[59] E Castro-aguirre, F Iñiguez-franco, H Samsudin, X Fang, and R Auras, "Poly (lactic acid) — mass production , processing , industrial applications , and end of life," *Advanced Drug Delivery Reviews*, vol. 107, pp. 333–366, 2016, ISSN: 0169-409X. DOI: 10.1016/j.addr.2016.03.010. [Online]. Available: http://dx.doi.org/10.1016/j.addr.2016.03.010.

[60] D. Tzetzis, K. Tsongas, and G. Mansour, "Determination of the mechanical properties of epoxy silica nanocomposites through fea-supported evaluation of ball indentation test results," *Journal of Materials Research*, vol. 20, pp. 1571–1578, 6 Nov. 2017, ISSN: 15161439. DOI: 10.1590/1980-5373-MR-2017-0454.

[61] N. Kurokawa and A. Hotta, "Regenerated cellulose nanofibers fabricated through electrospinning and saponification of cellulose acetate as reinforcement of polylactide composites," *Cellulose*, vol. 26, pp. 7797–7808, 13-14 Sep. 2019, ISSN: 1572882X. DOI: 10.1007/s10570-019-02623-6.

[62] R. Auras, L. Lim, S. M. Selke, and H. Tsuji, *Polylactic Acid, Synthesis, Structures, Properties, Processing, and Applications*. John Wiley and Sons, 2010.

[63] N. F. Zaaba and M. Jaafar, "A review on degradation mechanisms of polylactic acid: Hydrolytic, photodegradative, microbial, and enzymatic degradation," *Polymer Engineering and Science*, vol. 60, pp. 2061–2075, 9 2020, ISSN: 15482634. DOI: 10.1002/pen.25511.

[64] M. Funabashi, F. Ninomiya, and M. Kunioka, "Biodegradability evaluation of polymers by iso 14855-2," *International Journal of Molecular Sciences*, vol. 10, pp. 3635–3654, 8 Aug. 2009, ISSN: 14220067. DOI: 10.3390/ijms10083635.

[65] M. Shibata, S. Oyamada, S.-I. Kobayashi, and D. Yaginuma, "Mechanical properties and biodegradability of green composites based on biodegradable polyesters and lyocell fabric," *Journal of Applied Polymer Science*, vol. 92, pp. 3857–3863, 2004.

[66] M. S. Huda, A. K. Mohanty, L. T. Drzal, E Schut, and M Misra, "Green composites from recycled cellulose and poly(lactic acid): Physico-mechanical and morphological properties evaluation," *Journal of Materials Science*, vol. 40, pp. 4221–4229, 2005.

[67] A. K. Bledzki, A. Jaszkiewicz, and D. Scherzer, "Mechanical properties of pla composites with man-made cellulose and abaca fibres," *Composites Part A: Applied Science and Manufacturing*, vol. 40, pp. 404–412, 4 Apr. 2009, ISSN: 1359835X. DOI: 10.1016/j.compositesa.2009.01.002.

[68] B. Bax and J. Müssig, "Impact and tensile properties of pla/cordenka and pla/flax composites," *Composites Science and Technology*, vol. 68, pp. 1601–1607, 7-8 Jun. 2008, ISSN: 02663538. DOI: 10.1016/j.compscitech.2008.01.004.

[69] M. S. Huda, L. T. Drzal, A. K. Mohanty, and M. Misra, "Chopped glass and recycled newspaper as reinforcement fibers in injection molded poly(lactic acid) (pla) composites: A comparative study," *Composites Science and Technology*, vol. 66, pp. 1813–1824, 11-12 Sep. 2006, ISSN: 02663538. DOI: 10.1016/j.compscitech.2005.10.015.

[70] B. Geissler, M. Feuchter, S. Laske, M. Fasching, C. Holzer, and G. R. Langecker, "Strategies to improve the mechanical properties of high-density polylactic acid foams," *Journal of Cellular Plastics*, vol. 52, pp. 15–35, 1 Jan. 2016, ISSN: 15307999. DOI: 10.1177/0021955X14538274.

[71] B. Baghaei, M. Skrifvars, M. Rissanen, and S. K. Ramamoorthy, "Mechanical and thermal characterization of compression moulded polylactic acid natural fiber composites reinforced with hemp and lyocell fibers," *Journal of Applied Polymer Science*, vol. 131, 15 Aug. 2014, ISSN: 10974628. DOI: 10.1002/app.40534.

[72] Y. Chen, C. Ayranci, and T. Tang, "Modified burgers-reimschuessel model for moisture-sensitive polymers," *Journal of Polymer Science*, vol. 60, pp. 1539–1549, 9 Oct. 2021.

[73] Y. Chen, T. Tang, and C. Ayranci, "Moisture-induced anti-plasticization of polylactic acid: Experiments and modeling," *Journal of Applied Polymer Science*, vol. 139, 24 Jun. 2022, ISSN: 10974628. DOI: 10.1002/app.52369.

[74] C. Hall, *Polymer Materials, An Introduction for Technologists and Scientists*, 1st ed. The MacMillan Press Ltd., 1981, p. 208.

[75] S. M. Zhou and K. Tashiro, "Confirmation of universality of time-humidity superposition principle for various water-absorbable polymers through dynamic viscoelastic measurements under controlled conditions of relative humidity and temperature," *Journal of Polymer Science Part B: Polymer Physics*, vol. 39, pp. 1638–1650, 14 2001.

[76] P. Myllytie, L. Salmén, E. Haimi, and J. Laine, "Viscoelasticity and water plasticization of polymer-cellulose composite films and paper sheets," *Cellulose*, vol. 17, pp. 375–385, 2 2010, ISSN: 09690239. DOI: 10.1007/s10570-009-9376-z.

[77] O. Starkova and A. Aniskevich, "Limits of linear viscoelastic behavior of polymers," *Mechanics of Time-Dependent Materials*, vol. 11, pp. 111–126, 2 2007.

[78] E. M. Woo, "Moisture-temperature equivalency in creep analysis of a heterogeneous-matrix carbon fibre/epoxy composite," *Composites*, vol. 25, pp. 425–430, 6 1994, ISSN: 00104361. DOI: 10.1016/0010-4361(94)90098-1.

[79] K. Aniskevich, R. Krastev, and Y. Hristova, "Effect of long-term exposure to water on the viscoelastic properties of an epoxy-based composition," *Mechanics of Composite Materials*, vol. 45, pp. 137–144, 2 2009.

[80] X. J. Fan, S. W. Lee, and Q. Han, "Experimental investigations and model study of moisture behaviors in polymeric materials," *Microelectronics Reliability*, vol. 49, pp. 861–871, 8 2009.

[81] A. Valls-Lluch, W. Camacho, A. Ribes-Greus, and S. Karlsson, "Influence of water on the viscoelastic behavior of recycled nylon 6,6," *Journal of Applied Polymer Science*, vol. 85, pp. 2211–2218, 10 2002.

[82] F. Goldschmidt and S. Diebels, "Modelling and numerical investigations of the mechanical behavior of polyurethane under the influence of moisture," *Archive of Applied Mechanics*, vol. 85, pp. 1035–1042, 8 2015, ISSN: 14320681.

[83] W. D. Callister and D. G. Rethwisch, *Material Science and Engineering, An Introduction*, 8th ed. John Wiley and Sons, Inc., 2010, p. 1000.

[84] M. L. Williams, R. F. Landel, and J. D. Ferry, "The temperature dependence of relaxation mechanisms in amorphous polymers and other glass-forming liquids," *Journal of the American Chemical Society*, vol. 77, pp. 3701–3707, 14 1955.

[85] R. M. Christensen, *Theory of Viscoelasticity, An Introduction*, 2nd ed. Dover Publications Inc., 2003, p. 363.

[86] L. Sperling, *Introduction to Physical Polymer Science*. John Wiley and Sons, Inc, 2006.

[87] H. Ardebili, E. H. Wong, and M. Pecht, "Hygroscopic swelling and sorption characteristics of epoxy molding compounds used in electronic packaging," *IEEE Transactions on Components, Packaging and Manufacturing Technology*, vol. 26, pp. 206–214, 1 2003.

[88] Y. J. Chang, C. T. Chen, and A. V. Tobolsky, "Correlations between types of absorbed water molecules and water permeability in swollen polymer membranes," *Journal of Polymer Science Part B: Polymer Physics*, vol. 12, pp. 1–6, 1 1974.

[89] W.-I. Cha, S.-H. Hyon, and Y. Ikada, "Microstructure of poly(vinyl alcohol) hydrogels investigated with differential scanning calorimetry," *Die Makromolekulare Chemie*, vol. 194, pp. 2433–2441, 9 1993, ISSN: 0025-116X. DOI: 10.1002/macp.1993.021940902.

[90] A. Higuchi and T. Iijima, "D.s.c. investigation of the states of water in poly(vinyl alcohol) membranes," *Polymer*, vol. 26, pp. 1207–1211, 1985.

[91] W. N. Findley, *Creep and relaxation of nonlinear viscoelastic materials : with an introduction to linear viscoelasticity*, W. N. Findley, J. S. Lai, and K. Onaran, Eds. Dover Publications Inc., 1989, p. 380.

[92] B. Yang, W. M. Huang, C. Li, and L. Li, "Effects of moisture on the thermomechanical properties of a polyurethane shape memory polymer," *Polymer*, vol. 47, pp. 1348–1356, 4 2006, ISSN: 00323861. DOI: 10.1016/j.polymer.2005.12.051.

[93] M. Pannico and P. L. Manna, "Sorption of water vapor in poly (l-lactic acid): A time-resolved ftir spectroscopy investigation," *Frontiers in Chemistry*, vol. 7, pp. 1–10, April 2019. DOI: 10.3389/fchem.2019.00275.

[94] B. C. Hancock, S. D. Clas, and K. Christensen, "Micro-scale measurement of the mechanical properties of compressed pharmaceutical powders. 1: The elasticity and fracture behavior of microcrystalline cellulose," *International Journal of Pharmaceutics*, vol. 209, 2000. [Online]. Available: www.elsevier.com/locate/ijpharm.

[95] L. Mascia, Y. Kouparitsas, D. Nocita, and X. Bao, "Antiplasticization of polymer materials: Structural aspects and effects on mechanical and diffusion-controlled properties," *Polymers*, vol. 12, 4 Apr. 2020, ISSN: 20734360.

[96] N. Jain, A. Verma, and V. K. Singh, "Dynamic mechanical analysis and creep-recovery behaviour of polyvinyl alcohol based cross-linked biocomposite reinforced with basalt fiber," *Materials Research Express*, vol. 6, 10 2019.

[97] Y. Nakazato, S. Zhu, A. Usuki, and M. Kato, "Analysis and prediction of creep viscoelasticity in nylon 6 clay hybrid nanocomposites," *Journal of Solid Mechanics*, vol. 4, pp. 856–863, 6 2010.

[98] A. L. Simal and A. R. Martin, "Structure of heat-treated nylon 6 and 6.6 fibers. i. the shrinkage mechanism," *Journal of Applied Polymer Science*, vol. 68, 3 1998.

[99] L. A. D. G. Oriani and A. L. Simal, "Structure of heat-treated nylon 6 fibers. i. application of the arrhenius equation," *Journal of Polymer Science*, vol. 46, pp. 1973–1985, 11 1992, ISSN: 10974628. DOI: 10.1002/app.1992.070461110.

[100] M. Teodorescu, M. Bercea, and S. Morariu, "Biomaterials of pva and pvp in medical and pharmaceutical applications: Perspectives and challenges," *Biotechnology Advances*, vol. 37, pp. 109–131, 1 Jan. 2019, ISSN: 07349750. DOI: 10.1016/j.biotechadv.2018.11.008.

[101] T. Gaaz *et al.*, "Properties and applications of polyvinyl alcohol, halloysite nanotubes and their nanocomposites," *Molecules*, vol. 20, pp. 22 833–22 847, 12 Dec. 2015, ISSN: 14203049. DOI: 10.3390/molecules201219884.

[102] M. C. Lin, C. W. Lou, J. Y. Lin, T. A. Lin, Y. S. Chen, and J. H. Lin, "Biodegradable polyvinyl alcohol vascular stents: Structural model and mechanical and biological property evaluation," *Materials Science and Engineering: C*, vol. 91, pp. 404–413, Oct. 2018, ISSN: 09284931. DOI: 10.1016/j.msec.2018.05.030.

[103] D. Li *et al.*, "Preparation of plasticized poly (lactic acid) and its influence on the properties of composite materials," *PLoS ONE*, vol. 13, pp. 1–15, 3 2018, ISSN: 19326203. DOI: 10.1371/journal.pone.0193520.

[104] M. A. Rahman *et al.*, "Biocomposites based on lignin and plasticized poly (l -lactic acid)," *Journal of Applied Polymer Science*, pp. 202–214, 2013.

[105] G. Baschek, G. Hartwig, and F. Zahradnik, "Effect of water absorption in polymers at low and high temperatures," *Polymer*, vol. 40, pp. 3433–3441, 1999.

[106] "Polylactic acid market size, share and trends analysis report by end-use (packaging, textile, agriculture, automotive and transport, electronics), by region (north america, apac, europe), and segment forecasts, 2021 - 2028," Grand View Research, 2021, p. 130. [Online]. Available: https://www.grandviewresearch.com/industry-analysis/polylactic-acid-pla-market.

[107] Y. Ramot, M. Haim-Zada, A. J. Domb, and A. Nyska, "Biocompatibility and safety of pla and its copolymers," *Advanced Drug Delivery Reviews*, vol. 107, pp. 153–162, 2016, ISSN: 18728294. DOI: 10.1016/j.addr.2016.03.012. [Online]. Available: http://dx.doi.org/10.1016/j.addr.2016.03.012.

[108] V. K. Holm, S. Ndoni, and J. Risbo, "The stability of poly(lactic acid) packaging films as influenced by humidity and temperature," *Journal of Food Science*, vol. 71, pp. 40–44, 2 2006.

[109] R. A. Cairncross, J. G. Becker, S. Ramaswamy, and R. O'Connor, "Moisture sorption, transport, and hydrolytic degradation in polylactide," *Applied Biochemistry and Biotechnology*, vol. 131, pp. 774–785, 1-3 2006, ISSN: 02732289. DOI: 10.1385/ABAB:131:1:774.

[110] A. Singh, R. M. Guedes, D. Paiva, and F. D. Magalhães, "Experiment and modelling of the strain-rate-dependent response during in vitro degradation of pla fibres," *SN Applied Sciences*, vol. 2, pp. 1–18, 2 2020, ISSN: 25233971. DOI: 10.1007/s42452-020-1964-4. [Online]. Available: https://doi.org/10.1007/s42452-020-1964-4.

[111] E. C. L. A. M. Harris, "Improving mechanical performance of injection molded pla by controlling crystallinity," *Journal of Applied Polymer Science*, vol. 107, pp. 2246–2255, 2008.

[112] M. Niaounakis, E. Kontou, and M. Xanthis, "Effects of aging on the thermomechanical properties of poly(lactic acid)," *Journal of Applied Polymer Science*, vol. 119, pp. 472–481, 2011, ISSN: 00218995. DOI: 10.1002/app.

[113] D. M. Nieto, M. Alonso-García, M.-A. Pardo-Vicente, and L. Rodríguez-Parada, "Product design by additive manufacturing for water environments: Study of degradation and absorption behavior of pla and petg," *Polymers*, vol. 13, p. 1036, 7 2021, ISSN: 20734360. DOI: 10.3390/polym13071036.

[114] P. Kakanuru and K. Pochiraju, "Moisture ingress and degradation of additively manufactured pla, abs and pla/sic composite parts," *Additive Manufacturing*, vol. 36, p. 101 529, June 2020, ISSN: 22148604. DOI: 10.1016/j.addma.2020.101529. [Online]. Available: https://doi.org/10.1016/j.addma.2020.101529.

[115] S. Farah, D. G. Anderson, and R. Langer, "Physical and mechanical properties of pla , and their functions in widespread applications — a comprehensive review," *Advanced Drug Delivery Reviews*, vol. 107, pp. 367–392, 2016, ISSN: 0169-409X. DOI: 10.1016/j.addr.2016.06.012. [Online]. Available: http://dx.doi.org/10.1016/j.addr.2016.06.012.

[116] A. S. Khan, O. Lopez-Pamies, and R. Kazmi, "Thermo-mechanical large deformation response and constitutive modeling of viscoelastic polymers over a wide range of strain rates and temperatures," *International Journal of Plasticity*, vol. 22, pp. 581–601, 4 2006, ISSN: 07496419. DOI: 10.1016/j.ijplas.2005.08.001.

[117] G. L. Siparsky, K. J. Voorhees, J. R. Dorgan, and K. Schilling, "Water transport in polylactic acid (pla), pla/polycaprolactone copolymers, and pla/polyethylene glycol blends," *Journal of Polymers and the Environment*, vol. 5, pp. 125–136, 3 1997, ISSN: 10647546. DOI: 10.1007/BF02763656.

[118] E. A. Schmitt, D. R. Flanagan, and R. J. Linhardt, "Importance of distinct water environments in the hydrolysis of poly(dl-lactide-co-glycolide)," *Macromolecules*, vol. 27, pp. 743–748, 1994.

[119] M. Algarni, "The influence of raster angle and moisture content on the mechanical properties of pla parts produced by fused deposition modeling," *Polymers*, vol. 13, pp. 1–12, 2 2021, ISSN: 20734360. DOI: 10.3390/polym13020237.

[120] E. H. Backes, L. de N. Pires, L. C. Costa, F. R. Passador, and L. A. Pessan, "Analysis of the degradation during melt processing of pla/biosilicate® composites," *Journal of Composites Science*, vol. 3, p. 52, 2 2019.

[121] "Astm e104-20 standard practice for maintaining constant relative humidity by means of aqueous solutions," American Society for Testing and Materials, Tech. Rep., 2020, p. 5.

[122] J. Crank, *The Mathematics of Diffusion*. Oxford University Press, 1975, p. 421.

[123] Y. Y. Leu and W. S. Chow, "Kinetics of water absorption and thermal properties of poly(lactic acid)/organomontmorillonite/poly(ethylene glycol) nanocomposites," *Journal of Vinyl and Additive Technology*, vol. 17, pp. 40–47, 1 2011, ISSN: 10835601. DOI: 10.1002/vnl.20259.

[124] "Astm d3822-14 (2020) standard test method for tensile properties of single textile fibers," Tech. Rep., 2020.

[125] "Astm d2990-17 standard test methods for tensile, compressive, and flexureal creep and creep-rupture of plastics," Tech. Rep., 2017.

[126] J. Dong, C. Mei, J. Han, S. Lee, and Q. Wu, "3d printed poly(lactic acid) composites with grafted cellulose nanofibers: Effect of nanofiber and post-fabrication annealing treatment on composite flexural properties," *Additive Manufacturing*, vol. 28, pp. 621–628, May 2019, ISSN: 22148604. DOI: 10.1016/j.addma.2019.06.004. [Online]. Available: https://doi.org/10.1016/j.addma.2019.06.004.

[127] M. Drieskens, R. Peeters, J. Mullens, D. Franco, P. J. Lemstra, and D. G. Hristova-Bogaerds, "Structure versus properties relationship of poly(lactic acid). i. effect of crystallinity on barrier properties," *Journal of Polymer Science Part B: Polymer Physics*, vol. 47, pp. 2247–2258, 2009. DOI: 10.1002/polb. [Online]. Available: http://arxiv.org/abs/cond-mat/0406218%0Ahttp://dx.doi.org/10.1002/polb.

[128] H. Tsuji and H. Muramatsu, "Blends of aliphatic polyesters. iv. morphology, swelling behavior, and surface and bulk properties of blends from hydrophobic poly(l-lactide) and hydrophilic poly(vinyl alcohol)," *Journal of Applied Polymer Science*, vol. 81, pp. 2151–2160, 2001.

[129] S Amaya and S Sugiyama, "Development of mems using biodegradable polymer material," 2013, ISBN: 9781467359832.

[130] A. V. Quintero *et al.*, "Printing and encapsulation of electrical conductors on polylactic acid (pla) for sensing applications," 2014, pp. 532–535, ISBN: 9781479935086. DOI: 10.1109/MEMSYS.2014.6765695.

[131] C. J. Robin and K. N. Jonnalagadda, "Effect of size and moisture on the mechanical behavior of su-8 thin films," *Journal of Micromechanics and Microengineering*, vol. 26, 2 Jan. 2016, ISSN: 13616439. DOI: 10.1088/0960-1317/26/2/025020.

[132] K. B. Lee, *Principles of microelectromechanical systems*. WILEY, 2010.

[133] C. C. Nguyen, V. K. T. Ngo, H. Q. Le, and W. L. Li, "Influences of relative humidity on the quality factors of mems cantilever resonators in gas rarefaction," *Microsystem Technologies*, vol. 25, pp. 2767–2782, 7 Jul. 2019, ISSN: 09467076. DOI: 10.1007/s00542-018-4239-x.

[134] P. K. Bajpai, I. Singh, and J. Madaan, "Development and characterization of pla-based green composites: A review," *Journal of Thermoplastic Composite Materials*, vol. 27, pp. 52–81, 1 2014, ISSN: 08927057. DOI: 10.1177/0892705712439571.

[135] V. K. Thakur, M. K. Thakur, P. Raghavan, and M. R. Kessler, "Progress in green polymer composites from lignin for multifunctional applications: A review," *ACS Sustainable Chemistry and Engineering*, vol. 2, pp. 1072–1092, 5 2014, ISSN: 21680485. DOI: 10.1021/sc500087z.

[136] G. Koronis and A. Silva, *Green Composites for Automotive Applications*. Woodhead Publishing, 2019.

[137] K. Jha, R. Kataria, J. Verma, and S. Pradhan, "Potential biodegradable matrices and fiber treatment for green composites: A review," *AIMS Materials Science*, vol. 6, pp. 119–138, 1 2019, ISSN: 23720468. DOI: 10.3934/matersci.2019.1.119.

[138] A. K. Bledzki and A. Jaszkiewicz, "Mechanical performance of biocomposites based on pla and phbv reinforced with natural fibres - a comparative study to pp," *Composites Science and Technology*, vol. 70, pp. 1687–1696, 12 2010, ISSN: 02663538. DOI: 10.1016/j.compscitech.2010.06.005. [Online]. Available: http://dx.doi.org/10.1016/j.compscitech.2010.06.005.

[139] A. K. Bledzki and J Gassan, "Composites reinforced with cellulose based fibres," *Progress in Polymer Science*, vol. 24, pp. 221–274, 1999.

[140] V. Placet, O. Cisse, V. Guicheret-Retel, F. Trivaudey, and L. Boubakar, "Viscoelastic behaviour of single hemp fibre under constant and cyclic humidity environment - experiment and modelling," *ICCM International Conferences on Composite Materials*, vol. 2015-July, July 2015.

[141] S. Oza, H. Ning, I. Ferguson, and N. Lu, "Effect of surface treatment on thermal stability of the hemp-pla composites: Correlation of activation energy with thermal degradation," *Composites Part B: Engineering*, vol. 67, pp. 227–232, 2014, ISSN: 13598368. DOI: 10.1016/j.compositesb.2014.06.033.

[142] A. Jabbar, M. Tausif, H. R. Tahir, A. Basit, M. R. A. Bhatti, and G. Abbas, "Polylactic acid/lyocell fibre as an eco-friendly alternative to polyethylene terephthalate/cotton fibre blended yarns and knitted fabrics," *Journal of The Textile Institute*, vol. 111, pp. 129–138, 1 Jan. 2020, ISSN: 17542340. DOI: 10.1080/00405000.2019.1624070.

[143] G. Rajeshkumar *et al.*, "Environment friendly, renewable and sustainable poly lactic acid (pla) based natural fiber reinforced composites – a comprehensive review," *Journal of Cleaner Production*, vol. 310, p. 127 483, May 2021, ISSN: 09596526. DOI: 10.1016/j.jclepro.2021.127483. [Online]. Available: https://doi.org/10.1016/j.jclepro.2021.127483.

[144] J. Ganster and H. P. Fink, "Novel cellulose fibre reinforced thermoplastic materials," *Cellulose*, vol. 13, pp. 271–280, 3 Jun. 2006, ISSN: 09690239. DOI: 10.1007/s10570-005-9045-9.

[145] M. Sawpan, K. Pickering, and A. Fernyhough, "Hemp fibre reinforced poly(lactic acid) composites," *Advanced Materials and Processes*, vol. 29-30, pp. 337–340, 2007, ISSN: 1662-8985. [Online]. Available: http://www.scientific.net/AMR.29-30.337.

[146] N. Graupner, "Improvement of the mechanical properties of biodegradable hemp fiber reinforced poly(lactic acid) (pla) composites by the admixture of man-made cellulose fibers," *Journal of Composite Materials*, vol. 43, pp. 689–702, 6 2009, ISSN: 00219983. DOI: 10.1177/0021998308100688.

[147] B. Baghaei, M. Skrifvars, and L. Berglin, "Manufacture and characterisation of thermoplastic composites made from pla/hemp co-wrapped hybrid yarn prepregs," *Composites Part A: Applied Science and Manufacturing*, vol. 50, pp. 93–101, 2013, ISSN: 1359835X. DOI: 10.1016/j.compositesa.2013.03.012. [Online]. Available: http://dx.doi.org/10.1016/j.compositesa.2013.03.012.

[148] L. Suryanegara, A. N. Nakagaito, and H. Yano, "The effect of crystallization of pla on the thermal and mechanical properties of microfibrillated cellulose-reinforced pla composites," *Composites Science and Technology*, vol. 69, pp. 1187–1192, 7-8 Jun. 2009, ISSN: 02663538. DOI: 10.1016/j.compscitech.2009.02.022.

[149] M. A. Elsawy, K. H. Kim, J. W. Park, and A. Deep, "Hydrolytic degradation of polylactic acid (pla) and its composites," *Renewable and Sustainable Energy Reviews*, vol. 79, pp. 1346–1352, November 2017, ISSN: 18790690. DOI: 10.1016/j.rser.2017.05.143. [Online]. Available: http://dx.doi.org/10.1016/j.rser.2017.05.143.

[150] M. Bulota, S. Tanpichai, M. Hughes, and S. J. Eichhorn, "Micromechanics of tempo-oxidized fibrillated cellulose composites," *ACS Applied Materials and Interfaces*, vol. 4, pp. 331–337, 1 Jan. 2012, ISSN: 19448244. DOI: 10.1021/am201399q.

[151] M. A. Sawpan, K. L. Pickering, and A. Fernyhough, "Improvement of mechanical performance of industrial hemp fibre reinforced polylactide biocomposites," *Composites Part A: Applied Science and Manufacturing*, vol. 42, pp. 310–319, 3 2011, ISSN: 1359835X. DOI: 10.1016/j.compositesa.2010.12.004. [Online]. Available: http://dx.doi.org/10.1016/j.compositesa.2010.12.004.

[152] S. H. Lee, S. Wang, and Y. Teramoto, "Isothermal crystallization behavior of hybrid biocomposite consisting of regenerated cellulose fiber, clay, and poly(lactic acid)," *Journal of Applied Polymer Science*, vol. 108, pp. 870–875, 2 Apr. 2008, ISSN: 00218995. DOI: 10.1002/app.26853.

[153] M. M. Kim, B. S. Kim, J. R. Ha, S. K. Kim, J. W. Yi, and J. Y. Lim, "Interfacial optimization of lyocell fabric/pla with silane treatments," *Advanced Materials Research*, vol. 123-125, pp. 1155–1158, 2010, ISSN: 10226680. DOI: 10.4028/www.scientific.net/amr.123-125.1155.

[154] J. H. Lin, A. P. Chen, J. Y. Lin, T. A. Lin, and C. W. Lou, "Manufacturing technique and mechanical properties of environment-protective composite nonwoven fabrics," *Advanced Materials Research*, vol. 287-290, pp. 2673–2676, 2011, ISSN: 10226680. DOI: 10.4028/www.scientific.net/AMR.287-290.2673.

[155] C. Woodings, *Regenerated cellulose fibers*. CRC Press LLC, 2001.

[156] S. Zhang *et al.*, "Regenerated cellulose by the lyocell process, a brief review of the process and properties," *BioResources*, vol. 13, pp. 4577–4592, 2 2018.

[157] Y. Zhang *et al.*, "Biodegradable regenerated cellulose-dispersed composites with improved properties via a pickering emulsion process," *Carbohydrate Polymers*, vol. 179, pp. 86–92, Jan. 2018, ISSN: 01448617. DOI: 10.1016/j.carbpol.2017.09.065.

[158] A. Karakoç, A. Miettinen, J. Virkajarvi, and R. Joffe, "Effective elastic properties of biocomposites using 3d computational homogenization and x-ray microcomputed tomography," *Composite Structures*, vol. 273, Oct. 2021, ISSN: 02638223. DOI: 10.1016/j.compstruct.2021.114302.

[159] B. Raju, S. R. Hiremath, and D. R. Mahapatra, "A review of micromechanics based models for effective elastic properties of reinforced polymer matrix composites," *Composite Structures*, vol. 204, pp. 607–619, Nov. 2018, ISSN: 02638223. DOI: 10.1016/j.compstruct.2018.07.125.

[160] F. Vilaseca, R. D. Rey, R. Serrat, J. Alba, P. Mutje, and F. X. Espinach, "Macro and micro-mechanics behavior of stifness in alkaline treated hemp core fibres polypropylene-based composites," *Composites Part B: Engineering*, vol. 144, pp. 118–125, Jul. 2018, ISSN: 13598368. DOI: 10.1016/j.compositesb.2018.02.029.

[161] V. Mazzanti, R. Pariante, A. Bonanno, O. R. de Ballesteros, F. Mollica, and G. Filippone, "Reinforcing mechanisms of natural fibers in green composites: Role of fibers morphology in a pla/hemp model system," *Composites Science and Technology*, vol. 180, pp. 51–59, May 2019, ISSN: 02663538. DOI: 10.1016/j.compscitech.2019.05.015. [Online]. Available: https://doi.org/10.1016/j.compscitech.2019.05.015.

[162] N. Pan, "The elastic constants of randomly oriented fiber composites: A new approach to prediction," *Science and Engineering of Composite Materials*, vol. 5, pp. 63–72, 2 1996.

[163] G. Jiang *et al.*, "Structure and properties of regenerated cellulose fibers from different technology processes," *Carbohydrate Polymers*, vol. 87, pp. 2012–2018, 3 Feb. 2012, ISSN: 01448617. DOI: 10.1016/j.carbpol.2011.10.022.

[164] Z. Hashin, "Complex moduli of viscoelastic composites-ii. fiber reinforced materials," *International Journal of Solids and Structures*, vol. 6, pp. 797–807, 6 1970, ISSN: 00207683. DOI: 10.1016/0020-7683(70)90018-1. [Online]. Available: http://dx.doi.org/10.1016/0020-7683(70)90018-1.

[165] J. C. Halpin, *Primer on Composite Materials Analysis*, 1st ed. CRC Press, 1992, p. 240.

[166] *How is biomid fiber made*, 2018. [Online]. Available: https://biomidfiber.com/.

[167] I. I. Qamhia, "Experimental and analytical characterization of regenerated/-nano cellulose composites," University of Wisconsin-Milwaukee, 2014. [Online]. Available: http://dc.uwm.edu/etd.

[168] M. Legault, *Bio-composites update: Beyong eco-branding*, Jun. 2013. [Online]. Available: https://www.compositesworld.com/articles/biocomposites-update-beyond-eco-branding.

[169] "Astm d3379-75 standard test method for tensile strength and young's modulus for high-modulus single-filament materials," Tech. Rep., 1989.

[170] L Lim, R Auras, and M Rubino, "Processing technologies for poly (lactic acid)," *Progress in Polymer Science*, vol. 33, pp. 820–852, 2008. DOI: 10.1016/j.progpolymsci.2008.05.004.

[171] F. EW, S. HJ, and W. G, "Investigation of the structure of solution grown crystals of lactide copolymers by means of chemical reactions," *Kolloid-Zeitschrift und Zeitschrift für Polymere*, pp. 980–990, 251 1973.

[172] A. Pei, Q. Zhou, and L. A. Berglund, "Functionalized cellulose nanocrystals as biobased nucleation agents in poly(l-lactide) (plla) - crystallization and mechanical property effects," *Composites Science and Technology*, vol. 70, pp. 815–821, 5 May 2010, ISSN: 02663538. DOI: 10.1016/j.compscitech.2010.01.018.

[173] L. Suryanegara, A. N. Nakagaito, and H. Yano, "Thermo-mechanical properties of microfibrillated cellulose-reinforced partially crystallized pla composites," *Cellulose*, vol. 17, pp. 771–778, 4 2010, ISSN: 09690239. DOI: 10.1007/s10570-010-9419-5.

[174] Z. Ren, R. Guo, H. Bi, X. Jia, M. Xu, and L. Cai, "Interfacial adhesion of polylactic acid on cellulose surface: A molecular dynamics study," *ACS Applied Materials and Interfaces*, vol. 12, pp. 3236–3244, 2 Jan. 2020, ISSN: 19448252. DOI: 10.1021/acsami.9b20101.

[175] L. Monette, M. P. Anderson, and G. S. Grest, "The meaning of the critical length concept in composites: Study of matrix viscosity and strain rate on the average fiber fragmentation length in short-fiber polymer composites," *Polymer Composites*, vol. 14, pp. 101–115, 2 1993, ISSN: 15480569. DOI: 10.1002/pc.750140204.

[176] S. R. Ryu and D. J. Lee, "Effects of fiber aspect ratio, fiber content, and bonding agent on tensile and tear properties of short-fiber reinforced rubber," *KSME International Journal*, vol. 15, pp. 35–43, 1 2001, ISSN: 12264865. DOI: 10.1007/BF03184796.

[177] I. Robinson and J. Robinson, "The effect of fibre aspect ratio on the stiffness of discontinuous fibre-reinforced composites," *Composites*, vol. 25, p. 499, 7 1994.

[178] S. Houshyar, R. A. Shanks, and A. Hodzic, "The effect of fiber concentration on mechanical and thermal properties of fiber-reinforced polypropylene composites," *Journal of Applied Polymer Science*, vol. 96, pp. 2260–2272, 6 Jun. 2005, ISSN: 00218995. DOI: 10.1002/app.20874.

[179] I. H. Sahputra, A. Alexiadis, and M. J. Adams, "Effects of moisture on the mechanical properties of microcrystalline cellulose and the mobility of the water molecules as studied by the hybrid molecular mechanics–molecular dynamics simulation method," *Journal of Polymer Science, Part B: Polymer Physics*, vol. 57, pp. 454–464, 8 Apr. 2019, ISSN: 10990488. DOI: 10.1002/polb.24801.

[180] H. Cheung, M. Ho, K. Lau, F. Cardona, and D. Hui, "Natural fibre-reinforced composites for bioengineering and environmental engineering applications," *Composites Part B: Engineering*, vol. 40, pp. 655–663, 7 Oct. 2009, ISSN: 13598368. DOI: 10.1016/j.compositesb.2009.04.014.

[181] Y. K. Dasan, A. H. Bhat, and F. Ahmad, "Polymer blend of pla/phbv based bionanocomposites reinforced with nanocrystalline cellulose for potential application as packaging material," *Carbohydrate Polymers*, vol. 157, pp. 1323–1332, Feb. 2017, ISSN: 01448617. DOI: 10.1016/j.carbpol.2016.11.012.

[182] Y. Chen, T. Tang, and C. Ayranci, "Linear viscoelasticity of bio-based composites of polylactic acid and regenerated cellulose fibers: Modeling and experimental validation," 2022.

[183] T. Sun, C. Yu, W. Yang, J. Zhong, and Q. Xu, "Experimental and numerical research on the nonlinear creep response of polymeric composites under humid environments," *Composite Structures*, vol. 251, Nov. 2020, ISSN: 02638223. DOI: 10.1016/j.compstruct.2020.112673.

[184] A. Moudood, A. Rahman, N. M. L. Huq, A. Öchsner, M. M. Islam, and G. Francucci, "Mechanical properties of flax fiber-reinforced composites at different relative humidities: Experimental, geometric, and displacement potential function approaches," *Polymer Composites*, vol. 41, pp. 4963–4973, 12 Dec. 2020, ISSN: 15480569. DOI: 10.1002/pc.25766.

[185] S. Panthapulakkal and M. Sain, "Injection-molded short hemp fiber/glass fiber-reinforced polypropylene hybrid composites -mechanical, water absorption and thermal properties," *Journal of Applied Polymer Science*, vol. 103, pp. 2432–2441, 4 Feb. 2007, ISSN: 00218995. DOI: 10.1002/app.25486.

[186] V. A. Alvarez, A. N. Fraga, and A. Vázquez, "Effects of the moisture and fiber content on the mechanical properties of biodegradable polymer-sisal fiber biocomposites," *Journal of Applied Polymer Science*, vol. 91, pp. 4007–4016, 6 Mar. 2004, ISSN: 00218995. DOI: 10.1002/app.13561.

[187] C. P. Chow, X. S. Xing, and R. K. Li, "Moisture absorption studies of sisal fibre reinforced polypropylene composites," *Composites Science and Technology*, vol. 67, pp. 306–313, 2 Feb. 2007, ISSN: 02663538. DOI: 10.1016/j.compscitech.2006.08.005.

[188] X. Lu, M. Q. Zhang, M. Z. Rong, G. Shi, and G. C. Yang, "All-plant fiber composites. ii: Water absorption behavior and biodegradability of unidirectional sisal fiber reinforced benzylated wood," *Polymer Composites*, vol. 24, pp. 367–379, 3 2003, ISSN: 15480569. DOI: 10.1002/pc.10036.

[189] T. Bechtold and C. B. Schimper, "Hydrolysis of regenerated cellulose fibres for textile and other applications," *Advances in Textile Biotechnology*, pp. 312–327, Jan. 2010. DOI: 10.1533/9780857090232.2.312.

[190] M. M. Lu, C. A. Fuentes, and A. W. V. Vuure, "Moisture sorption and swelling of flax fibre and flax fibre composites," *Composites Part B: Engineering*, vol. 231, Feb. 2022, ISSN: 13598368. DOI: 10.1016/j.compositesb.2021.109538.

[191] Y. Zhou, M. Fan, and L. Chen, "Interface and bonding mechanisms of plant fibre composites: An overview," *Composites Part B: Engineering*, vol. 101, pp. 31–45, Sep. 2016, ISSN: 13598368. DOI: 10.1016/j.compositesb.2016.06.055.

[192] L. T. Lim, I. J. Britt, and M. A. Tung, "Sorption and transport of water vapor in nylon 6,6 film," *Journal of Applied Polymer Science*, vol. 71, pp. 197–206, 2 Jan. 1999, ISSN: 00218995. DOI: 10.1002/(SICI)1097-4628(19990110)71:2⟨197::AID-APP2⟩3.0.CO;2-J.

[193] S. M. K. Thiagamani, M. E. Hoque, S. Krishnasamy, C. Muthukumar, and S. Siengchin, *Vibration and Damping Behavior of Biocomposites*, 1st ed. CRC Press, 2022.

[194] F. Tian, Y. Pan, and Z. Zhong, "A long-term mechanical degradation model of unidirectional natural fiber reinforced composites under hydrothermal ageing," *Composites Science and Technology*, vol. 142, pp. 156–162, Apr. 2017, ISSN: 02663538. DOI: 10.1016/j.compscitech.2017.01.021.

[195] S. Neumann and G. Marom, "Stress dependence of the coefficient of moisture diffusion in composite materials," *Polymer Composites*, vol. 6, pp. 9–12, 1 1985.

[196] C. H. Shen and G. S. Springer, "Moisture absorption and desorption of composite materials," *Journal of Composite Materials*, vol. 10, pp. 2–20, 1 1976, ISSN: 1530793x. DOI: 10.1177/002199837601000101.

[197] D. W. Wei, H. Wei, A. C. Gauthier, J. Song, Y. Jin, and H. Xiao, "Superhydrophobic modification of cellulose and cotton textiles: Methodologies and applications," *Journal of Bioresources and Bioproducts*, vol. 5, pp. 1–15, 1 Feb. 2020, ISSN: 23699698. DOI: 10.1016/j.jobab.2020.03.001.

Appendix A: Supplementary Information Related to Chapter 4

The constants in equation 4.13 are given by:

$F_6 = C_1C_8C_{15}$

$F_5 = C_2C_8C_{15} + C_1C_9C_{15} + C_1C_8C_{16}$

$F_4 = C_3C_8C_{15} + C_2C_9C_{15} + C_1C_{10}C_{15} + C_2C_8C_{16} + C_1C_9C_{16} + C_1C_8C_{10}$

$F_3 = C_3C_9C_{15} + C_2C_{10}C_{15} + C_3C_8C_{16} + C_2C_9C_{16} + C_1C_{10}C_{16} + C_2C_8C_{10} + C_1C_9C_{10}$

$F_2 = C_3C_{10}C_{15} + C_3C_9C_{16} + C_2C_{10}C_{16} + C_3C_8C_{10} + C_2C_9C_{10} + C_1C_{10}C_{10}$

$F_1 = C_3C_{10}C_{16} + C_3C_9C_{10} + C_2C_{10}C_{10}$

$F_0 = C_3C_{10}C_17$

$D_7 = C_8C_{11} + C_4C_{15}$

$D_6 = C_9C_{11} + C_8C_{12} + C_5C_{15} + C_4C_{16}$

$D_5 = C_{10}C_{11} + C_9C_{12} + C_8C_{13} + C_6C_{15} + C_5C_{16} + C_4C_{10}$

$D_4 = C_{10}C_{12} + C_9C_{13} + C_8C_{14} + C_7C_{15} + C_6C_{16} + C_5C_{10}$

$D_3 = C_{10}C_{13} + C_9C_{14} + C_7C_{16} + C_6C_{10}$

$D_2 = C_{10}C_{14} + C_7C_{10}$

$C_1 = 8\mu_{m1}\mu_{m2}$

$C_2 = 8(E_{m2}\mu_{m1} + E_{m1}\mu_{m2} + E_{m2}\mu_{m2})$

$C_3 = 8E_{m1}E_{m2}$

$C_4 = 3E_{m2}\mu_{m2}[(-1 + V_f)E_{m2}(1/E_f)\mu_{m1}^2\mu_{m2}\xi_1 + \mu_{m1}^2\mu_{m2}(1 + V_f\xi_1)]$

$C_5 = 3E_{m2}\mu_{m2}[E_{m2}\mu_{m1}^2 + V_fE_{m2}\mu_{m1}^2\xi_1 - 2(-1+V_f)E_{m1}E_{m2}(1/E_f)\mu_{m1}\mu_{m2}\xi_1 + 2E_{m1}\mu_{m1}\mu_{m2}(1+$
$V_f\xi_1) + E_{m2}\mu_{m1}\mu_{m2}(1 + V_f\xi_1)]$

$C_6 = 3E_{m2}\mu_{m2}[2E_{m1}E_{m2}\mu_{m1} + 2V_f E_{m1}E_{m2}\mu_{m1}\xi_1 - (-1+V_f)E_{m1}^2E_{m2}(1/E_f)\mu_{m2}\xi_1 + E_{m1}^2\mu_{m2}(1+V_f\xi_1) + E_{m1}E_{m2}\mu_{m2}(1+V_f\xi_1)]$

$C_7 = 3E_{m2}\mu_{m2}(E_{m1}^2E_{m2} + V_f E_{m1}^2E_{m2}\xi_1)$

$C_8 = (1-V_f)\mu_{m1}\mu_{m2} + E_{m2}(1/E_f)\mu_{m1}\mu_{m2}(V_f+\xi_1)$

$C_9 = E_{m2}\mu_{m1} - V_f E_{m2}\mu_{m1} + (1-V_f)E_{m1}\mu_{m2} + (1-V_f)E_{m2}\mu_{m2} + E_{m1}E_{m2}(1/E_f)\mu_{m2}(V_f+\xi_1)$

$C_{10} = E_{m1}E_{m2} - V_f E_{m1}E_{m2}$

$C_{11} = 5E_{m2}\mu_{m2}[(-1+V_f)E_{m2}(1/E_f)\mu_{m1}^2\mu_{m2}\xi_2 + \mu_{m1}^2\mu_{m2}(1+V_f\xi_2)]$

$C_{12} = 5E_{m2}\mu_{m2}[E_{m2}\mu_{m1}^2 + V_f E_{m2}\mu_{m1}^2\xi_2 - 2(1+V_f)E_{m1}E_{m2}(1/E_f)\mu_{m1}\mu_{m2}\xi_2 + 2E_{m1}\mu_{m1}\mu_{m2}(1+V_f\xi_2) + E_{m2}\mu_{m1}\mu_{m2}(1+V_f\xi_2)]$

$C_{13} = 5E_{m2}\mu_{m2}[2E_{m1}E_{m2}\mu_{m1} + 2V_f E_{m1}E_{m2}\mu_{m1}\xi_2 - (-1+V_f)E_{m1}^2E_{m2}(1/E_f)\mu_{m2}\xi_2 + E_{m1}^2\mu_{m2}(1+V_f\xi_2) + E_{m1}E_{m2}\mu_{m2}(1+V_f\xi_2)]$

$C_{14} = 5E_{m2}\mu_{m2}(E_{m1}^2E_{m2} + V_f E_{m1}^2E_{m2}\xi_2)$

$C_{15} = (1-V_f)\mu_{m1}\mu_{m2} + E_{m2}(1/E_f)\mu_{m1}\mu_{m2}(V_f+\xi_2)$

$C_{16} = E_{m2}\mu_{m1} - V_f E_{m2}\mu_{m1} + (1-V_f)E_{m1}\mu_{m2} + (1-V_f)E_{m2}\mu_{m2} + E_{m1}E_{m2}(1/E_f)\mu_{m2}(V_f+\xi_2)$

Appendix B: Matlab code related to Chapter 2 and Chapter 3

Here is a section by section illustration of the code. Using Code for Onogi's data using PVA DP 600 at 20°C as an example

Head of the file includes close all variables and matlab windows. Also, it give the necessary details on data file preparation, notes about the unit, algorithms for the fitting, related assumptions and some necessary explanations.

```
%############################################################
%Modified Burgers Reimschuessel model
%############################################################


clear all
close all
%Section 0: Some illustrations for this file
%1. Data file preparation:
%    - All data in excel file of CSV
%    - First column is time, no heading, pay attention to the ...
   provided unit
%    - Second column is the corresponding valune, no heading, pay ...
   attention to the provided unit
%2. Default algorithm of fitting is the so-called Trust-region ...
   nonlinear least square fit, in which the starting points
%   and upper and lower limit of the fitting parameters are ...
   recommended to specify. Order of magnitude would work for
%   starting points
%3. Before this algorithm is running, use the Matlab fit function ...
   tool box (cftool in command window) to try and find
%   the best parameters: StartPoint, Upper, Lower
%4. It is assumed that the experiment is running in an ideal step ...
   strain at the begining of the test. That is to say,
%   the instantaneous elastic strain, taken by spring E_2 is ...
   uncoupled with other parameters. However, other material
%   material's viscoelastic parameters E_1, mu_1 and mu_2 are all ...
```

```
   coupled and has to be fitted. In this code, the value
%   of E_2 is provided in each fitting for the stress relaxation test.
%5. In this function the Burger's model in Kelvin representation ...
   with creep solution is used.
%   - E_1 is the Kelvin part elastic modulus, the elastic modulus of ...
   the recoverble creep part
%   - E_2 is the Maxweel part elastic modulus, the instantaneous ...
   elastic modulus
%   - mu_1 is the Kelvin part viscosity, the viscosity of the ...
   recoverble creep part
%   - mu_2 is the Maxwell part viscosity, the reason for the ...
   irrecoverable part
%6. In this code, we are working with Onogi 1962's PVA data, with ...
   degree of polymerization 600, at 20 degree
%   Their moisture absorption data are given with respect to the ...
   conditioning RH. However, the one-to-one correspondence
%   of the RH and the water content in the material is given. Thus, ...
   we are using water content as independent variable
%   Here is the conversion chart:
%      RH%        Water Content%
%      00            0.0
%      33            4.5
%      45            6.4
%      60            8.5
%      75           15.5
```

In the first section, the original data is read from the data file. Then, a figure window is created and maximized to plot the data. The hold is turned on to allow all experimental data and later the fitting curves to be plotted on the same figure.

```
%Section 1: Read the Original Data and Plot the Original Data
% This section is intended to create a figure and plot the original ...
   experimental data
%  Figure initilization:
fig1 = figure;
fig1.WindowState = 'maximized';
%  Read the data file:
%   In all the dataset, time in seconds and Relaxation Modulus in MPa
RH0relaxation = readmatrix('0RH.xlsx');
RH33relaxation = readmatrix('33RH.xlsx');
RH45relaxation = readmatrix('45RH.xlsx');
RH60relaxation = readmatrix('60RH.xlsx');
RH75relaxation = readmatrix('75RH.xlsx');
%  Plot the data
plot(RH0relaxation(:,1),RH0relaxation(:,2),'r*',...
'MarkerSize',12)%Plot the experimental data at water content level 0
hold on %Make sure all plot on the same figure
plot(RH33relaxation(:,1),RH33relaxation(:,2),'ro',...
'MarkerSize',12)%Plot the experimental data at water content level 4.5
plot(RH45relaxation(:,1),RH45relaxation(:,2),'rs',...
```

```
'MarkerSize',12)%Plot the experimental data at water content level 6.4
plot(RH60relaxation(:,1),RH60relaxation(:,2),'rd',...
'MarkerSize',12)%Plot the experimental data at water content level 8.5
plot(RH75relaxation(:,1),RH75relaxation(:,2),'r+',...
'MarkerSize',12)%Plot the experimental data at water content level 15.5
%Section 1 END: Read the Original Data and Plot the Original Data
```

In the second section, the stress relaxation curve from Burger's model is fitted to the experimental data. The fit function is used to fit and give the fitted parameters. The fitting and the goodness of fit is provided and stored. The process is conducted for multiple times, corresponding to the multiple moisture levels. Only the fist moisture level with complete comments is shown here in this report.

```
%Section 2: Fit the stress relaxation data
%a is r_1
%b is r_2
%c is A
relax_function = ...
    fittype('(5590/(b-a))*((c-a)*exp(-a*x)-(c-b)*exp(-b*x))');%Define ...
    the fit type, a customized function, which is the creep function ...
    here
options = fitoptions(relax_function);%Take out the options structure ...
    of fit
options.StartPoint = [1 1.1 0.01] ;% Set the start point of the fit
options.Lower = [0 0 0];%Set the lower limit of the range
options.Upper = [10 10 10];%Set the upper limit of the range
[f1,gof1] = fit(RH0relaxation(:,1),RH0relaxation(:,2),...
relax_function,options)%FIT! And give the goodness of fit
t = 0:1e4;%Generate the time points
relax = (5590/(f1.b-f1.a))*((f1.c-f1.a)*exp(-f1.a*t)...
-(f1.c-f1.b)*exp(-f1.b*t));%Put the time points into the fitted function
plot(t,relax,'b','LineWidth',2)%Plot the fitted curve

relax_function = ...
    fittype('(4840/(b-a))*((c-a)*exp(-a*x)-(c-b)*exp(-b*x)) ...
    ');%Define the fit type, a customized function, which is the ...
    creep function here
options = fitoptions(relax_function);%Take out the options structure ...
    of fit
options.StartPoint = [1 1.1 0.01] ;% Set the start point of the fit
options.Lower = [0 0 0];%Set the lower limit of the range
options.Upper = [10 10 10];%Set the upper limit of the range
[f2,gof2] = fit(RH33relaxation(:,1),RH33relaxation(:,2),...
relax_function,options)%FIT! And give the goodness of fit
clear relax
relax = (4840/(f2.b-f2.a))*((f2.c-f2.a)*exp(-f2.a*t)-...
(f2.c-f2.b)*exp(-f2.b*t));%Put the time points into the fitted function
plot(t,relax,'b','LineWidth',2)%Plot the fitted curve
```

```
relax_function = ...
    fittype('(3097/(b-a))*((c-a)*exp(-a*x)-(c-b)*exp(-b*x)) ...
    ');%Define the fit type, a customized function, which is the ...
    creep function here
options = fitoptions(relax_function);%Take out the options structure ...
    of fit
options.StartPoint = [1 1.1 0.01] ;% Set the start point of the fit
options.Lower = [0 0 0];%Set the lower limit of the range
options.Upper = [10 10 10];%Set the upper limit of the range
[f3,gof3] = fit(RH45relaxation(:,1),RH45relaxation(:,2),...
relax_function,options)%FIT! And give the goodness of fit
clear relax
relax = (3097/(f3.b-f3.a))*((f3.c-f3.a)*exp(-f3.a*t)-...
(f3.c-f3.b)*exp(-f3.b*t));%Put the time points into the fitted function
plot(t,relax,'b','LineWidth',2)%Plot the fitted curve


relax_function = ...
    fittype('(906/(b-a))*((c-a)*exp(-a*x)-(c-b)*exp(-b*x)) ...
    ');%Define the fit type, a customized function, which is the ...
    creep function here
options = fitoptions(relax_function);%Take out the options structure ...
    of fit
options.StartPoint = [1 1.1 0.01] ;% Set the start point of the fit
options.Lower = [0 0 0];%Set the lower limit of the range
options.Upper = [10 10 10];%Set the upper limit of the range
[f4,gof4] = fit(RH60relaxation(:,1),RH60relaxation(:,2),...
relax_function,options)%FIT! And give the goodness of fit
clear relax
relax = (906/(f4.b-f4.a))*((f4.c-f4.a)*exp(-f4.a*t)-...
(f4.c-f4.b)*exp(-f4.b*t));%Put the time points into the fitted function
plot(t,relax,'b','LineWidth',2)%Plot the fitted curve

relax_function = ...
    fittype('(260/(b-a))*((c-a)*exp(-a*x)-(c-b)*exp(-b*x)) ...
    ');%Define the fit type, a customized function, which is the ...
    creep function here
options = fitoptions(relax_function);%Take out the options structure ...
    of fit
options.StartPoint = [1 1.1 0.01] ;% Set the start point of the fit
options.Lower = [0 0 0];%Set the lower limit of the range
options.Upper = [10 10 10];%Set the upper limit of the range
[f5,gof5] = fit(RH75relaxation(:,1),RH75relaxation(:,2),...
relax_function,options)%FIT! And give the goodness of fit
clear relax
relax = (260/(f5.b-f5.a))*((f5.c-f5.a)*exp(-f5.a*t)-...
(f5.c-f5.b)*exp(-f5.b*t));%Put the time points into the fitted function
plot(t,relax,'b','LineWidth',2)%Plot the fitted curve
```

At the end of this section, the plot is modified for a better view. Including:adding labels, legend, title and change the font size of the fonts in this figure. There is only

one note here. For the legend, we are intended to tell the difference between the experimental data of different moisture levels. Therefore, each of them will have a different shape on the data point and has to be demonstrated in the legend part. However, for the model fitted curves for each moisture level and the author's fitting in different moisture level, there is no need to tell the difference of the fitting curves between the different moisture levels. They all shown as blue solid line or block solid line. So only one legend is needed for our fitting curve. In the Matlab, when the number of legend provided in the code is less than the number of curves in the figure, it will only label the first plotted curves with the legends.

```
% Adjust the plot settings for this viscoelastic model fitting plot
xlabel('\bf Time(s)') %Define the x-label text
ylabel('\bf Relaxation Modulus (MPa)') %Define the y-label text
legend({'0%','4.5%','6.4%','8.5%','15.5%','Fit with Burgers ...
   model'},'FontSize',16,'Location','best') %Put the legend on
title('Onogi 1962: PVA films with DP 600 under 25^o C') %Put the ...
   title of the chart on
ax=gca;%The following is to adjust the figure properties
ax.XAxis.FontSize = 14;%font size of x-ticks
ax.YAxis.FontSize = 14;%font size of y-ticks
ax.XLabel.FontSize = 16;%font size of x-label
ax.YLabel.FontSize = 16;%font size of y-label
ax.Title.FontSize = 18;%font size of title
%Section 2 END: Fit the stress relaxation data
```

In the third section, the fitted parameters are stored and the Burger's model parameters are back calculated and stored.

```
%Section 3: Parameters with respect to moisture
% Input the calculated E_2 data
E_2 = [5590 4840 3097 906 260]';

r_1 = [f1.a, f2.a, f3.a, f4.a, f5.a]';
r_2 = [f1.b, f2.b, f3.b, f4.b, f5.b]';
A = [f1.c, f2.c, f3.c, f4.c, f5.c]';
p_1 = (r_1+r_2)./(r_1.*r_2);
p_2 = ones(length(r_1),1)./(r_1.*r_2);

mu_2 = p_2.*A.*E_2;
E_1 = (mu_2)./(p_1 - ones(length(A),1)./(A)-p_2.*A);
mu_1 = (p_2.*E_2)./(p_1 - ones(length(A),1)./(A)-p_2.*A);
```

In the fourth section, the evolution of model parameters are plotted and the moisture decay model is fitted to the data. First making preparations for the fitting and plot, that includes generate a continuous moisture variable and create a figure to contain the four subplots of the four Burger's model parameters:

```
%Section 4: Plot the evolution of model parameters with respect to ...
   moisture content and fit the moisture model==========
% This section is intended to plot the extracted model parameters ...
   with respect to moisture and fit with the CTA moisture
% decay model. In this script, it is the modified nonlinear ...
   Reimschuessel's model with Gaussian's function.
%  Initialization
C = [0, 4.5 6.4 8.5 15.5]'; %The experimental moisture levels
C_cont = 0:0.01:16; %Generate a continuous moisture levels
fig2 = figure; %Create a new figure
fig2.WindowState = 'maximized'; %Maximize the window size
```

In each of the subplot, the evolution of each parameters with respect to moisture is fitted first. Then the fitting results is plotted with the fitted parameters. Finally, the format of the subplot is tuned and the fitting results as well as the goodness of fit (Adjusted R^2) is shown in the command window.

```
%Section 4: Plot the model parameters evolution
C = [0, 4.5 6.4 8.5 15.5]';

C_cont = 0:0.01:16;% generate a continuous moisture levels
fig2 = figure;
fig2.WindowState = 'maximized';
subplot(2,2,1);
plot(C,E_1,'ro','MarkerSize',12)%Plot the E_1 with respect to moisture
hold on
E_1_function = ...
   fittype('A+(20637-A)*exp(-B*x)+C*x*exp(-D*x)');%Define the fit ...
   type, a customized function, so called Reimschuessel's model
%E_1 initial is fixed, the value at 0 moisture content, which is ...
   1962.65 MPa
%A is E_1 final
%B is the parameter decay rate
%C is the magnitude of hydrogen bonding reinforcement
%D is the reinforcement effect decay rate
options = fitoptions(E_1_function);%Take out the options structure ...
   of fit
options.StartPoint = [0 0.3 1e3 0.3];% Set the start point of the fit
options.Lower = [0 0 0 0.25];
```

```
options.Upper = [Inf 10 Inf 1];
[fE1,gofE1] = fit(C,E_1,E_1_function,options);%FIT! And give the ...
    goodness of fit
E_1_fit = fE1.A+(20637-fE1.A)*exp(-fE1.B*C_cont)+...
fE1.C.*C_cont.*exp(-fE1.D.*C_cont);
plot(C_cont,E_1_fit,'b','LineWidth',2)
%Finally adjust the figure properties to make it looks good
xlabel('\bf Moisture(%)')
ylabel('\bf E_1 (MPa)')
ax=gca;%The following is to adjust the figure properties
ax.XAxis.FontSize = 16;%font size of x-ticks
ax.YAxis.FontSize = 16;%font size of y-ticks
ax.XLabel.FontSize = 16;%font size of x-label
ax.YLabel.FontSize = 16;%font size of y-label
ax.Title.FontSize = 16;%font size of title

subplot(2,2,2);
plot(C,E_2,'ro','MarkerSize',12)%Plot the E_1 with respect to moisture
hold on
E_2_function = fittype('A+(5590-A)*exp(-B*x)+C*x*exp(-D*x)');%Define ...
    the fit type, a customized function, which is the creep function ...
    here
%E_2 initial is fixed, the value at 0 moisture content, which is ...
    1725 MPa
%k is the magnification rate
options = fitoptions(E_2_function);%Take out the options structure ...
    of fit
options.StartPoint = [100 0.1 1e3 0.5];% Set the start point of the fit
options.Lower = [0 0 0 0];
options.Upper = [Inf 1 Inf Inf];
[fE2,gofE2] = fit(C,E_2,E_2_function,options);%FIT! And give the ...
    goodness of fit
E_2_fit = fE2.A+(5590-fE2.A)*exp(-fE2.B*C_cont)+fE2.C.*...
C_cont.*exp(-fE2.D.*C_cont);
plot(C_cont,E_2_fit,'b','LineWidth',2)
%Finally adjust the figure properties to make it looks good
xlabel('\bf Moisture(%)')
ylabel('\bf E_2 (MPa)')
ax=gca;%The following is to adjust the figure properties
ax.XAxis.FontSize = 16;%font size of x-ticks
ax.YAxis.FontSize = 16;%font size of y-ticks
ax.XLabel.FontSize = 16;%font size of x-label
ax.YLabel.FontSize = 16;%font size of y-label
ax.Title.FontSize = 16;%font size of title

subplot(2,2,3);
plot(C,mu_1,'ro','MarkerSize',12)%Plot the E_1 with respect to moisture
hold on
mu_1_function = ...
    fittype('A+(1.819e6-A)*exp(-B*x)+C*x*exp(-D*x)');%Define the fit ...
    type, a customized function, which is the creep function here
%mu_1 initial is fixed, the value at 0 moisture content, which is ...
    4418.48 MPa min
%k is the magnification rate
```

```
options.StartPoint = [100 0.3 1e5 0.5];% Set the start point of the fit
options.Lower = [0 0 0 0];
options.Upper = [Inf 1 Inf Inf];
[fmu1,gofmu1] = fit(C,mu_1,mu_1_function,options);%FIT! And give the ...
    goodness of fit
mu_1_fit = fmu1.A+(1.819e6-fmu1.A)*exp(-fmu1.B*C_cont)+...
fmu1.C.*C_cont.*exp(-fmu1.D.*C_cont);
plot(C_cont,mu_1_fit,'b','LineWidth',2)
%Finally adjust the figure properties to make it looks good
xlabel('\bf Moisture(%)')
ylabel('\bf \mu_1 (MPa s)')
ax=gca;%The following is to adjust the figure properties
ax.XAxis.FontSize = 16;%font size of x-ticks
ax.YAxis.FontSize = 16;%font size of y-ticks
ax.XLabel.FontSize = 16;%font size of x-label
ax.YLabel.FontSize = 16;%font size of y-label
ax.Title.FontSize = 16;%font size of title

subplot(2,2,4);
plot(C,mu_2,'ro','MarkerSize',12)%Plot the E_1 with respect to moisture
hold on
mu_2_function = ...
    fittype('A+(1.276e8-A)*exp(-B*x)+C*x*exp(-D*x)');%Define the fit ...
    type, a customized function, which is the creep function here
%mu_2 initial is fixed, the value at 0 moisture content, which is ...
    201212.93 MPa min
%a is the final viscosity, if no hydrogen bonding was formed
%k is the magnification rate of the normal mu_2 decreasing due to ...
    the increased free volume
%c is the magnification rate of the hydrogen bonding caused more ...
    energy loss
options = fitoptions(mu_2_function);%Take out the options structure ...
    of fit
options.StartPoint = [100 0.3 1e5 0.5];% Set the start point of the fit
options.Lower = [0 0 0 0];
options.Upper = [Inf 1 Inf Inf];
[fmu2,gofmu2] = fit(C,mu_2,mu_2_function,options);%FIT! And give the ...
    goodness of fit
mu_2_fit = fmu2.A+(1.276e8-fmu2.A)*exp(-fmu2.B*C_cont)+...
fmu2.C.*C_cont.*exp(-fmu2.D*C_cont);
plot(C_cont,mu_2_fit,'b','LineWidth',2)
%Finally adjust the figure properties to make it looks good
xlabel('\bf Moisture(%)')
ylabel('\bf \mu_2 (MPa s)')
ax=gca;%The following is to adjust the figure properties
ax.XAxis.FontSize = 16;%font size of x-ticks
ax.YAxis.FontSize = 16;%font size of y-ticks
ax.XLabel.FontSize = 16;%font size of x-label
ax.YLabel.FontSize = 16;%font size of y-label
ax.Title.FontSize = 16;%font size of title

% sgtitle('Evolution of model parameters with repsect to moisture ...
    content')
% sgt.FontSize = 20;
```

```
%Output the fitted equations and the goodness of fit
fE1
fprintf('Adjusted R-square of E_1 %f\n',gofE1.adjrsquare)
fE2
fprintf('Adjusted R-square of E_2 %f\n',gofE2.adjrsquare)
fmu1
fprintf('Adjusted R-square of mu_1 %f\n',gofmu1.adjrsquare)
fmu2
fprintf('Adjusted R-square of mu_2 %f\n',gofmu2.adjrsquare)
```

In the last section, both our model predictions and the experimental data are plotted on the same figure. Similarly, a figure in maximized window is created.And the parameters are initialized.

```
C_cont = 0:0.01:20;% generate a continuous moisture levels
fig3 = figure;
E_1_fit = ...
    fE1.A+(20637-fE1.A)*exp(-fE1.B*C_cont)+fE1.C.*C_cont.*exp(-fE1.D.*C_cont);
E_1_fit = E_1_fit./((20637).*ones(1,length(E_1_fit)));
plot(C_cont,E_1_fit,'b','LineWidth',2)
yline(0.2)
xlabel('\bf Moisture(wt%)')
ylabel('\bf E_1 / E_{10}')
ylim([0, 2])
ax=gca;%The following is to adjust the figure properties
ax.XAxis.FontSize = 16;%font size of x-ticks
ax.YAxis.FontSize = 16;%font size of y-ticks
ax.XLabel.FontSize = 16;%font size of x-label
ax.YLabel.FontSize = 16;%font size of y-label
ax.Title.FontSize = 16;%font size of title

fig4 = figure;
E_2_fit = ...
    fE2.A+(5590-fE2.A)*exp(-fE2.B*C_cont)+fE2.C.*C_cont.*exp(-fE2.D.*C_cont);
E_2_fit = E_2_fit./((5590).*ones(1,length(E_2_fit)));
plot(C_cont,E_2_fit,'b','LineWidth',2)
yline(0.2)
xlabel('\bf Moisture(wt%)')
ylabel('\bf E_2 / E_{20}')
ylim([0, 2])
ax=gca;%The following is to adjust the figure properties
ax.XAxis.FontSize = 16;%font size of x-ticks
ax.YAxis.FontSize = 16;%font size of y-ticks
ax.XLabel.FontSize = 16;%font size of x-label
ax.YLabel.FontSize = 16;%font size of y-label
ax.Title.FontSize = 16;%font size of title

fig5 = figure;
mu_1_fit = fmu1.A+(1.819e6-fmu1.A)*exp(-fmu1.B*C_cont)+...
fmu1.C.*C_cont.*exp(-fmu1.D.*C_cont);
```

```
mu_1_fit = mu_1_fit./((1.819e6).*ones(1,length(mu_1_fit)));
plot(C_cont,mu_1_fit,'b','LineWidth',2)
yline(0.2)
xlabel('\bf Moisture(wt%)')
ylabel('\bf \mu_1 / \mu_{10}')
ylim([0, 3])
ax=gca;%The following is to adjust the figure properties
ax.XAxis.FontSize = 16;%font size of x-ticks
ax.YAxis.FontSize = 16;%font size of y-ticks
ax.XLabel.FontSize = 16;%font size of x-label
ax.YLabel.FontSize = 16;%font size of y-label
ax.Title.FontSize = 16;%font size of title

fig6 = figure;
mu_2_fit = fmu2.A+(1.276e8-fmu2.A)*exp(-fmu2.B*C_cont)+...
fmu2.C.*C_cont.*exp(-fmu2.D*C_cont);
mu_2_fit = mu_2_fit./((1.276e8).*ones(1,length(mu_2_fit)));
plot(C_cont,mu_2_fit,'b','LineWidth',2)
yline(0.2)
xlabel('\bf Moisture(wt%)')
ylabel('\bf \mu_2 / \mu_{20}')
ylim([0, 3])
ax=gca;%The following is to adjust the figure properties
ax.XAxis.FontSize = 16;%font size of x-ticks
ax.YAxis.FontSize = 16;%font size of y-ticks
ax.XLabel.FontSize = 16;%font size of x-label
ax.YLabel.FontSize = 16;%font size of y-label
ax.Title.FontSize = 16;%font size of title


%Making predictions here
%Section 4: Prediction and Comparison
%CTA model parameters ========================================
%E_1
E_1i = 20637; %MPa
E_1f = fE1.A; %MPa
k_E1 = fE1.B; % 1/%
k_HE1 = fE1.C; %MPa
k_DE1 = fE1.D; % %

%E_2
E_2i = 5590; %MPa
E_2f = fE2.A; %MPa
k_E2 = fE2.B; %Unitless
k_HE2 = fE2.C; %MPa
k_DE2 = fE2.D; % %
%mu_1
mu_1i = 1.819e6; %MPa*s
mu_1f = fmu1.A; %MPa*s
k_mu1 = fmu1.B; %Unitless
k_Hmu1 = fmu1.C; %MPa
k_Dmu1 = fmu1.D; % %
%mu_2
mu_2i = 1.276e8; %MPa*s
```

```
mu_2f = fmu2.A; %MPa
k_mu2 = fmu2.B; %Unitless
k_Hmu2 = fmu2.C; %MPa
k_Dmu2 = fmu2.D; % %
% CTA model parameters ====================================


fig3=figure;
fig3.WindowState = 'maximized';
plot(RH0relaxation(:,1),RH0relaxation(:,2),'r*','MarkerSize',12) ...
    %Plot the original data at water content level 0
hold on %Make sure all plot on the same figure
plot(RH33relaxation(:,1),RH33relaxation(:,2),'ro','MarkerSize',12) ...
    %Plot the original data at water content level 4.5
plot(RH45relaxation(:,1),RH45relaxation(:,2),'rs','MarkerSize',12) ...
    %Plot the original data at water content level 6.4
plot(RH60relaxation(:,1),RH60relaxation(:,2),'rd','MarkerSize',12) ...
    %Plot the original data at water content level 8.5
plot(RH75relaxation(:,1),RH75relaxation(:,2),'r+','MarkerSize',12) ...
    %Plot the original data at water content level 15.5

t_predict = 0:1e4;

%At 0% moisture concentration
C = 0;
E_1 = E_1f+(E_1i-E_1f)*exp(-k_E1*C) + k_HE1.*C.*exp(-k_DE1.*C);
E_2 = E_2f+(E_2i-E_2f)*exp(-k_E2*C) + k_HE2.*C.*exp(-k_DE2.*C);
mu_1 = mu_1f+(mu_1i-mu_1f)*exp(-k_mu1*C) + k_Hmu1.*C.*exp(-k_Dmu1.*C);
mu_2 = mu_2f+(mu_2i-mu_2f)*exp(-k_mu2*C) + k_Hmu2.*C.*exp(-k_Dmu2.*C);
p_1 = mu_1/E_1 + mu_2/E_1 + mu_2/E_2;
p_2 = (mu_1*mu_2)/(E_1*E_2);
q_1 = mu_2;
q_2 = (mu_1*mu_2)/(E_1);
r_1 = (p_1 - sqrt(p_1^2-4*p_2))/(2*p_2);
r_2 = (p_1 + sqrt(p_1^2-4*p_2))/(2*p_2);
R_predict = (1/(sqrt(p_1^2-4*p_2)))*((q_1 - ...
    q_2*r_1)*exp(-r_1*t)-(q_1 - q_2*r_2)*exp(-r_2*t));
plot(t_predict,R_predict,'b','LineWidth',2)


%At 4.5% moisture concentration
clear R_predict
C = 4.5;
E_1 = E_1f+(E_1i-E_1f)*exp(-k_E1*C) + k_HE1.*C.*exp(-k_DE1.*C);
E_2 = E_2f+(E_2i-E_2f)*exp(-k_E2*C) + k_HE2.*C.*exp(-k_DE2.*C);
mu_1 = mu_1f+(mu_1i-mu_1f)*exp(-k_mu1*C) + k_Hmu1.*C.*exp(-k_Dmu1.*C);
mu_2 = mu_2f+(mu_2i-mu_2f)*exp(-k_mu2*C) + k_Hmu2.*C.*exp(-k_Dmu2.*C);
p_1 = mu_1/E_1 + mu_2/E_1 + mu_2/E_2;
p_2 = (mu_1*mu_2)/(E_1*E_2);
q_1 = mu_2;
q_2 = (mu_1*mu_2)/(E_1);
r_1 = (p_1 - sqrt(p_1^2-4*p_2))/(2*p_2);
r_2 = (p_1 + sqrt(p_1^2-4*p_2))/(2*p_2);
R_predict = (1/(sqrt(p_1^2-4*p_2)))*((q_1 - ...
```

```
    q_2*r_1)*exp(-r_1*t)-(q_1 - q_2*r_2)*exp(-r_2*t));
plot(t_predict,R_predict,'b','LineWidth',2)


%At 6.4% moisture concentration
clear R_predict
C = 6.4;
E_1 = E_1f+(E_1i-E_1f)*exp(-k_E1*C) + k_HE1.*C.*exp(-k_DE1.*C);
E_2 = E_2f+(E_2i-E_2f)*exp(-k_E2*C) + k_HE2.*C.*exp(-k_DE2.*C);
mu_1 = mu_1f+(mu_1i-mu_1f)*exp(-k_mu1*C) + k_Hmu1.*C.*exp(-k_Dmu1.*C);
mu_2 = mu_2f+(mu_2i-mu_2f)*exp(-k_mu2*C) + k_Hmu2.*C.*exp(-k_Dmu2.*C);
p_1 = mu_1/E_1 + mu_2/E_1 + mu_2/E_2;
p_2 = (mu_1*mu_2)/(E_1*E_2);
q_1 = mu_2;
q_2 = (mu_1*mu_2)/(E_1);
r_1 = (p_1 - sqrt(p_1^2-4*p_2))/(2*p_2);
r_2 = (p_1 + sqrt(p_1^2-4*p_2))/(2*p_2);
R_predict = (1/(sqrt(p_1^2-4*p_2)))*((q_1 - ...
    q_2*r_1)*exp(-r_1*t)-(q_1 - q_2*r_2)*exp(-r_2*t));
plot(t_predict,R_predict,'b','LineWidth',2)


%At 8.5% moisture concentration
clear R_predict
C = 8.5;
E_1 = E_1f+(E_1i-E_1f)*exp(-k_E1*C) + k_HE1.*C.*exp(-k_DE1.*C);
E_2 = E_2f+(E_2i-E_2f)*exp(-k_E2*C) + k_HE2.*C.*exp(-k_DE2.*C);
mu_1 = mu_1f+(mu_1i-mu_1f)*exp(-k_mu1*C) + k_Hmu1.*C.*exp(-k_Dmu1.*C);
mu_2 = mu_2f+(mu_2i-mu_2f)*exp(-k_mu2*C) + k_Hmu2.*C.*exp(-k_Dmu2.*C);
p_1 = mu_1/E_1 + mu_2/E_1 + mu_2/E_2;
p_2 = (mu_1*mu_2)/(E_1*E_2);
q_1 = mu_2;
q_2 = (mu_1*mu_2)/(E_1);
r_1 = (p_1 - sqrt(p_1^2-4*p_2))/(2*p_2);
r_2 = (p_1 + sqrt(p_1^2-4*p_2))/(2*p_2);
R_predict = (1/(sqrt(p_1^2-4*p_2)))*((q_1 - ...
    q_2*r_1)*exp(-r_1*t)-(q_1 - q_2*r_2)*exp(-r_2*t));
plot(t_predict,R_predict,'b','LineWidth',2)


%At 15.5% moisture concentration
clear R_predict
C = 15.5;
E_1 = E_1f+(E_1i-E_1f)*exp(-k_E1*C) + k_HE1.*C.*exp(-k_DE1.*C);
E_2 = E_2f+(E_2i-E_2f)*exp(-k_E2*C) + k_HE2.*C.*exp(-k_DE2.*C);
mu_1 = mu_1f+(mu_1i-mu_1f)*exp(-k_mu1*C) + k_Hmu1.*C.*exp(-k_Dmu1.*C);
mu_2 = mu_2f+(mu_2i-mu_2f)*exp(-k_mu2*C) + k_Hmu2.*C.*exp(-k_Dmu2.*C);
p_1 = mu_1/E_1 + mu_2/E_1 + mu_2/E_2;
p_2 = (mu_1*mu_2)/(E_1*E_2);
q_1 = mu_2;
q_2 = (mu_1*mu_2)/(E_1);
r_1 = (p_1 - sqrt(p_1^2-4*p_2))/(2*p_2);
r_2 = (p_1 + sqrt(p_1^2-4*p_2))/(2*p_2);
R_predict = (1/(sqrt(p_1^2-4*p_2)))*((q_1 - ...
```

```
    q_2*r_1)*exp(-r_1*t)-(q_1 - q_2*r_2)*exp(-r_2*t));
plot(t_predict,R_predict,'b','LineWidth',2)


%adjust the plot settings ...
    ========================================================================
xlabel('\bf Time(s)')
ylabel('\bf Relaxation Modulus (MPa)')
legend({'0 wt%','4.5 wt%','6.4 wt%','8.5 wt%','15.5 ...
    wt%','Model'},'FontSize',40,'Location','northeast')
ax=gca;%The following is to adjust the figure properties
ax.XAxis.FontSize = 40;%font size of x-ticks
ax.YAxis.FontSize = 40;%font size of y-ticks
ax.XLabel.FontSize = 40;%font size of x-label
ax.YLabel.FontSize = 40;%font size of y-label
ax.Title.FontSize = 40;%font size of title
axis(ax, [0 12000 0 6500])
% set(gca, 'XScale','log') %Set the x scale to be logrithm
% set(gca, 'YScale','log') %Set the x scale to be logrithm

%Calculate the overall adjusted R-square ...
    ============================================================
C = [0 4.5 6.4 8.5 15.5];
time = {RH0relaxation(:,1), RH33relaxation(:,1), ...
    RH45relaxation(:,1), RH60relaxation(:,1), RH75relaxation(:,1)};
experimental = {RH0relaxation(:,2), RH33relaxation(:,2), ...
    RH45relaxation(:,2), RH60relaxation(:,2), RH75relaxation(:,2)};
total_average_number = ...
    (mean(RH0relaxation(:,2))+mean(RH33relaxation(:,2))...
+mean(RH45relaxation(:,2))...
+mean(RH60relaxation(:,2))+mean(RH75relaxation(:,2)))/5;
for i=1:5
    total_average = ...
        ones(length(experimental{i}),1).*total_average_number;
    E_1 = E_1f+(E_1i-E_1f)*exp(-k_E1*C(i)) + ...
        k_HE1.*C(i).*exp(-k_DE1.*C(i));
    E_2 = E_2f+(E_2i-E_2f)*exp(-k_E2*C(i)) + ...
        k_HE2.*C(i).*exp(-k_DE2.*C(i));
    mu_1 = mu_1f+(mu_1i-mu_1f)*exp(-k_mu1*C(i)) + ...
        k_Hmu1.*C(i).*exp(-k_Dmu1.*C(i));
    mu_2 = mu_2f+(mu_2i-mu_2f)*exp(-k_mu2*C(i)) + ...
        k_Hmu2.*C(i).*exp(-k_Dmu2.*C(i));
    p_1 = mu_1/E_1 + mu_2/E_1 + mu_2/E_2;
    p_2 = (mu_1*mu_2)/(E_1*E_2);q_1 = mu_2;
    q_2 = (mu_1*mu_2)/(E_1);
    r_1 = (p_1 - sqrt(p_1^2-4*p_2))/(2*p_2);
    r_2 = (p_1 + sqrt(p_1^2-4*p_2))/(2*p_2);
    % Calculate the predicted compliance of each of the data point ...
        with respect to experimental
    compliance_predict = (1/(sqrt(p_1^2-4*p_2)))*((q_1 - ...
        q_2*r_1)*exp(-r_1*time{i})-(q_1 - q_2*r_2)*exp(-r_2*time{i}));
    % calculate the residual sum of square
    residual_temp = compliance_predict - experimental{i};
    residual(i) = sum(residual_temp.^2);
```

```
   clear residual_temp
   total_temp = total_average-experimental{i};
   total(i) = sum(total_temp.^2);
   clear total_temp
   clear total_average
end
R_square = 1-(sum(residual))/(sum(total));
adj_R_square = 1-((1-R_square)*(368-1))/(368-20-1)
```

Appendix C: Matlab code related to Chapter 4

Firstly, initialize the file and system, then load the processed experimental results:

```
clear all
close all

%Read all the data files
Composite56_data = load('56Composite20220502Corrected.mat');
Composite28_data = load('28Composite20220603.mat');
PurePLA_data = load('PurePLA20220521.mat');
```

Then, plot the experimental results with error bars and adjust the plot

```
fig1 = figure;
errorbar(PurePLA_data.Time,PurePLA_data.compliance_report,...
PurePLA_data.compliance_error,...
    's','MarkerSize',10,'MarkerEdgeColor',...
    'blue','MarkerFaceColor','blue','Color','blue')
hold on
errorbar(Composite28_data.Time,Composite28_data.compliance_report,...
Composite28_data.compliance_error,...
    's','MarkerSize',10,'MarkerEdgeColor','black',...
    'MarkerFaceColor','black',...
    'Color','black')
errorbar(Composite56_data.Time,Composite56_data.compliance_report,...
Composite56_data.compliance_error,...
    's','MarkerSize',10,'MarkerEdgeColor','red','MarkerFaceColor','red',...
    'Color','red')
legend({'Pure PLA','2.8 wt% Composite','5.6 wt% ...
   Composite'},'FontSize',16,'Location','best')
xlabel('\bf Time (s)')
ylabel('\bf Creep Compliance (1/GPa)')
ax=gca;%The following is to adjust the figure properties
ax.XAxis.FontSize = 14;%font size of x-ticks
ax.YAxis.FontSize = 14;%font size of y-ticks
ax.XLabel.FontSize = 16;%font size of x-label
```

```
ax.YLabel.FontSize = 16;%font size of y-label
ax.Title.FontSize = 18;%font size of title
xlim([0 1000])
ylim([0.2 0.7])
```

Thirdly, fit the pure PLA data with creep function and extract the Burgers model parameters:

```
% Figure 2, fit the pure PLA with Burgers model then use HTP model ...
   to predict the 5.6 wt% composite, then compare with the raw data.
fig2 = figure;
fig2.Position = [100 100 1000 800];
MarkerSizeValue = 8;
LineWidthValue = 3;
FontSizeValue = 20;

creep_function = ...
   fittype('1/2.460+(1/a)*(1-exp(((-a)*x/b)))+x/c');%Define the fit ...
   type, a customized function, which is the creep function here
% a is E_1
% b is mu_1
% c is mu_2
%Note that E_2 is extracted from the instantaneous elastic compliance.
options = fitoptions(creep_function);%Take out the options structure ...
   of fit
options.StartPoint = [0 0 0];% Set the start point of the fit
options.Lower = [5 50 1500];%Set the lower limit of the parameters
options.Upper = [Inf Inf Inf];%Set the upper limit of the parameters
[f2PLA,gof2] = fit(PurePLA_data.Time',PurePLA_data.compliance_report'...
,creep_function,...
options)%FIT! And give the goodnes1600s of fit
t=0:0.1:900;
creep = ...
   1/2.460+(1/f2PLA.a)*(1-exp(((-f2PLA.a)*t/f2PLA.b)))+t/f2PLA.c;%Put ...
   the time points into the fitted function
plot(t,creep,'blue','LineWidth',LineWidthValue)%Plot the fitted curve
hold on
errorbar(PurePLA_data.Time,PurePLA_data.compliance_report,...
PurePLA_data.compliance_error,...
    's','MarkerSize',MarkerSizeValue,'MarkerEdgeColor','blue',...
    'MarkerFaceColor','blue','Color','blue')
```

Fourthly, make calculation for the Halpin-Tsai-Pagano model in Laplace transformed domain.

```
%The following is the HTP model prediction
%For BioMid fibers
```

```
E_f = 49.68; %Fiber elastic modulus, GPa
S_f = 1/E_f; %Fiber compliance, 1/GPa
Fiber_L = 4.7e3; %Fiber length, um, measured by the chopped pellets
Fiber_d = 12.5; %Fiber diameter, um, measured by the microscope

%For PLA
E_1 = f2PLA.a; %Burgers E_1, GPa
E_2 = 2.460; %Burgers E_2, GPa
mu_1 = f2PLA.b; %Burgers mu_1, GPa s
mu_2 = f2PLA.c; % Burgers mu_2, GPa s

xi_1 = 2*Fiber_L/Fiber_d; %H-T model Semi-empirical parameter, ...
   related to fiber aspect ratio
xi_2 = 2;

phi = 0.0235; %Fiber volume fraction
syms s % create the symbolic variable
%Construct the transformed composites creep compliance in ...
   longitudinal direction i=1
J_f = S_f/s;
J_m = 1/(mu_2*s^2)+1/(E_2*s) + 1/(E_1*s+mu_1*s^2);
eta = (J_m/J_f-1)/(J_m/J_f+xi_1);
J_1 = 1/((1/J_m)*((1+xi_1*eta*phi)/(1-eta*phi)));
%Construct the transformed composites creep compliance in transverse ...
   direction i=2
J_f = S_f/s;
J_m = 1/(mu_2*s^2)+1/(E_2*s) + 1/(E_1*s+mu_1*s^2);
eta = (J_m/J_f-1)/(J_m/J_f+xi_2);
J_2 = 1/((1/J_m)*((1+xi_2*eta*phi)/(1-eta*phi)));
%Halpin-Pagano's model
J_c = 1/((3/8)*(1/J_1)+(5/8)*(1/J_2))
G_C = ilaplace(J_c)%Perform inverse Laplace
fplot(G_C,[0 900],'black','Linewidth',LineWidthValue) %Plot this ...
   symbolic function, transformed composite relaxation modulus, ...
   with time range of 0 to 1800s
%HTP model prediction ends here
%Plot the theoretically corrected data 73.5% area of the measured ...
   area, gives 6.8 MPa creep stress
errorbar(Composite28_data.Time,Composite28_data.compliance_report,...
Composite28_data.compliance_error,...
    's','MarkerSize',MarkerSizeValue,'MarkerEdgeColor','black',,,,
    'MarkerFaceColor','black','Color','black')


phi = 0.0470; %Fiber volume fraction
syms s % create the symbolic variable
%Construct the transformed composites creep compliance in ...
   longitudinal direction i=1
J_f = S_f/s;
J_m = 1/(mu_2*s^2)+1/(E_2*s) + 1/(E_1*s+mu_1*s^2);
eta = (J_m/J_f-1)/(J_m/J_f+xi_1);
J_1 = 1/((1/J_m)*((1+xi_1*eta*phi)/(1-eta*phi)));
%Construct the transformed composites creep compliance in transverse ...
   direction i=2
```

```
J_f = S_f/s;
J_m = 1/(mu_2*s^2)+1/(E_2*s) + 1/(E_1*s+mu_1*s^2);
eta = (J_m/J_f-1)/(J_m/J_f+xi_2);
J_2 = 1/((1/J_m)*((1+xi_2*eta*phi)/(1-eta*phi)));
%Halpin-Pagano's model
J_c = 1/((3/8)*(1/J_1)+(5/8)*(1/J_2))
G_C = ilaplace(J_c)%Perform inverse Laplace
fplot(G_C,[0 900],'red','Linewidth',LineWidthValue) %Plot this ...
   symbolic function, transformed composite relaxation modulus, ...
   with time range of 0 to 1800s
%HTP model prediction ends here


%Plot the theoretically corrected data 73.5% area of the measured ...
   area, gives 6.8 MPa creep stress
errorbar(Composite56_data.Time,Composite56_data.compliance_report,...
Composite56_data.compliance_error,...
's','MarkerSize',MarkerSizeValue,'MarkerEdgeColor','red',...
'MarkerFaceColor','red','Color','red')
% Adjust the plot settings.
legend({'0.0PLA/RCF model fitting',...
    '0.0PLA/RCF experimental',...
    '2.8PLA/RCF model prediction',...
    '2.8PLA/RCF experimental',...
    '5.6PLA/RCF model prediction',...
    '5.6PLA/RCF experimental'},...
    'FontSize',FontSizeValue,'Location','south')
xlabel('\bf Time (s)')

ylabel('\bf Compliance (1/GPa)');

ax=gca;%The following is to adjust the figure properties
ax.XAxis.FontSize = FontSizeValue;%font size of x-ticks
ax.YAxis.FontSize = FontSizeValue;%font size of y-ticks
ax.XLabel.FontSize = FontSizeValue;%font size of x-label
ax.YLabel.FontSize = FontSizeValue;%font size of y-label
ax.Title.FontSize = FontSizeValue;%font size of title
xlim([0 1000])
ylim([0 0.65])
```

Appendix D: Matlab code related to Chapter 5

Firstly, load the experimental data

```
clear all
close all
%%
%Load the experimental data
Composite56_data = load('56Composite20220502Corrected.mat');
Group98_data = load('CompGroup98on20220616.mat');
%Load the experimental data
```

Then, input the parameters and call the numerical solving function

```
%%
%Making analytical calculation for dry composites and numerical ...
    calculation for wet composites==========================
ΔT = 0.5;
n = 900/ΔT+1;
C_B_surface = 0.420;
C_PLA_surface = 0.122;
k_d_final = 0.73855;
k_w_final = 6.3408e-4;
%Use the best fitted parameters to make prediction
[J_dry_Ct, Numerical_time, Numerical_compliance] = ...
    Wet_Surface_Inner_Numerical_fit_counter(n, ΔT, k_d_final, ...
    k_w_final, C_B_surface, C_PLA_surface);
```

The details of the numerical solving function is shown below:

```
function [J_dry_Ct, Numerical_time, ...
    Numerical_compliance]=Wet_Surface_Inner_Numerical_fit_counter(n, ...
    ΔT, k_d, k_w, C_B_surface, C_PLA_surface)
%Input arguments:
%     n: %number of discretization points
```

```
%     ΔT: %Delta t and Delta \tau. Time discretization gap, in seconds
%     k_d: %Exponential Damage Parameter, can be played
%     k_w: %Inner layer thickness proportional function constant, ...
   can be played
%     dry_data: dry composites experimental data
%     wer_data: wet composites experimental data

%Output arguments:
%     J_dry_Ct: dry composites creep compliance in t-domain
%     Numerical_time: time points of the numerical solution
%     Numerical_compliance: compliance points of the numerical solution



%Modified Burgers-Reimschuessel model parameters
    %For PLA
    %E_1
    P_0E1 = 8.794; %GPa
    P_fE1 = 0; %GPa
    k_pE1 = 0.707; % %
    k_AE1 = 12.88;
    k_DE1 = 0.7257;
    %E_2
    P_0E2 = 2.460; %GPa
    P_fE2 = 0; %GPa
    k_pE2 = 0.1768; % %
    k_AE2 = 5.032;
    k_DE2 = 4.058;
    %mu_1
    P_0mu1 = 632.16; %GPa*s
    P_fmu1 = 0; %GPa*s
    k_pmu1 = 0.4889; % %
    k_Amu1 = 4125;
    k_Dmu1 = 4.337;
    %mu_2
    P_0mu2 = 8.892e3; %GPa*s
    P_fmu2 = 0; %GPa*s
    k_pmu2 = 1.461; % %
    k_Amu2 = 4.553e4;
    k_Dmu2 = 1.462;
    %For BioMid fibers
    P_0EB = 49.68; % GPa
    P_fEB = 26.70; %GPa
    k_pEB = 0.2092; % %
    k_AEB = 4.74;
    k_DEB = 10.17;
    %Modified Burgers-Reimschuessel model parameters
    W = 0.056; %Fiber weight fraction
    rho_C = 1/((W/1.5)+((1-W)/1.24));%Composites density, assuming ...
       no voids, fiber density 1.5 while matrix density 1.24
    phi = ((rho_C)/(1.5))*W; %Fiber volume fraction calculated from ...
       fiber weight fraction
    syms s % create the symbolic variable s, the independent ...
       variable in Laplace domain
```

```
    syms t % create the symbolic variable time t


%     fig1 = figure;
%     fig1.Position = [500 100 1000 800];
%The following is the Dry group
    C_PLA = 0; %Moisture content of the PLA matrix
    C_c = 0; %Moisture content of the composites
    C_B = (C_c-0.944*C_PLA)/(0.056); %Moisture content of the BioMid ...
       fibers by calculation
    %For BioMid fibers
    E_B = ...
       P_fEB+(P_0EB-P_fEB)*exp(-k_pEB*C_B)+k_AEB*C_B*exp(-k_DEB*C_B); ...
       %Fiber elastic modulus, GPa
    S_B = 1/E_B; %Fiber compliance, 1/GPa
    %For PLA
    E_1 = P_fE1+(P_0E1-P_fE1)*exp(-k_pE1*C_PLA)...
    +k_AE1*C_PLA*exp(-k_DE1*C_PLA);
    E_2 = P_fE2+(P_0E2-P_fE2)*exp(-k_pE2*C_PLA)+...
    k_AE2*C_PLA*exp(-k_DE2*C_PLA);
    mu_1 = P_fmu1+(P_0mu1-P_fmu1)*exp(-k_pmu1*C_PLA)+...
    k_Amu1*C_PLA*exp(-k_Dmu1*C_PLA);
    mu_2 = P_fmu2+(P_0mu2-P_fmu2)*exp(-k_pmu2*C_PLA)+...
    k_Amu2*C_PLA*exp(-k_Dmu2*C_PLA);
    %Halpin-Tsai model semi-empirical parameters
    Fiber_L = 4.7e3; %Fiber length, um, measured by the chopped pellets
    Fiber_d = 12.5; %Fiber diameter, um, measured by the microscope
    xi_1 = 2*Fiber_L/Fiber_d; %H-T model Semi-empirical parameter, ...
       related to fiber aspect ratio
    xi_2 = 2;
    %Halpin-Tsai-Pagano model prediction
    %Construct the transformed composites creep compliance in ...
       longitudinal direction i=1
    J_f = S_B/s;
    J_m = 1/(mu_2*s^2)+1/(E_2*s) + 1/(E_1*s+mu_1*s^2);
    eta = (J_m/J_f-1)/(J_m/J_f+xi_1);
    J_1 = 1/((1/J_m)*((1+xi_1*eta*phi)/(1-eta*phi)));
    %Construct the transformed composites creep compliance in ...
       transverse direction i=2
    J_f = S_B/s;
    J_m = 1/(mu_2*s^2)+1/(E_2*s) + 1/(E_1*s+mu_1*s^2);
    eta = (J_m/J_f-1)/(J_m/J_f+xi_2);
    J_2 = 1/((1/J_m)*((1+xi_2*eta*phi)/(1-eta*phi)));
    %Halpin-Pagano's model
    J_c = 1/((3/8)*(1/J_1)+(5/8)*(1/J_2));
    J_dry_Ct = ilaplace(J_c);%Perform inverse Laplace

%     fplot(J_dry_Ct,[0 900],'red','Linewidth',2) %Plot this ...
   symbolic function, transformed composite relaxation modulus, ...
   with time range of 0 to 1800s
%     hold on
    %HTP model prediction ends here
    %Plot the dry composites data
%     ...
```

```
   errorbar(Composite56_data.Time,Composite56_data.compliance_report,...
Composite56_data.compliance_error,...
%         's','MarkerSize',8,'MarkerEdgeColor','red',...
'MarkerFaceColor','red','Color','red')
% Dry group ends here

%The following is the 98% RH group Exponential Fiber Damage
    %For Inner Layer
    %Moisture contente for calculation
    C_PLA_inner = 0.906; %Moisture content of the PLA matrix, in wt%
    C_c_inner = 1.313; %Moisture content of the composites
    C_B_inner = (C_c_inner-0.944*C_PLA_inner)/(0.056); %Moisture ...
       content of the BioMid fibers by calculation
    %For BioMid fibers
    E_B_inner = P_fEB+(P_0EB-P_fEB)*exp(-k_pEB*C_B_inner)+...
    k_AEB*C_B_inner*exp(-k_DEB*C_B_inner); %Fiber elastic modulus, GPa
    %Damage coefficient function change here==========
    C_d_inner = exp(-k_d*C_c_inner);
    %Damage coefficient function change here==========
    E_B_inner = C_d_inner*E_B_inner;%Damaged Fiber Young's modulus ...
       in the inner layer
    S_B_inner = 1/E_B_inner; %Fiber compliance, 1/GPa
    %For PLA
    E_1 = P_fE1+(P_0E1-P_fE1)*exp(-k_pE1*C_PLA_inner)+...
    k_AE1*C_PLA_inner*exp(-k_DE1*C_PLA_inner);
    E_2 = P_fE2+(P_0E2-P_fE2)*exp(-k_pE2*C_PLA_inner)+...
    k_AE2*C_PLA_inner*exp(-k_DE2*C_PLA_inner);
    mu_1 = P_fmu1+(P_0mu1-P_fmu1)*exp(-k_pmu1*C_PLA_inner)+...
    k_Amu1*C_PLA_inner*exp(-k_Dmu1*C_PLA_inner);
    mu_2 = P_fmu2+(P_0mu2-P_fmu2)*exp(-k_pmu2*C_PLA_inner)+...
    k_Amu2*C_PLA_inner*exp(-k_Dmu2*C_PLA_inner);
    %Halpin-Tsai model semi-empirical parameters
    Fiber_L = 4.7e3; %Fiber length, um, measured by the chopped pellets
    Fiber_d = 12.5; %Fiber diameter, um, measured by the microscope
    xi_1 = 2*Fiber_L/Fiber_d; %H-T model Semi-empirical parameter, ...
       related to fiber aspect ratio
    xi_2 = 2;
    %Halpin-Tsai-Pagano model prediction
    %Construct the transformed composites creep compliance in ...
       longitudinal direction i=1
    J_f = S_B_inner/s;
    J_m = 1/(mu_2*s^2)+1/(E_2*s) + 1/(E_1*s+mu_1*s^2);
    eta = (J_m/J_f-1)/(J_m/J_f+xi_1);
    J_1 = 1/((1/J_m)*((1+xi_1*eta*phi)/(1-eta*phi)));
    %Construct the transformed composites creep compliance in ...
       transverse direction i=2
    J_f = S_B_inner/s;
    J_m = 1/(mu_2*s^2)+1/(E_2*s) + 1/(E_1*s+mu_1*s^2);
    eta = (J_m/J_f-1)/(J_m/J_f+xi_2);
    J_2 = 1/((1/J_m)*((1+xi_2*eta*phi)/(1-eta*phi)));
    %Halpin-Pagano's model
    G_c_inner = ((3/8)*(1/J_1)+(5/8)*(1/J_2))/s^2; % Stress ...
       relaxation modulus in Laplace domain
    % J_c_inner = 1/G_c_inner; %Inner layer creep compliance in s domain
```

```
G_Ct_inner = ilaplace(G_c_inner);% Stress relaxation modulus in ...
   t domain
% J_Ct_inner = ilaplace(J_c_inner); %Inner layer creep ...
   compliance in t domain
%Inner Layer Ends here
% fplot(J_Ct_inner,[0 900],'black','Linewidth',2) %Plot the ...
   inner layer creep compliance


%For Surface Layers
%    C_PLA_surface = 0.122; %Moisture content of the PLA matrix, in wt%
%    C_B_surface = 0.420; %Moisture content of the BioMid fibers by ...
  calculation
C_c_surface = 0.056*C_B_surface + (1-0.056)*C_PLA_surface; ...
   %Moisture content of the composites

%For BioMid fibers
E_B_surface = P_fEB+(P_0EB-P_fEB).*exp(-k_pEB.*C_B_surface)+...
k_AEB.*C_B_surface.*exp(-k_DEB.*C_B_surface);
%Damage coefficient function change here==========
C_d_surface = exp(-k_d*C_c_surface);
%Damage coefficient function change here==========
E_B_surface = C_d_surface.*E_B_surface;
S_B_surface = 1/E_B_surface;
%For PLA
E_1 = P_fE1+(P_0E1-P_fE1)*exp(-k_pE1*C_PLA_surface)+...
k_AE1*C_PLA_surface*exp(-k_DE1*C_PLA_surface);
E_2 = P_fE2+(P_0E2-P_fE2)*exp(-k_pE2*C_PLA_surface)+...
k_AE2*C_PLA_surface*exp(-k_DE2*C_PLA_surface);
mu_1 = P_fmu1+(P_0mu1-P_fmu1)*exp(-k_pmu1*C_PLA_surface)+...
k_Amu1*C_PLA_surface*exp(-k_Dmu1*C_PLA_surface);
mu_2 = P_fmu2+(P_0mu2-P_fmu2)*exp(-k_pmu2*C_PLA_surface)+...
k_Amu2*C_PLA_surface*exp(-k_Dmu2*C_PLA_surface);
%Halpin-Tsai model semi-empirical parameters
Fiber_L = 4.7e3; %Fiber length, um, measured by the chopped pellets
Fiber_d = 12.5; %Fiber diameter, um, measured by the microscope
xi_1 = 2*Fiber_L/Fiber_d; %H-T model Semi-empirical parameter, ...
   related to fiber aspect ratio
xi_2 = 2;
%Halpin-Tsai-Pagano model prediction
%Construct the transformed composites creep compliance in ...
   longitudinal direction i=1
J_f_surface = S_B_surface/s;
J_m = 1/(mu_2*s^2)+1/(E_2*s) + 1/(E_1*s+mu_1*s^2);
eta = (J_m/J_f_surface-1)/(J_m/J_f_surface+xi_1);
J_1 = 1/((1/J_m)*((1+xi_1*eta*phi)/(1-eta*phi)));
%Construct the transformed composites creep compliance in ...
   transverse direction i=2
J_f_surface = S_B_surface/s;
J_m = 1/(mu_2*s^2)+1/(E_2*s) + 1/(E_1*s+mu_1*s^2);
eta = (J_m/J_f_surface-1)/(J_m/J_f_surface+xi_2);
J_2 = 1/((1/J_m)*((1+xi_2*eta*phi)/(1-eta*phi)));
%Halpin-Pagano's model
G_c_surface = ((3/8)*(1/J_1)+(5/8)*(1/J_2))/s^2; % Stress ...
```

```
    relaxation modulus in Laplace domain
G_Ct_surface = ilaplace(G_c_surface);% Stress relaxation modulus ...
    in t domain
%Surface Layers Ends here


%Numerical solution of the Voight parallel model with varying ...
    thickness
%Thickness variation function change here==========
f_t = exp(-k_w*t); %Inner layer thickness proportion function
%Thickness variation function change here==========
t = 0;
G_S0 = double(subs(G_Ct_surface));
G_I0 = double(subs(G_Ct_inner));

DG_S = diff(G_Ct_surface); %derivative of surface layer stress ...
    relaxation modulus, a symbolic function
DG_I = diff(G_Ct_inner); %derivative of inner layer stress ...
    relaxation modulus, a symbolic function


M = zeros(n);
b = ones(n,1);
f = zeros(n,1);

t = 0; % The first equation, n = 0
f(1) = double(subs(f_t));
M(1,1) = f(1)*G_I0 + (1-f(1))*G_S0;

t = 1*ΔT; %t = t_1, n = 1
f(2) = double(subs(f_t));
M(2,1) = (1-f(1))*(ΔT/2)*double(subs(DG_S)) + ...
    f(1)*(ΔT/2)*double(subs(DG_I)); %J_0 coefficient
t = 0;
M(2,2) = (1-f(1))*(G_S0 + (ΔT/2)*double(subs(DG_S))) + ...
    f(1)*(G_I0 + (ΔT/2)*double(subs(DG_I))); %J_1 coefficient

i_options = 2:(n-1);
counter_total = length(i_options);
counter = 1;%For construction of the wait bar, starting from 1
h = waitbar(0, 'Calculation in progress');%For construction of ...
    the wait bar, initialize the wait bar

for i = i_options
    tic
    t = i*ΔT;
    f(i+1) = double(subs(f_t));
    M(i+1,1) = (1-f(i+1))*(ΔT/2)*double(subs(DG_S)) + ...
        f(i+1)*(ΔT/2)*double(subs(DG_I)); %J_0 coefficient
    for j = 1:(i-1)
        t = (i-j)*ΔT;
        M(i+1,j+1) = 2*((1-f(i+1))*(ΔT/2)*double(subs(DG_S)) + ...
            f(i+1)*(ΔT/2)*double(subs(DG_I)));
    end
```

```
        t = 0;
        M(i+1,i+1) = (1-f(i+1))*(G_S0 + (ΔT/2)*double(subs(DG_S))) + ...
            f(i+1)*(G_I0 + (ΔT/2)*double(subs(DG_I)));

        bar_str = ['Calculation in progress...', ...
            num2str(counter/counter_total*100),'% ', ...
            num2str(counter) ' of ' num2str(counter_total)]; %Wait ...
            bar display string
        waitbar(counter/counter_total,h,bar_str);%Update the wait bar
        counter = counter + 1; %Wait bar counter + 1, for next round
        toc
    end

    Numerical_compliance = M^-1 * b;
    Numerical_time = 0:ΔT:(n-1)*ΔT;

end
```

The adjusted R^2 values is calculated below:

```
%Make calculation of the adjusted R_square
SS_RES = 0;
SS_TOT = 0;
y_i_bar = mean(Group98_data.compliance_report);
for i = 1:19
    SS_RES = SS_RES + (Group98_data.compliance_report(i) - ...
        Numerical_compliance(((n-1)/(18))*(i-1)+1))^2;
    SS_TOT = SS_TOT + (Group98_data.compliance_report(i) - y_i_bar)^2;
end
R_square = 1 - (SS_RES)/(SS_TOT); %Calculate the R_square
R_square_adj = 1 - (1-R_square)*(19-1)/(19-2-1);
%Use the best fitted parameters to make prediction end
%Making analytical calculation for dry composites and numerical ...
    calculation for wet composites end
```

Finally make the plot

```
%%
%Plot
fig1 = figure;
fig1.Position = [500 100 1000 800];

% 98% RH composites plot
plot(Numerical_time,Numerical_compliance,'k--','LineWidth',2)
hold on
errorbar(Group98_data.Time,Group98_data.compliance_report,...
Group98_data.compliance_error,...
    's','MarkerSize',8,'MarkerEdgeColor','black',...
    'MarkerFaceColor','black','Color','black')
```

```
% Dry composites plot
fplot(J_dry_Ct,[0 900],'red','Linewidth',2) %Plot this symbolic ...
    function, transformed creep compliance
errorbar(Composite56_data.Time,Composite56_data.compliance_report,...
Composite56_data.compliance_error,...
    's','MarkerSize',8,'MarkerEdgeColor','red',...
    'MarkerFaceColor','red','Color','red')

% Plot settings
legend({'98% RH, HTP with Surface-Inner layer model prediction, ...
    numerical',...
    '98% RH, creep under 22% RH, experimental results',...
    'Dry 5.6 wt% (4.68 vol.%) prediction by Halpin-Tsai-Pagano ...
       model, analytical',...
    'Dry 5.6 wt% (4.68 vol.%) Composite experimental results'},...
    'FontSize',16,'Location','best')
xlabel('\bf Time (s)')
ylabel('\bf Creep Compliance (1/GPa)')
ax=gca;%The following is to adjust the figure properties
ax.XAxis.FontSize = 14;%font size of x-ticks
ax.YAxis.FontSize = 14;%font size of y-ticks
ax.XLabel.FontSize = 16;%font size of x-label
ax.YLabel.FontSize = 16;%font size of y-label
ax.Title.FontSize = 18;%font size of title
xlim([0 1000])
ylim([0.2 0.65])
%Plot

%%
%Moisture content plot
fig2 = figure;
fig2.Position = [100 100 1000 800];

Time_experiment = 0:50:900;
MC_experiment = [1.313 1.274 1.256 1.243 1.233 1.223 1.217 1.209 ...
    1.202 1.194 1.193 1.181 1.178 1.171 1.168 1.163 1.158 1.157 1.157];
MC_StandardDeviation = [0.049 0.052 0.044 0.044 0.046 0.050 0.049 ...
    0.053 0.053 0.052 0.052 0.052 0.050 0.050 0.048 0.054 0.050 ...
    0.050 0.054];
errorbar(Time_experiment,MC_experiment,MC_StandardDeviation,...
    's','MarkerSize',8,'MarkerEdgeColor',...
    'blue','MarkerFaceColor','blue','Color','blue')
hold on

Time = 0:1:900;
C_c_inner = 1.313;
C_c_surface = 0.056*C_B_surface + (1-0.056)*C_PLA_surface;
C_c = exp(-k_w_final.*Time).*C_c_inner + ...
    (1-exp(-k_w_final.*Time)).*C_c_surface;
plot(Time, C_c, 'LineWidth', 2)

ylim([0 1.5])
legend({'5.6 wt% composites from 98%RH to Room 24% RH, 21.7 - ...
```

```
    22.1^oC, July 12',...
     'Model prediction'},...
     'FontSize',16,'Location','best')
xlabel('\bf Time (s)')
ylabel('\bf Moisture Content (wt%)')

ax=gca;%The following is to adjust the figure properties
ax.XAxis.FontSize = 14;%font size of x-ticks
ax.YAxis.FontSize = 14;%font size of y-ticks
ax.YAxis.Color = 'blue';%font size of y-ticks
ax.XLabel.FontSize = 16;%font size of x-label
ax.YLabel.FontSize = 16;%font size of y-label
ax.Title.FontSize = 18;%font size of title
```

Appendix E: Original data of Chapter 3

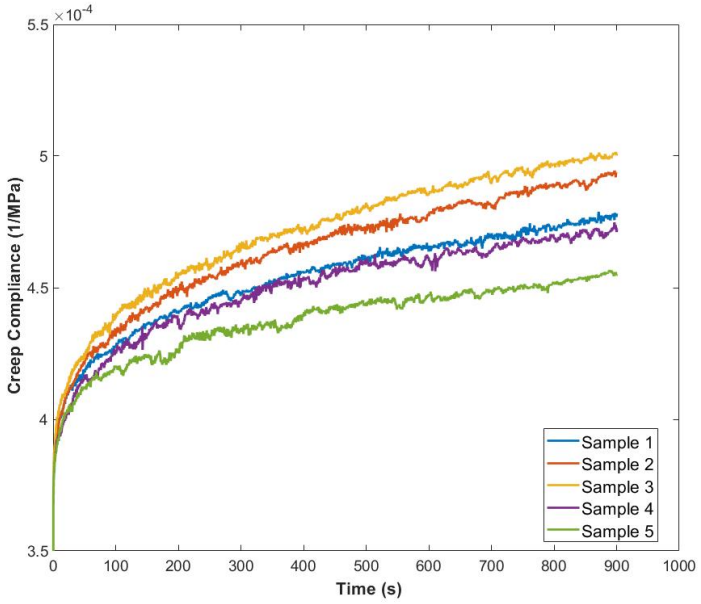

Figure E.1: Original data of creep compliance of dry samples

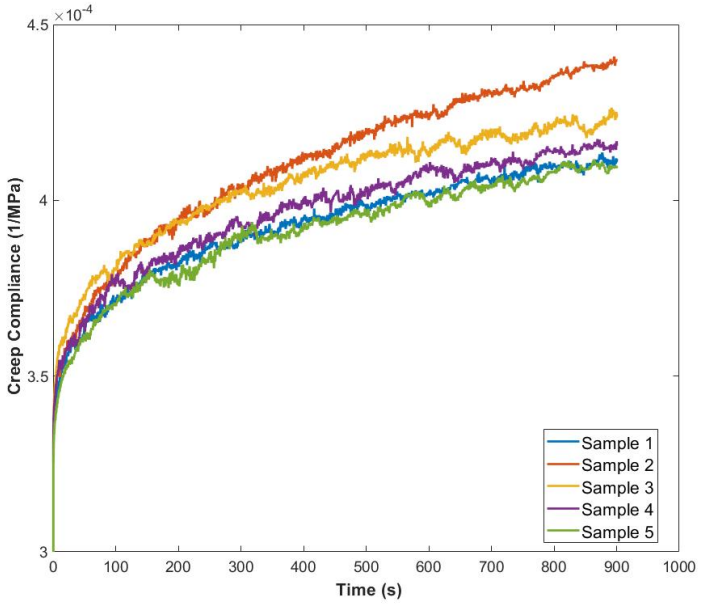

Figure E.2: Original data of creep compliance of samples conditioned under 33% RH

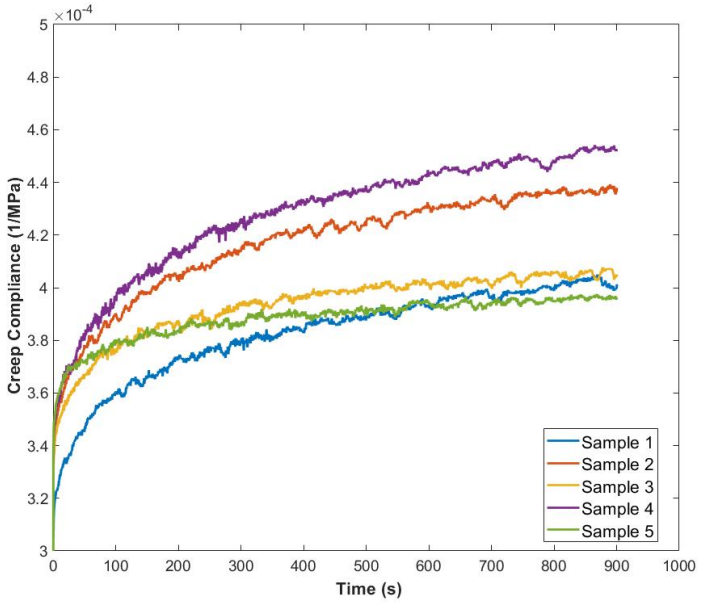

Figure E.3: Original data of creep compliance of samples conditioned under 75% RH

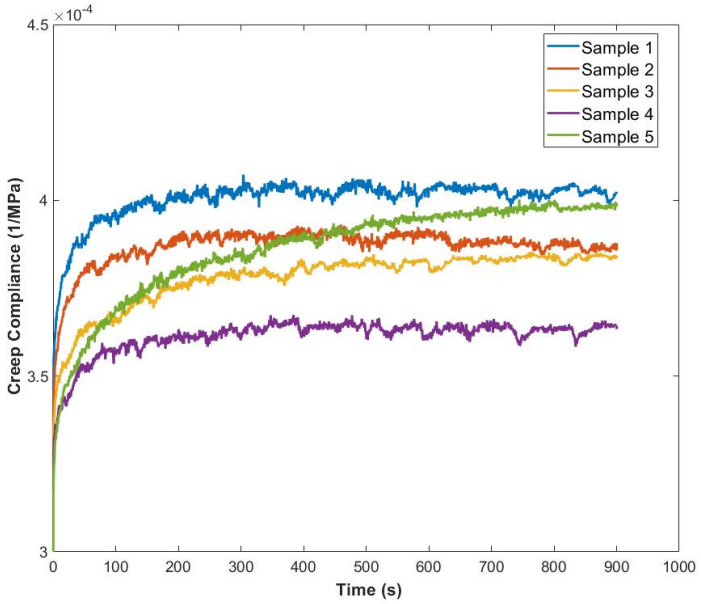

Figure E.4: Original data of creep compliance of samples conditioned under 98% RH

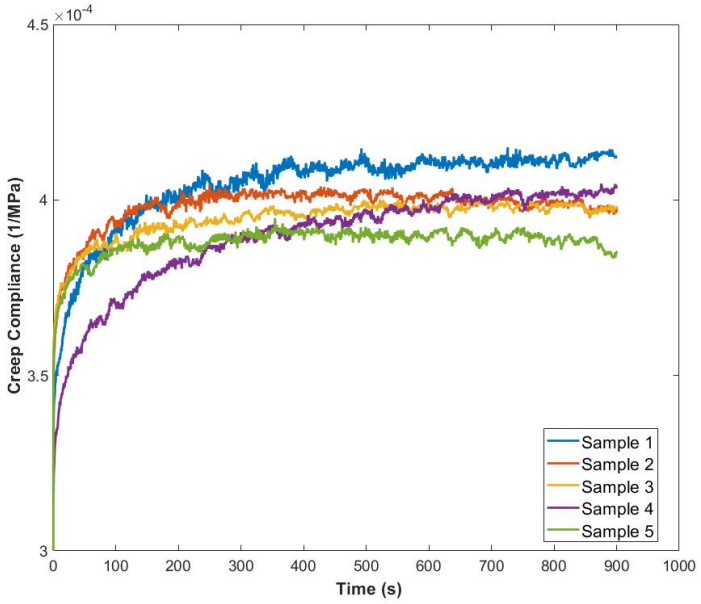

Figure E.5: Original data of creep compliance of samples immersed in distilled water

Appendix F: Original data of Chapter 4

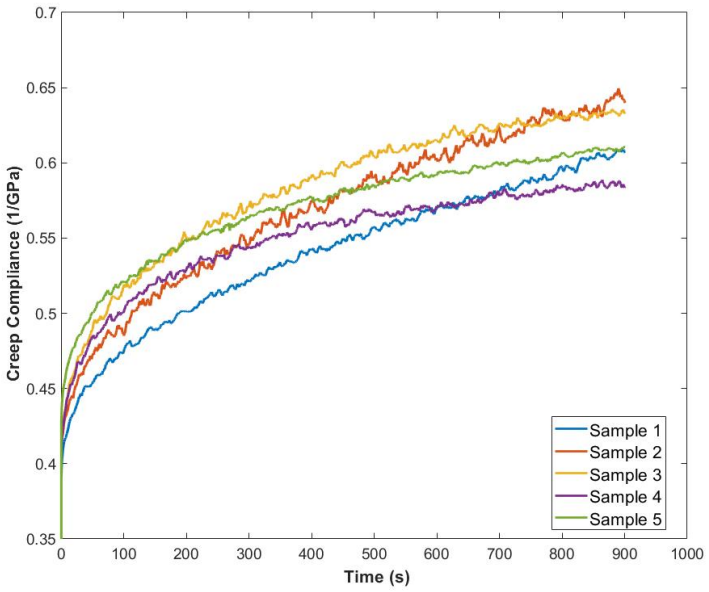

Figure F.1: Original data of creep compliance of pure PLA

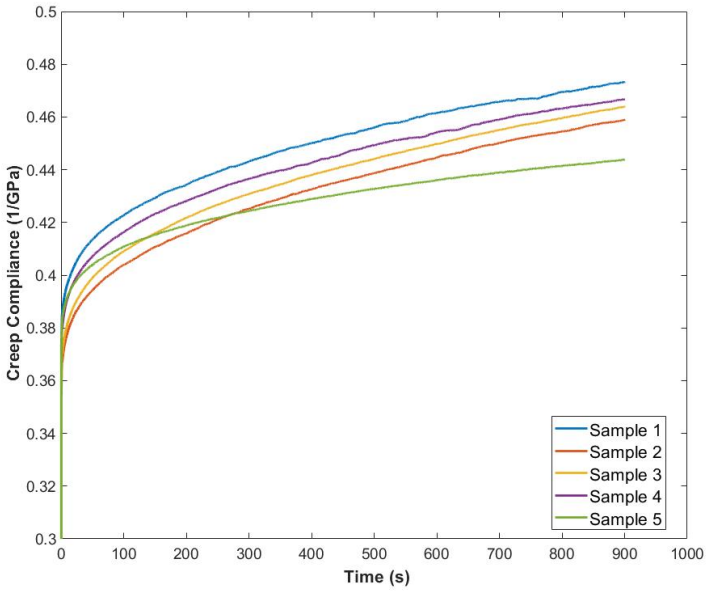

Figure F.2: Original data of creep compliance of 2.8 wt% RCF reinforced PLA composites

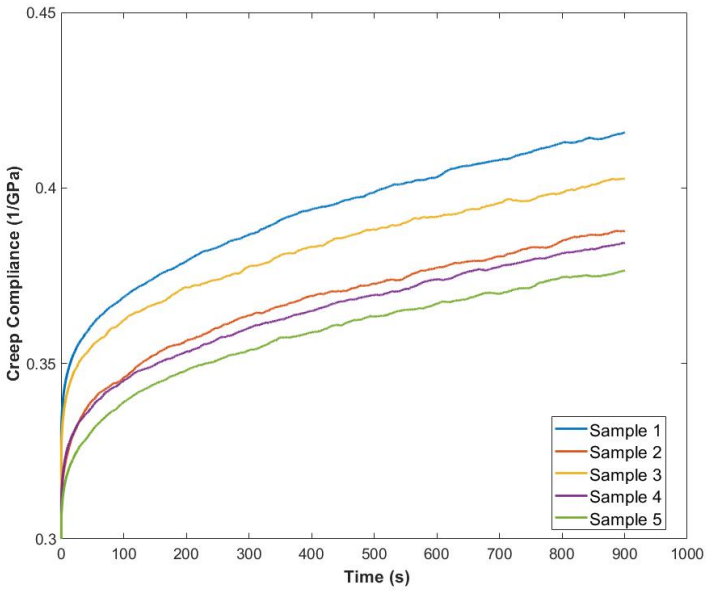

Figure F.3: Original data of creep compliance of 5.6 wt% RCF reinforced PLA composites

Appendix G: Original data of Chapter 5

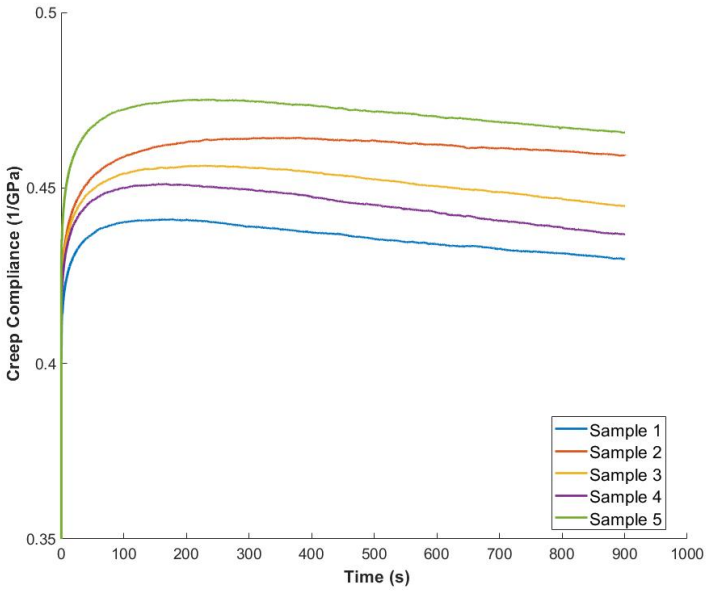

Figure G.1: Original data of creep compliance of composites conditioned under 98% RH and creeped under 24% RH